# A THREE STEP APPROACH TO THE DEGRADATION OF NATURAL ORGANIC MATTER (NOM) FROM WATER SOURCES.

---


**by**

**NQOBILE GUGULETHU NDLANGAMANDLA**


submitted in accordance with the requirements for the degree of

**MASTERS OF SCIENCE**

in

**CHEMISTRY**

at the

**UNIVERSITY OF SOUTH AFRICA**


| | | |
|---|---|---|
| **Supervisor** | **:** | **Dr Thabo TI Nkambule** |
| **Co-supervisors** | **:** | **Prof Bhekie B Mamba** |
| | **:** | **Prof Titus AM Msagati** |
| | **:** | **Dr Alex T Kuvarega** |


**June 2017**

## DECLARATION

Name: Nqobile Gugulethu Ndlangamandla

Student number: 57669082

Degree: Masters in Chemistry

Exact wording of the title of the dissertation or thesis as appearing on the copies submitted for examination:

**A THREE STEP APPROACH TO THE DEGRADATION OF NATURAL ORGANIC MATTER (NOM) FROM WATER SOURCES**

I declare that the above dissertation/thesis is my own work and that all the sources that I have used or quoted have been indicated and acknowledged by means of complete references.

_____ _____

SIGNATURE DATE

## DEDICATION

I dedicate this work to the most high God, the master of the universe, who protected me, guided me and opened the opportunity for me to pursue with my Master's degree. To my parents (Nomusa Nene and Z.M Ndlangamandla), my grandmother, my siblings and my late grandfather for believing in me and encouraging me.

## ACKNOWLEDGEMENTS

I would like to take this opportunity to thank the following people and institutions:

God Almighty for his love, protection and guidance throughout my Master's studies.

My supervisors Dr Thabo T.I. Nkambule, Dr Alex T. Kuvarega, Prof Titus A.M. Msagati and Prof Bhekie B. Mamba for their supervision, support, guidance and encouragement. I would not have been this far if it was not for their patience and love.

I would like to thank Prof Johannes H. Haarhoff for his mentorship throughout my MSc studies.

Dr Nyoni and Mr. Amza Sacko for their assistance with various instruments. I would also like to thank the department of Physics for the solar simulator and XRD analysis; the department of Chemistry for TGA.

I would like to thank the University of South Africa (UNISA) for giving me the opportunity to pursue my MSc studies. National Research Foundation (NRF), Water Research Commision (WRC) and Nanotechnology and Water sustainability unity for financial support.

I would like to thank the following water treatment utilities for their guidance and assistance throughout the sampling rounds: Magalies Water treatment plant; Rietvlei Water treatment plant; Umgeni Water treatment plant; Midvaal Water treatment plant; Veolia Water treatment plant; Plettensberg Bay Water treatment plant and Lepelle water treatment plant.

A special thanks to my mother Nomusa Nene for her support, love, encouragement, patience and prayers throughout. My whole family (a special thanks to Zamo Zwane for his support) for their understanding, encouragement and support.

Lastly, I would like to thank my colleagues and friends (a special thanks to Nozipho Gumbi, Welldone Moyo, Dineo Bopape and Nhamo Chaukura) for their love, support and encouragement during hard lab times.

## CONFERENCES AND PUBLICATIONS

The results presented in this dissertation have been presented in regional and national conferences and a part of it has been submitted for publication in peer reviewed journals.

### Conferences

### Oral presentation

1. NG Ndlangamandla, AT Kuvarega, TAM Msagati, BB Mamba, Thabo TI Nkambule “A three step approach to the degradation of Natural Organic Matter (NOM) from water sources ". Annual student Research and Innovation showcase, 19-21 August 2015, UNISA, South Africa.

2. NG Ndlangamandla, AT Kuvarega, TAM Msagati, BB Mamba, Thabo TI Nkambule " Natural Organic Matter (NOM) removal efficiency by various South African water treatment plants: Towards the development of a rapid NOM degradation protocol ". Water Institute of Southern Africa (WISA), 15-19 May 2016, Durban.

3. NG Ndlangamandla, AT Kuvarega, TAM Msagati, BB Mamba, Thabo TI Nkambule "A novel degradation approach for the efficient removal of Natural Organic Matter (NOM) from water sources ". 17th WaterNet/WARFSA/GWP-SA, 26-28 October 2016, Botswana.

### Poster presentation

1. NG Ndlangamandla, AT Kuvarega , TAM Msagati , BB Mamba , Thabo TI Nkambule " Photocatalytic degradation of Natural Organic Matter (NOM) in water using N, Pd co-doped $TiO_2$ & MWCNTs/N, Pd co-doped $TiO_2$". NanoAfrica international conference, 3-6 April 2016, UNISA, South Africa.

2. NG Ndlangamandla, AT Kuvarega, TAM Msagati, BB Mamba, Thabo TI Nkambule “A three step approach to the degradation of Natural Organic Matter (NOM) from water sources ". AVISHKAR competition, 11-12 December 2015, University of Pune, India.

## Publications

1. NG Ndlangamandla, AT Kuvarega, TAM Msagati, BB Mamba, Thabo TI Nkambule “Evaluating the character of Natural Organic Matter (NOM) and its removal efficiency by various South African water treatment plants: towards the development of a rapid NOM degradation protocol” (submitted, Water SA, 2016).
2. NG Ndlangamandla, AT Kuvarega, TAM Msagati, BB Mamba, Thabo TI Nkambule “A novel degradation approach for the efficient removal of Natural Organic Matter (NOM) from water sources” (submitted, Physics and Chemistry of Earth, 2016).

## ABSTRACT

Natural Organic Matter (NOM) is a complex blend of organic compounds that forms naturally *via* the degradation of plant and animal materials into water sources. NOM in water negatively affects water quality (by causing odor, taste and color problems), negatively affects consumers health (through the disinfection by-products formation which are carcinogenic), increases costs in plant operations (by causing membrane fouling and high coagulant dosage demand) and negatively impacts the ecosystem (through bacterial regrowth and deterioration of surface water sources). In addition, the complexity and the size of NOM hinders most of the available water treatment processes that are in place in South Africa and worldwide from effectively and efficiently removing NOM from water sources. The varying character of NOM in various sources makes it difficult to remove NOM as its composition is not uniform; it depends on the climate, topology, industrial and agricultural activities around a particular area. Hence there is a need for methods that can effectively characterize and degrade NOM (such as photodegradation using $TiO_2$) into smaller pieces for easy removal during water treatment processes.

The characterization of NOM in water was done by collecting samples from different water treatment plants located in various South African geographic locations. The purpose was to get a better understanding regarding the type and the composition of NOM occurring in water. The treatment plants of interest were Magalies Water (MP1, MP2 and MP3); Rietvlei Water (RV); Umgeni Water (HL, UM, MT and AM); Lepelle Water (LE, LO and LF); Midvaal Water (MV); Veolia Water (VP and VH) and Plettenberg Bay Water (P). The sampling was done during the period of September 2015 to September 2016 in order to account for seasonal variations. Samples were collected after each treatment stage for each treatment plant in order to study the treatability of NOM by various treatment processes. Conventional characterization methods such as dissolved organic carbon (DOC), ultra-violet at 254 nm ($UV_{254}$) and specific UV-absorbance (SUVA); and advanced methods such as fluorescence excitation-emission matrix (FEEM) were employed in order to have a broad understanding on the character of NOM occurring in South African water sources.

Furthermore, N, Pd co-doped $TiO_2$ (NPT) and MWCNTs/N, Pd co-doped $TiO_2$ (CT) were successfully synthesized *via* sol-gel method and characterized using FTIR (to confirm for the available functional groups), UV-Vis (to study the effect of doping $TiO_2$ with N and Pd and the effect of the presence of MWCNTs on the absorption edge of $TiO_2$), XRD (to verify the presence of the crystalline phases), Raman (to determine the nature of $TiO_2$ and to verify the presence of MWCNTs), SEM (for morphology), EDS (for elemental composition) and TGA (for thermal stability and to evaluate the amount of MWCNTs present on the nanocomposite). NPT and CT were then tested for their photodegradation efficiency on various NOM containing samples collected from selected treatment plants.

Conventional NOM characterization methods include both the on-site characterization (pH, turbidity and conductivity); and bulk characterization (DOC, $UV_{254}$ and SUVA). The pH was used to determine the alkalinity or the acidity of the water; and it was found to be in a range of 2.50-9.13 with Midvaal (MV) raw water being the most alkaline and Preekstoel (VP) being the most acidic water. The turbidity (a measure of the amount of all the clay particles and colloids in water) of all the water samples at their final stages of the treatment process was found to be in the range of 0.00-3.00 NTU, with the Flag Boshielo Water (LF) having the highest turbidity value and the Magalies Water (MP1) having the lowest turbidity. Lastly, the water conductivity was found to be in the range of 135.3–781.3 mS/cm, with the Olifantspoort plant (LO) having the highest conductivity and Plettenberg Bay plant (P) plant having the lowest conductivity. Bulk characterization results showed that the VP raw water had the highest SUVA value (i.e. 7.24 $\ell \cdot mg^{-1}$ m) thus high content of high molecular weight and hydrophobic NOM compared to other raw water sources. Regardless of the observed high SUVA in VP raw water; the P plant showed the highest DOC removal efficiency of 90.03% and Hazelmere (HL) plant showed the highest $UV_{254}$ removal of 88.07%. DOC and $UV_{254}$ were also used to study the effect of seasonal variations on NOM quantity, quality and treatability. It was shown that the DOC and $UV_{254}$ was high in autumn (R2) compared to other seasons due to the aromatic nature of the soluble compounds found in leaves, which end up deposited into water sources during the autumn season.

Advanced NOM characterization technique, FEEM, gave more and deeper understanding about the composition of NOM in water. FEEM showed that all the raw water samples contain, amongst others, the aromatic protein fraction. NOM fractions (humic and fulvic) were also observed albeit in different quantities in raw waters of VP, HL and P treatment plants. FEEM also proved that the observed high $UV_{254}$ removal efficiency for VP, HL and P treatment plants was because of the presence of high content of humic substances in the raw waters of these treatment plants. FEEM was also used to link the treatability of NOM to various treatment processes (i.e coagulation and filtration) of P treatment plant. Water after the coagulation showed little traces of humic and fluvic components compared to the raw water samples. Whereas, water after filtration showed very little or no traces of humic fractions.

The N, Pd co-doped $TiO_2$ (0.0-1.0%) was evaluated for its photodegradation efficiency towards NOM containing water samples under visible-light irradiation. The highest photodegradation of 58.8% was achieved with NPT (0.5% Pd) on MV raw water samples. The results were in close approximation to those of conventional processes applied at MV treatment plant (60.0%). NPT (0.5% Pd) was also used to conduct the treatability studies with NOM containing samples obtained from various raw water samples. The results showed different $UV_{254}$ (aromatic content of NOM) removal efficiencies thus proving the varying character of NOM from various water sources. On the other hand, MWCNTs/N, Pd co-doped $TiO_2$ (CT) (0.5 - 5.0%) nanocomposites were evaluated for their photocatalytic efficiency towards P raw water samples. It was observed that the highest photocatalytic activity was with 1.0% MWCNTs. About 91.2% ($UV_{254}$) reduction was achieved with CT (1.0% MWCNTs), which is much higher compared to 68.2% achieved with NPT (1.0% Pd). The observed enhanced $UV_{254}$ reduction is attributable to the large surface area of $TiO_2$ which allows bigger amounts of NOM to be adsorbed onto the surface of the $TiO_2$. Adsorption of high amounts of NOM on the surface of the $TiO_2$ permits the photogenerated radicals to have enough time to interact with NOM.

## TABLE OF CONTENTS

***Section*** ***Page***

## LIST OF FIGURES

## LIST OF TABLES

***Table*** ***Description*** ***Page***

## LIST OF ABBREVIATIONS

| | |
|---|---|
| AOC | Assimilable Organic Carbon |
| AOPs | Advanced oxidation processes |
| ATR | Attenuated Total Reflectance |
| BDOC | Biodegradable Dissolved Organic Carbon |
| BAS | Biologically Active Sand |
| CB | Conduction band |
| CdO | Cadmium oxide |
| CHA | Charged Hydrophobic Acids |
| CNTs | Carbon nanotubes |
| CT | MWCNTs/ N, Pd co-doped $TiO_2$ |
| DBPs | Disinfection By-products |
| DOC | Dissolved Organic Carbon |
| EDS | Electron Data System |
| EC | Enhanced Coagulation |
| FEEM | Fluorescence Excitation-Emission Matrices |
| FT-IR | Fourier-Transform Infrared |
| GAC | Granular Activated Carbon |

| | |
|---|---|
| HAAs | Haloacetic Acids |
| HS | Humic Substances |
| HPI | Hydrophilic |
| HPO | Hydrophobic |
| HPOA | Hydrophobic Acids |
| HPON | Hydrophobic Neutrals |
| OH | Hydroxyl |
| IEX | Ion Exchange |
| LC-OCD | Liquid Chromatography Organic Carbon Detection |
| LMW | Low Molecular Weight |
| NF | Nanofiltration |
| NOM | Natural Organic Matter |
| NPT | N, Pd co-doped $TiO_2$ |
| NTU | Nepholometric Turbidity Units |
| NMR | Nuclear Magnetic Resonance |
| MWCNTs | Multiwalled carbon nanotubes |
| ParaFac | Parallel Factor |
| PAC | Powdered Activated Carbon |

| | |
|---|---|
| PRAM | Polarity Rapid Assessment Method |
| Py-GC-MS | Pyrolysis gas chromatography-mass spectrometry |
| RC | Retention Coefficient |
| RO | Reverse Osmosis |
| SA | South Africa |
| SEM | Scanning Electron Microscopy |
| SEC | Size Exclusion Chromatography |
| SHA | Slightly Hydrophobic Acids |
| SWCNTs | Single-walled carbon nanotubes |
| SPE | Solid Phase Extraction |
| SANS | South African National Standards |
| SUVA | Specific Ultraviolet Absorbance |
| $SnO_2$ | Tin dioxide |
| TGA | Thermogravimetric Analysis |
| $TiO_2$ | Titanium dioxide |
| TOC | Total Organic Carbon |
| TPI | Transphilic |
| TPIN | Transphilic Neutrals |

| | |
|---|---|
| THMFP | Trihalomethane Formation Potential |
| THMs | Trihalomethanes |
| UF | Ultrafiltration |
| UV | Ultraviolet |
| UV-Vis | Ultraviolet visible |
| USEPA | United States Environmental Protection Agency |
| VB | Valence band |
| VHA | Very Hydrophobic Acids |
| WHO | World Health Organization |
| $WO_3$ | Tungsten trioxide |
| XRD | X-Ray Diffraction |
| ZnO | Zinc oxide |

# CHAPTER 1
# INTRODUCTION

## 1.1 BACKGROUND

Water is such an important resource. Its scarcity and pollution have a great impact on human life, industrial production, food production and the environment. South Africa (SA) only receives about 450 mm rainfall against a global average of 870 mm, and this makes SA the 30$^{th}$ driest country in the world (Haldenwang 2011; World Cup Report 2011). It is expected that by 2025 the South African water supply will exceed the demand and this is mainly due to increased population growth, urbanization and rapid industrialization (Haldenwang 2011; Kuvarega *et al.*, 2012a).

Water scarcity is currently affecting most regions in the world and it is expected to have a greater impact even in the areas which are currently recognized as water rich (**Figure 1.1**) (Nkambule *et al*., 2012a). Floods and droughts have been reported to be the main impacts of climate change on water availability both in South Africa and worldwide (Delpla *et al*., 2009). In that note, issues of water scarcity has a huge effect on energy production; it is for this reason that areas that are suffering from water scarcity are also suffering from energy inefficiency (WWAP 2012).

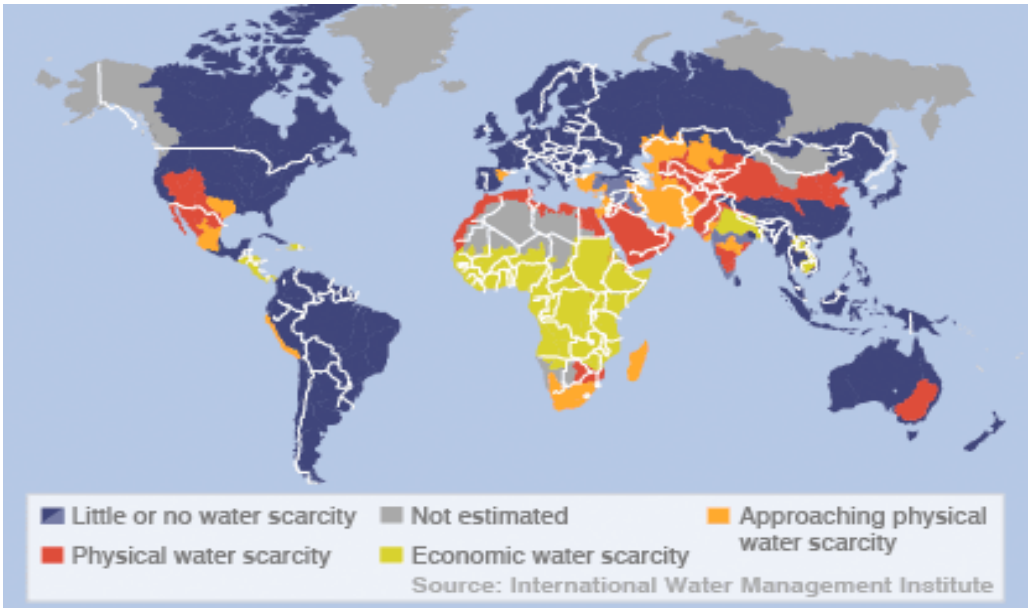


**Figure 1.1: An illustration of the global water scarcity pattern (WWAP 2012).**

Furthermore, water pollution brought about by the presence of toxic contaminants such as heavy metals, inorganics and organics in water is also a global concern. Poor water quality negatively affect the health of human beings and animals; it also has a negative impact on ecosystem services, tourism, agriculture and industrial production (WWAP 2012). One of the well-known organics that compromises water quality when it is present in high amounts is natural organic matter (NOM).

NOM is a complex and heterogeneous concoction of organic compounds that forms naturally through the breaking down of plant and animal remains into water systems and it is present in all natural waters (Kim & Yu 2005; Wu *et al*., 2003; Fabris *et al*., 2008; Nkambule *et al.,* 2012a). In terms of its chemical structure, NOM is a negatively charged molecule with carboxylic groups and phenols being the predominant fractions; it also consist of amines, purines and ketones (Anderson 2013). The composition and the type of NOM in water is not uniform and it is dependent on the climate, geology, topography, industrial and agricultural conditions being practised in that particular location. As a result, an understanding of the character of NOM and the recognition of the local conditions are very

important when developing methods for its characterization or removal from water (Nkambule *et al.,* 2012a).

NOM has both the non humic (hydrophilic) and humic (hydrophobic) fractions (**Figure 1.2**) (Matilainen *et al*., 2011; Anderson 2013). The non-humic fraction is largely aliphatic in nature and is composed predominantly of hydrophilic organic acids and low molecular weight compounds which are amenable to microbial attack (Lee 2005). In contrast, the humic fraction is mainly aromatic in nature and consists of humin, fulvic acids and humic acids. The hydrophobic fraction can be effectively removed from water using enhanced coagulation (Ritson *et al*., 2014).

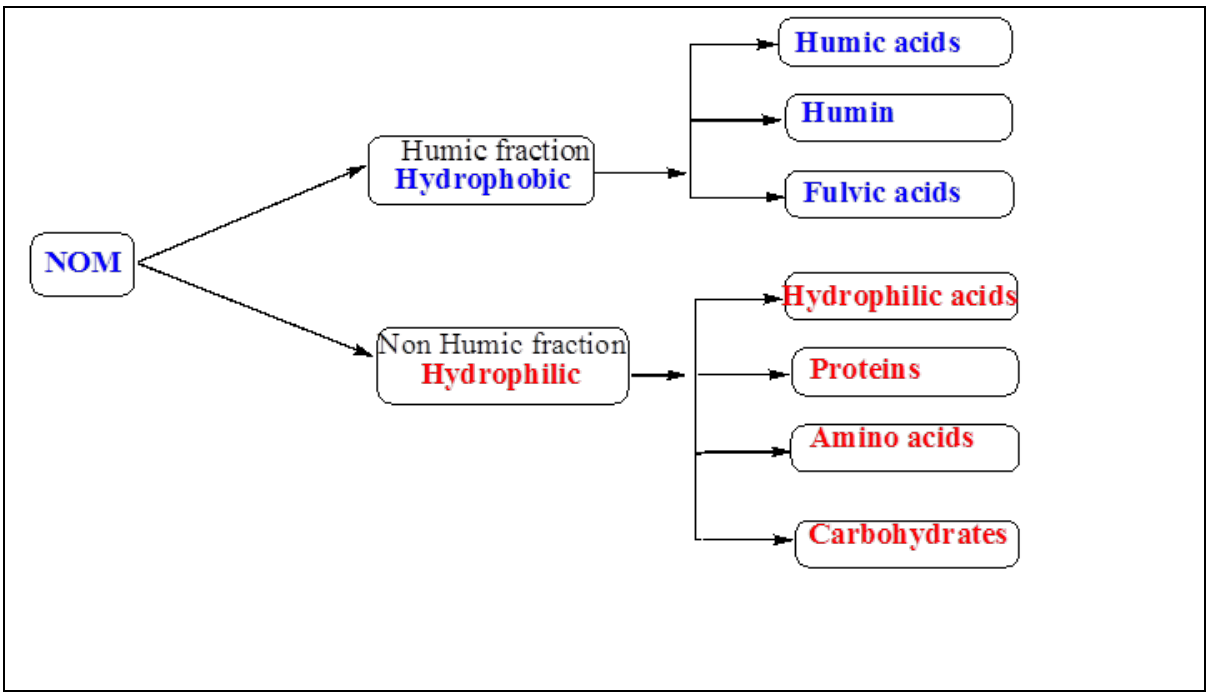


**Figure 1.2: A Classification of NOM.**

The impact of NOM in water includes reduced water quality due to: (i) bad taste and unpleasant odour, responsible for the colouration (usually yellowish) of the water; (ii) promotion of bacterial regrowth; (iii) results in climate change (amount of precipitation); (iv) high content of complexed heavy metals; and (v) formation of disinfectant by-products (DBPs) during the disinfection stage of the water treatment (Matilainen *et al*., 2011; Anderson 2013). The presence of NOM in water

affects other water treatment processes such as membrane filtration by causing membrane fouling and coagulation by increasing the coagulant dosages required for water treatment (Fabris *et al.,* 2008). All the above mentioned issues can in turn have adverse effect on the environment and also affect human health (Nkambule *et al.,* 2011).

NOM in water interferes with the effectiveness of downstream water treatment processes to remove micro-pollutants from the water source because of its large size and complexity (Nkambule *et al.,* 2012b). Therefore, the removal of NOM is an essential part of the water treatment process, irrespective of whether the water is going to be used for industrial purposes or as drinking water in households (Lamsal *et al*., 2011; Mikola *et al*., 2013). Some of the mostly utilised NOM removal methods are coagulation and filtration. However, for the above-mentioned, the hydrophilic fractions of NOM are not effectively removed in water than the hydrophobic fractions. Thus, there is a need for the development of new methods for the removal of NOM, which are able to remove even the more persistent hydrophilic fractions of NOM from aqueous media.

However, prior to the effective removal of NOM from its source; adequate NOM characterization must be conducted. The molecular weight, aromaticity, functional group distribution and elemental composition of NOM affect its removal efficiency (Nkambule *et al*., 2009). Different methods, including resin adsorption, nuclear magnetic resonance (NMR) spectroscopy, SUVA, $UV_{254}$, DOC, FEEM, fourier transform ion cyclotron resonance mass spectrometry, polarity rapid assessment method (PRAM) and multidimensional NMR techniques, have been used for the effective characterization of NOM in water (Matilainen *et al.,* 2011).

Owing to the large molecular size of NOM, most of the water treatment processes are unable to effectively remove it from water sources. NOM blocks the pores of membranes, for example, thus making it difficult for other pollutants present in water to be effectively removed (Matilainen *et al.*, 2010a). Thus a method that will degrade NOM into smaller fractions, which can then be easily removed using existing water treatment processes, is required. In this study, an advanced method that utilizes the nanomaterials/nanocomposites technology for the effective

removal of NOM from water sources has been adopted. Specifically, the method involves a photocatalyst that reacts with NOM in the presence of a light source. The light source triggers the catalyst to produce reactive oxygen species that degrade NOM into smaller and sometimes less harmful species. Alternatively, the NOM is photodegraded into carbon dioxide and water (Comninellis *et al*., 2008). The photodegradation technology is far less costly and economically sustainable as it uses solar light as the energy source. Additionally, this technology is able to tackle pollutants that are not easily removed using the currently available technologies. Nanoparticles (nanomaterials/nanocomposites) are of interest because of their increased degradation potential brought about by a large surface area to mass ratio, which improves the adsorbing capacity of the material. Materials with reduced size tend to have a high mobility, which allows large volumes of water to be effectively treated using a small amount of the material and thus making the technology very cost effective (Comninellis *et al*., 2008).

## 1.2 PROBLEM STATEMENT

Various NOM removal methods have been employed in the treatment of South African waters, such as enhanced coagulation, oxidation, activated carbon filtration and membrane filtration. However, these methods can only remove NOM from water to a certain extent, and there are a lot of limitations and challenges associated with these methods. NOM in water causes membrane fouling and decline of flux; which in turn increases operational costs (Fabris *et al*., 2008). Moreover, when NOM is removed from water by activated carbon filtration, it decreases the removal efficiency of other pollutants by competing for the adsorption sites with these pollutants (Matilainen *et al*., 2010b).

The primary objective of drinking water treatment plants (WTPs) is to produce water that does not pose any health risks to the end-users (Lee 2005). However, the presence of NOM in water compromises this objective because it can cause odour, taste and colour problems that negatively affect the aesthetic quality of the water (Dlamini *et.al.*, 2012). Furthermore, the hydrophilic fraction of NOM is a major contributor of biodegradable organic carbon, which promotes microbiological regrowth in the water distribution system (Murray & Parsons 2004; Świetlik &

Sikorska 2006; Matilainen & Sillanpää 2010; Baghoth 2012). The hydrophilic NOM fraction is more likely to be present in the later stages of the water treatment and reacts with chlorine to form disinfection by products (DBPs) that are carcinogenic and can cause cardiac defects (Cedergren *et al*., 2002; Haarhoff *et al*., 2009). Haloacetic acids (HAAs) is one of the most abundant group of DBPs that have the highest concentration in drinking water (Fabris *et al.*, 2008). HAAs can cause reproductive and developmental defects in humans (Sobantu & Moodley 2014; Nkambule *et al.,* 2009).

The South African WTPs rely largely on surface water feedstock; the quality of this water is compromised due to high runoffs and other indirect reuse (Haarhoff *et al*., 2009). NOM in South African waters has been reported to be not uniform in different locations due to geology, climate changes and human activities practised in the various regions (Haarhoff *et al*., 2009; Nkambule *et al*., 2012c). The character of NOM in the same location may also differ seasonally due to issues of rainfall events, drought or floods and snowmelts runoff (Matilainen *et al*. 2010b). It is noteworthy that the amount of NOM has been increasing over the years and this may be due to the climate change and a decline in acid deposition (Delpla *et al.,* 2009). Equally important, the quality of NOM has been also changing in the past years; this can be observed with the increase in UV, colour and SUVA values of NOM thereby changing the treatability of NOM in water (Matilainen & Sillanpää 2010). Thus there is a need to characterize NOM in order to develop effective methods for its removal.

Most of the water treatment entities in South Africa uses DOC, $UV_{254}$ and SUVA as their NOM characterization methods. However, these methods do not give enough information about the composition of NOM in water; SUVA and DOC/UV only serve as qualitative and quantitative tools, respectively, for the analyses of NOM. Methods that are currently available for the characterization of NOM are ineffective and this is the main reason why challenges in the effective removal of NOM from water still persists. In order to get a deeper understanding about the composition of NOM, advanced characterization methods such as FEEM were used (Nkambule *et al*., 2012a).

Despite recent advances in the characterization of NOM, significant work still needs to be carried out with regards to the composition of NOM in South African waters and worldwide. SA has five different water types based on its geographic locations and not much work has been reported that represents all these water types. Although Nkambule *et.al*., (2012a) and Dlamini *et.al*., (2012) reported on this, the information is not enough to make valid conclusions with regards to the composition of NOM in SA. Moreover, most work conducted thus far addresses the treatability of NOM using a particular/single stage treatment process (mostly enhanced coagulation). However, not enough information has been provided with regards to the treatability of NOM throughout the entire treatment process.

In addition, the complexity and the magnitude of the NOM make it difficult for the currently available methods to effectively remove it from water. One of the reasons why NOM has a large size is that humic substances tend to aggregate even to the extent of forming micelle-like structures (Matilainen 2007). Therefore a new and effective method for the treatment of NOM is required. Photodegradation is a potential solution for the degradation of large NOM molecule into smaller fractions so that they can be effectively removed from water.

## 1.3 JUSTIFICATION FOR THIS RESEARCH PROJECT

The character of NOM occurring in water sources located in different South-African regions is not uniform due to various sources of NOM and this means there is no single water treatment method that can be used by all water treatment plants (Mamba *et al*., 2009; Nkambule *et al*., 2012a). The first step towards NOM removal in water is its characterization, therefore in this study samples were collected in various South African drinking water treatment plants via extensive sampling. The obtained samples were characterized using conventional and advanced methods in order to have a broad understanding on the character of NOM occurring in various geographic locations in South Africa.

Owing to the size and complexity of NOM, the available water treatment technologies are unable to effectively remove NOM from the water. Therefore, treatment methods that can degrade NOM into smaller molecules prior to its

removal are required. This study is focused on the application of $TiO_2$-doped nanomaterials and nanocomposites in the photodegradation of NOM in the presence of a solar energy source. As a justification for the economic viability of this technology, a solar energy source was used instead of UV (Kuvarega *et al*., 2012a). The use of $TiO_2$ semiconductor is attractive because of its photocatalytic properties, which allows it to be used for the photocatalytic degradation of environmental pollutants. However, $TiO_2$ is limited by the electron-hole recombination and large band gap and thus cannot be activated in the visible region (Yu *et al*., 2008; Yang *et al*., 2010; Khairy & Zakaria 2014). Doping $TiO_2$ with non-metals such as nitrogen reduces the band gap of the material thus increasing its photocatalytic activity under visible light (Kuvarega & Mamba 2016).

Nitrogen has a similar atomic size and low ionization energy to oxygen, thus this dopant can easily replace oxygen from the lattice (Yang *et al*., 2010). Moreover using noble metals such as palladium can effectively reduce electron-hole recombination thus enhancing its photocatalytic activity in the visible region (Kuvarega *et al*., 2012b; Riaz 2013). Noble metals can form heterojunction at the $TiO_2$/Pd interface, thus allowing the effective transfer of electrons from the valence band (VB) to the conduction band (CB) of the $TiO_2$, as Pd is of lower Fermi level compared to $TiO_2$. Although noble metals are expensive, their properties make them irreplaceable to the current technological applications (Kuvarega *et al*., 2011).

Co-doping $TiO_2$ (doping with more than one dopant) has drawn a lot of attention because it has higher photocatalytic activity compared to mono-doping. Co-doping provides a synergistic effect of dopants on the material's performance (Luo *et al*., 2015). Doping $TiO_2$ with both N and Pd effectively reduces the band gap of $TiO_2$ thus making it most active in the visible region (Nkambule *et al.,* 2012a). Moreover, it also reduces electron-hole recombination, which enhances the photoactivity of $TiO_2$.

On the other hand, carbon nanotubes (CNTs), which are good supports of semiconductors such as $TiO_2$, have recently attracted research attention due to their distinctive properties such as large surface area, and high chemical and

mechanical stability. Consequently, using nanocomposites such as CNTs/$TiO_2$ has a great impact on the photoactivity performance of $TiO_2$ under a visible light source (Gao *et al.,* 2009). This is mainly due to the unique properties of CNTs, which make them good photosensitizers and good adsorbents (Kuvarega *et.al*., 2012b).

## 1.4 OBJECTIVES OF THE STUDY

The objectives of this study were as follows:

To characterize NOM occurring in selected South African water sources. (This was done in order to understand the character of NOM occurring in South African waters).

Synthesis of N, Pd co-doped $TiO_2$ (NPT) and MWCNTs/N, Pd $TiO_2$ (CT) using sol-gel method; and their characterization using TGA, XRD, FTIR, Raman, UV-Vis, SEM and EDS.

(For the development of an effective NOM degradation method that will complement the existing NOM removal processes).

The evaluation of NPT and CT for NOM removal on samples collected from selected treatment plants.

(For the optimization of the developed NOM degradation method for the effective removal of NOM in water).

## 1.5 DISSERTATION OUTLINE

The rest of this dissertation is structured as follows:

**Chapter 2** (Literature review) gives a review of the literature relating to the study undertaken. It begins with a brief discussion on water scarcity and pollution, and goes on to describe NOM, its negative impact when it is present in water, its characterization methods and challenges associated with its characterization and removal. Thereafter, the NOM degradation approaches

(enzymatic, advanced oxidation processes and nanomaterial/nanocomposites) as the effective NOM removal methods are discussed before giving a brief overview of using different dopants to enhance the photoactivity of $TiO_2$ in the visible region. With respect to the overview of different dopants, particular attention is paid to the use of nanomaterials (NPT) and nanocomposites (CT). The chapter concludes by highlighting problems associated with the application of nanomaterials and nanocomposites in industry.

**Chapter 3** (Experimental methodology) gives detailed experimental procedures and methods that were followed in order to meet the objectives of this study.

**Chapter 4** (Evaluating the character of NOM and its removal by South African water treatment plants) presents results on the characterization of the NOM present in water after every treatment step for the seven South African water treatment plants.

**Chapter 5** (Synthesis, characterization and application of N, Pd co-doped $TiO_2$ in the photodegradation of NOM present in water) describes the characterization and application of NPT in the degradation of NOM under visible light.

**Chapter 6** (Synthesis, characterization and application of MWCNTs/N, Pd $TiO_2$ for the photocatalytic degradation of NOM in water). Describes the characterization and application of CT in the degradation of NOM under visible light.

**Chapter 7** (Conclusion and recommendations): This chapter presents the conclusions and perspectives for further work.

**References**: The references cited in the text are listed at the end of each chapter.

**Appendix**: Additional information including tables and figures for all the NOM characterization results, treatability of NOM using NPT and CT can be found in this section.

## REFERENCES


Anderson, L.E. (2013). Anion exchange resin technology for natural organic matter. MSc dissertation, Dalhousie University.

Baghoth, S.A. (2012). Characterizing natural organic matter in drinking water treatment processes and trains. UNESCO-IHE institute for Water Education, MSc dissertation, The Netherlands University.

Cedergren, M.I., Selbing, A.J, Löfman, O. & Källen, B.A.J. (2002). Chlorination by-products and nitrate in drinking water and risk for congenital cardiac defects. *Environ Res*, **89 (2)**:124-130.

Chen, J., Gu, B., LeBoeuf, E.J., Pan, H. & Dai, S. (2002) Spectroscopic characterization of the structural and functional properties of natural organic matter fractions. *Chemosphere*, **48**:59-68.

Comninellis, C., Kapalka, A., Malato, S., Parsons, S.A., Poulios, I. & Mantzavinos, D. (2008). Advanced oxidation processes for water treatment : advances and trends for R & D. *J Chem Technol Biotechnol*, **776**:769-776.

World Cup Legacy Report (2011). South Africa: A water scarce country. 58-73.

Delpla, I, Jung, A. V., Baures, E., Clement, M. & Thomas, O. (2009). Impacts of climate change on surface water quality in relation to drinking water production. *Environ Int*, **35 (8)**:1225-1233.

Dlamini, S. & Haaroff, J.B.M. (2012). The profiling and treatability of Natural organic matter in South African raw water sources using enhanced coagulation. MSc dissertation, University of Johannesburg.

Fabris, R., Chow, C. W. K., Drikas, M., & Eikebrokk, B. (2008). Comparison of NOM character in selected Australian and Norwegian drinking waters. *Water Research*, **42**:4188–4196.

Gao, B., Chen, G.Z. & Li Puma, G. (2009). Carbon nanotubes/titanium dioxide

(CNTs/$TiO_2$) nanocomposites prepared by conventional and novel surfactant wrapping sol-gel methods exhibiting enhanced photocatalytic activity. *Applied Catalysis B: Environmental*, **89 (3-4)**:503–509.

Gao, B., Chen, G.Z. & Li Puma, G. (2009). Carbon nanotubes/titanium dioxide (CNTs/$TiO_2$) nanocomposites prepared by conventional and novel surfactant wrapping sol-gel methods exhibiting enhanced photocatalytic activity. *Applied Catalysis B: Environmental*, **89 (3-4)**:503–509.

Gopal, K., Tripathy, S.S., Bersillon, J.L. & Dubey, S.P. (2007). Chlorination by-products, their toxicodynamics and removal from drinking water. *J Hazard Mater*, **140 (1-2)**:1-6.

Haldenwang, B. (2011). The state of water in South Africa. *Natural Env*, **7 (01)**:1–5.

Haarhoff, J., Kubare, M., Mamba, B., Krause, R., Nkambule, T., Matsebula, B. & Menge, J. (2009).NOM characterization and removal at six Southern African water treatment plants. *Drink Water Eng. Sci. Discuss*, **2**:231-257.

Khairy, M. & Zakaria, W. (2014). Effect of metal-doping of $TiO_2$ nanoparticles on their photocatalytic activities toward removal of organic dyes. *Egypt J Pet*, **23 (4)**:419-426.

Kim, H.C. & Yu, M.J. (2005). Characterization of natural organic matter in conventional water treatment processes for selection of treatment processes focused on DBPs control. *Water Res*, **39**:4779-4789.

Kuvarega, A.T., Krause, R.W.M. & Mamba, B.B. (2011). Nitrogen / Palladium-Codoped $TiO_2$ for Efficient Visible Light Photocatalytic Dye Degradation. *Society*, 22110–22120.

Kuvarega, A.T., Krause R.W.M. & Mamba, B.B. (2012a). Photocatalytic performance of nitrogen-platinum group metal co-doped $TiO_2$ supported on carbon

nanotubes for visible-light degradation of organic pollutants in water. PhD thesis, University of Johannesburg.

Kuvarega, A.T., Krause, R.W.M. & Mamba, B.B. (2012b). Multiwalled carbon nanotubes decorated with nitrogen, palladium co-doped $TiO_2$ (MWCNT/N, Pd co-doped $TiO_2$) for visible light photocatalytic degradation of Eosin Yellow in water. *J Nanopart Res*, **14:776.**

Kuvarega, A.T. & Mamba, B.B. (2016). $TiO_2$ -based photocatalysis: Toward visible light-responsive photocatalysts through doping and fabrication of Carbon-based nanocomposites. *Critical Reviews in Solid State and Materials Sciences*,1–52.

Lamsal, R., Walsh, M.E. & Gagnon, G.A. (2011). Comparison of advanced oxidation processes for the removal of natural organic matter. *Water Res*, **45 (10)**:3263-3269.

Lee, M.K. (2005). Application of White-rot Fungi for the Biodegradation of Natural Organic Matter in Wastes. MSc dissertation, RMIT University.

Luo, X. Chen, C., Yang, J., Wang, J., Yan, Q, Shi, H. & Wang, C. (2015). Characterization of La/Fe/$TiO_2$ and Its Photocatalytic Performance in Ammonia Nitrogen Wastewater. *Int. J. Environ. Res. Public health*, **12 (11)**:14626–39.

Matilainen, A, Gjessing, E.T., Lahtinen, T., Hed, L., Bhatnagar, A. & Sillanpää, M. (2011). An overview of the methods used in the characterisation of natural organic matter (NOM) in relation to drinking water treatment. *Chemosphere*, **83 (11)**:1431-1442.

Matilainen, A. & Sillanpää, M. (2010a). Removal of natural organic matter from drinking water by advanced oxidation processes. *Chemosphere*, **80 (4)**:351-365.

Matilainen, A., Vepsäläinen, M. & Sillanpää, M. (2010b). Natural organic matter removal by coagulation during drinking water treatment: A review. *Adv Colloid Interface Sci*, **159 (2)**:189-197.

Matilainen, A. (2007). Removal of the Natural Organic Matter in the different stages of the drinking water treatment process removal of the Natural Organic Matter in the different stages of the drinking water treatment process. PhD thesis, Tampere University of Technology.

Mikola, M., Rämö, J., Sarpola, A. & Tanskanen, J. (2013). Removal of different NOM fractions from surface water with aluminium formate. *Sep Purif Technol*, **118**:842-846.

Murray, C.A. & Parsons, S.A. (2004). Removal of NOM from drinking water: Fenton's and photo-Fenton's processes. *Chemosphere*, **54**:1017-1023.

Nkambule, T.I., Krause, R.W, Mamba, B.B. & Haarhoff, J. (2009a). Removal of natural organic matter from water using ion-exchange resins and cyclodextrin polyurethanes. *Phys. Chem. Earth*, **34 (13-16)**:812-818.

Nkambule, T.I., Krause, R.W.M., Mamba, B.B. & Haarhoff, J. (2009b). Characterisation of Natural Organic Matter (NOM) and its removal using cyclodextrin polyurethanes. *Water SA,* **35 (2)**:200-203.

Nkambule, T.I., Krause, R.W.M., Haarhoff, J. & Mamba, B.B. (2011). Treatability and characterization of Natural Organic Matter (NOM) in South African waters using newly developed methods. *Phys. Chem. Earth*, **36 (14-15)**:1159-1166.

Nkambule, T. I., Krause, R. W. M., Haarhoff, J., & Mamba, B. B. (2012a). Natural Organic Matter (NOM) in South african waters: characterization of NOM, treatability and method development for effective NOM removal from water. Ph.D thesis, University of Johannesburg.

Nkambule, T.I., Krause, R.W.M., Haarhoff, J. & Mamba, B.B. (2012b). Natural organic matter (NOM) in South African waters: NOM characterisation using combined assessment techniques. *Water SA*, **38 (5)**:697-706.

Nkambule, T.I., Krause, R.W.M., Haarhoff, J. & Mamba, B.B. (2012c). The characterisation of natural organic matter (NOM) in South African waters. *Water Sci. Technol. Water Supply*, **12:**648-657.

Riaz, N. (2013). Iron doped $TiO_2$ photocatalysts for environmental applications : fundamentals and progress. *Int Proc on Biol and Biomed*, 72-77.

Ritson, J.P., Graham, N.J.D., Templeton, M.R., Clark, J.M., Gough, R. & Freeman, C. (2014). The impact of climate change on the treatability of dissolved organic matter (DOM) in upland water supplies : A UK perspective. *Sci. Total Environ*, 473-474:714-730.

Sobantu, P. & Moodley, K.G. (2014). Development of methods for the separation and characterization of natural organic matter in dam. MTech , Durban University of Technology.

Świetlik, J. & Sikorska, E. (2006). Characterization of natural organic matter fractions by high pressure size-exclusion chromatography, specific UV absorbance and total luminescence spectroscopy. *Polish J. Environ. Stud*, **15 (1)**:145-153.

Wu, F.C., Evans, R.D. & Dillon, P.J. (2003). Separation and characterization of NOM by high-performance liquid chromatography and on-line three-dimensional excitation emission matrix fluorescence detection. *Environ Sci. Technol*, **37 (16)**:3687-3693.

WWAP (World Water Assessment Programme). World Water Development Report Volume 4: Managing Water under Uncertainty and Risk. Vol 1. 2012.

Yang, G., Jiang, Z., Yang, G. & Yan, Z. (2010). Preparation of highly visible-light active N-doped $TiO_2$ photocatalyst. *J. Mater. Chem*, **20 (25)**: 5301.

Yu, H., Quan, X., Chen, S., Zhao, H. & Zhang, Y. (2008). $TiO_2$-carbon nanotube heterojunction arrays with a controllable thickness of $TiO_2$ layer and their first application in photocatalysis. *J. Photochem. Photobiol. A Chem*, **200 (2-3)**:301-306.

# CHAPTER 2
# LITERATURE REVIEW

## 2.1 INTRODUCTION

This chapter is a review of literature on natural organic matter (NOM), its characterization and removal methods as well as the environmental and health risks it poses if it is present in undesirable amounts in water systems. The removal of NOM and the various processes used for the treatment of NOM, including advanced and innovative methods for the degradation of NOM (e.g. nanomaterial/nanocomposites, advanced oxidation processes and enzymatic), are discussed in detail. A brief overview on the use of different dopants to enhance $TiO_2$ photoactivity under the visible light range is also presented with particular attention being paid to the use of nanomaterial and nanocomposites. Lastly, the problems associated with the application of nanomaterials and nanocomposites in industry are highlighted.

## 2.2 WHAT IS NATURAL ORGANIC MATTER (NOM)?

Natural organic matter (NOM) is a heterogeneous mixture of organic compounds formed naturally through the decomposition of plants and animals remains into water systems. NOM is a problem in the water treatment industry because its presence in water poses a lot of negative challenges such as, compromised water quality; poses health risks to the consumers by causing DBPs which are carcinorgenic; deteriotoriation of pipelines during water transportation; bacterial regrowth in the distribution system etc. NOM also increases operational costs by enhancing the coagulation demand during coagulation, blocking pores of activated carbon and membrane filtration during the treatment process. Based on these issues, NOM must be properly removed from water sources.

NOM is composed of different organic compounds, from highly aliphatic to highly coloured aromatic compounds (Nkambule *et al*., 2012a). Owing to the negatively charged carboxylic groups found on its surface, NOM is overall negatively charged and has a range of molecular sizes and chemical compositions (Anderson 2013). For this reason, NOM has both hydrophilic and the hydrophobic components (Matilainen *et al*., 2010b).

The hydrophobic component consists of fulvic and humic acids and is made up of phenolic structures, aromatic carbon and conjugated double bonds, and is responsible for the brownish colour observed in most surface water sources (Goslan *et al.,* 2004; Roe 2011). Almost 50-75% of the total organic carbon (TOC) is humic in nature (Wu *et al*., 2003; Roe 2011; Baghoth 2012; Sobantu & Moodley 2014). The difference between the humic and fulvic acids is attributed to their solubility; with humic acid soluble only at higher pH levels (pH >2) and fulvics soluble at all pH levels (Chen *et al.*, 2002; Sobantu & Moodley 2014). Research has shown that humic substances, specifically humic acids and humin, are resistant to microbial degradation (Grinhut *et al.,* 2007). The charge density of both humic and non-humic substances is not uniform, with the humics having higher charge density compared to the non-humic. Owing to their high charge density, humic substances can be easily removed in water using techniques such as coagulation (Roe 2011).

In addition, NOM is mainly composed of carbon, oxygen, hydrogen and nitrogen elements, with humic acids having the lower content of oxygen but high in carbon compared to fulvic acids (Lee 2005). Conversely, the hydrophilic component has a high content of aliphatic carbons and nitrogenous compounds, such as amino acids, carbohydrates and sugars (Matilainen *et al.,* 2011; Metsämuuronen *et al.,* 2012).

Lastly, NOM in water consist of lignin, cutin, proteins, polyphenols and other polymers as its main building blocks (Wu *et al.*, 2003; Grinhut *et al.*, 2007; Fabris *et al*., 2008; Peleato 2013). NOM can be derived from both the sources within the aquatic environment (autochtonous) and from external sources (allochthonous) (Wershaw *et al.,* 2005; Nkambule *et al.,* 2012a). Basically, the allochtonous NOM

is dependent on the type of plant and animal remains that finds their ways to the water sources. In plants, for example, the soluble compounds that can be easily leached from the plant's tissue are the main components of NOM (Wershaw *et al.,* 2005). Allochthonous NOM has a high content of fulvic acids and is highly aromatic, while autochthonous has a low fulvic acid content and C:N ratio (Lee 2005; Roe 2011).

### 2.2.1 Formation of disinfectant by-products from NOM

Water disinfection was recognised as one of the fundamental developments in the past century for improving human health (Latifoglu 2003; Bond *et al.,* 2014). Disinfecting water is important because it destroys micro-organisms that can cause water-borne diseases such as cholera, with chlorine being the preferred disinfectant because of its high oxidising potential (Latifoglu 2003; Gopal *et al.,* 2007; Bond *et al.,* 2014; Ozdemir 2014). NOM in water results in the formation of DBPs during the disinfection step (chlorination) of the water treatment process (Nkambule *et al.,* 2012b; Sobantu & Moodley 2014; Urbanowska & Kabsch-Korbutowicz 2016).

More than 600 DBP compounds have been identified and their formation in drinking water is based on factors such as pH, temperature, contact time, dose, presence of inorganic compounds and the type of NOM present in water. The main DBP compounds which are found in high concentrations in drinking water throughout the world are trihalomethanes (THMs) and haloacetic acids (HAAs) (Fabris *et al*., 2008; Matilainen & Sillanpää 2010). THMs are volatile and can be categorised into chloroform, bromoform dichlorobromomethane and dibromochloromethane (Cedergren *et al*., 2002; Latifoglu 2003). Based on the United States Environmental Protection Agency (USEPA), the allowable THMs and HAAs limits in water is 80 µg/L and 60 µg/L, respectively (USEPA 2012; Anderson 2013; Ozdemir 2014). The type of DBPs formed is dependent on the type of NOM present in water and the treatment processes being used by that particular plant (Kim & Yu 2007). The highest contributor of DBP precursors is the hydrophilic fraction of NOM, however, even the hydrophobic fraction does contributes to the disinfectant by-product formation (DBPF) if it is not effectively

removed after coagulation (Matilainen & Sillanpää 2010; Li *et al.,* 2014). In contrast, Kim *et al*., (2006) reported that humic substances are the main contributor of DBPF.

Various alternative approaches have been found to be more effective in one way or the other compared to the use of chlorine to disinfect water (Gopal *et al.,* 2007). One of the proposed ways of reducing DBPs in water is to reduce the chlorine dosages and/or remove as much NOM as possible before the disinfection step (Wei-Bin *et al.,* 2013; Bond *et al.,* 2014; Do *et al.,* 2015). Other researchers have suggested the use of chloramine as a disinfectant instead of chlorine (Pifer & Fairey 2012). However, the switch to chloramine is accompanied by some disadvantages, such as corrosion in the distribution system and increased occurrence of nitrification (Pifer & Fairey 2012). Moreover, when compared with chlorine, chloramine is considered to be a less effective disinfectant as it requires longer contact time and produces volatile by-products that are responsible for bad taste and malodour in water (Gopal *et al.,* 2007). Conversely, the use of iodine and bromine (to produce iodamines or bromamines, respectively) can cause the formation of more hazardous DBPs compared to the chlorinated precursors because they are highly reactive to the hydrophilic fraction of NOM (Matilainen & Sillanpää 2010; Li *et al.,* 2014).

The characteristics and amount of NOM depends on the climate, topography and geology, the type of agricultural and industrial activities practised in that particular location (Nkambule *et al.*, 2012b). In most cases upland and agricultural locations that are densely vegetated are reported to be very turbid and have a high content of humic substances, whereas lowland areas are high in non-humic substances (Roe 2011). Equally important, seasonal variations have a great impact on NOM character, and most researchers have concluded that there is high NOM quantity during summer season due to high temperature and heavy storms, which can end up depositing about 50% NOM into water sources (Roe 2011). In addition, due to issues of climate change, changes in soil acidity and land use variations over the years, the quantity of NOM has increases in source waters (Roe 2011). Therefore, understanding the character of the NOM in water is of utmost importance, also

taking into consideration the local conditions, so that technologies or methods for the removal of NOM can be developed (Nkambule *et al.,* 2012b).

## 2.3 METHODS FOR THE CHARACTERIZATION OF NOM

### 2.3.1 General parameters used for the characterization of NOM

It is worth noting that there is no single tool that can give all the information required for the characterization of NOM, however, a combined application of different tools and methods that can effectively characterize and remove NOM from water (Chen *et al.*, 2002). The commonly used methods for the characterization of NOM are DOC, $UV_{254}$, SUVA, FEEM, biodegradable dissolved organic carbon (BDOC) and elemental composition (FTIR). Of these characterization methods, DOC, $UV_{254}$ and SUVA are being used by most of South African water treatment plants (Nkambule *et al.*, 2012a). All these methods are limited as they only give information regarding amount of NOM present in water; however, they provide limited information about the composition of NOM (Matilainen *et al.,* 2011). Consequently, FEEM is used because it enables access to information relating to the composition of NOM. Moreover, since NOM is the main cause of colouration in water, the amount of colour present can be utilized to determine the amount of NOM in water. All these methods only provide information about the amount (DOC/UV-Vis) and quality (SUVA) of NOM present in water; however, they provide limited information about the character of NOM (Matilainen *et al*., 2011). The characterization techniques mentioned above are discussed individually in the section that follows.

### 2.3.2 Total organic carbon (TOC)/ dissolved organic carbon (DOC) analysis

TOC represents all non-purgeable organic carbon present in a water sample, whereas DOC is the amount of organic carbon in water after it has been filtered through a 0.45 µm filter (Matilainen *et al.*, 2011; Nkambule, *et al*., 2012; Haarhoff *et a*l., 2013; Anderson 2013). Both TOC and DOC methods involve oxidation (either with UV persulfate or high thermal combustion) of the organic carbon present in the water to form carbon dioxide. The resulting $CO_2$ is then quantified

using infra-red spectroscopy and the quantity of $CO_2$ detected is equivalent to the amount of organic carbon in that sample (Matilainen *et al.,* 2011; Nkambule *et al.,* 2012c). Before the amount of DOC/TOC is measured, the inorganic compounds are removed *via* acid treatment (Nkambule *et al.,* 2012a). According to the South African National Standards (SANS), the maximum allowed DOC amount is 10 mg/ ℓ, while the World Health Organisation (WHO) allowable standard is 5 mg/ ℓ (Nkambule *et al.,* 2011).

### 2.3.3 Ultraviolet and visible absorption spectroscopy (UV-Vis) analysis

Studies have shown that any wavelength within the range 220 to 300 nm is appropriate for the measurements of NOM (Matilainen *et al.,* 2011; Anderson 2013). However, the molar absorptivity values differ due to the various chromophores present in the NOM. More specifically, 220 nm corresponds to both the aromatic and carboxylic chromophores, whereas, 254 nm is associated with the aromatic character of the molecule and is used to measure the amount of NOM and disinfectant by-product formation potential (DBPFP) (Matilainen *et al.,* 2011; Anderson 2013). Furthermore, whilst 214 nm is associated with nitrites and nitrates, 272 nm is used to predict the trihalomethane formation, and 300 nm is used by Rand Water and other treatment plants to quantify DOC (Nkambule *et al*., 2012c). Although UV-Vis can be used for the prediction of functionalities indicated above, its use is limited to molecules that can absorb UV light. To this end, not all NOM fractions have a potential to absorb light, especially low molecular NOM fractions which are aliphatic in nature (Roe 2011; Ritson *et al*., 2014).

### 2.3.4 Specific UV-absorbance (SUVA) analysis

As illustrated in Equation 2.1, the hydrophobicity of NOM can be determined using SUVA (Thebe *et al*., 2000; Fabris *et al.,* 2008; Baghoth *et al.,* 2011; Anderson 2013).

$$\mathrm{SUVA}\left(\frac{\mathrm{L}}{\mathrm{mg}}.\mathrm{m}\right) = \frac{\mathrm{UV}_{254}\left(\mathrm{cm}^{-1}\right)\times 100\left(\frac{\mathrm{cm}}{\mathrm{m}}\right)}{\mathrm{DOC}\left(\frac{\mathrm{mg}}{\mathrm{L}}\right)} \qquad [2.1]$$

When SUVA > 4, this proves the availability of high molecular weight and hydrophobic organic matter of NOM in water. Whereas SUVA < 2 indicates a presence of mainly hydrophilic and low molecular weight organic compounds (Uyak *et al.,* 2008; Ates *et al.,* 2009; Roe 2011; Li *et al.,* 2014). There is a good correlation between high SUVA values and the treatability of NOM by coagulation (Matilainen *et al.,* 2011; Nkambule *et al.,* 2012a). Moreover, it has been shown that SUVA is related to disinfectant by-product formation (DBPF) and water that has a high SUVA tend to have a high potential of forming DBPs in water (Anderson 2013; Li *et al.,* 2014).

### 2.3.5 Fluorescence analysis

Fluorescence, unlike UV-vis for example, provides information with regards to functional groups, heterogeneity, structure, conformation as well as dynamic characteristics related to the intermolecular and intramolecular interactions of the molecule of interest (Chen *et al.*, 2003). There is a positive correlation between TOC and fluorescence peaks with $R^2$ value ranging between 0.88–0.9 (Roe 2011). Literature indicates that fluorescence is a good predictor for DBPF compared to SUVA due to its sensitive (Ritson *et al.,* 2014). However, the complexity of NOM limits the application of this technique due to the overlapping of the spectra which is often observed and this results in some difficulties when it comes to the interpretation of the spectra ( Chen *et al*., 2003).

#### 2.3.5.1 Fluorescence excitation-emission matrix (FEEM) spectroscopy

FEEM spectroscopy is the simple and very sensitive technique that is used to determine various forms of humic substances and by extension the composition of NOM (Chen *et al*., 2003). This method can also be utilized to indicate which components of NOM is being removed by the various water treatment processes. McKnight *et al*., (2001) reported that FEEM can differentiate between various forms of humic substances originating from different sources. When compared to other characterization techniques such as UV-Vis, FEEM measurements are less prone to interferences and are very selective (Persson & Wedborg 2001).

In this technique, a sample is excited with a light source usually at a particular wavelength and the emitted light is at a different wavelength (Baghoth 2012). For a chromophore present in NOM to be excited, it first needs to absorb energy in accordance to the Beer's Lambert law (Peleato 2013). Beer's law states that the absorbance is dependent on the concentration of the chromophore of interest, molar absorptivity and path length of the cell being used. The absorbance (A) is what contributes to the excitation of the chromophore. For complex molecules such as NOM with multiple chromophores, the molar absorptivity is used to differentiate those chromophores (Peleato 2013). By gathering all the emission spectra at different excitation wavelengths the excitation emission matrix (EEM) is obtained (Baghoth 2012). The location and size of the EEM peaks depend on the composition of the NOM. The importance of this method lies on its ability to detect changes in properties of the species of interest (Kim *et al.,* 2006; Nkambule, *et al.,* 2012c).

#### 2.3.5.2 Parallel factor analysis

Parallel factor analysis (PARAFAC) is used for identifying specific components of the sample that can fluoresce. It models EEM data into individual components of fluorophores, and can differentiate components into protein-like and humic-like forms (Nkambule *et al*., 2012a; Pifer & Fairey 2012). Peak picking methods were previously used to identify the fluorescent components of a sample, however, molecules with complex structures such as NOM were not properly delt with due to multiple chromophores. PARAFAC on the other hand, is more efficient because it allows individual components of NOM to be extracted for further analysis (Nkambule *et al*., 2012a; Pifer & Fairey 2012). Nonetheless, the non-linear response of PARAFAC hinders it to deal with light scattering regions (Peleato 2013).

### 2.3.6 Biological analyses

Biological tests are developed to determine the biodegradable organic matter content of water and are based on two concepts which are: biodegradable organic carbon (BDOC) and assimilable organic carbon (AOC) (Matilainen *et al*., 2011). The two biological tests are discussed briefly in the following section.

#### 2.3.6.1 Biodegradable organic carbon (BDOC)

BDOC, which is calculated according to equation 2.2, determines the fraction of DOC assimilated and mineralized by heterotrophic microbes (Baghoth 2012; Nkambule *et al*., 2012b). The idea is to reduce BDOC as much as possible since its availability on the treated water enhances bacterial regrowth in the distribution system (Matilainen *et al*., 2011). Consequently, bacterial regrowth can then results in biofilm formation in the pipelines, deterioration of water quality and enhancement of water turbidity; which in turn increases operational costs (Matilainen *et al*., 2011; Nkambule *et al*., 2012c; Papageorgiou *et al*., 2016).

Furthermore, BDOC is mainly determined via inoculation, either with suspended bacteria or with the bacterium fixed on a sand (Haarhoff *et al*., 2009). A research conducted by Nkambule *et.al.* (2012c) where BDOC was measured by studying the effect of a bacteria (fixed on the biological activated sand) on DOC of the water sample over a period of six days showed a 20-65 % DOC removal efficiency for various treatment plants, with the water that was high in humic substances having the highest reduction potential (Nkambule *et al.,* 2012a). Equally important, BDOC can be used as a water treatment process control parameter, because it has a potential of indicating the quantity of disinfect required during the disinfection step of the water treatment process (Haarhoff *et al*., 2009).

$$BDOC = DOC_{initial} - DOC_{final} \qquad [2.2]$$

#### 2.3.6.2 Assimilable organic carbon (AOC).

AOC is a distribution system water quality control parameter that is used to determines the bacterial regrowth based on the amount of nutrients present in water (Matilainen *et al*., 2011). It represents the part of biodegradable organic matter that can be easily assimilated by microbes and can be converted to cell mass (Haarhoff *et al*., 2009; Croft 2012). AOC consists of low molecular weight NOM molecules, with less than 1000 Dalton weight (Haarhoff *et al*., 2009). Even though AOC contributes of only about 1.0–10 % of the total organic carbon in water, however, it is regarded as one of the most effective biological water stability indicators (Liu *et al*., 2015).

### 2.3.7 Fractionation

Through fractionation, different groups of NOM molecules are selectively separated based on their chemical and physical properties (Chen *et al.*, 2002). NOM can be fractionated into hydrophobic and hydrophilic compounds based on their affinity for water (Haarhoff *et al*., 2009). The hydrophilic fraction has a polarised molecular structure which makes it readily soluble in polar solvents because of its composition which involves mainly proteins, amino acids and carbohydrates (Haarhoff *et al*., 2009). Whereas, the hydrophobic fraction has a high affinity for organic solvents (Haarhoff *et al*., 2009). The two fractionation methods that are relevant for the separation of NOM (resin fractionation and gel permission chromatography) are discussed briefly in the following section.

#### 2.3.7.1 Resin fractionation

One of the most commonly used approaches for differentiating between hydrophilic and hydrophobic NOM is to characterize them as organic materials that are either absorbed or not absorbed by Amberlite XAD resins (Wershaw *et al.,* 2005; Kim & Yu 2007). This method is used for isolating humic fractions from water, with XAD-4 resin adsorbing transphilic NOM (i.e. weakly hydrophobic acid fractions) and XAD-8 isolating hydrophobic NOM (i.e. high molecular weight NOM

with aromatic character) (Nkambule *et al.,* 2012a; Urbanowska & Kabsch-Korbutowicz 2016).

In addition, hydrophilic fractions are not adsorbed by neither of the above mentioned resins; instead, they are separated using WA-10 (weak anionic resin) and AG-MP-50 (cation resin) (Matilainen *et al.,* 2011; Roe 2011). The rapid resin fractionation method, which is based on XAD resins, separates dissolved organic carbons into four portions based on their molecular weight and character. These fractions are: (i) slightly hydrophobic acids (SHA); (ii) very hydrophobic acids (VHA); (iii) neutral hydrophilics (NEU); and (iv) charged hydrophilics (Nkambule *et al*., 2012a). Most importantly, this method is less time consuming and economically favorable because not much of the sample is required for analysis (Urbanowska & Kabsch-Korbutowicz 2016).

#### 2.3.7.2 Gel permission chromatography

This fractionation method involves a continuous flow of analyte through the stationary phase *via* molecular diffusion (Amy *et al*., 2015). As opposed to chromatographic methods that separate compounds based on chemical or physical interactions, gel permission chromatography separates compounds based on their molecular size. Very large molecules have a short retention time because they do not enter the gel pores of the stationary phase and are thus eluted first (Amy *et al.*, 2015). Some of the properties that may influence the elution rates are the type and grade of the gel, the composition of the eluent used, the type of the organic material being eluted and the standard synthetic chemicals used for the calibration of the gel column (Amy *et al.*, 2015). Since NOM is heterogeneous in terms of size, this method is well suited for the separation of NOM components since they will be differentiated based on their weight and size (Nkambule *et al*., 2012b).

### 2.3.8 Elemental composition

#### 2.3.8.1 Atomic force microscopy (AFM) analysis

Measuring the conformation and the size of NOM under various local conditions is another way of undertaking structural analysis of the NOM. This is conducted by using atomic force microscopy (AFM). AFM is a photon correlation spectroscopy that gives better chemical and structural data on NOM, in relation to bacteria-NOM adhesion forces (Matilainen *et al*., 2011).

#### 2.3.8.2 FTIR analysis

Fourier transform infrared (FTIR) is used for defining the functional groups present on the molecules. For the FTIR, the obtained absorption spectrum is a unique fingerprint of that molecule (Matilainen *et al*., 2011). However, the interpretation of the results may be complicated in the case of NOM because it is a complex molecule.

In this study, $UV_{254}$, DOC, SUVA, which are the conventional characterization methods were used by various water treatment plants to quantify NOM in water, whereas, FEEM (advance NOM characterization method) was employed to effectively characterize NOM; which is the first objective of the study. This is because molecular weight, aromaticity, functional group distribution and elemental composition of NOM contribute greatly on NOM removal from water sources. Both the conventional and the advanced characterization methods were used in this study in order to obtain enough information regarding the quantity, quality and the composition of the NOM in water.

## 2.4 METHODS USED FOR THE REMOVAL OF NOM

Nkambule *et al.*, (2009) reported that the problem of water availability is expected to increase in the coming years even in those areas that are presently recognised as water rich. This challenge requires a thorough research to find effective, robust and cost effective novel methods for water treatment that are energy efficient,

while minimizing the use of chemicals which could have negative impacts on the environment. Methods that have been commonly used to remove NOM are coagulation, activated carbon filtration, membrane filtration and oxidation and these are discussed individually in the section that follows.

### 2.4.1 Coagulation

Coagulation has been used to reduce colour, turbidity and to eliminate pathogens during the water treatment process (Anderson 2013). However, because the conditions that are used for colour removal and turbidity are not exactly the same as those of NOM removal, enhanced coagulation is often used (Matilainen *et al*., 2010b). In the enhanced coagulation process, more coagulant is used compared to the baseline coagulation process, and this allows the removal of about 80% of NOM from the water source (Murray & Parsons 2004; Lobanga *et al.*, 2013). Nevertheless, increasing the coagulant dosage, with the purpose of removing NOM will increase sludge production, which is difficult to treat due to the high content of metal ions (Murray & Parsons 2004). Equally important, if not all of the hydrophobic fraction is removed during the coagulation process, the untreated hydrophobic fraction can result in an increase of the disinfectant by-product formation (DBPF) (Wei-Bin *et al*., 2013). Moreover, the hydrophilic fraction of NOM is not effectively removed by coagulation compared to the hydrophobic fraction (Matilainen *et al.,* 2010). This is because the hydrophilic fraction has the high amount of acidic functional groups, which are reluctant to be destabilized by the coagulation process (Matilainen 2007).

### 2.4.2 Oxidation

Pre-oxidation removes NOM more efficiently than the coagulation process (Matilainen *et al*., 2010). Ozonation, which also removes odour, colour and taste in water, is the preferred form of pre-oxidation method (Matilainen *et al*., 2010). According to Wei-Bin *et.al.,* (2013), oxidation *via* ozonation has a potential of decreasing the SUVA values of the water samples due to the increase in low molecular mass fractions. Ozonation is commonly effected through either pre-ozonation or post-ozonation (Pei *et al.*, 2007). Pre-ozonation increases the

biodegradability of NOM in water, thus enhancing its removal by increasing the biological activity in the filter of biologically activated carbon (BAC) filtration (Matilainen *et al*., 2010a). Wei-Bin *et.al.,* (2013) conducted a study whereby BAC was used for the reduction of trihalomethanes formation potential and it was found that BAC also reduces the $UV_{254}$ and SUVA of the raw water samples. Post-ozonation, on the other hand has been shown to enhance the reduction of TOC in the coagulation step of the water treatment process (Pei *et al*., 2007). Depending on the type of raw water entering the treatment plant and the preferred treatment any of the two processes (i.e. pre- or post-ozonation) can be used.

### 2.4.3 Activated carbon filtration

Activated carbon (AC) has been proven to be the effective adsorbent for water filtration (Lobanga & Haarfoff 2012). However, AC is often colonized by heterotrophic biomass to form biological AC, which reduces the portion of biodegradable and assimilated elements in water (Wei-Bin *et al*., 2013). During the filtration process, taste, odour, pesticides, industrial chemicals and algal toxins are efficiently removed (Lobanga & Haarfoff 2012). While NOM can also be removed during the filtration processes, it decreases the efficiency of the removal of other pollutants by competing for the active sites with smaller target molecules. Previous studies have shown that lower molecular weight species are more adsorbable on activated carbon (Matilainen 2007). This is because the lower the size of the molecule, the easier for it to enter the nanopores, thus excluding the macromolecules (Matilainen 2007).

### 2.4.4 Membrane filtration

Reverse osmosis, ultrafiltration, microfiltration and nanofiltration are pressure driven membrane filtration methods with various levels of NOM removal potential (Metsämuuronen *et al.*, 2012). Reverse osmosis and ultrafiltration membranes have been widely used to separate NOM based on its molecular sizes. Due to its properties such as easier maintenance, small size and very high water quality produced, this technology is a serious contender for replacing conventional water treatment processes (Zularisam *et al.,* 2006). Furthermore, membrane filtration is

environmental friendly, capable of handling a wide range of fluctuations in feed quality and it has a low energy consumption potential. Although research has shown that ultrafiltration and microfiltration can be employed in the removal of microparticles and macromolecules, which include dissolved organic matter (DOM), it does not directly deal with DBPs (Zularisam *et al.*, 2006). One of the disadvantages of using membranes include membrane fouling, which results in a decline of flux (Ates *et al*., 2009). In order to minimise this adverse effect, pre-treatment with coagulation is usually applied.

### 2.4.5 Degradation of NOM

Most conventional methods used for NOM removal in WTPs uses chemicals, which result in the production of large quantities of sludge with high concentrations of NOM and thus posing serious disposal problems for the authorities (Lee 2005; Solarska *et al*., 2009). Consequently, research into the development of alternative methods that degrade NOM into harmless products is a priority. Such methods include enzymatic, UV based advanced oxidation processes, and the use of nanomaterials and nanocomposites. In this study, nanomaterials and nanocomposites were adopted for use in the effective degradation of NOM into smaller and possibly harmless by-products. Before delving on the application of nanomaterials and nanocomposites in the degradation of NOM, the other degradation techniques are discussed.

#### 2.4.5.1 Enzymatic degradation of NOM

Bioremediation technology, which involves the use of microorganisms such as fungi and bacteria, or isolated enzymes to degrade organic pollutants into harmless products, has been given much attention because it is environmentally friendly, cost-effective, and limits by-product formation (Lee 2005). This method removes biodegradable organic matter, and thus reduce chlorine demand during the disinfection step of the water treatment process as there will be no or very little NOM available to react with free chlorine (Lee 2005). This technology is not only applied in drinking water treatment to purify water, it is also applied in the treatment of concentrated NOM wastes from water treatment processes. As an

added advantage, the use of enzymes and bacteria to degrade NOM results in the formation of NOM fraction with lower molecular weight (Wershaw *et al*., 2005).

Some of the studies reported on this technology involve the use of saprotrophic fungi and white rot fungi (WRF) to degrade humic substances (Gramss *et al*., 1999; Grinhut *et al*., 2007). The activity of WRF is based on their non-specific extracellular oxidative enzyme system, which may include lignin peroxidase, laccase and manganese-dependent peroxidase that completely mineralize lignin to $CO_2$ and $H_2O$. The non-specificity of these enzymes allows them to oxidize a wide number of compounds with some structural similarity to the lignin substructures. These enzymes have been used to degrade the humic substances and this has resulted in the formation of carboxyl and phenoxy radicals (Solarska *et al.*, 2009). Solarska *et al.,* (2009) have reported that the biodegradation of NOM has resulted in the formation of low molecular weight compounds (i.e. organic and fulvic acids) and low molecular weight humics.

Enzymes are generally substrate-specific, and by binding to the specific substrate in the NOM molecule, the enzyme can then start degrading that part of the molecule into smaller pieces, which are easier to remove from the water source using specific treatment processes (Solarska *et al,.* 2009). Enzymes break certain bonds in the NOM structure, which other methods fail to do. The amino acids, carbohydrates, proteins and carboxylic acids found in source water vary in their susceptibility to microbial biodegradability (Solarska *et al.,* 2009).

#### 2.4.5.2 UV based advanced oxidation processes

Advanced oxidation processes (AOPs) are a combination of methods used to oxidize NOM from waters, which include $TiO_2$/UV, UV/$H_2O_2$, $O_3$/UV, Fenton and photo-Fenton processes, and ultrasound. Thus AOPs include all the processes where hydroxyl radicals ($OH^{\bullet}$) are being formed as an intermediate through different methods (Comninellis *et al.,* 2008; Lamsal *et al.*, 2011).

In these processes, the $H_2O_2$ molecule is divided into two hydroxyl radicals after absorbing photons and these radicals attack organic molecules under certain

conditions to produce end products such as water, $CO_2$ and inorganic acids (Galindo *et al.*, 2000). However, these radicals can react with carbonate and bicarbonate ions, which are commonly available in raw water, thus reducing the amount of hydroxyl radicals available to react with the NOM (Lamsal *et al.,* 2011). Three major approaches under this category, which are discussed briefly in section 2.4.5.2.1-2.4.5.2.3, are photo assisted Fenton ($UV/H_2O_2$), photocatalytic processes ($TiO_2/UV$) and ozone based applications ($O_3/UV$).

#### 2.4.5.2.1 Photo assisted Fenton ($UV/H_2O_2$)

During treatment with UV, NOM molecules are oxidized and the aromatic fractions are reduced. High molecular weight NOM is converted into low biodegradable compounds (Matilainen & Sillanpää 2010). The generated hydroxyl radicals reduce both TOC and DBP formation potential in raw water. At the appropriate hydrogen peroxide concentration and right UV dose, NOM can be completely mineralized into inorganic molecules (Matilainen & Sillanpää 2010).

#### 2.4.5.2.2 Photocatalytic processes ($TiO_2/UV$)

These processes use oxygen as the oxidizing agent and a semiconductor metal oxide as catalyst (Huang *et al*., 2008). The first step involves the absorption of UV irradiation by the $TiO_2$, which triggers the excitement of electrons from the valence band (VB) to the conduction band (CB). This in turn triggers the formation of hydroxyl radicals and the formation of holes on the VB (Nkambule *et al.,* 2012a). Organic compounds like NOM are then degraded by hydroxyl radicals in the solution and by electron-holes on the $TiO_2$ surface (Huang *et al*., 2008). Oxidation reactions can be affected by the water matrix, solution pH, catalyst concentration, light wavelength and intensity (Matilainen & Sillanpää 2010).

#### 2.4.5.2.3 Ozone based applications ($O_3/UV$)

Ozone is primarily used as a disinfectant and for the management of taste and odour in water treatment (Bose & Reckhow 2007). Ozone selectively interacts with NOM *via* an electrophilic addition to double bonds, which leads to its degradation

(Matilainen & Sillanpää 2010). However, this process can also results to the formation of oxidation by-products, as well as possible release of entrapped compounds. These by-products may results in biological regrowth in the water system (Matilainen *et al.*, 2007). Moreover, hydroxyl radicals ($OH^{\bullet}$) that are formed when ozone decomposes in water also react with NOM *via* a direct, fast and non-selective reaction (Van Geluwe *et al*., 2011). The hydroxyl formation potential in this case is much lower compared to in the case of AOPs.

#### 2.4.5.3 Photodegradation using nanomaterials

Nanomaterials exhibit improved biological, chemical, physical properties and functionality due to their nanoscale sizes (Joshi *et al.*, 2008). These materials have stimulated significant research interest and are thought to elucidate a lot environmental pollution issues. A number of n-type semiconductors, for example $TiO_2$, ZnO, CdS, $SnO_2$ and $WO_3$, are regarded as good photocatalysts for the degradation of organic pollutants present in water sources (Jwo *et al.*, 2005; Kuvarega *et.al*., 2012a). Nevertheless, most of these photocatalysts are limited by a large band gap, very high electron-hole recombination, and their instability in water that can cause the decomposition of the catalyst itself (Kuvarega & Mamba 2016). Be that as it may, photocatalysis using $TiO_2$ has received considerable attention in view of its application in the decontaminating of the environment (e.g. cleaning of windows, glasses and tiles) (Nosaka *et al.*, 2005).

$TiO_2$ is a semiconductor photocatalyst with chemical and biological stability, non-toxicity, insolubility in water, high photocatalytic activity, acidic and basic media, availability and low cost (Kuvarega *et al*., 2011; Riaz 2013). $TiO_2$ can effectively mineralize organic pollutants to smaller molecules (Nkambule *et al.*, 2012d). It usually exist in three polymorphs, which are rutile, brookitile and anatase (Chatterjee & Dasgupta 2005; Hanaor & Sorrell 2011). The anatase phase is metastable while the rutile and brookitle phases are stable. The anatase polymorph can easily and irreversibly transform to the rutile phase at high temperatures (Hanaor & Sorrell 2011). The anatase phase is mostly preferred for water purification due to its lower density, higher electron mobility and low dielectric constant (Kuvarega *et.al*., 2012a).

The principle behind the activation of $TiO_2$ involves the absorption of light with a wavelength equal to or higher than the band gap of $TiO_2$, causing the excitation of electrons from the VB to the CB thus creating holes in the VB (**Figure 2.1**) (Kuvarega *et al.*, 2011; Ubonchonlakate *et al.*, 2012). On the contrary, an energy source with a wavelength that is lesser than the band gap of $TiO_2$ can cause dissipation of energy in a form of heat (Yang *et al.,* 2014).

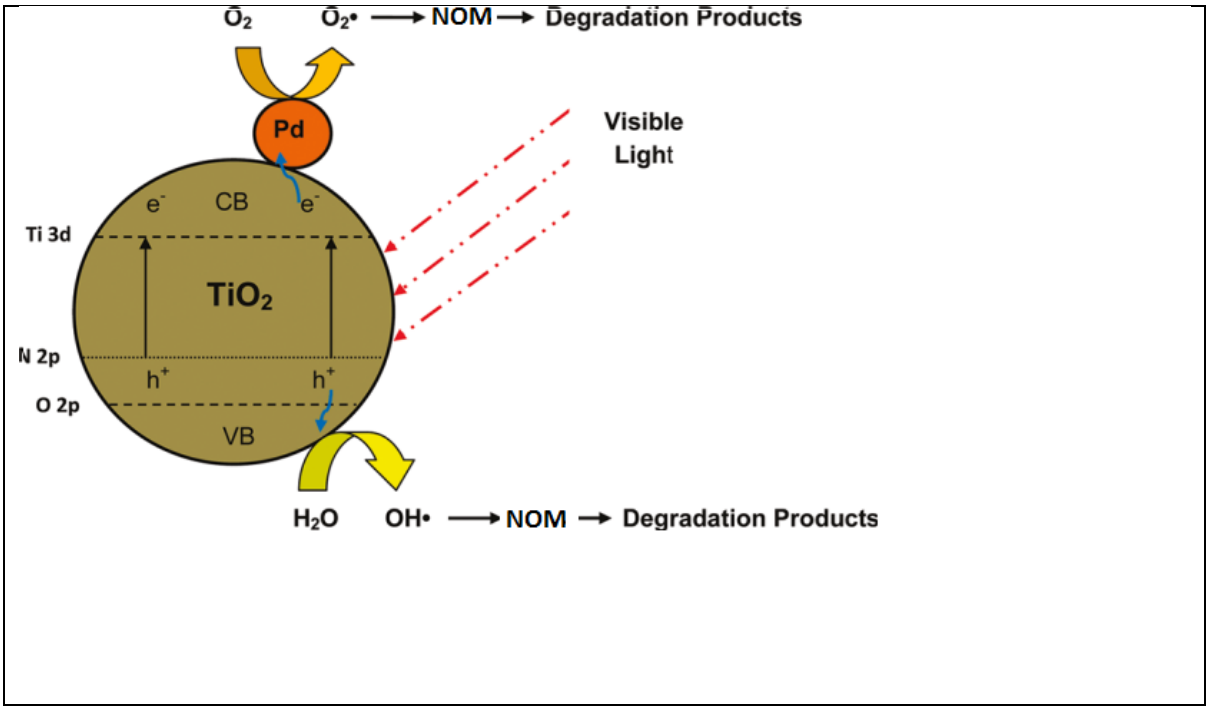


**Figure 2.1: Proposed scheme for the photodegradation of NOM by NPT** (adopted with modification from Kuvarega *et al.,* 2011).

The holes in the VB can react with OH and water from the surface of the particle to form highly reactive $OH^{\bullet}$ (Yang *et al*., 2014; Seifvand & Kowsari 2016). The generated hydroxyl radicals then attack any organic compound available on the surface of the material to form mainly $CO_2$ and $H_2O$ (Ubonchonlakate *et al*., 2012). On the other hand, oxygen (which is an electron acceptor) can be reduced by the electrons of the CB to form superoxide radical anions (Chatterjee & Dasgupta 2005). Therefore, the absence of oxygen can suppress the photoactivity of $TiO_2$.

Although photocatalysis based on $TiO_2$ has a wide band gap (3.2 eV), there is a very small portion (4%) of the solar spectrum that can be used to sensitize $TiO_2$ (Cheng *et al*., 2012; Khairy & Zakaria 2014; Luo *et al.*, 2015). The limited portion of the spectrum reduces the photocatalytic efficiency of the $TiO_2$ under solar light, which in turn limits the potential of $TiO_2$ as a suitable technology in environmental remediation (Yang *et al*., 2010; Kuvarega *et al.*, 2012b; Jiang *et al.*, 2012; Yang *et al.*, 2014). $TiO_2$ also suffers from electron-hole recombination, which deactivates the photoactivity process and negatively affects the quantum yield (Nosaka *et al*., 2005; Nkambule *et al.*, 2012d; Yang *et al.*, 2014).

It is thus important to develop methods that can shift the absorption of light from the UV to the visible region without compromising the photoactivity of $TiO_2$ (Burda *et al.,* 2003; Nosaka *et al.*, 2005). The use of solar simulation as a light source is cost effective compared to UV light (Burda *et al.*, 2003). Various methods such as dye sensitization, adding inert support, physical implantation, binary oxides and chemical doping using metals and non-metals have been employed in order to make the $TiO_2$ active under visible light (Chatterjee & Dasgupta 2005; Najjar *et al*., 2015; Mahlambi *et al*., 2015). Chemical doping is achieved by introducing impurities next to the VB or CB, with the sole purpose of modifying the properties of $TiO_2$ (Di Paola *et al.*, 2012; Seifvand & Kowsari 2016). A good dopant reduces the band gap of $TiO_2$ by increasing the VB level but leaving the CB untouched (Kuvarega *et al.*, 2011). Also, the dopant should not introduce instability in the $TiO_2$ material and must also decrease electro-hole recombination (Kuvarega *et.al*., 2012a). Various methods have been employed for dopping $TiO_2$, however, the sol-gel method has been given much attention because it is fast and versatile and allows metal or non-metals to be incorporated into the sol thus allowing a direct interaction between the dopant and the support during the gelation step (Chatterjee & Dasgupta 2005).

#### 2.4.5.3.1 The use of non-metals as dopants

Non-metals have been used as $TiO_2$ dopants with the purpose of reducing the band gap of the material (Casbeer *et al.*, 2012; Yang *et al.*, 2014). Doping $TiO_2$ requires the following considerations:

(1) It is important to know whether the dopant is introduced in the interstitial or substitutional manner since this can have a great impact on the properties of the doped $TiO_2$; and
(2) It is important to know the effect of the dopant on the stability of the material (Kuvarega *et al.,* 2012b).

Various non-metals such as N, C, F, B and S have been investigated for their effectiveness in the enhancement of the photocatalytic activity of titanium dioxide under visible light illumination (Cheng *et al.*, 2012; Yang *et al.*, 2014). Doping with nitrogen or carbon has been shown to shift the absorption spectra by 50 nm towards the visible region (Wang & Lewis 2006).

Studies have shown that introducing anionic species like nitrogen can result in the reduction of the band gap thus improving the photoactivity of the $TiO_2$ in the visible region (Kuvarega *et al.*, 2011; Cheng *et al.*, 2012; Luo *et al.*, 2015). Nitrogen has the same size and low ionization energy as oxygen, and it can easily and effectively substitute oxygen through the mixing of N 2p orbital with O 2p orbital within the $TiO_2$ band-gap (Kuvarega *et al*., 2011). Moreover, N can form an intra-band-gap impurity energy state between the CB and VB of $TiO_2$, thus reducing the band gap of the $TiO_2$ material (Yang *et al.*, 2014).

It is important to take into consideration the various experimental conditions (e.g. temperature) for the preparation of the photocatalyst, since these conditions determine the properties of the resulting material (Riaz 2013). Additionally, the conditions followed to perform photodegradation experiments such as catalyst concentration, concentration of the pollutant, the type of irradiation source, reaction temperature and pH of the reaction mixture must also be taken into consideration (Riaz 2013). Cheng *et al.*, (2012) evaluated the effect of N-doped $TiO_2$ on the degradation of Rhodium B (RhB) dye and reported that doping $TiO_2$ (with up to 3% of N) resulted in the enhancement of the photoactivity of $TiO_2$. The catalytic enhancement is attributable to the narrowing of the band gap of the $TiO_2$. The high number of hydroxyl radicals available on the surface, which react with the targeted pollutant also contributed to this enhancement (Cheng *et al.*, 2012). Photodegradation studies of 2-propanol using N doped $TiO_2$ material and guanine

carbonate, guanine hydrochloride and urea as nitrogen sources have shown that guanidine carbonate is much more efficient than urea and guanine hydrochloride in the degradation of 2-propanol. The doped $TiO_2$ was also found to have a higher degradation efficiency than the undoped (Nosaka *et al.*, 2005).

A comparative study done by Burda *et.al*., (2003) on the degradation of methylene blue dye has revealed that doping $TiO_2$ (for up to 8% N) caused the enhancement of the photodegradation of the dye in the visible region when $TiO_{2-x}N_x$ was used instead of the pristine $TiO_2$ material. Yang *et.al.*, (2010) has synthesized a number of nitrogen doped $TiO_2$ using the solvothermal method and tested their photoactivity using methylene blue and methyl orange dyes under a visible light source. The results showed that the doped material had an enhanced photoactivity under visible region when compared with pristine $TiO_2$ (Yang *et al*., 2010).

Other than reducing the band gap, more work still needs to be conducted to increase the photodegradation efficiency of $TiO_2$ even further. Most researchers are now focusing their efforts on using metals as dopants for $TiO_2$. Metals can collect a huge number of electrons thus eliminating the issue of electron-hole recombination by improving the separation of electrons and holes on the surface of $TiO_2$ (Li & Li 2002; Ubonchonlakate *et al*., 2012; Kuvarega *et al*., 2012b; Riaz 2013; Najjar *et al*., 2015; Seifvand & Kowsari 2016). It has also been shown that these metals can significantly increase the photocatalytic activity by reducing the band gap of $TiO_2$ (Nkambule *et al.,* 2012d).

Reducing the band gap of the material makes it active under visible light. To this end, the type of metal dopant being used and its concentration has a huge impact in reducing the band gap and electron-hole recombination of the material (Kuvarega *et al*., 2012b). Recent reports have revealed that doping $TiO_2$ material with non-metals requires harsh conditions to prepare the material (Kuvarega *et al*., 2012b). Various types of metals have been used as dopants for $TiO_2$ material; these include alkali metals, transition metals, rare earth metals and platinum group metals (Kuvarega & Mamba 2016). Although noble metals such as Au, Pd and Pt are regarded as stable under photocatalytic irradiation, they are very expensive (Kuvarega *et.al*., 2012a). Based on this, most researchers are focusing their

efforts on finding an alternative using cost effective and readily available transition metals such as Ni, Mn, Cu, Fe, Cr, Co and Zn (Choi & Kang 2007; Khairy & Zakaria 2014; Bashiri *et al*., 2016).

#### 2.4.5.3.2 Transition metals

Transition metal dopants can enhance the photoactivity of $TiO_2$ by reducing electron-hole recombination (since the photogenerated electrons can be trapped by metals) thus increasing the lifetime of the holes (Yang *et al.*, 2014). They also reduce the band gap of $TiO_2$, making it active under the visible region (Khairy & Zakaria 2014). Among the transition metals used as dopants for $TiO_2$, are noble metals such as Ru, Au, Rh, Pt, Ir, Pd, Ag and Os (Kuvarega *et.al*., 2012b). These metals can result in the formation of a Schottky barrier at the $TiO_2$/metal interface, thus inhibiting electron-hole recombination (Kuvarega *et al*., 2012b; Riaz 2013). When Khairy *et.al*., (2014) studied the effect of Cu and Zn doped on $TiO_2$ material for the photodegradation of methyl orange, it was shown that doping $TiO_2$ with these metals caused a red shift in the absorption edge and also reduced the band gap of the $TiO_2$. This led to the enhancement of the photoactivity of the doped materials compared to when pristine $TiO_2$ was used (Khairy & Zakaria 2014).

According to the work conducted by Ubonchonlakate *et.al.,* (2012), which was based on the antibacterial efficiency of $TiO_2$-Ag and $TiO_2$-Ag-PEG composites films against *P.aeruginosa* bacteria, the doped $TiO_2$ gave a higher degradation activity than the pristine $TiO_2$. For the Ag-$TiO_2$ film, the enhanced photodegradation activity was mainly due to the silver reducing the electron-hole recombination after photo-excitation, which then increases the photoactivity of $TiO_2$. Moreover, it was shown that the absorption edge for the doped $TiO_2$ material shifted to longer wavelength, making the material much more active under the visible region. The enhanced degradation efficiency associated with $TiO_2$ doped with Ag is attributable to the ions being photoactive under UV-A and UV-C, which then leads to higher UV inactivation of the targeted bacteria. Similar findings were observed by Li & Li (2002) who conducted a comprehensive study on Au-$TiO_2$ and gold-deposited $TiO_2$; a reduction of the methylene blue dye was observed in this case. The presence of Au (of up to 0.5%) resulted in the decrease of electron-hole

recombination, which in turn resulted to the increase in the activity of the doped $TiO_2$ compared to pure $TiO_2$. Most importantly, the findings confirmed that the absorption of $TiO_2$ underwent the red shift, which was accompanied by a reduced band gap of $TiO_2$.

Seifvand and Kowsari (2016), prepared Pd doped $TiO_2$ in ionic liquid using the sol-gel method for the photodegradation of $NO_X$ and CO. The obtained results showed an enhanced degradation for the doped $TiO_2$, which is attributable to the palladium reducing the electron-hole recombination. It was also concluded that the observed results were due to the Schottky-barrier formed at the photocatalyst/metal interface which then reduced the electron-hole recombination effect.

In a separate study involving the application of Pd-doped $TiO_2$ in the degradation of the C.I. Acid Yellow 23 (AY23) under UV illumination, doping $TiO_2$ for up to 0.75% Pd with the catalyst dose of 600 mg/L and 300 ˚C calcining temperature resulted in an enhanced degradation of the targeted pollutant (Najjar *et al*., 2015). A 82% TOC reduction after 120 minutes was noted. Another reason for the observed enhanced degradation efficiency could be due to uniform dispersion of mono dispersed palladium particles (Najjar *et al*., 2015).

Nevertheless, the main disadvantage of using transition metals as dopants is their ease of leaching in water; which can be harmful to the consumer (Kuvarega *et al*., 2012b). In addition, using transition metals can reduce the stability of the material which then prompts long term leaching of the dopant; thus resulting in a gradual decrease in the photoactivity of the material (Wang & Lewis 2006; Kuvarega *et al*., 2012b). As mentioned above, doping with non-metal requires hash conditions and has low reproducibility. Based on these shortcomings, researchers are now focusing on co-doping as an alternative and preferred route for enhancing the photoactivity of $TiO_2$ by inducing a synergistic effect on $TiO_2$.

#### 2.4.5.3.3 Co-doping

Co-doping (metal to metal, double non-metal, metal to non-metal) has attracted much attention due to the synergistic effects on the photoactivity of $TiO_2$ (Kuvarega *et al*., 2012a; Nkambule *et al*., 2012d; Yang *et al*., 2014). Co-doping reduces the band gap of $TiO_2$, which then allows $TiO_2$ to be effective under visible region; while reducing electron-hole recombination (Yang *et al.,* 2014). It also enhances the physical properties of $TiO_2$, such as surface area and crystal size, while preventing the transformation between anatase and rutile polymorphs (Kuvarega *et al.,* 2012b).

Studies using La/Fe co-doped $TiO_2$ to photodegrade ammonia nitrogen in wastewater have shown that the co-doped $TiO_2$ has the highest photodegradation efficiency as compared to single doped and pristine $TiO_2$ (Luo *et al*., 2015). The enhanced degradation efficiency is due to larger surface, reduced band gap and electron-hole recombination, which increases the photoactivity of $TiO_2$. In addition, a review by Yang *et.al*., (2014) shows that N-metal co-doped $TiO_2$ is the most effective photocatalyst than pristine $TiO_2$ and N-$TiO_2$ for the degradation of various pollutants in water. In the same work, the doping of $TiO_2$ with both Ag and N was reported to enhance the photodegradation of methylene blue dye under visible light when compared with single dopant and pristine $TiO_2$. This is mainly because the co-doped $TiO_2$ has a photo-response under visible range due to the N anions reducing the band gap of $TiO_2$, and the Ag reduced electron-hole recombination (Yang *et al*., 2014). A study of the sol-gel synthesis of PdO/TiON catalyst and its application in various bacterial indicators has revealed that the presence of palladium enhances the photocatalytic activity of the catalyst when compared with the TiON and PdO/$TiO_2$; this provides evidence for the existence of the synergistic effect of co-doping (Wu *et al*., 2009).

Nkambule *et.al.*, (2012a) reported that N-Pd co-doped $TiO_2$ has NOM removal efficiencies of 96, 15 and 38% for hydrophobic, transphilic and hydrophilic fractions, respectively. This removal efficiency was very high relative to conventional treatment methods for the removal of NOM. The high removal efficiency is due to the large surface area of $TiO_2$, reduced band gap by N atoms,

reduced electron-hole recombination by Pd and the synergistic effect of co-doping with both metal and non-metal. It was also observed that visible light was more effective and efficient than UV light in the degradation of the hydrophobic fraction of NOM. Similar dopants (N, Pd co-doped $TiO_2$, N-doped and $TiO_2$) were used for the degradation of Eosin Yellow dye under visible irradiation (Kuvarega *et al*., 2011). This proves the synergistic effect of co-doping, which reduces the band gap and electron-hole recombination of the material. This work then focuses on using N, Pd co-doped $TiO_2$ to degrade various NOM samples collected from different South African water treatment plants.

#### 2.4.5.4 Photodegradation using nanocomposites

Different forms of carbon based materials including graphite, activated carbon and nanotubes have been used to modify titanium dioxide with the purpose of making it more active under visible light (Mahlambi *et al*., 2015). Despite enhancing the photocatalytic activity of $TiO_2$, these nanocomposites prevent transformation between various phases of titania even at very high temperatures (Mahlambi *et al*., 2015).

##### 2.4.5.4.1 Carbon nanotubes

Carbon nanotubes (CNTs), can be visualized as a sheets of graphene rolled in such a way that it forms a cylinder with a planar hexagonal C-C bonds arrangement (Bokobza 2007). Their lengths range from micrometers to centimeters and their diameters are in a range of nanometers to tens of the same units (Bokobza 2007; Kuvarega *et al*., 2012b). Various methods have been used for the preparation of CNTs, these include laser ablation, arch-discharge and catalytic chemical vapour deposition methods (Bokobza 2007). The main disadvantage of CNTs is their poor dispersion character mainly due to van der Waals forces experienced in between the tubes, which results in agglomeration (Bokobza 2007). Owing to their exclusive structure and large surface area, these materials have attracted significant research attention (Yu *et al*., 2011; Di Paola *et al*., 2012). There are two main classes of CNTs, namely single-walled carbon nanotubes (SWCNTs) and multi-walled carbon nanotubes (MWCNTs).

Due to their high Young's modulus and tensile strength, CNTs can form nanocomposites with enhanced mechanical characteristics (Kuvarega *et.al*., 2012a). Moreover, the chirality and the number of the graphene walls present in CNTs play a huge role in the electronic properties of CNTs. Generally, single-walled carbon nanotubes (SWCNTs) are a combination of both semiconducting and metallic material, whereas multi-walled carbon nanotubes (MWCNTs) have a metallic conductivity property that is almost similar to metals (Yu *et al*., 2011; Kuvarega *et al*., 2012b).

Due to their nanoporous character, high mechanical stability and chemical stability, CNTs are excellent supports especially for semiconductors that possess photocatalytic activity (Yu *et al*., 2011; Kuvarega *et.al*., 2012a). Owing to these properties, most researchers are now exploring their use in various areas such as aerospace, energy, medicine, information and chemical industries (Bokobza 2007; Kuvarega *et al.*, 2012b).

Decorating CNTs with $TiO_2$ to produce the CNTs/$TiO_2$ nanocomposites has attracted a lot of attention from researchers; the properties of CNTs/$TiO_2$ nanocomposites are suited to deal with a number of global problems including water purification (Kuvarega *et al*., 2012b). These nanocomposites have improved properties and display cooperative effects (Yu *et al*., 2008; Gao *et al*., 2009; Yu *et al*., 2011). Although $TiO_2$ is an n-type semiconductor; the presence of CNTs allows the photogenerated electrons to freely move towards the CNT surface (minimizing electron-hole recombination), which may have a lower Fermi level (Kuvarega *et al*., 2012b). This in turn reduces the band gap of $TiO_2$ and also increases the lifetime of the holes in the VB thus increasing its photocatalytic activity. As depicted in **Figure 2.2**, in the presence of the activation energy of the visible light, the photogenerated electrons from the CNTs move freely towards the conduction band of $TiO_2$.

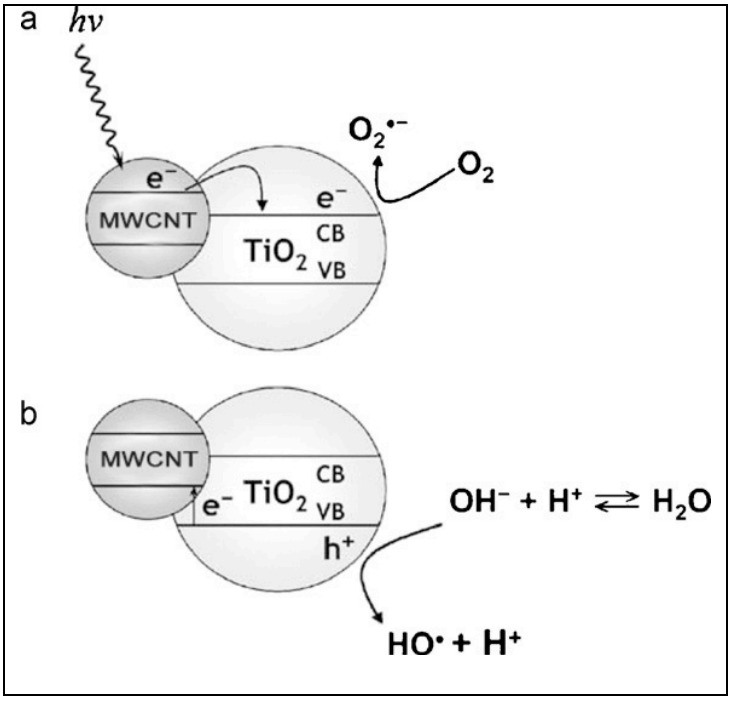


**Figure 2.2: Proposed scheme for the photocatalytic activity of MWCNTs/$TiO_2$** (Di Paola *et al*., 2012)**.**

In addition, CNTs are good adsorbents and composites of MWCNTs/$TiO_2$ increases the adsorption of the targeted pollutants into the surface of the material thus allowing the efficient degradation of the targeted pollutants (Kuvarega & Mamba 2016). For the effective degradation of pollutants, direct contact is required between the pollutant and the surface of the material since the generated radicals have a short lifetime. Most importantly, the conductive structure of these materials reduces the electron-hole recombination by forming hetero-junctions at the interface of the CNTs/$TiO_2$ nanocomposite (Kuvarega *et al*., 2012b).

Nanocomposite of CNTs/$TiO_2$ (with 20% highest CNTs loading) prepared *via* sol gel displayed superior photoactivity and photodegradation against methylene blue when compared with pure $TiO_2$ (Gao *et.al*., 2009). Similar findings were reported by Wang *et al.*, (2009) when MWCNTs/$TiO_2$ (also synthesized using sol-gel) was tested for the photodegradation of 2,6-dinitro-*p*-cresol (DNPC) in aqueous media. The high surface area of the MWCNTs/$TiO_2$, which increases the amount of adsorbed pollutants available for photodegradation, seems to be behind the increased levels of photodegradation associated with the MWCNTs/$TiO_2$ (Gao *et*

*a*l., 2009; Wang *et al*., 2009). It should also be noted that CNTs can also act as a light absorbing photosensitizer, which can trigger the generation of electrons, resulting in a high number of radicals being formed (Gao *et al*., 2009; Wang *et al*., 2009).

Similarly, Kang *et.al*., (2015) showed that MWCNTs/$TiO_2$ (prepared using solvothermal method) has a higher photodegradation efficiency towards copper sulfophthalocyanine under solar illumination compared to pristine $TiO_2$. The nanoscale diameter and high aspect ratio structure of the MWCNTs/$TiO_2$ allow them (MWCNTs) to accumulate a large number of photogenerated electrons, thus reducing electron-hole ratio, which then enhances the photoactivity of $TiO_2$ (Kang *et al*., 2015). Yu *et.al*., (2011) on the other hand concluded that the enhanced photoactivity of MWCNTs dispersed on the mesoporous titanium dioxide was because the MWCNTs acted as channels for the transfer of electrons thus reducing electron-hole recombination.

Most importantly, the work carried out by Lu & Su (2007) demonstrated that MWCNTs heated for 60 minutes at 400 ˚C caused an increase in the adsorption of NOM compared to pristine CNTs. After thermal treatment, a decrease in the negative charge content caused an increase in the adsorption of NOM. In a similar work, CNTs were compared with other adsorbents such as granular activated carbon (GAC) and it was observed that CNTs have superior adsorption capacity (Lu & Su 2007).

Kuvarega *et.al*., (2012a) prepared MWCNTs/N, Pd co-doped $TiO_2$ using the sol-gel method and evaluated its photoactivity against Eosin Yellow under visible irradiation. A comparative study involving solar light and UV light was also carried out, and a higher degradation under visible light was observed, and this was mainly because of small portion of UV (3-5%) in solar radiation. Moreover, the results of this study showed that the introduction of MWCNTs (up to 0.5%) in the material resulted in an enhanced degradation efficiency as compared to N, Pd co-doped $TiO_2$. The observed increase in the photocatalytic activity of $TiO_2$ was due to the synergistic effect of N, Pd $TiO_2$ with MWCNTs.

All literature findings quoted above shows the importance of introducing MWCNTs on $TiO_2$ material, and the resulting nanocomposites have proven to enhance photoactivity against various pollutants. However, not much research has been undertaken on $TiO_2$ doped with metal/non-metal decorating CNTs, and to the best of our knowledge no work has been reported on the use of MWCNTs/N, Pd co-doped $TiO_2$ to degrade NOM in water.

## 2.5 NANOPARTICLES AND THE ENVIRONMENT

Although nanomaterials have been widely used for environmental applications, there is a growing concern about their toxicity towards humans and environment. The concept of toxicity deals with the concentration of that material being present and also the time of exposure (Elsaesser & Howard 2012). Available toxicological information only targets the effect of inhaling nanomaterials present in air (Farré & Gajda-schrantz 2009).

The two main sources of nanomaterials involve both nature (e.g. forest fires and volcanic eruptions) and industries (e.g. automobile exhaust, welding and smelting) (Farré & Gajda-schrantz 2009). Previous research showed that reducing the material size can enhance its toxicity, regardless of the fact that the material is inert in its bulk form (such as $TiO_2$) (Farré & Gajda-schrantz 2009). Owing to the large surface area and reduced size of nanomaterials, they can efficiently interact with biological processes to produce grave toxicity (Farré & Gajda-schrantz 2009).

Nanomaterials are redox active and can cause the formation of reactive oxygen species, which can cause both cell damage and death (Farré & Gajda-schrantz 2009; Elsaesser & Howard 2012). Free radicals produced by these nanoparticles can affect cell integrity (Elsaesser & Howard 2012). Nanomaterials can affect the stability of a cell membrane through various processes (**Figure 2.3**) and this depends on the surface properties of the material (Elsaesser & Howard 2012).

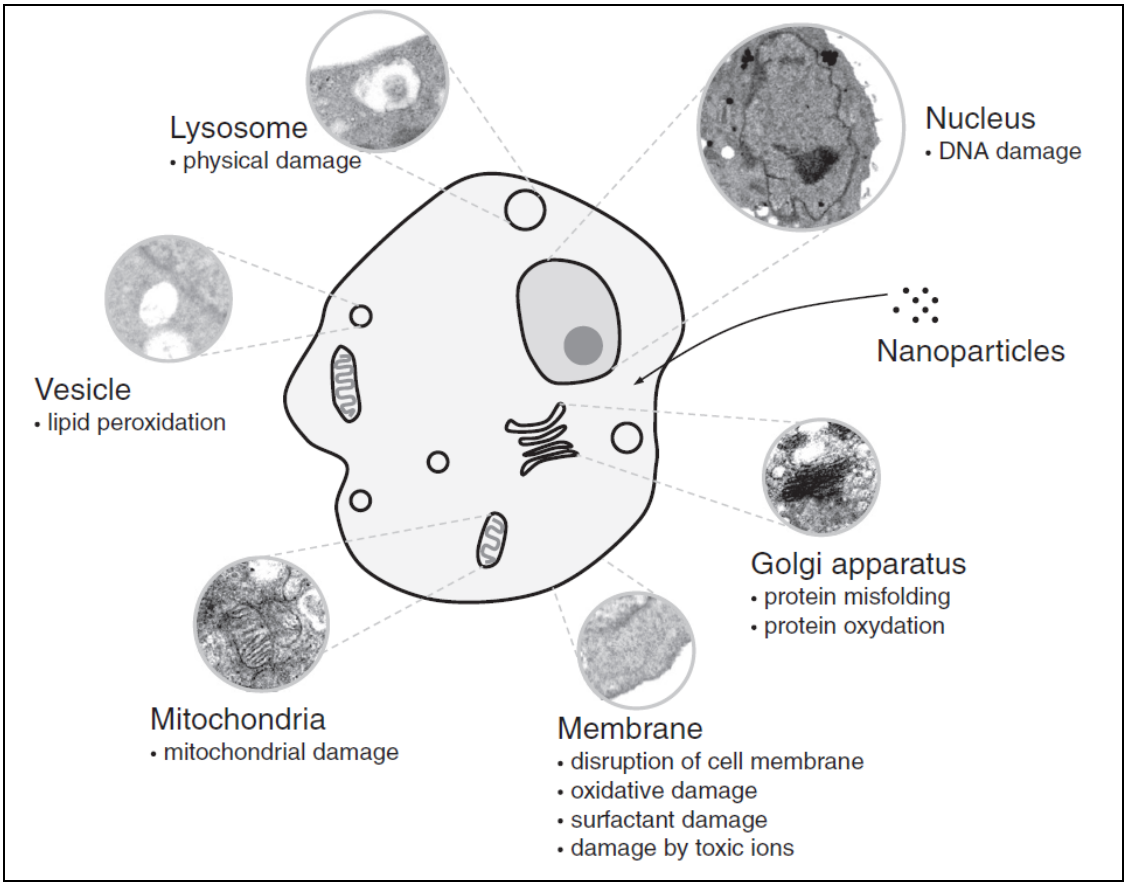


**Figure 2.3: Damages caused by nanomaterials in a cell (their targets and nanotoxicological pathways)** (Elsaesser & Howard 2012).

*In vitro* studies to understand the effect of nanoparticles on human health show that the main entry pathway of these materials into the body is through inhalation (Elsaesser & Howard 2012). Despite the body having its defense mechanisms, nanomaterials can reach the liver, brain, heart and other organs where they bio accumulate (Elsaesser & Howard 2012). CNTs, for example, have proven to negatively affect biota. These materials were reported as respiratory toxicants because they usually accumulate on gill surfaces of most fish (Farré & Gajda-schrantz 2009). Moreover, the metal catalyst in the CNTs may be more toxic compared to the treated or functionalized CNTs (Lu & Su 2007).

Although $TiO_2$ and CNTs/$TiO_2$ materials are effective in degrading most pollutants present in water, the main concern is that, since these materials are applied in their powdery form, separating them after use might be a problem in industry (Ubonchonlakate *et al*., 2012). Whereas in bench scale experiments these

materials are easily separated using filtration, in industry this may require costly treatment processes and more time (Kuvarega *et.al*., 2012a).

One of the feasible applications of nanomaterials in industry might be the decoration of these materials on activated carbon so that it can increase both the adsorption of the pollutants onto the material surface and the degradation or removal of the targeted pollutants. However, there is limited understanding of the toxicity of nanomaterial, and there is a need for a continuation in this aspect of nanomaterials research.

## 2.6 CONLUSION

The literature reviewed here has demonstrated the importance of characterizing NOM before its removal from the water. However, the characterization methods that are currently being used in South African water treatment plants do not give enough information about the composition of NOM present in water, and there is a need of introducing advanced methods such as FEEM in the industrial level or forming a collaboration between industries and institutions that already have this technique for the effectective characterization of NOM.

Studies focusing on the treatability of NOM throughout the treatment process are limited. Most researchers have looked at the effectiveness of NOM removal by one treatment step such as coagulation/enhanced coagulation process. This limits the understanding of NOM treatability throughout the treatment process. However, in order to develop methods that will complement the available NOM removal methods, the treatability of NOM throughout the treatment process must be clearly understood. Not only will this assist in identifying the NOM fractions that cannot be effectively removed, it will also provide guidelines in terms of where the newly developed method could be introduced in the treatment train.

Currently, the available water treatment processes do not effectively remove all the NOM present in water and this is mainly due to its large size and complex structure. NOM degradation methods that degrades NOM into smaller molecules for effective removal using the currently available treatment processes offers a

viable option for the treatment of water polluted with NOM. It is envisaged that such an approach will lead to the reduction or eradication of NOM and DBPs in our water sources.

## 2.7 REFERENCES


Amy, G.L., Collins, M.R., Kuo, C.J., & King, P.H. (2015). Comparing Gel Permeation Chromatography and Ultrafiltration for the Molecular Weight Characterization of Aquatic Organic Matter. *American water works*, **79 (1)**:43-49.

An, G., Ma, W., Sun, Z., Liu, Z., Han, B., Miao, S., Miao, Z. & Ding, K. (2007). Preparation of titania/carbon nanotube composites using supercritical ethanol and their photocatalytic activity for phenol degradation under visible light irradiation. *Carbon N Y*, **45 (9)**:1795-1801.

Anderson, L.E. (2013). Anion exchange resin technology for natural organic matter. MSc dissertation, Dalhousie University.

Ates, N., Yilmaz, L., Kitis, M. & Yetis, U. (2009). Removal of disinfection by-product precursors by UF and NF membranes in low-SUVA waters. *J Memb. Sci*, **328 (1-2)**:104-112.

Baghoth, S.A. (2012). Characterizing Natural organic matter in drinking water treatment processes and trains. UNESCO-IHE institute for Water Education, MSc dissertation, The Netherlands University.

Bashiri, R., Mohamed, N.M., Kait, C.F., Sufian, S., Khatani, M. & Hanaei, H. (2016). Effect of Preparation Parameters on Optical Properties of Cu and Ni Doped $TiO_2$ Photocatalyst. *Procedia Eng*, **148**:151-157.

Baughman R, Zakhidov A. & de Heer, W.A. (2002). Carbon Nanotubes-The Route Toward Applications. *Science*, **297**:787-792.

Bokobza, L. (2007). Multiwall carbon nanotube elastomeric composites: A review. *Polymer*, **48 (17)**:4907-4920.

Bond, T., Kamal, N.H.M., Bonnisseau, T. & Templeton, M.R. (2014). Disinfection by-product formation from the chlorination and chloramination of amines. *J Hazard. Mater*, **278**:288-296.

Bose, P. & Reckhow, D.A. (2007). The effect of ozonation on natural organic matter removal by alum coagulation. *Water Res*, **41 (7)**:1516-1524.

Burda, C., Lou, Y., Chen, X., Samia, A.C.S., Stout, J. & Gole, J.L. (2003). Enhanced Nitrogen Doping in $TiO_2$ Nanoparticles. *Nano Lett*, **3**:1049-1051.

Casbeer, E., Sharma, V.K. & Li, X.Z. (2012). Synthesis and photocatalytic activity of ferrites under visible light: A review. *Sep Purif. Technol*, **87**:1-14.

Cedergren, M.I., Selbing, A.J, Löfman, O. & Källen, B.A.J. (2002). Chlorination by-products and nitrate in drinking water and risk for congenital cardiac defects. *Environ Res*, **89 (2)**, 124-130.

Chatterjee, D. & Dasgupta, S. (2005). Visible light induced photocatalytic degradation of organic pollutants. *J. Photochem. Photobiol*, **6 (2-3)**:186-205.

Chen, J., Gu, B., LeBoeuf, E.J., Pan, H. & Dai, S. (2002). Spectroscopic characterization of the structural and functional properties of natural organic matter fractions. *Chemosphere*, **48**:59-68.

Chen, W., Westerhoff, P., Leenheer, J.A & Booksh, K. (2003). Fluorescence excitation - Emission matrix regional integration to quantify spectra for dissolved organic matter. *Environ. Sci. Technol*, **37**:5701-5710.

Cheng, X., Yu, X., Xing, Z. & Yang, L. (2012). Synthesis and characterization of N-doped $TiO_2$ and its enhanced visible-light photocatalytic activity. *Arab. J. Chem*, 1-5.

Choi, H.J. & Kang, M. (2007). Hydrogen production from methanol/water decomposition in a liquid photosystem using the anatase structure of Cu loaded $TiO_2$. *Int. J. Hydrogen Energy*, **32 (16)**:3841-3848.

Comninellis, C., Kapalka, A., Malato, S., Parsons, S.A., Poulios, I. & Mantzavinos, D. (2008). Advanced oxidation processes for water treatment : advances and trends for R & D. *J Chem Technol Biotechnol*, **776**. 769-776.

Cook, R.L. (2004). Coupling NMR to NOM. *Anal. Bioanal. Chem*, **378 (6)**:1484-1503.

Croft, J. (2012). Natural Organic Matter Characterization of Different Source and Treated Waters ; Implications for Membrane Fouling Control. MSc dissertation, University of Waterloo.

Di Paola, A., García-López, E., Marcì, G. & Palmisano, L. (2012). A survey of photocatalytic materials for environmental remediation. *J. Hazard. Mater*, 211-212:3-29.

Do, T.D., Chimka, J.R. & Fairey, J.L. (2015). An improved (and singular) disinfectant protocol for indirectly assessing organic precursor concentrations of trihalomethanes and dihaloacetonitriles. *Environ. Sci. Technol*, 1-30.

Elsaesser, A. & Howard, C.V. (2012). Toxicology of nanoparticles. *Adv. Drug Deliv. Rev*, **64 (2)**:129-137.

Fabris, R., Chow, C. W. K., Drikas, M., & Eikebrokk, B. (2008). Comparison of NOM character in selected Australian and Norwegian drinking waters. *Water Research*, **42**, 4188–4196.

Farré, M. & Gajda-schrantz, K. (2009). Ecotoxicity and analysis of nanomaterials in the aquatic environment. *Anal Bioanal Chem*, 81-95.

Galindo, C., Jacques, P. & Kalt, A. (2000). Photodegradation of the aminoazobenzene acid orange 52 by three advanced oxidation processes: UV/$H_2O_2$, UV/$TiO_2$ and VIS/$TiO_2$. *J. Photochem. Photobiol. A Chem*, **130**:35-47.

Gao, B., Chen, G.Z. & Li Puma, G., (2009). Carbon nanotubes/titanium dioxide (CNTs/$TiO_2$) nanocomposites prepared by conventional and novel surfactant wrapping sol-gel methods exhibiting enhanced photocatalytic activity. *Appl. Catal.*

*B Environ*, **89 (3-4)**, 503–509.

Gopal, K., Tripathy, S.S., Bersillon, J.L. & Dubey, S.P. (2007). Chlorination by-products, their toxicodynamics and removal from drinking water. *J Hazard Mater*, **140 (1-2)**:1-6.

Goslan, E.H., Wilson, D., Banks, J., Hillis, P., Campbell, A. & Parsons SA. (2004). Natural organic matter fractionation: XAD resins versus UF membranes. An investigation into THM formation. *Water Science and Technology: Water Supply*, **4**:113-119.

Gramss, G., Ziegenhagen, D. & Sorge, S. (1999). Degradation of soil humic extract by wood and soil-associated fungi, bacteria, and commercial enzymes. *Microbial Ecology*, **37 (2)**,140–151.

Grinhut, T., Hadar, Y. & Chen, Y. (2007). Degradation and transformation of humic substances by saprotrophic fungi: processes and mechanisms. *Fungal Biol. Rev*, **21**:179-189.

Haarhoff, J., Kubare, M., Mamba, B., Krause, R., Nkambule, T., Matsebula, B. & Menge, J. (2009). NOM characterization and removal at six Southern African water treatment plants. *Drink Water Eng. Sci. Discuss*, **2**:231-257.

Haarhoff, J., Mamba, B., Krause, R. & Staden, S.V. (2013). Natural organic matter in drinking water sources : its characterization and treatability. Water Research Commission report, University of Johannesburg, 1-89.

Hanaor, D.A.H. & Sorrell, C.C. (2011). Review of the anatase to rutile phase transformation. *J material Sci*, **46**: 855-874.

Huang, X., Leal, M. & Li, Q. (2008). Degradation of natural organic matter by $TiO_2$ photocatalytic oxidation and its effect on fouling of low-pressure membranes. *Water Res*, **42**:1142-1150.

Jiang, L., Wang, Y. & Feng, C. (2012). Application of photocatalytic technology in environmental safety. *Procedia Eng*, **45**:993-997.

Joshi, M., Bhattacharyya, A. & Ali, S.W. (2008). Characterization techniques for nanotechnology applications in textiles. *Indian J. Fibre Text. Res*, **33 (3)**:304-317.

Jwo, C.S., Tien, D.C., Teng TP, Chang, H., Tsung, T.T., Liao, C. & Lin, C. (2005). Preparation and UV characterization of $TiO_2$ nanoparticles synthesized by SANSS. *Rev. Adv. Mater. Sci*, **10 (3)**:283-288.

Kang, S.Z., Cui, Z. & Mu, J. (2015). Composite of Carboxyl - Modified Multi - walled Carbon Nanotubes and $TiO_2$ Nanoparticles : Preparation and Photocatalytic Activity. *Fullerenes, Nnanotubes, and Nanostructures*, **15**:81-88.

Khairy, M. & Zakaria, W. (2014). Effect of metal-doping of $TiO_2$ nanoparticles on their photocatalytic activities toward removal of organic dyes. *Egypt J Pet*, **23 (4)**:419-426.

Kim, H. C., & Yu, M. J. (2005). Characterization of natural organic matter in conventional water treatment processes for selection of treatment processes focused on DBPs control. *Water Research*, **39**:4779–4789.

Kim, H. C., Yu, M. J. & Han, I. (2006). Multi-method study of the characteristic chemical nature of aquatic humic substances isolated from the Han River, Korea. *Appl Geochemistry*, **21 (7)**:1226-1239.

Kim, H. C., & Yu, M. J. (2007). Characterization of aquatic humic substances to DBPs formation in advanced treatment processes for conventionally treated water. *J. Hazard. Mater*, **143 (1-2)**:486-493.

Kuvarega, A.T., Krause, R.W.M. & Mamba, B.B. (2011). Nitrogen / Palladium-Codoped $TiO_2$ for Efficient Visible Light Photocatalytic Dye Degradation. *Society*, 22110–22120.

Kuvarega, A.T., Krause, R.W.M. & Mamba, B.B. (2012a). Multiwalled carbon nanotubes decorated with nitrogen, palladium co-doped $TiO_2$ (MWCNT /N, Pd co-doped $TiO_2$) for visible light photocatalytic degradation of Eosin Yellow in water. *J Nanopart Res*, **14:776.**

Kuvarega, A.T., Krause R.W.M. & Mamba, B.B. (2012b). Photocatalytic performance of nitrogen-platinum group metal co-doped $TiO_2$ supported on carbon nanotubes for visible-light degradation of organic pollutants in water. PhD thesis, University of Johannesburg.

Kuvarega, A.T. & Mamba, B.B. (2016). $TiO_2$ -based Photocatalysis: Toward Visible Light-Responsive Photocatalysts Through Doping and Fabrication of Carbon-based Nanocomposites. *Critical Reviews in Solid State and Materials Sciences*,1–52.

Lamsal, R., Walsh, M. E., & Gagnon, G. A. (2011). Comparison of advanced oxidation processes for the removal of natural organic matter. *Water Research*, **45 (10)**, 3263–3269.

Latifoglu, A. (2003). Formation of trihalomethanes by the disinfection of drinking water. *Indoor Built Environ*, **12 (6)**:413-417.

Lee, M.K. (2005). Application of White-rot Fungi for the Biodegradation of Natural Organic Matter in Wastes. MSc dissertation, RMIT University.

Li, F.B. & Li, X.Z. (2002). Photocatalytic properties of gold/gold ion-modified titanium dioxide for wastewater treatment. *Appl. Catal. A Gen*, **228 (1-2)**:15-27.

Li, A., Zhao, X., Mao, R., Liu, H. & Qu, J. (2014). Characterization of dissolved organic matter from surface waters with low to high dissolved organic carbon and the related disinfection by-product formation potential. *J. Hazard. Mater*, **271**:228-235.

Liu, X., Wang, J., Liu, T., Kong, W. & He, X. (2015). Effects of Assimilable Organic Carbon and Free Chlorine on Bacterial Growth in Drinking Water. *plos one*, 1–11.

Lobanga, K.P. & Haarhoff, J. (2012). Natural organic matter removal from surface waters by enhanced coagulation, granular activated carbon adsorption and ion exchange. PhD thesis, University of Johannesburg.

Lobanga, K.P., Haarhoff, J. & van Staden, S.J. (2014). Treatability of South African surface waters by enhanced coagulation. *Water SA*, **40 (3)**:529-534. .

Lu, C. & Su, F. (2007). Adsorption of natural organic matter by carbon nanotubes. *Sep. Purif. Technol*, **58 (1)**:113-121.

Luo, X. Chen, C., Yang, J., Wang, J., Yan, Q, Shi, H. & Wang, C. (2015). Characterization of La/Fe/$TiO_2$ and Its Photocatalytic Performance in Ammonia Nitrogen Wastewater. *Int. J. Environ. Res. Public health*, **12 (11)**:14626–39.

Mahlambi, M.M., Mishra, A.K., Mishra, S.B., Krause, R.W.M., Mamba, B.B. & Raichur, A.M. (2015). $TiO_2$ Nanocatalysts Supported on a Hybrid Carbon-Covered Alumina Support : Comparison between Visible Light and UV Light Degradation of Rhodamine. *B Journal of Nanotech*, 2015:1-8.

Matilainen, A. (2007). Removal of the Natural Organic Matter in the different stages of the drinking water treatment process removal of the Natural Organic Matter in the different stages of the drinking water treatment process. PhD thesis, Tampere University of Technology.

Matilainen, A. & Sillanpää, M. (2010a). Removal of natural organic matter from drinking water by advanced oxidation processes. *Chemosphere*, **80 (4)**:351-365.

Matilainen, A., Vepsäläinen, M. & Sillanpää, M. (2010b). Natural organic matter removal by coagulation during drinking water treatment: A review. *Adv Colloid Interface Sci*, **159 (2)**:189-197.

Matilainen, A, Gjessing, E.T., Lahtinen, T., Hed, L., Bhatnagar, A. & Sillanpää, M. (2011). An overview of the methods used in the characterisation of natural organic matter (NOM) in relation to drinking water treatment. *Chemosphere*, **83 (11)**:1431-1442.

McKnight, D.M., Boyer, E.W., Westerhoff, P.K., Doran, P.T., Kulbe, T. & Andersen, D.T. (2001). Spectrofluorometric characterization of dissolved organic matter for indication of precursor organic material and aromaticity. *Limnology and*

*Oceanography*, **46**: 38-48.

Metsämuuronen, S., Sillanpää, M., Bhatnagar, A. & Mänttäri, M. (2012). Natural organic matter removal from drinking water by membrane technology. *Sep. Purif. Rev*, **43 (1)**:1-61

Murray, C.A. & Parsons, S.A. (2004). Removal of NOM from drinking water: Fenton's and photo-Fenton's processes. *Chemosphere*, **54**:1017-1023.

Najjar, R., Shokri, M. & Farsadi, S. (2015). Preparation of Pd-doped nano-$TiO_2$ in microemulsion and their application in photodegradation of C.I. Acid Yellow 23. *Desalin. Water Treat*, **54 (9)**:2581-2591.

Nkambule, T.I., Krause, R.W, Mamba, B.B. & Haarhoff, J. (2009a). Removal of natural organic matter from water using ion-exchange resins and cyclodextrin polyurethanes. *Phys. Chem. Earth*, **34 (13-16)**:812-818.

Nkambule, T.I., Krause, R.W.M., Mamba, B.B. & Haarhoff, J. (2009b). Characterisation of Natural Organic Matter (NOM) and its removal using cyclodextrin polyurethanes. *Water SA,* **35 (2)**:200-203.

Nkambule, T.I., Krause, R.W.M., Haarhoff, J. & Mamba, B.B. (2011). Treatability and characterization of Natural Organic Matter (NOM) in South African waters using newly developed methods. *Phys. Chem. Earth*, **36 (14-15)**:1159-1166.

Nkambule, T. I., Krause, R. W. M., Haarhoff, J., & Mamba, B. B. (2012a). Natural Organic Matter (NOM) in South african waters: characterization of NOM, treatability and method development for effective NOM removal from water. PhD thesis, University of Johannesburg.

Nkambule, T.I., Krause, R.W.M., Haarhoff, J. & Mamba, B.B. (2012b). Natural organic matter (NOM) in South African waters: NOM characterisation using combined assessment techniques. *Water SA*, **38 (5)**:697-706.

Nkambule, T.I., Krause, R.W.M., Haarhoff, J. & Mamba, B.B. (2012c). The characterisation of Natural Organic Matter (NOM) in South African waters. *Water Sci. Technol. Water Supply*, **12:**648-657.

Nosaka, Y., Matsushita, M., Nishino, J. & Nosaka, A.Y. (2005). Nitrogen-doped titanium dioxide photocatalysts for visible response prepared by using organic compounds. *Sci. Technol. Adv. Mater*, **6 (2)**:143-148.

Ozdemir, K. (2014). Characterization of Natural Organic Matter in Conventional Water Treatment Processes and Evaluation of THM Formation with Chlorine. *The Sci World Journ*, **2014**:1-7.

Pei, Y., Yu, J., Guo, Z, Zhang, Y., Yang, M., Zhang, J. & Junji, H. (2007). Pilot Study on Pre-Ozonation Enhanced Drinking Water Treatment Process. *Ozone Sci. Eng,* **29**:317-323.

Papageorgiou, A., Papadakis, N. & Voutsa, D. (2016). Fate of natural organic matter at a full-scale Drinking Water Treatment Plant in Greece. *Environ Sci Pollut Res*, **23**:1841–1851.

Peleato, N.M. (2013). Applications of principal component analysis of fluorescence excitation-emission matrices for characterization of natural organic matter in water treatment. MSc dissertation, University of Toronto.

Persson, T. & Wedborg, M. (2001). Multivariate evaluation of the fluorescence of aquatic organic matter. *Analytica Chimica Acta*, **434**: 179-192.

Pifer, A. D., & Fairey, J. L. (2012). Improving on $SUVA_{254}$ using fluorescence-PARAFAC analysis and asymmetric flow-field flow fractionation for assessing disinfection byproduct formation and control. *Water Research*, **46 (9)**: 2927–2936.

Riaz, N. (2013). Iron doped $TiO_2$ photocatalysts for environmental applications : fundamentals and progress. *Int Proc on Biol and Biomed*, 72-77.

Ritson, J.P., Graham, N.J.D., Templeton, M.R., Clark, J.M., Gough, R. & Freeman, C. (2014). The impact of climate change on the treatability of dissolved organic

matter (DOM) in upland water supplies : A UK perspective. *Sci. Total Environ*, 473-474:714-730.

Roe, J.L. (2011). Characterising natural organic matter in surface waters and the minimisation of disinfection by-product formation. PhD thesis, The University of Birmingham.

Seifvand, N. & Kowsari, E. (2016). Synthesis of Mesoporous Pd-Doped $TiO_2$ Templated by a Magnetic Recyclable Ionic Liquid for Efficient Photocatalytic Air Treatment. *Ind. Eng. Chem. Res*, **55 (40)**:10533-10543.

Sobantu, P. & Moodley, K.G. (2014). Development of methods for the separation and characterization of natural organic matter in dam. MTech , Durban University of Technology.

Solarska, S., May, T., Roddick, F A., & Lawrie, A. C. (2009). Isolation and screening of natural organic matter-degrading fungi. *Chemosphere*, **75 (6)**:751-758.

Świetlik, J. & Sikorska, E. (2006). Characterization of natural organic matter fractions by high pressure size-exclusion chromatography, specific UV absorbance and total luminescence spectroscopy. *Polish J. Environ. Stud*, **15 (1)**:145-153.

Thebe, T., Swartz, C.D., Morrison, I.R., Engelbrecht, W.J. & Loewenthal, R.E. (2000). Characterisation of Natural Organic Matter in South African coloured surface waters. *Water Institute of Southern Africa (WISA) Biennial Conference, Sun City, South Africa, 28 May -1 June 2000*, 1-11.

United States Environmental Protection Agency (USEPA) 2012 of the Drinking Water Standards and Health Advisories.

Uboncholakate, K., Sikong, L. & Saito, F. (2012). Photocatalytic disinfection of P.aeruginosa bacterial Ag-doped $TiO_2$ film. *Procedia Eng*, **32**:656-662.

Urbanowska, A. & Kabsch-Korbutowicz, M. (2016) Characteristics of Natural Organic Matter removed from water along with its treatment. *Envi Prot Engin*, **42 (2)**:183-195.

Uyak, V., Ozdemir, K. & Toroz, I. (2008). Seasonal variations of disinfection by-product precursors profile and their removal through surface water treatment plants. *Sci. Total Environ*, **390 (2-3)**:417-424.

Van Geluwe, S., Vinckier, C., Braeken, L. & Van der Bruggen, B. (2011). Ozone oxidation of nanofiltration concentrates alleviates membrane fouling in drinking water industry. *J. Memb. Sci*, **378 (1-2)**:128-137.

Wang, G. S., Liao, C. H., & Wu, F. J. (2001). Photodegradation of humic acids in the presence of hydrogen peroxide. *Chemosphere*, **42**, 379–387.

Wang, H. & Lewis, J.P. (2006). Second-generation photocatalytic materials: anion-doped $TiO_2$. *J. Phys. Condens*. *Matter*, **18 (2)**:421-434.

Wang, H., Wang, H.L. & Jiang, W.F. (2009). Solar photocatalytic degradation of 2, 6-dinitro-*p*-cresol (DNPC) using multi-walled carbon nanotubes (MWCNTs)-$TiO_2$ composite photocatalysts. *Chemosphere*, **75 (8)**:1105-1111.

Wei-Bin, T., Jie-Chung, L. & Jian-Yun, H. (2013). A Study of Removing SUVA and Trihalomethanes by Biological Activated Carbon. *International journal of environmental, Chemical, Ecological, Geological and Geophisical Engineering*, **7 (10)**:680-683.

Wershaw, R.L., Leenheer, J.A. & Cox, L. (2005). Characterization of dissolved and particulate natural organic matter (NOM) in Neversink Reservoir, New York Scientific Investigations Report 2005-5108. *US Geol. Surv. Sc.i Investi*.

Wu, F. C., Evans, R. D., & Dillon, P. J. (2003). Separation and characterization of NOM by high-performance liquid chromatography and on-line three-dimensional excitation emission matrix fluorescence detection. *Environmental Science and Technology*, **37 (16)**, 3687–3693.

Yang, G., Jiang, Z., Yang, G. & Yan, Z. (2010). Preparation of highly visible-light active N-doped $TiO_2$ photocatalyst. *J. Mater. Chem*, **20 (25)**: 5301.

Yang, Z., Lan-lan, Q., Peng-wei, T. & You-xian, Z. (2014). Review of N and Metal co-Doped $TiO_2$ for Water Purification under Visible Light Irradiation. *Int. Conf. Environ. Chem. Biol*, **78 (7)**:139-142.

Yu, H., Quan, X., Chen, S., Zhao, H. & Zhang, Y. (2008). $TiO_2$-carbon nanotube heterojunction arrays with a controllable thickness of $TiO_2$ layer and their first application in photocatalysis. *J. Photochem. Photobiol. A Chem*, **200 (2-3)**:301-306.

Yu, J., Ma, T. & Liu, S. (2011). Enhanced photocatalytic activity of mesoporous $TiO_2$ aggregates by embedding carbon nanotubes as electron-transfer channel. *Phys. Chem. Chem. Phys*, **13 (8)**:3491-3501.

Zularisam, A. W., Ismail, A. F. & Salim, R. (2006). Behaviours of natural organic matter in membrane filtration for surface water treatment - a review. *Desalination*, **194 (1-3)**:211-231.

# CHAPTER 3
# EXPERIMENTAL METHODOLOGY

## 3.1 INTRODUCTION

In this chapter the detailed experimental procedures and characterization methods that were followed in order to achieve the objectives of this study are presented.

## 3.2 REAGENTS AND SOLVENTS

Unless otherwise specified, all chemicals and reagents were from Sigma-Aldrich and were utilized with no further purification. Deionized water was utilized for dilution purposes and for TOC measurements.

## 3.3 OVERVIEW OF THE EXPERIMENTAL PROCEDURE

The methodology involved: (i) water sampling, which was characterized using pH, turbidity, conductivity, UV-Vis, DOC, SUVA and FEEM; (ii) synthesis using the modified sol-gel method and characterization of N, Pd co-doped $TiO_2$ (also referred as NPT) and MWCNTs/N, Pd co-doped $TiO_2$ (1% Pd) (also referred as CT) using FTIR, UV-Vis, Raman, TGA, XRD, SEM and EDS (iii) evaluation of the photoactivity of NPT and CT for the photodegradation of NOM in water (**Figure 3.1**).

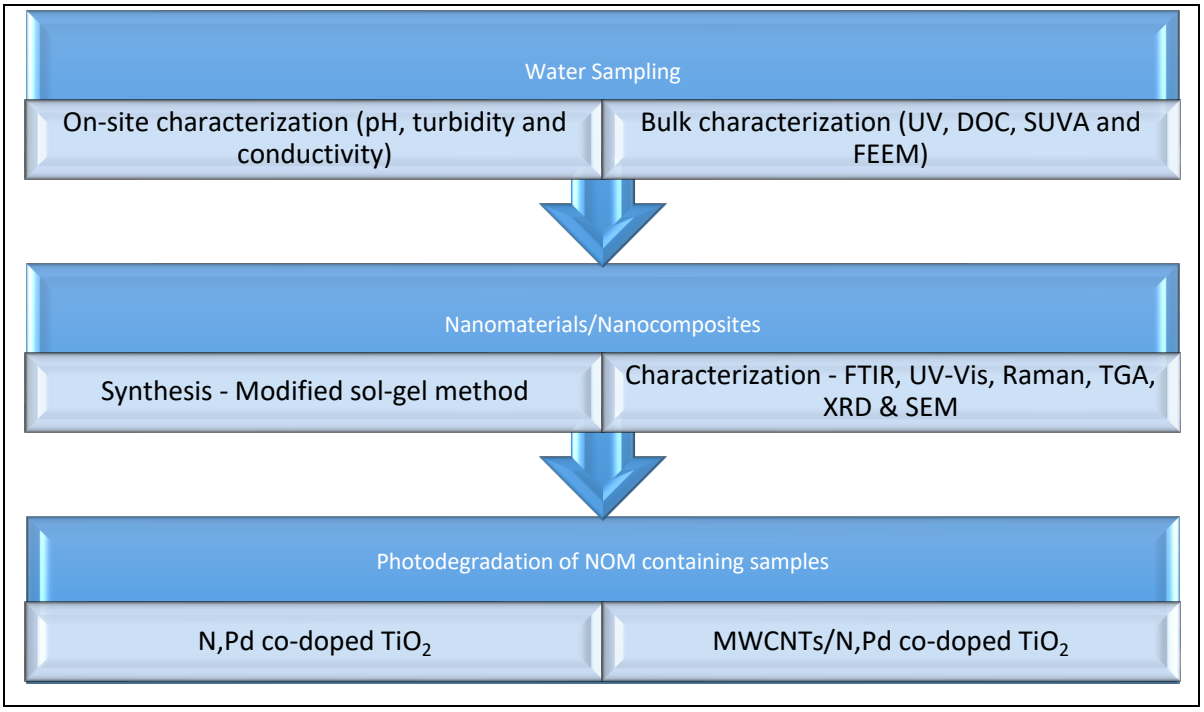


**Figure 3.1: Experimental flow diagram.**

## 3.4 SAMPLING

Water samples were collected using 1 ℓ glass bottles. The sample bottles were filled to the brim with water, with no head space in order to reduce any possible contamination which may occur as a result of trapped air. The majority of the samples were collected using a bucket hooked with a rod, while others were collected from the tap. The water samples were then stored in a cooler box loaded with ice cubes during the transportation of the samples. The sample's pH, electrical conductivity (EC) and turbidity were measured on site using a YSI professional plus portable multi-meter, which was calibrated prior to use with a pH 7/4 buffer and a 1413/12880 $\mu Scm^{-1}$ electrical conductivity solutions at 25 ˚C. Turbidity measurements were carried out using an orion AQ 3010 turbidity meter after calibrating it using calibrant 1-500 (Nephlometric Turbidity Units (NTU)), calibrant 2–100 NTU, calibrant 3-20 NTU and calibrant 4–0.02 NTU. Triplicate measurements were taken for each sample and the average ±standard error of the mean (SEM) was recorded. Upon arrival at the laboratory, the water samples were

kept in the refrigerator at 4 ˚C until further treatment and analyses (usually within 72 hours of sampling).

## 3.5 SAMPLING SITES

In order to accomplish the first objective of this work; which is to characterize NOM occurring in various water treatment plants across South Africa, extensive sampling was conducted and samples were collected after each treatment stage for each treatment plant (**Figure 3.2**). This was done with the aim of understanding the treatability of NOM and the efficiency of the various processes in their removal of NOM from water (Markechová *et al.*, 2013).

The treatment plants of interests are:

a) Magalies Water treatment plant (S25.6713˚/E27.2376˚) (MP1, MP2 and MP3), which draws its water from the Hartebeespoort Dam. This water is hypertrophic with high concentrations of nutrients, mainly algal blooms.

b) Rietvlei Water treatment plant (RV (S25.8773˚/E28.2644˚)) has its raw water drawn from the Rietvlei Dam. This water is categorized as eutrophic (supplemented by Highveld) mainly due to high return flows and agricultural run-offs. The water suffers from bad taste and odour. The plant has been experiencing water quality variation, algal issues and the clogging of the filters.

c) Umgeni Water treatment plant (HL (S29˚36.8726'/E031˚03.3145'), UM (S30˚19.7733'/E030˚403876'), MT (S30˚28.5690'/E030˚36.4260') and AM (S30.0350˚/E0.8901˚E) is categorized as montaigne water with high NOM content and low colour. It originates from warmer places of the Amatolo and Drakensberg area. The HL plant draws its water from Hazelmere Dam; UM from Umzinto Dam, MT from Mtwalume Dam and AM from Nungwane Dam.

d) Lepelle water treatment plant LE(S23˚56.676/E029˚59.1381'), LO(S24˚21.315'/E029˚45.5561') and LF(S24˚46.3454'/E29˚25.5491') is categorised as oligotrophic and has a low content of nutrients. The LE

water originates from Ebenezer Dam and is currently suffering from high algal blooms and has a low content of NOM. The LO water is from the Olifants River and has its catchments being affected by intensive mining activities (de Villiers & Mkwelo 2009). Lastly, the LF originates from Flag Boshielo Dam and has subsistence farming occurring in the catchment, which has resulted into land degradation due to soil erosion (Dabrowski *et al.*, 2014).

e) Midvaal Water (MV (S29.9303˚/E26.7972˚)) treatment plant draws its water from the Vaal River, which has a high urban development next to the water source. The water has high plant and NOM content.

f) Veolia Water treatment plant (VP (S34˚24.512'/E19˚12.474') and (VH (S34˚24.512'/E19˚12.474')) has VP drawing its surface water from De Bos Dam and is a highly coloured with moderate NOM content. VH draws its borehole water from Gateway and Hemel-en-Aarde boreholes, both of which have high content of manganese and iron.

g) Plettenberg Bay (P (S34.0575˚/E23.3645˚) Water treatment plant originates from Keurbooms River and is categorized as water that is high in colour and has a high content of humic substances.

**Table 3.1** shows the description of sampling codes used for the various stages of the water treatment processes from all the seven water treatment plants that were sampled. It also provides the sampling dates at which the samples were collected. It is important to note that for Magalies Water, all the plants uses one raw water source that is then channelled to three different sub-treatment plants (MP1, MP2 and MP3). Samples were collected from seven water treatment plants with different geographic locations in order to accommodate the various types of water present in South African water sources. Additionally, samples were collected in various rounds with the purpose of accommodating the effect of seasonal variation on NOM character.

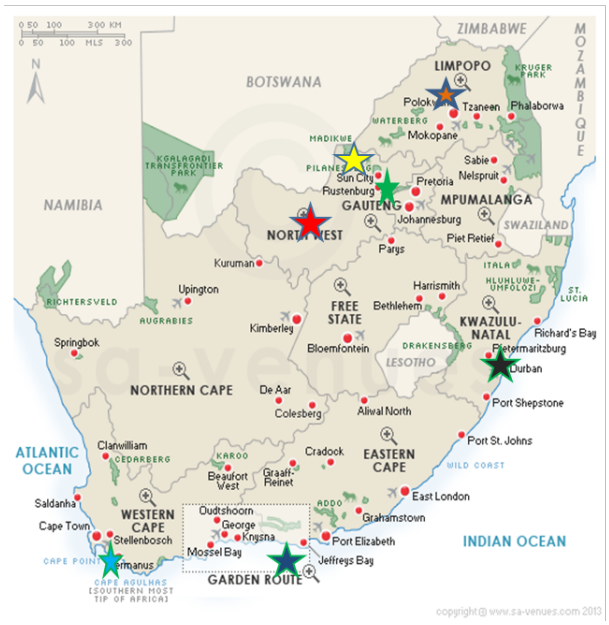


**Figure 3.2: The locations (shown by stars of various colors on the map) of the different sampling sites (google maps).**

**Table 3.1: Description of sampling codes from various water treatment plants**

| Water treatment plant | Code description/treatment stage | Sample Code | Sampling dates |
|---|---|---|---|
| **Magalies plant 1** | Raw water | MP1-1 | 11th November 2015, 06th May 2016 & 22nd July 2016 |
| | After dissolved air flotation | MP1-2 | |
| | After filtration | MP1-3 | |
| | After granular activated carbon | MP1-4 | |
| | After disinfection | MP1-5 | |
| **Magalies plant 2** | After pre-treatment | MP2-1B | |
| | After dissolved air flotation | MP2-2 | |

| | | | |
|---|---|---|---|
| | After sedimentation | MP2-3 | |
| | After filtration | MP2-4 | |
| | After disinfection | MP2-5 | |
| **Magalies plant 3** | After sedimentation | MP3-2 | |
| | After COCO dissolved air floatation | MP3-3 | |
| | After disinfection | MP3-5 | |
| **Rietvlei plant** | Raw water | RV-1 | 23rd November 2015, 26th February 2016, 30th April 2016, 5th July 2016 & 27th September 2016 |
| | After coagulation/flocculation | RV-2 | |
| | After granular activated carbon | RV-3 | |
| | After dissolved air flotation/filtration | RV-4 | |
| | After disinfection | RV-5 | |
| **Lepelle Northern water - Ebenezer plant** | Raw water | LE-1 | 24th February 2016, 05th May 2016, 30th June 2016 & 29th September 2016 |
| | After aeration | LE-2 | |
| | After coagulation/flocculation | LE-3 | |
| | After filtration | LE-4 | |
| | After disinfection | LE-5 | |
| **Lepelle Northern water- Olifantspoort plant** | Raw water | LO-1 | |
| | After settling (coagulation/ flocculation) | LO-2 | |
| | After filtration | LO-3 | |
| | After disinfection | LO-4 | |

| | | | |
|---|---|---|---|
| **Lepelle Northern water-Flag Boshielo plant** | Raw water | LF-1 | |
| | After settling (coagulation/ flocculation) | LF-2 | |
| | After filtration | LF-3 | |
| | After disinfection | LF-4 | |
| **Midvaal water** | Raw water | MV-1 | 2nd March 2016, 3th May 2016, 28th June 2016 & 26th September 2016 |
| | After pre-ozonation | MV-2 | |
| | Before flotation | MV-3 | |
| | After chemical dosing | MV-4 | |
| | After flotation | MV-5 | |
| | Before settling | MV-6 | |
| | After settling | MV-7 | |
| | After filtration | MV-8 | |
| | After disinfection | MV-9 | |
| **Plattenberg Bay plant** | Raw water | P-1 | 20th June 2016 & 20th September 2016 |
| | After flocculation | P-2 | |
| | After sedimentation | P-3 | |
| | After filtration | P-4 | |
| | After disinfection | P-5 | |
| **Veolia Water - Preekstoel (Surface water)** | Raw water | VP-1 | 21st June 2016 & 19th September 2016 |
| | After mixing | VP-2 | |
| | After sedimentation | VP-3 | |
| | After filtration | VP-4 | |
| | After disinfection | VP-5 | |

| | | | |
|---|---|---|---|
| **Veolia Water - Hermanus plant (Borehole water)** | Raw water | VH-1 | |
| | After filtration (Manganese) | VH-4 (Mn) | |
| | After filtration (Iron) | VH-4 (Fe) | |
| **Amanzimtoti plant** | Raw water | AM-1 | 24th June 2016 & 22nd September 2016 |
| | After coagulation | AM-2 | |
| | After clarification | AM-3 | |
| | After filtration | AM-4 | |
| | After disinfection | AM-5 | |
| **Hazelmere plant** | Raw water | HL-1 | |
| | After coagulation | HL-2 | |
| | After clarification | HL-3 | |
| | After filtration | HL-4 | |
| | After disinfection | HL-5 | |
| **Umzinto plant** | Raw water | UM-1 | |
| | After coagulation | UM-2 | |
| | After clarification | UM-3 | |
| | After filtration | UM-4 | |
| | After disinfection | UM-5 | |
| **Mtwalume plant** | Raw water | MT-1 | |
| | After coagulation | MT-2 | |
| | After clarification | MT-3 | |
| | After filtration | MT-4 | |
| | After disinfection | MT-5 | |

## 3.6 CHARACTERIZATION OF WATER SAMPLES

### 3.6.1 Dissolved organic carbon (DOC) analysis

The water samples were initially filtered using a 25 mm diameter Acrodisc syringe filters with 0.45 µm pore size. Prior to DOC analysis, the TOC analyser (Teledyne Tekmar, TOC Torch) was calibrated using potassium hydrogen phthalate (KHP) standards of 2, 5, 10, 20 mg/ ℓ concentrations and was used to measure the DOC (Nkambule *et al.*, 2009). Clean vials (40 mℓ with Teflon septum caps) were used for DOC analysis. The water samples were not filled up to the brim in order to minimize formation of air bubbles while DOC measurements were being carried out. Measurements were carried out in triplicates and an average DOC value for each water sample was recorded.

### 3.6.2 UV-Vis analysis

A UV-Vis spectrometer (Lambda 650 S, Perkin Elmer) was used to measure the UV character of all the water samples. For each water sample, a full wavelength spectrum was obtained in the range 200 to 800 nm (Nkambule *et al.*, 2009). Furthermore, the absorbance at each of the four wavelengths (i.e. 214, 254, 272, and 300 nm) were measured for each sample (Nkambule *et al.*, 2011). All the absorbance values were converted to per meter by multiplying each value of UV by 100. The data obtained was used to calculate SUVA according to Equation 3.1).

### 3.6.3 SUVA analysis

The specific ultra violet absorbance (SUVA) for each water sample was calculated using the following formula:

$$\mathrm{SUVA}\left(\frac{\mathrm{L}}{\mathrm{mg}}.\mathrm{m}\right)=\frac{\mathrm{UV_{254}}(\mathrm{cm^{-1}})\times 100\left(\frac{\mathrm{cm}}{\mathrm{m}}\right)}{\mathrm{DOC}\left(\frac{\mathrm{mg}}{\mathrm{L}}\right)} \qquad [3.1]$$

### 3.6.4 FEEM analysis

FEEM (Horiba AquaLog model spectrometer) was used to better understand the character of NOM present in water. Deionized water was used for calibration in order to perform the Aqualog validation test. The FEEM utilises xenon excitation as a light source and 10 nm band pass excitation and emission slits. In order to obtain EEMs, the excitation wavelengths were increased from 200 to 800 nm with a band pass of 5 nm. Finally, for each of the excitation wavelengths, the emission at longer wavelengths was detected at 0.3 nm intervals (Nkambule *et al*., 2012a).

A blank (deionized water with the known DOC) was subtracted from the fluorescence spectra of the sample in order to account for Raleigh scattering, which is a huge problem when using this spectrometer. For monitoring and correction of both the excitation spectrum for the emission detector and the absorbance signals, the reference detector of the AquaLog spectrometer was used. The transmission detector was utilised for recording the transmission spectrum of the sample under the same spectral-band pass and resolution conditions as the fluorescence EEM data.

## 3.7 SYNTHESIS OF NPT NANOMATERIALS

A modified sol-gel procedure was used to synthesize NPT and ammonium hydroxide was used as a source of nitrogen, hydrolysis reagent and palladium diamine dichloride solvent for the Pd precursor (**Figure 3.3**). To 2-propanol (25 mℓ), titanium isopropoxide (5 mℓ) was added and stirred for 10 minutes to form solution B. The relevant palladium diamine dichloride (0.006 g, 0.012 g, 0.015 g, 0.018 g, 0.02 g and 0.030 g) was dissolved in ammonia to give Pd: Ti ratio of 0.2%, 0.4%, 0.5%, 0.6%, 0.8% and 1.0% respectively; this solution (solution A) was then added slowly and under vigorous stirring to the solution B for 1 hour. The resulting solution was evaporated overnight in oven at 80 ˚C to yield a powdery solid, which was calcined in an electric furnace for 2 hours at 500 ˚C. The powdery solid was thereafter characterized by FTIR, UV-Vis, Raman, XRD, TGA and SEM in order to obtain structural, thermal, and morphological information (Kuvarega *et al*., 2011).

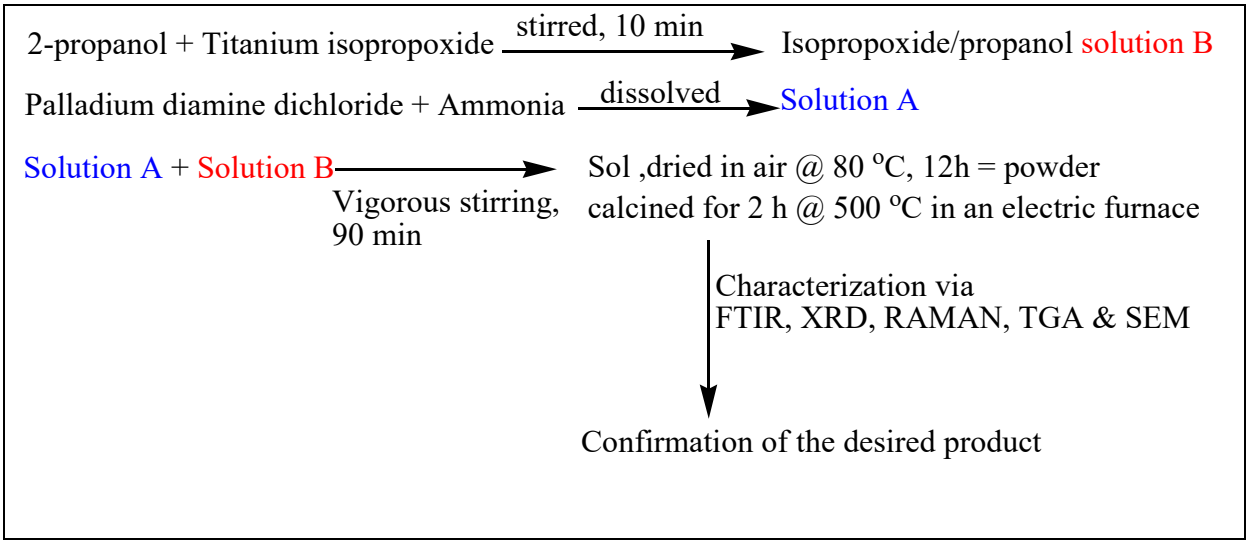


**Figure 3.3: Modified sol-gel method for synthesis of NPT.**

## 3.8 SYNTHESIS OF CT NANOCOMPOSITES

CT nanocomposites were prepared based on the method described by Kuvarega *et.al.* (2012a) (**Figure 3.4**). The relevant MWCNTs (0.01 g, 0.02 g, 0.05 g and 0.13 g) was dispersed in a mixture of 2-propanol, (50 mℓ) and titanium isopropoxide (10 mℓ) to give a MWCNT:$TiO_2$ percentage of 0.5%, 1.0%, 3.0% and 5.0%, respectively. The mixture was sonicated at room temperature for 45 min to improve MWCNTs dispersion. Palladium diamine dichloride (0.015 g; Pd: Ti ratio of 0.5%) was dissolved in ammonia (3 mℓ). The solution was then slowly added to the MWCNTs / solution B mixture while stirring vigorously for 90 min and the resultant suspension was dried overnight in an oven set at 80 ˚C. The resulting powder was calcined for 2 h at 350 ˚C in air in an electric furnace and thereafter characterized by FTIR, UV-Vis, Raman, XRD, TGA and SEM in order to obtain structural, thermal, and morphological information (Kuvarega *et al.*, 2012a).

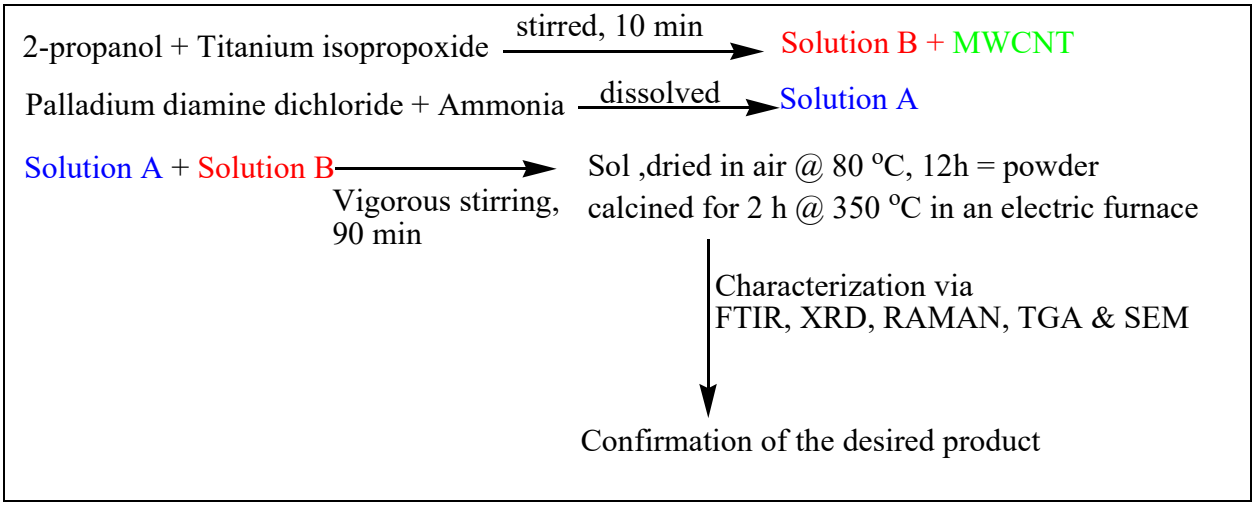


**Figure 3.4: Modified sol-gel method for synthesis of CT nanocomposites.**

## 3.9 CHARACTERIZATION OF NANOMATERIALS AND NANOCOMPOSITES

### 3.9.1 Fourier Transform Infrared (FTIR) and Raman spectroscopy

FTIR spectra were carried out using a Perkin Elmer (FT-ATR Spectrum 100) spectrometer, using a spectral resolution of 4 $cm^{-1}$ and averaging a total number of 4 scans. The samples were analysed in their powder form.

Raman analysis was carried out on a Raman II FT-Raman module equipped with Vertex-70 FTIR spectrometer. The resolution of 4 $cm^{-1}$ was used and a total number of 64 scans/samples was performed.

### 3.9.2 X-ray diffraction (XRD) spectroscopy

XRD analysis was conducted using Rigaku Smartlab. Japan X-ray diffractometer was operated with a Cu Kα radiation source at a 0.15406 nm wavelength and produced at 45 kV and 200 mA. Powdered samples were mounted on a Si sample holder using a bracket sample stage. Measurements were conducted at 2 θ degree angles over the range of 0° to 80°. The results were generated using Smartlab Rigaku control software PDXL.

### 3.9.3 Ultra-violet visible (UV-Vis) spectroscopy

UV-Vis spectroscopy was for determining the optical properties of the materials and results were generated using diffuse reflectance UV-Vis absorption spectrophotometry on a UV-Vis spectrometer (Lambda 650 S) integrating sphere attachment. $BaSO_4$ was used as the standard.

Diffuse reflectance was then used to construct the Kubelka-Munk function (Equation 3.2), which is a basic method used to define the band gap of the powdered materials (Murphy 2007).

$$K = \frac{(1-R)^2}{2R} = F(R) \qquad [3.2]$$

Where *K* is reflectance in terms of Kubelka-Munk, *R* is a reflectance parameter and *F(R)* corresponds to the Kulbeka-Munk function.

In addition, the band gap ($E_g$) and the absorption coefficient (α) are related as in terms of Equation 3.3 (Kuvarega *et al.*, 2012b):

$$\alpha hv = A(hv - Eg)^n \qquad [3.3]$$

Where *α* corresponds to the absorption coefficient, *A* is a constant, *hv* refers to the energy of light, $E_g$ for the band gap and n is a constant that depends on the type of the transition mode of the band gap of that material.

When the allowed transition is indirect then n = 2, whereas n = ½ with the direct allowed transition. For semiconductors such as $TiO_2$, n = 2, however, doping the material may cause changes in this parameter (Kuvarega *et al.*, 2011).

### 3.9.4 Thermogravimetric analysis (TGA)

To obtain thermal stability data, TGA was performed on a Discovery TGA 5500 Thermal Analyzer at a heating rate of 10 ˚C/min over a range of 30 to 900 ˚C under nitrogen flow.

### 3.9.5 Scanning Electron Microscopy (SEM) and Energy Dispersive X-ray (EDS)

SEM and EDS were conducted using SEM JOEL IT 300 & OXFORD integrated system instrument. Powdered samples were loaded on the carbon tape and mounted on the sample holder.

## 3.10 EVALUATION AND PHOTOCATALYTIC ACTIVITY OF NPT AND CT

The photocatalytic performance of the NPT (0.2-1.0% Pd) was evaluated by quantifying the NOM degradation rate under a visible light source. NPT (0.05 g) was added in 50 mℓ of NOM containing samples. A solar simulator (HAL-320, ASAHI spectral, Japan. A 300 W Xenon lamp), at a distance of 34 cm from a reaction beaker, was used as a light source (**Figure 3.5**). Preciding the photodegradation reactions, the suspension was sonicated for 10 min and stirred using a magnetic stirrer in the absence of any light source for 1 h to permit for adsorption equilibrium (Kuvarega 2012). Aliquots of the suspension (3 mℓ) were withdrawn using a 6 mℓ Neomedic disposable syringe and filtered through a 0.45 µm Pall Acrodisc GHP membrane filter at 30 min intervals for 180 minutes. The amount of NOM in the filtered samples, for purpose of studying the effect of the catalyst on NOM, was monitored using a UV-Vis spectrometer. A similar procedure was used to investigate the photocatalytic activity of CT (0.5–5.0 % MWCNTs).

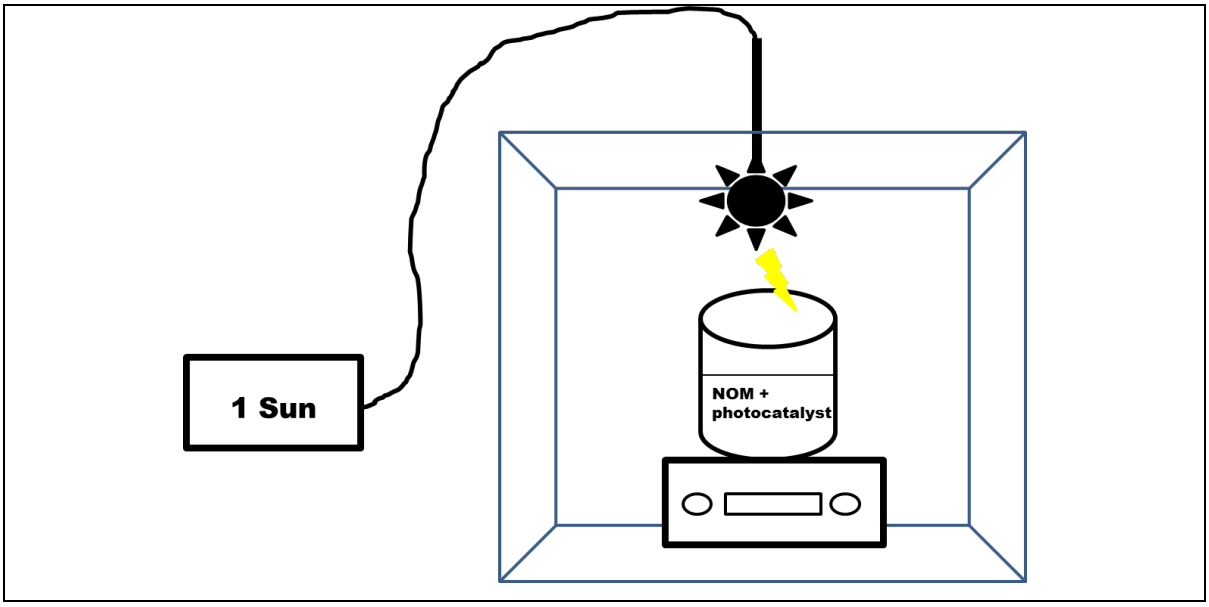


Power source NOM containg sample on magnetic stirrer, housed in a dark

**Figure 3.5: Experimental set-up for photocatalytic degradation of NOM.**

## 3.11 DATA HANDLING

All the raw data obtained was handled using excel and OriginPro 8 software.

## 3.12 REFERENCES


Dabrowski, J., Oberholster, P.J. & Dabrowski, J.M. (2014). Water quality of Flag Boshielo Dam, Olifants River, South Africa : Historical trends and the impact of drought. *Water SA*, **40 (2)**:345-358.

de Villiers, S. & Mkwelo, S.T. (2009) Has monitoring failed the Olifants River, Mpumalanga?. *Water SA*, **35 (5)**:671-676.

Kuvarega, A.T., Krause, R.W.M. & Mamba, B.B. (2011). Nitrogen / Palladium-Codoped $TiO_2$ for Efficient Visible Light Photocatalytic Dye Degradation. *Society*, 22110–22120.

Kuvarega, A.T., Krause R.W.M. & Mamba, B.B. (2012a). Photocatalytic performance of nitrogen-platinum group metal co-doped $TiO_2$ supported on carbon nanotubes for visible-light degradation of organic pollutants in water. PhD thesis, University of Johannesburg.

Kuvarega, A.T., Krause, R.W.M. & Mamba, B.B. (2012b). Multiwalled carbon nanotubes decorated with nitrogen, palladium co-doped $TiO_2$ (MWCNT/N, Pd co-doped $TiO_2$) for visible light photocatalytic degradation of Eosin Yellow in water. *J Nanopart Res*, 14:776.

Mamba, B.B., Krause, R.W., Matsebula, B. & Haarhoff, J. (2009). Monitoring natural organic matter and disinfection by-products at different stages in two South African water treatment plants. *Water SA*, **35 (1)**:121-127.

Markechová, D., Tomková, M. & Sádecká. J. (2013). Fluorescence excitation-emission matrix spectroscopy and parallel factor analysis in drinking water treatment: A review. *Polish J. Environ. Stud*, **22 (5)**:1289-1295.

Murphy, A.B. (2007). Band-gap determination from diffuse reflectance measurements of semiconductor films, and application to photoelectrochemical water-splitting. *Sol. Energy Mater. Sol. Cells*, **91 (14)**:1326-1337.

Nkambule, T.I., Krause, R.W, Mamba, B.B. & Haarhoff, J. (2009a). Removal of natural organic matter from water using ion-exchange resins and cyclodextrin polyurethanes. *Phys. Chem. Earth*, **34 (13-16)**:812-818.

Nkambule, T.I., Krause, R.W.M., Mamba, B.B. & Haarhoff, J. (2009b). Characterisation of natural organic matter (NOM) and its removal using cyclodextrin polyurethanes. *Water SA*, **35 (2)**:200-203.

Nkambule, T.I., Krause, R.W.M., Haarhoff, J. & Mamba, B.B. (2011). Treatability and characterization of Natural Organic Matter (NOM) in South African waters using newly developed methods. *Phys. Chem. Earth*, **36 (14-15)**:1159-1166.

Nkambule, T. I., Krause, R. W. M., Haarhoff, J., & Mamba, B. B. (2012). Natural Organic Matter (NOM) in South African waters: characterization of NOM, treatability and method development for effective NOM removal from water. PhD thesis, University of Johannesburg.

# CHAPTER 4
# EVALUATING THE CHARACTER OF NOM AND ITS REMOVAL BY SOUTH AFRICAN WATER TREATMENT PLANTS

## 4.1 INTRODUCTION

NOM in water compromises the water quality. This in turn poses a threat on the effectiveness of the available water treatment processes in the removal of NOM and other micro-pollutants present in water. Based on this information, most water treatment plants have now added NOM on their list of priority pollutants to be removed during the water treatment processes (Dlamini *et.al.,* 2012). Most of the water treatment plants are dependent on surface water as their feed, and this type of water is often compromised due to high agricultural run-offs, floods, droughts and other water re-use which negatively affects its supply (Haarhoff *et al.,* 2009).

This chapter provides a deeper understanding about the character of NOM occurring in South African waters and evaluate the effectiveness of various water treatment processes used by specific South African water treatment plants for the removal of NOM. The first step towards the removal of NOM from water is its characterization; since the character of NOM is not uniform across different water sources. Conventional methods such as DOC, $UV_{254}$ and SUVA are typically used for the characterization of NOM, however, these methods do not provide enough information about the composition of the NOM in water. Therefore, advanced characterization methods such as FEEM are required to close this information gap. Once the character of NOM is defined or understood then various NOM removal methods can be employed. The South African National Standards (SANS) and the World Health Organisation (WHO) have set the maximum allowable DOC levels at 10 mg/ℓ and 5 mg/ℓ, respectively (Nkambule *et al*., 2011). In principle, the readily available water treatment processes should be able to reduce NOM in water to below the acceptable standards (Mamba *et al*., 2009).

## 4.2 CONVENTIONAL METHODS FOR THE CHARACTERIZATION OF NOM

### 4.2.1 pH, turbidity and conductivity of the water

In the water industry pH is used to determine the alkalinity or the acidity of the water (Ashery *et al.,* 2010). The measured pH values of the WTPs under investigation ranged from 2.50 to 9.13 (**Table 9 &10 (Appendix)**). The pH values of the raw and final water are generally alkaline, with the most alkaline value recorded for Midvaal (MV). The raw water from the Preekstoel (VP-1) treatment plant is the most acidic water, and this could be because this water is very high in ion content (**Figure 4.1 (A)**). In principle, processes such as biofiltration also depend on pH for their proper functioning (Funes *et al.,* 2014). Thus the high pH levels of VP and VH final water could be due to the Fe and Mn not being effectively removed from the raw water source of the VH plant. This could be due to the presence of NOM in the water, which has been reported to compromise the removal of Fe and Mn (Ashery *et al.,* 2010). If Fe and Mn ions are not effectively removed from the solution, they tend to compete with $H^+$ ions for the active site on the biofilter or biosorbent surface (Zhang *et al.*, 2014). This affects the pH of the water of both the VH and VP due to the fact that the treated water from VH is then blended with the treated water from VP.

Similarly, the effectiveness of the coagulation process is also relient on the pH of the water (Nkambule *et al.,* 2011). The pH levels of the water before the coagulation process can affect the removal of NOM from that particular water source (Mamba *et al.*, 2009). The higher the pH, the lower the efficiency of NOM removal, and vice versa. This is because at lower pH levels, NOM can easily aggregate, which promotes an efficient removal of NOM from water (Mamba *et al.,* 2009). Furthermore, the effect of pH on NOM removal was also studied by Ashery *et al.*, (2010), and it was shown that the optimum removal was obtained when the water pH was adjusted to 5-6 before the addition of alum coagulant. This raise another important point; it is also important for the pH of the feed water to be determined prior to the coagulation step. In addition, according to the South African Target Water Quality, the allowable no risk pH should is between 6 and 9;

and it can be concluded from the results of the pH measurements that all the final water samples meet the allowable operational limits.

The turbidity of the water (**Figure 4.1 (B)**) can, on the other hand, be used as an indicator of the total amount of clay particles and colloids present in water (Nkambule *et al.,* 2012b). Ashery *et al*., (2010) studied the effect of pH on turbid water and observed that the optimum turbidity removal was at around pH 5–6 when using alum coagulant. In instances where the turbidity of water is higher than the accepted standards, processes such as flocculation and filtration could be affected during the water treatment (Obi *et al.,* 2009). Turbidity can also affect the effectiveness of chlorine during the disinfection step (Mamba *et al.,* 2009). The acceptable values of turbidity in water is between 0 to 1 NTU, and water with higher turbidity values may cause problems such as the ones mentioned above (Mamba *et al*., 2009).

In this study, the turbidity of all the water samples at their final stages of the treatment process was found to be in the range 0.0-3.0 NTU, with the Flag Boshielo Water plant (LF) having the highest turbidity value and the Magalies Water (MP1) having the lowest turbidity (**Figure 4.1 (B)**). The turbidity levels were found to decrease as the water passed through various treatment steps (**Table 1-11 (Appendix)**). The standard error of the mean values prove that the quality of raw water kept on changing for various sampling rounds. This can be attributed to natural causes such as floods, droughts and human activities performed near the raw water sources, which end up polluting the water sources.

Lastly, **Figure 4.1 (C)** shows the water conductivity measurement for the various WTPs. Water conductivity is highly dependent on the concentration of ions with the ability to transfer electrical current (Obi *et al.,* 2009). When the ion content in water is high, it increases the tendency of bursting of pipes and also may affect the health of the consumer by causing skin problems (Obi *et al.,* 2009). The allowable conductivity level for no risk is < 700 mS/cm. The measured levels of conductivity (**Figure 4.1 (C)**) of water samples was found to be in the range of 86.83-781.30 mS/cm, with the Ebenezer plant (LE) having the lowest conductivity and Olifantspoort plant (LO) having the highest conductivity. Moreover, the measured

conductivity values of the water samples varied from plant to plant. An increase in conductivity measurements was however observed as the water was being taken through the various treatment processes (**Table 1-11 (Appendix)**), mostly because of the introduction of various ions through the chemicals that were being used in the water treatment stages (Mamba *et al.,* 2009).

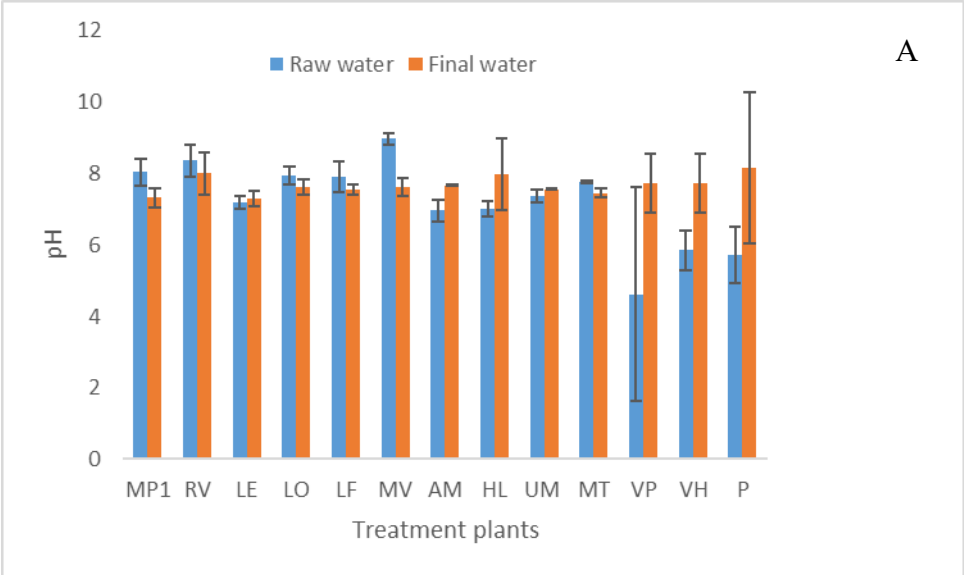


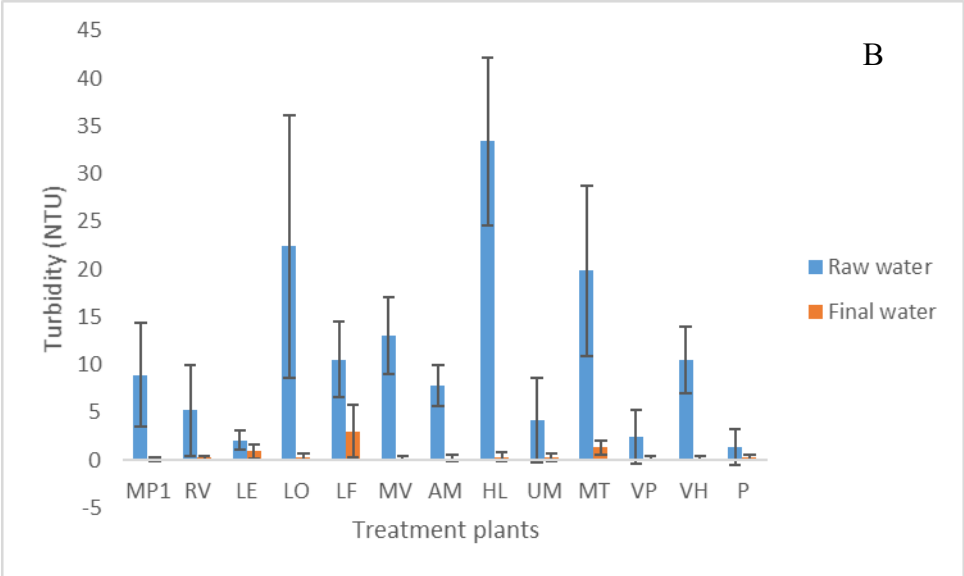

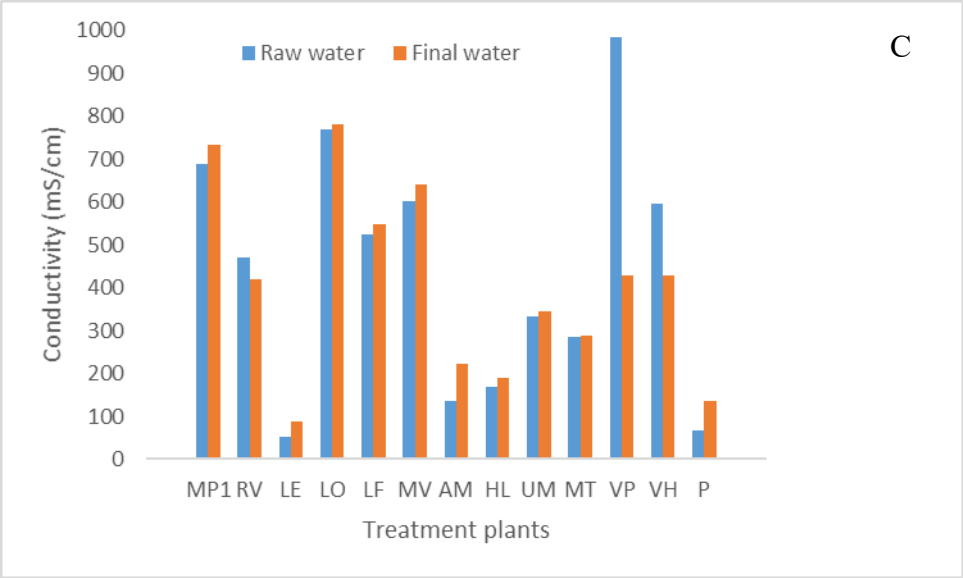


**Figure 4.1: pH (A), turbidity (B) and conductivity (C) measurements for the various WTPs.**

### 4.2.2 Removal of DOC

DOC levels varied throughout the water treatment process (**Table 1-11 (Appendix)**) for the various treatment plants. Secondly, it must be noted that the final water from most of the water treatment plants have DOC values below the allowable standards placed by both WHO and SANS (**Figure 4.2 (A)**), with MT plant and VH plant having the highest and lowest DOC values, respectively. In addition, these results also show that the plants from Umgeni (Durban, KwaZulu Natal) have the highest levels of NOM. This is concordant to literature reports that this water is montaigne with high NOM content and low colour (Dlamini *et.al.,* 2012).

The removal efficiency of DOC from water by the various water treatment plants is not similar, with P having the highest and HL having the lowest NOM removal (**Figure 4.2 (B)**). This is because the various treatment plants use different treatment processes and chemical dosages to treat the water. However, some plants with similar treatment processes still showed different NOM removal efficiencies (e.g. UM and MT). The observed differences in DOC removal could be

due to the different chemical dosages that is applied by UM and MT plants. The non-uniform character of NOM present in the raw waters of the two plants (**Appendix C**) also contributes to the observed differences in NOM removal. The character of the NOM of the raw water from the two plants (UM and MT) is different even though both plants are located within an hour from each other in Kwazulu-Natal. This significant difference is attributed to the different geology, topography and human activities (industrial and agricultural) being practised around the two raw water sources (Nkambule *et al.,* 2009). The raw water for UM is located in an area with high industrial, farming and other human-related activities, which occur upstream of the raw water source. MT on the other hand, has its water quality impacted by sand mining, which increases the water turbidity. These activities could be the core factor for the observed differences in DOC removal efficiency. Some studies have proven that the character of NOM can become non-uniform over the years due to natural causes such as increase in temperatures and decrease in acid deposition; and other human related activities such as industrial and agricultural activities (Evans *et al*., 2005).

A slight increase in the amount of DOC was observed for LE-3 (after sedimentation) in all the rounds of sampling as compared to LE-1 (raw water) and (after aeration) LE-2 (**Table 5 (Appendix)**). Degradation occurring on the edges of the sedimentation tank is often responsible for increased amounts of DOC levels (Mamba *et al*., 2009).

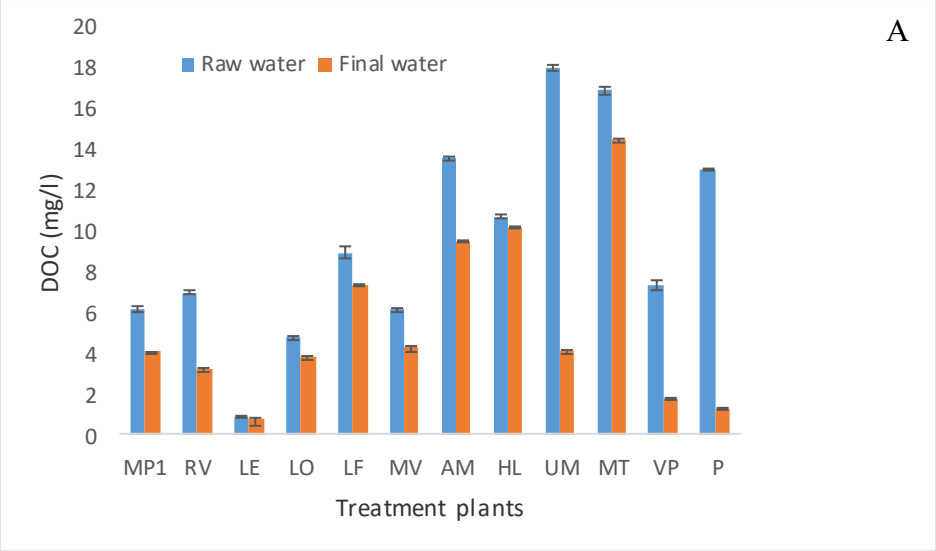

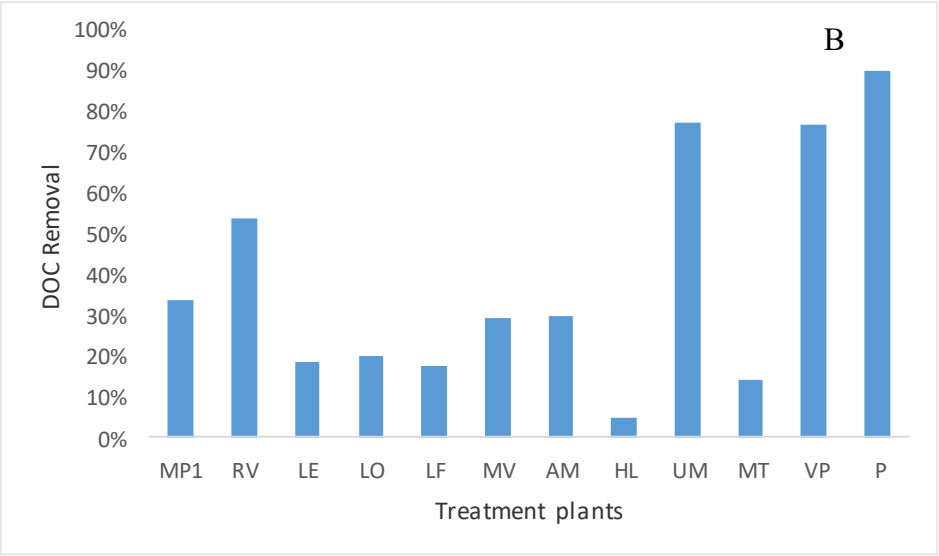


**Figure 4.2: DOC (A) and % DOC removal (B) for various WTPs.**

### 4.2.3 UV-Vis analysis of various water treatment plants

Any wavelength ranging from 220 to 280 nm is appropriate for the measurements of NOM (Nkambule *et al.,* 2012a). However, the molar absorptivity values vary due to the range of chromophores present in NOM. Specifically, the wavelength of 254 nm is associated with the aromatic character of the molecule and is also used in industries for the maximum absorption of NOM molecule (Nkambule *et al.,* 2009). Furthermore, 214 nm is associated with nitrites and nitrates, and 272 nm is the best predictor for the formation of trihalomethanes (Nkambule *et al.,* 2012b).

A decrease in the absorbance values of $UV_{254}$ from raw water to final water was observed for all the treatment plants (**Figure 4.3 (A)**), suggesting that the aromatic character of NOM is decreasing. Moreover, the raw water of all the plants under investigation generally has high $UV_{214}$ values, with the raw water of the VP plant having the highest $UV_{214}$ absorbance value (**Appendix B**). This mean that the raw water of the VP plant consists of a high nitrate and nitrite content. However, it should be noted that the $UV_{214}$ absorbance values decreases after the subsequent treatment steps. Also, the $UV_{272}$ absorbance values were found to be high, which means that the water has a great potential to form trihalomethanes (THMs). As

with the $UV_{214}$ absorbance values, the $UV_{272}$ absorbance values also decreased after the subsequent treatment steps.

Overall, the raw water from the Preekstoel (VP) and Plettenberg Bay (P) plants consists of NOM with high aromatic content and THM formation potential compared to the other water treatment plants. The water from these plants was also brownish relative to the water of all the other plants. These observations are in line with a study undertaken by Thebe *et.al*., (2000), which showed that the surface waters located along the coastal belt of the Southern Cape consists of high NOM concentrations with high colour content.

In addition, the obtained results show that the HL plant has the highest percentage removal of the aromatic content of NOM (as measured by the decrease of the $UV_{254}$) and LE has the lowest removal of aromatics (**Figure 4.3 (B)**). From these findings it can be concluded that most of the NOM in the water was removed by coagulation, which targets mainly the hydrophobic fraction (and by extension the aromatic character) of NOM. Similar findings, which were reported by Thebe *et.al.,* (2000), attribute this to the ease of removal associated with humic substances (i.e. compared to non-humic substances). Moreover, the observed difference in the removal efficiency of aromatic content of NOM ($UV_{254}$) could be due to the different types of coagulants being used by these plants. Equally important, the type of water (including its pH) being treated needs to be compatible with the type of coagulant being used in order to achieve optimum removal of the targeted pollutant (Mamba *et al.,* 2009).

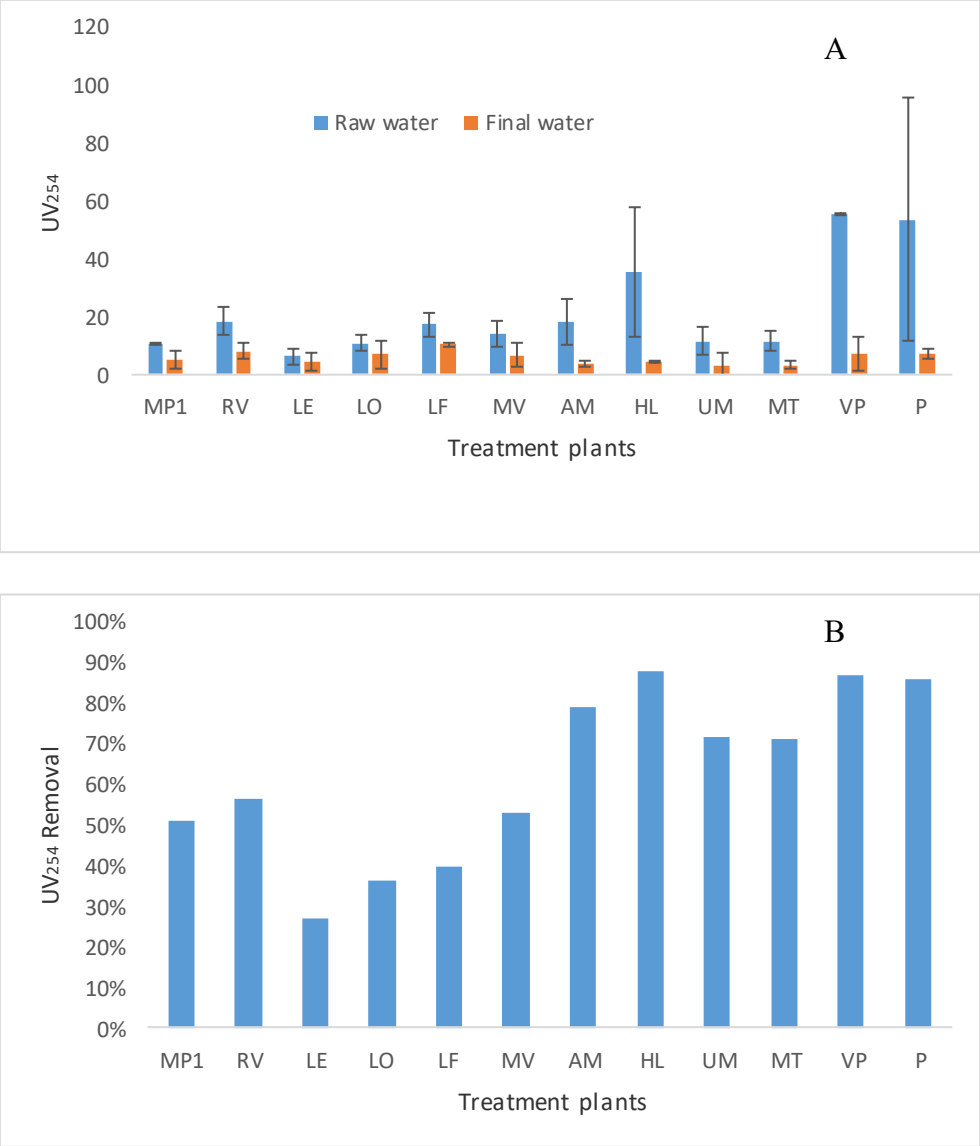


**Figure 4.3: $UV_{254}$ (A) and % $UV_{254}$ removal (B) for various WTPs.**

The raw water in most of the WTPs showed a relatively high absorbance compared to the water that was collected from other treatment steps (**Figure 4.4**). This was expected since the raw water consists of all the suspended particles and colloids which might also absorb some UV light (Nkambule *et al.*, 2012c). Moreover, there was a decrease in the UV absorbance after every treatment step in most plants, proving the effectiveness of the treatment processes in removing NOM and these results were consistent to what was observed by Nkambule *et.al.,* (2012a). RV-4 (after dissolved air filtration) absorbs higher than RV-3 (after GAC) and it also has a higher DOC content (**Figure 4.4 (A)**). This could be due to the

filters not being properly cleaned, thus overloaded or some defects in the filtration unit itself (Obi *et al.,* 2009). This possibly indicates that the filters need to be backwashed properly.

In addition, MV-2 (after pre-ozonation) and MV-4 (after chemical dosing) have higher absorbance values compared to MV-1 (**Figure 4.4 (B)**), and this might be due to the addition of chemicals (ozone during ozonation and ferric chloride with cationic polymer during chemical dosing) which could have reacted with the pollutants that were initially present in water. Accordingly, by-products (especially in the case of MV-2 which is the pre-ozonation process) can be formed and might absorb high UV compared to raw water sample (**Figure 4.4 (C)**). The same was observed for LE plant (**Figure 4.4 (B)**), with LE-5 having the highest DOC, $UV_{254}$ and turbidity compared to the water from the former treatment step and this could be due to the same reason as explained above. As expected from the brownish colour, the raw water sample for Plettenberg Bay (P) absorbed higher than the other samples (**Figure 4.4 (D)**). It can also be observed that P-4 (after filtration) absorbs lower than P-5 (after disinfection), this can be due to the sand filters being used by this plant, and this can prove the effectiveness of the filters in removing pollutants present in water. This allows the effective removal of most of the NOM present in water before the disinfection step thus limiting the formation of disinfectant by-products (DBPs) which are carcinorgenic to humans.

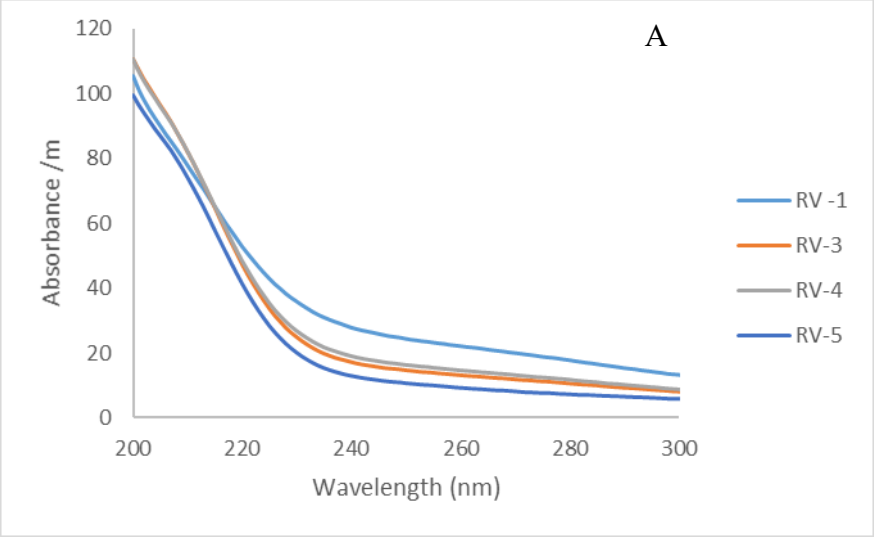

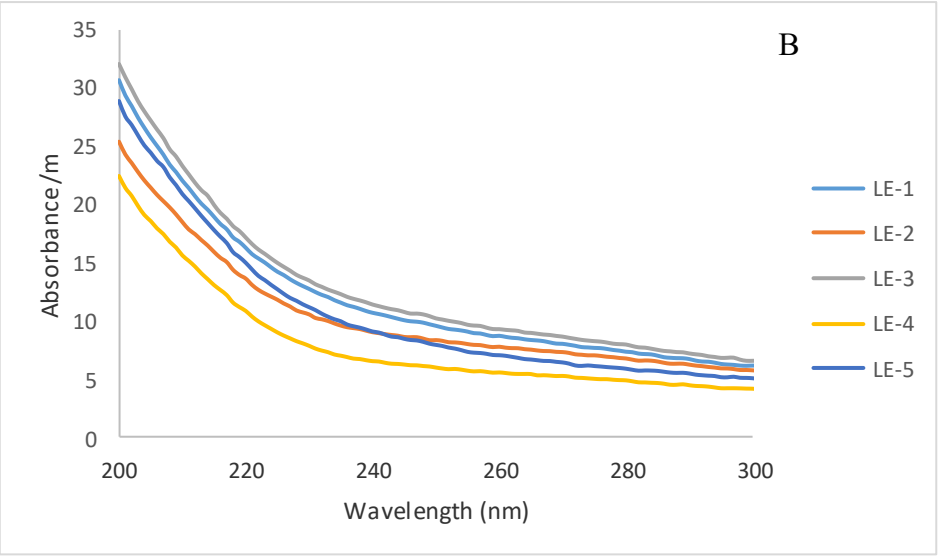
B
35
30
25
20
15
10
5
0
Absorbance/m
200
220
240
260
280
300
Wavelength (nm)
LE-1
LE-2
LE-3
LE-4
LE-5

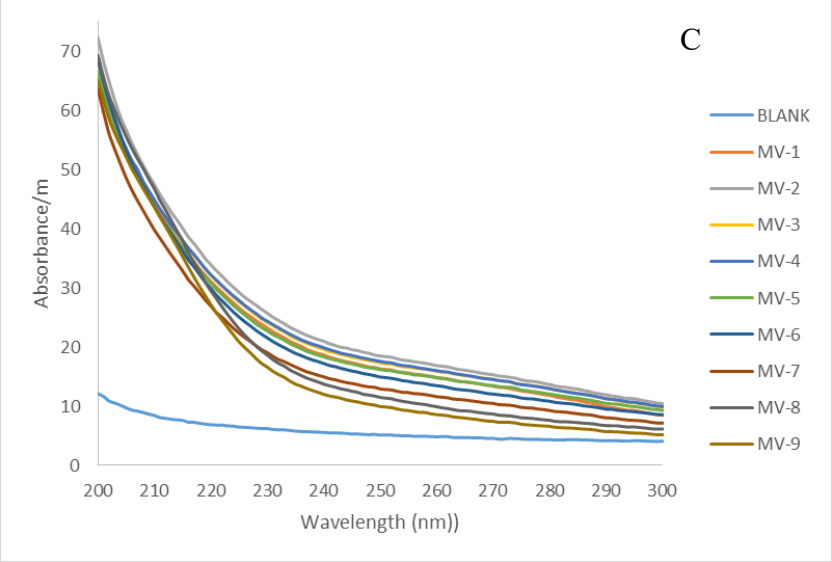
C
70
60
50
40
30
20
10
0
Absorbance/m
200
210
220
230
240
250
260
270
280
290
300
Wavelength (nm))
BLANK
MV-1
MV-2
MV-3
MV-4
MV-5
MV-6
MV-7
MV-8
MV-9

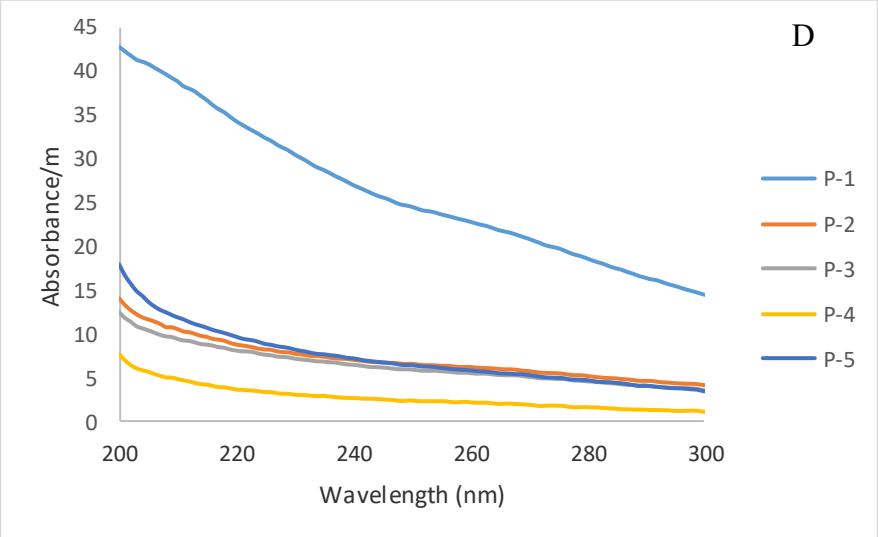


**Figure 4.4: UV scan for the Rietvlei plant (A), Ebenezer plant (B), Midvaal plant (C) and Plettenberg Bay treatment plant (D).**

### 4.2.4 SUVA analysis of various water treatment plants

The raw water for Magalies (MP1, 2 & 3) and Umzinto (UM) plants have SUVA values that are less than 2 (1.76 and 1.16 $\ell \cdot mg^{-1} \cdot m$ respectively) (**Figure 4.5**), meaning that the NOM is made up of non-humic substances and is hydrophilic in nature with their final water being more hydrophilic than the corresponding raw waters (1.42 and 0.87 $\ell \cdot mg^{-1} \cdot m$ respectively) (Świetlik & Sikorska 2006; Mamba *et al.,* 2009). For the RV, LE, LO, MV, AM and MT plants, the nature of NOM in the respective raw water is transphilic (3.87, 3.06, 2.38, 2.45, 2.26 and 2.02 $\ell \cdot mg^{-1} \cdot m$ respectively) and it remained in that form (2.77, 2.38, 2.46, 1.40, 0.87 and 0.90 $\ell \cdot mg^{-1} \cdot m$ respectively) throughout the treatment process for most of the plants except for MV, AM and MT plants which became hydrophilic. Lastly, the raw water for Preekstoel (VP), Hazelmere (HL) and Plettenberg Bay (P) was found to be hydrophobic in nature (7.74, 5.91 and 4.26, $\ell \cdot mg^{-1} \cdot m$ respectively), with the VP plant being the most hydrophobic (i.e. highly aromatic) (Nkambule *et al*., 2009; Haarhoff *et al.,* 2009; Matilainen *et al.,* 2011). Furthermore, the brownish colour of the raw waters is evidence of the high amount of humic substances in raw water

(Thebe *et al.*, 2000). Previous findings have shown that water with high SUVA has high DOC removal potential (Nkambule *et al*., 2012a). However, this study noted that this was not always the case because the DOC and $UV_{254}$ removal efficiency was observed to be a function of the type of coagulants used, coagulant dosages and the effectiveness of filters used by various treatment plants. For example, the VP plant, which had the highest SUVA values compared to the other water treatment plants did not show the highest DOC and $UV_{254}$ removal. Similarly, the UM plant, which registered the lowest SUVA values did not register the lowest $UV_{254}$ percentage removal. Furthermore, the results indicate that the character of NOM kept on changing throughout the treatment process (**Table 24-41 (Appendix)**).

The results also show that the SUVA increases in the order LE-2 (after aeration) > LE-1 (raw) and LE-5 (final) > LE-4 (after filtration) (**Table 28 (Appendix)**). From these findings, it is clear that addition of the coagulants and disinfectants to the water containing this type of NOM results in increased SUVA values (i.e. NOM becoming more transphilic in nature). Similar findings were observed for SUVA increasing in the order: LO-4 (final) > LO-3 (after filtration) and LF-4 (final) > LF-3 (after filtration) (**Table 29** & **30 (Appendix)**) and this could be due to a similar reason. Overall, the type of NOM present in the raw water sources for LE, LO and LF was not the same, even though all of these plants are located in the Limpopo Province. The difference in the SUVA values is probably due to the different industrial and agricultural activities being practised near the raw water sources. Similar results were observed for HL, AM, UM and MT plants which are located in KwaZulu Natal.

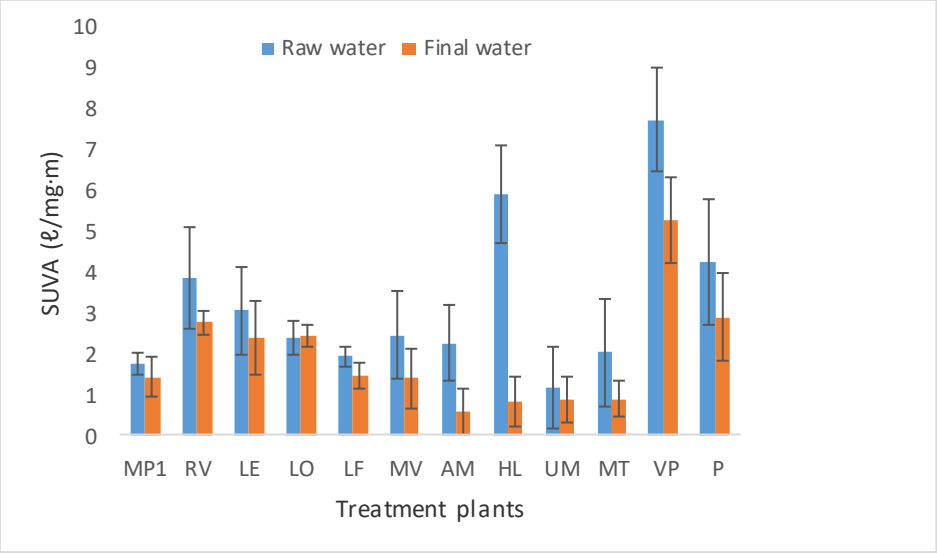


**Figure 4.5: SUVA values for samples from various water treatment plants.**

## 4.3 ADVANCED CHARACTERIZATION METHODS

### 4.3.1 Fluorescence excitation emission matrices (FEEM)

The principle behind FEEM is based on the fact that after a sample have been excited at a particular wavelength, a number of emission scans over various wavelengths are obtained and are used to define the composition of NOM. This technique is very useful as it has the ability to determine the amount and the nature of fluorophores being analysed. A FEEM label description graph, which shows the regional distribution of NOM fractions in water samples, is shown below in **Figure 4.6**. Unlike conventional characterization techniques such as DOC, UV and SUVA; which only defines the quantity and quality of NOM in water, respectively; FEEM has the potential of further defining the character of NOM (Nkambule *et al*., 2012a). Bieroza *et.al*., (2010) described FEEM as a process evaluating and optimizing tool for water treatment plants that is able to determine the properties of organic matter and the removal efficiency of dissolved organic matter throughout the treatment train. Thus this study focuses on using FEEM to better understand the composition of NOM occurring in various South African raw water sources. Equally important, it was also used to study the treatability of NOM by various treatment processes of the P treatment plant.

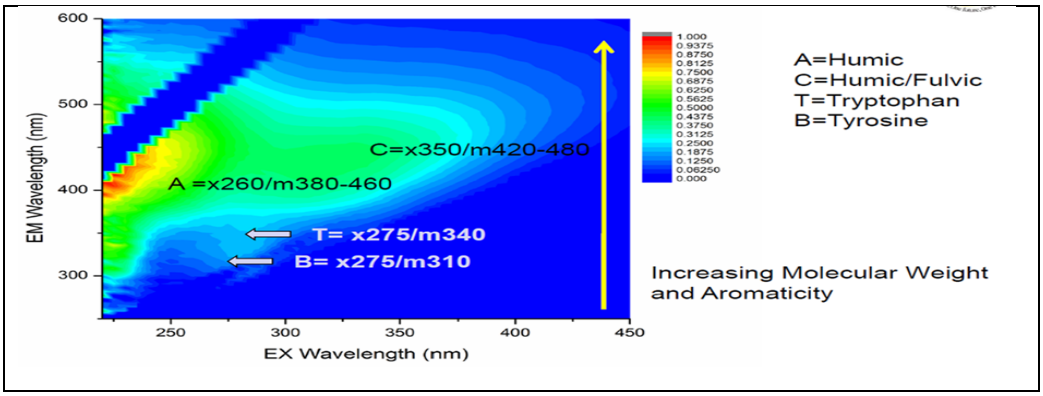


**Figure 4.6: An example of FEEM spectra for the classification of the EEM region of a raw water sample (Nkambule *et al*., 2012a).**

The fluorescence EEM spectra of the raw water samples for the RV and MV treatment plants showed a similar regional distribution of the NOM fractions. To this end, the FEEM spectra for the raw water samples of the RV (**Figure 4.7 (A)**) and MV (**Figure 4.7 (B)**) treatment plants indicates the presence of humic (A), trytophan (T) and tyrosine (B) fractions. Over and above the occurrence of these compounds, the RV water sample was found to contain the humic/fulvic-like fraction (C).

NOM fractions (humic and fulvic) were also observed albeit in different quantities in raw waters of VP, HL and P treatment plants (**Figures 4.7 (E)-(F)**). From these results, it can be concluded that the high $UV_{254}$ removal efficiency that was observed for these plants (VP, HL and P) was due to the presence of high amounts of humic substances in these treatment plants. The higher the amount of aromatics (shown by high $UV_{254}$) in water, the easier for that water to be treated through coagulation.

All the raw water samples (**Figures 4.7–4.8**) were found to contain, amongst others, the aromatic protein fraction, which has excitation (EX) and emission (EM) wavelength boundaries of 200-250 nm and 280-320 nm, respectively. Furthermore, the NOM of the raw water samples for the Lepelle treatment plant is

composed exclusively of the aromatic protein fraction (**Figures 4.7 (C)-(D)**). These results once again emphasize the notion of varying character of NOM that is found in various water sources. Most importantly, it highlights how the FEEM can be used to determine the NOM (humic substance) removal efficiency during the various stages of the water treatment process (Nkambule *et al*., 2012b). **Figure 4.8 (B)** indicates that after the coagulation process, most of the humic and fluvic components had already been removed. This proves that coagulation deals mostly with those molecules that are hydrophobic in nature (Matilainen *et al*., 2010; Lobanga *et al*., 2013; Bello *et al*., 2014). Moreover, water that has gone through the filtration process has very little or no traces of humic fractions (**Figure 4.8 (C)**). This is a good indication that the filters being used by the Plettenberg Bay (P) plant effectively remove organic pollutants (humic substances) from water.

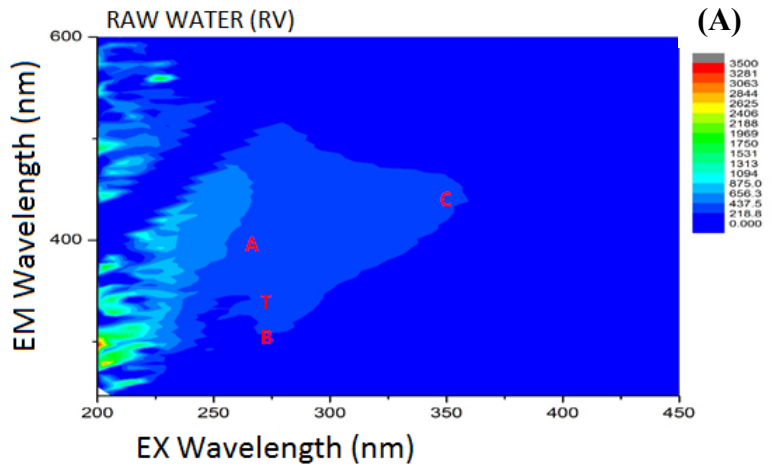


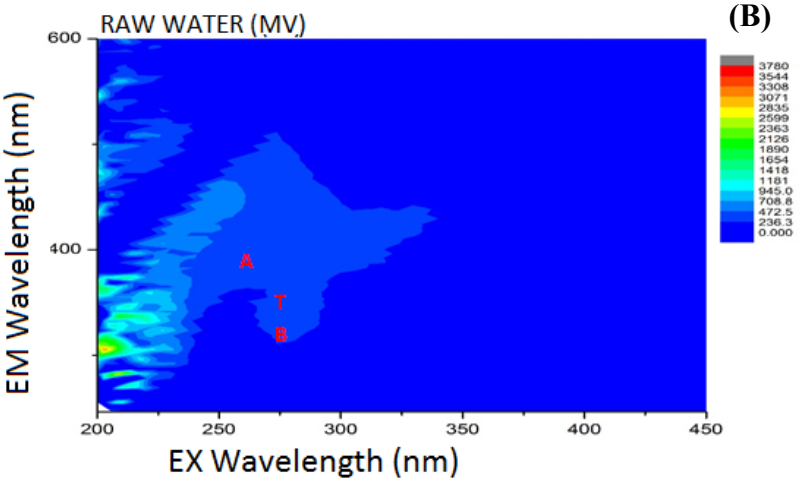

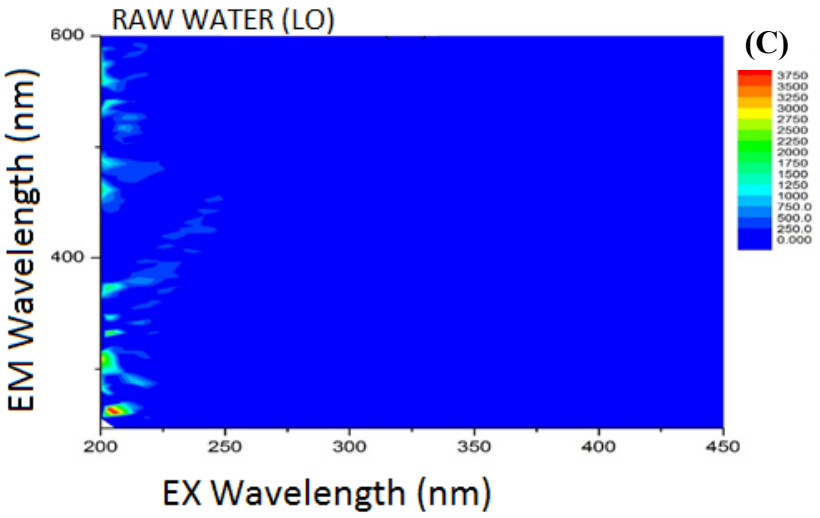
RAW WATER (LO)
(C)
EM Wavelength (nm)
EX Wavelength (nm)
600
400
200
250
300
350
400
450
3750
3500
3250
3000
2750
2500
2250
2000
1750
1500
1250
1000
750.0
500.0
250.0
0.000

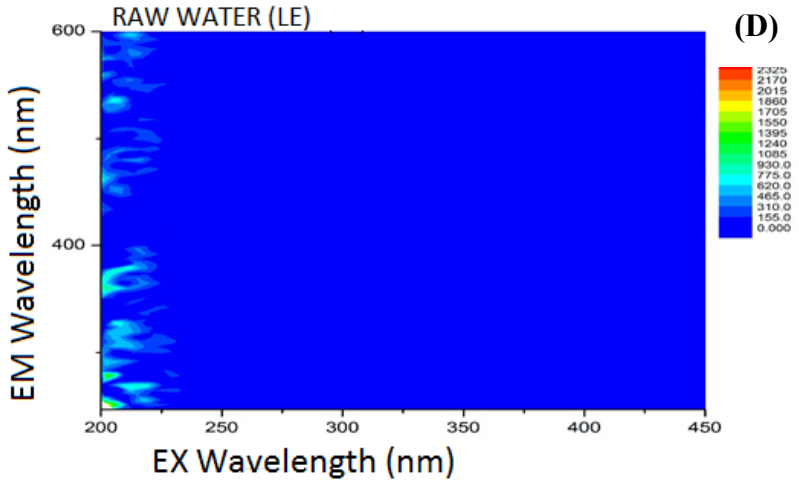
RAW WATER (LE)
(D)
EM Wavelength (nm)
EX Wavelength (nm)
600
400
200
250
300
350
400
450
2325
2170
2015
1860
1705
1550
1395
1240
1085
930.0
775.0
620.0
465.0
310.0
155.0
0.000

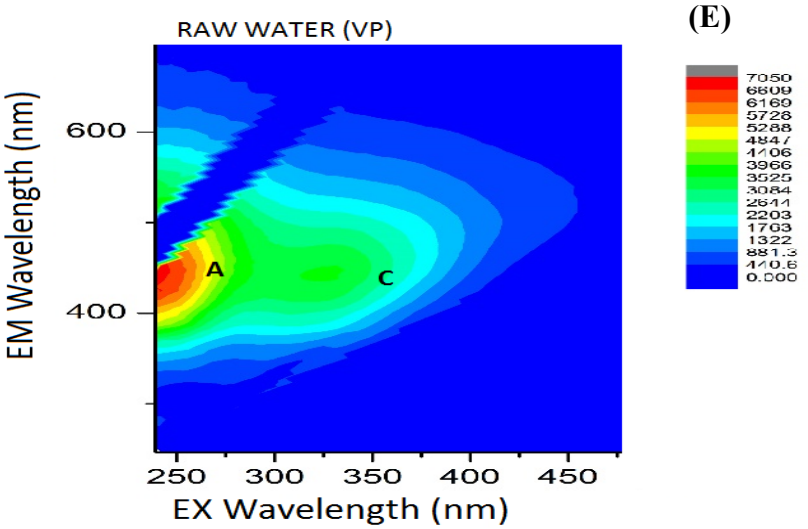
RAW WATER (VP)
(E)
EM Wavelength (nm)
EX Wavelength (nm)
600
400
250
300
350
400
450
A
C
7050
6609
6169
5728
5288
4847
4406
3966
3525
3084
2644
2203
1763
1322
881.3
440.6
0.000

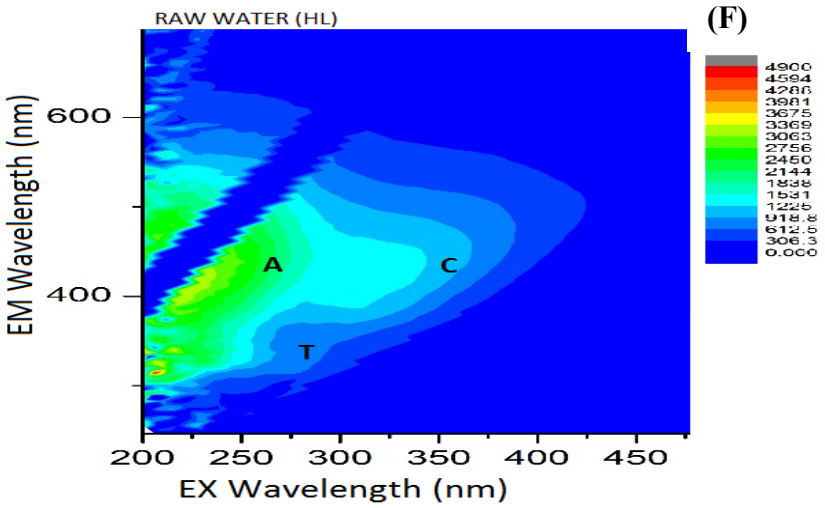


**Figure 4.7: FEEM spectra of the RV (A), MV (B), LO (C), LE (D), VP (E), HL (F) raw water.**

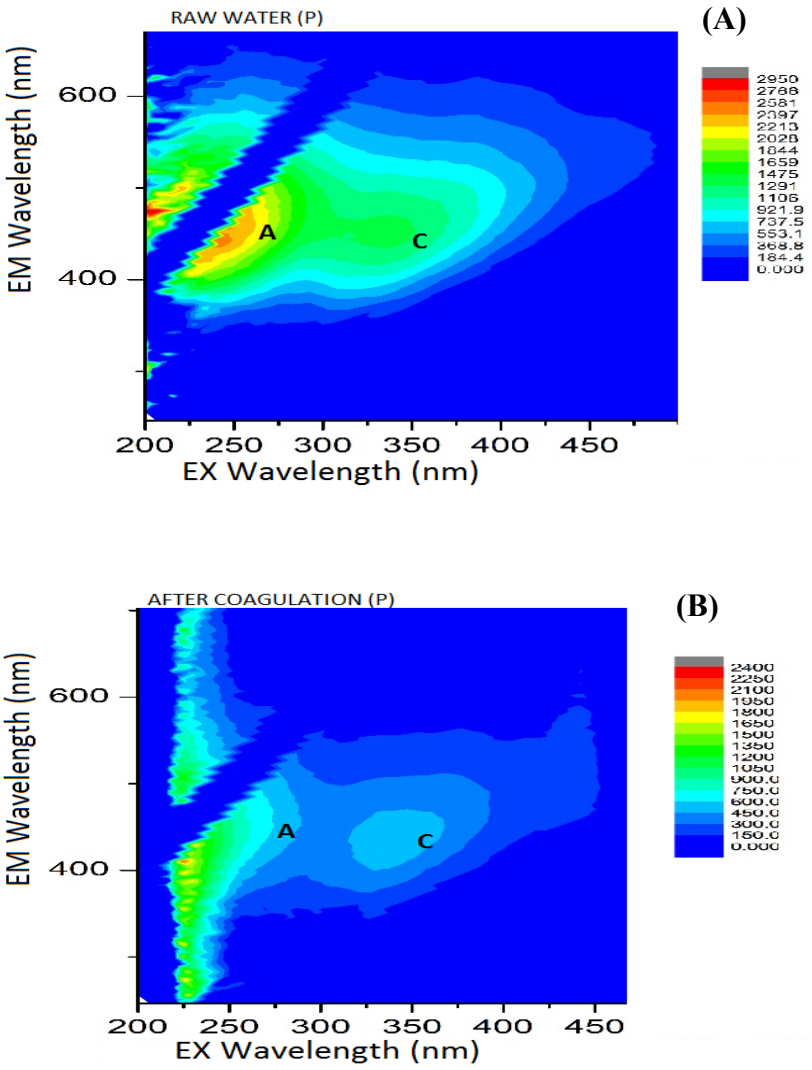

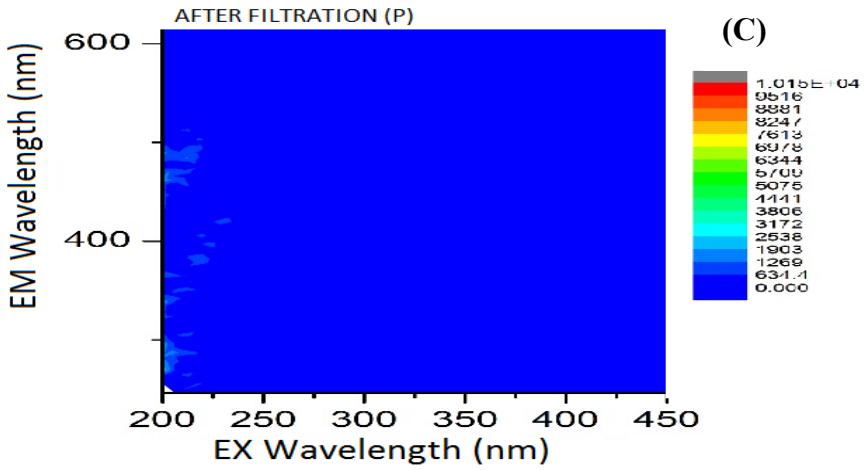


**Figure 4.8: FEEM spectra of the (A) raw water sample of the P treatment plant prior to treatment; (B) water sample of the P treatment plant after coagulation; and (C) water sample of the P treatment plant after filtration.**

## 4.4 EFFECT OF SEASONAL VARIATIONS ON NOM TREATABILITY

The effect of seasonal variations on the treatability of the NOM of the RV treatment plant was studied (**Figure 4.9**). RV treatment plant was selected based on the fact that the sampling rounds performed for this plant covered all the seasons, while other plants shows two to three seasons (interchangeably) only. The seasonal variations with regards to $UV_{254}$, which defines the aromatic character of NOM, was autumn>winter>spring>summer, whereas for DOC it was autumn>summer>winter>spring. These results shows that the highest levels of aromatic content of NOM (as evidenced by $UV_{254}$ measurements) and DOC were found during the autumn (R2) season.

NOM is derived both from internal (autochtonous) and external (allochtonous) sources. During windy and rainy seasons, allochtonous NOM becomes dominant. The source of allochtonous NOM is mainly plant and animal remains that find their way into the water resources (Wershaw *et al*., 2005). Thus the observed high levels of DOC and $UV_{254}$ in autumn can be attributed to the leaves from the trees that become deposited into the water sources. Leaves consist of aromatic components which are the main contributor of the enhanced aromatic ($UV_{254}$) readings of NOM in water. Additionally, literature shows that increased levels of

DOC over a period of years is most likely to be due to the addition of hydrophobic NOM fractions into the water sources (Sharp *et al.*, 2006).

The observed high levels of DOC during the summer compared to spring and winter could be due to issues of high run-offs, which tend to introduce various forms of pollutants (plants and animal remains) into the raw water sources. The observed trend could also be due to microbial effect, as microbes are usually more active during the warm summer months and autumn season (drier times). Microbes facilitates the release of DOC from the soil, which then finds its way to the raw water sources, when there is enough rainfall (Sharp *et al.*, 2006). The activity of some microbes towards the degradation of NOM is also temperature dependent (Ritson *et al.*, 2014). Uyak *et.al.,* (2008) observed that there were high levels of DOC in spring and autumn due to issues of runoffs and precipitations, which release various forms of NOM from the soil's upper layer into the water sources. The main point, which was confirmed in this study, is that the chemical character of NOM is highly influenced by changes in climatic conditions.

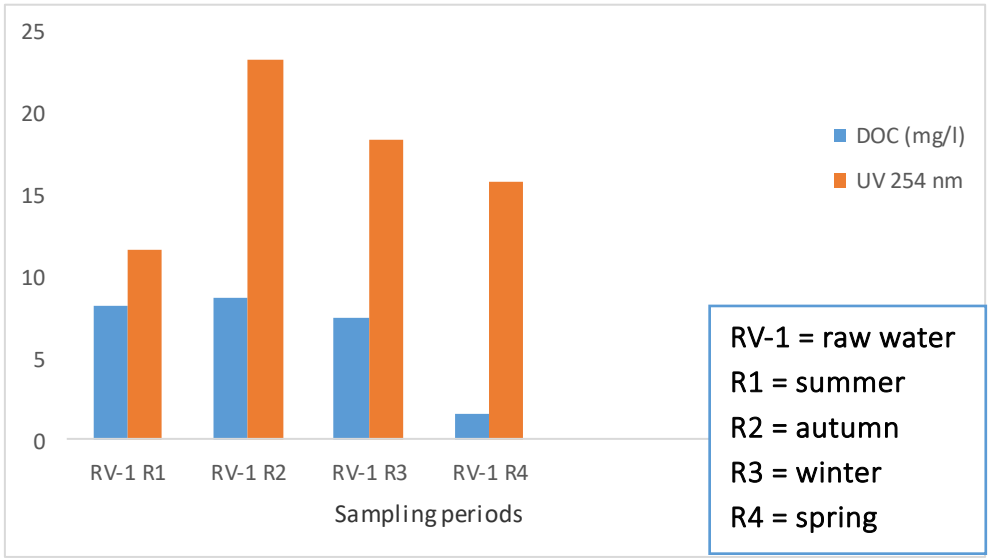


**Figure 4.9: Effect of seasonal variations on $UV_{254}$ and DOC for RV treatment plant.**

The results in **Figure 4.10** show that high SUVA was observed in spring and autumn for the RV treatment plant; low SUVA values (NB: SUVA < 2 indicates presence of hydrophilic material) were experienced during summer. Since DOC is inversely proportional to SUVA, the high spring SUVA levels are attributable to low DOC levels. The high autumn SUVA levels (NB: SUVA between 2 and 4 indicates presence of transphilic organic material) could be due to the aromatic fraction that are found in leaves, which find their way into water resources thus increasing the hydrophobicity of the NOM. Teixeira & Nunes (2016) observed that the hydrophobicity of NOM was high in summer and spring seasons compared to winter and autumn which are hot and cold seasons respectively. Summer and spring were also shown to have high $UV_{254}$ (aromatic content of NOM) (Teixeira & Nunes 2016).

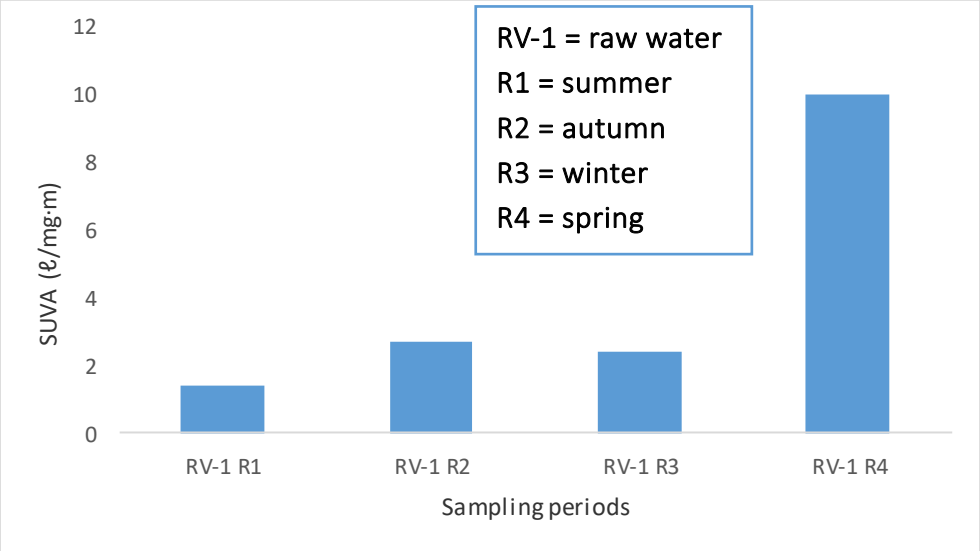


**Figure 4.10: The SUVA measurements for the RV treatment plant.**

It was expected that the raw water with the high $UV_{254}$ and SUVA will experience a high removal of aromatic content of NOM (Teixeira & Nunes 2016). This is due to the fact that the highly aromatic hydrophobic fractions (which are determined by $UV_{254}$) are more amenable to their removal using the coagulation process (Matilainen *et al.,* 2010; Ritson *et al.,* 2014). The results obtained in this study, however, do not seem to indicate any direct correlation between the high $UV_{254}$

and SUVA levels and high DOC removal rates (**Figure 4.11**). As explained previously (section 4.2.4), this could be due to poor treatment optimisation (such as coagulant dosages and type).

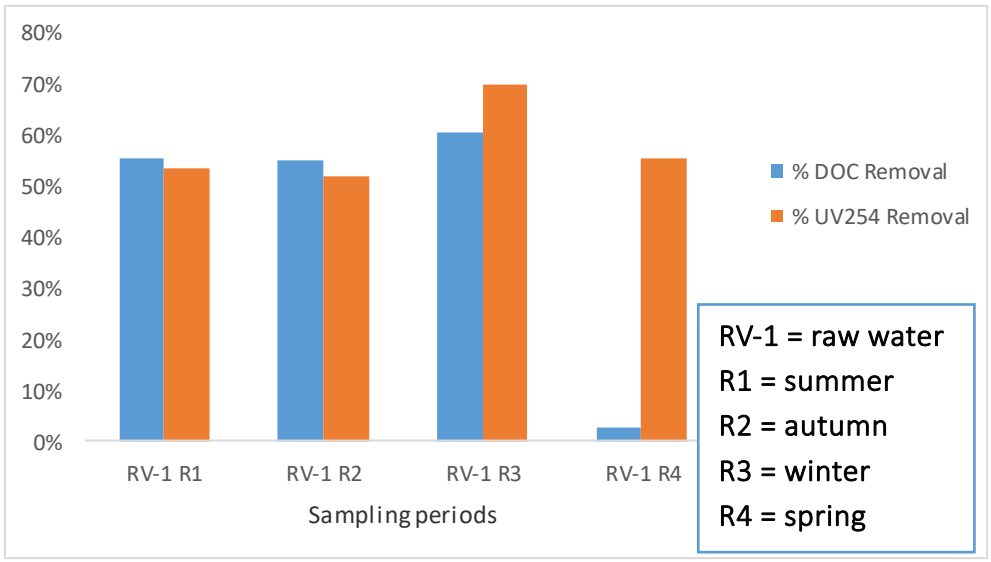


**Figure 4.11: Percentage $UV_{254}$ and DOC removal for the RV treatment plant.**

## 4.5 CONCLUSION

For every sampling round, the pH, turbidity and conductivity measurements were different across the different treatment plants, thus proving the variation in the water quality at these plants. We were able to demonstrate using the DOC, UV-Vis and SUVA results, both the quantitative and qualitative variation of the NOM across the different seasons and locations of the treatment plants. As expected, conventional methods (DOC, UV analysis, SUVA, turbidity, conductivity and pH) that were employed for the characterization of NOM do not give enough information about the chemical character or composition of the NOM but are instead limited to providing information about the quantity (DOC and UV-Vis) and the quality (SUVA) of NOM in the water. However, in order to effectively remove NOM from water, its composition needs to be well understood. Therefore, advanced characterisation methods (such as FEEM), which provide such information are required. To this end, the FEEM results have shown that NOM

samples with high humic substances (e.g. in HL, P and VP treatment plants) were effectively treated as they showed high $UV_{254}$ (aromatic character of NOM) removal percentages. FEEM also provided information regarding the treatability of NOM throughout the water treatment train.

Effective characterization of NOM in water can lead towards the improvement of its removal efficiency. The observed differences in the treatability of NOM can be due to the fact that the character and the amount of NOM in various regions is not the same. Moreover, due to the fact that various treatment plants use various treatment processes it is expected that the removal efficiencies of pollutants in water could be different. Conversely, even though some treatment plants can have similar treatment steps, however, the chemical dose used by each treatment plant might not be the same. All these factors play a role on the removal efficiency of NOM in water.

Lastly, the effect of seasonal variations on NOM quantity, quality and treatability was studied. It was shown that the DOC and $UV_{254}$ was high in autumn compared to the other seasons. This was due to the aromatic nature of the soluble compounds found in leaves, which end up deposited into water sources. It was also concluded that there was no correlation between $UV_{254}$, DOC and SUVA to percentage DOC and $UV_{254}$ (aromatic content of NOM) removal in water.

## 4.6 REFERENCES


Ashery, A.F., Radwan, K. & Rashed, M.I.G.A. (2010). The effect of pH control on turbidity and NOM removal in conventional water treatment. *Fifteenth International Water Technology Conference, Alexandia, Egypt,*1-16.

Bieroza, M.Z., Bridgeman, J. & Baker, A. (2010). Fluorescence spectroscopy as a tool for determination of organic matter removal efficiency at water treatment works. *Drink. Water Eng. Sci*, **3 (1)**, 63-70.

Bello, O., Hamam, Y. & Djouani, K. (2014). Coagulation process control in water treatment plants using multiple model predictive control. *Alexandria Eng J*, **53 (4)**:939-948.

Dlamini, S. & Haarhoff, J.B.M. (2012). The profiling and treatability of Natural organic matter in South African raw water sources using enhanced coagulation. MSc dissertation, University of Johannesburg.

Evans, C.D., Monteith, D.T. & Cooper, D.M. (2005). Long-term increases in surface water dissolved organic carbon: Observations, possible causes and environmental impacts. *Environ Pollut*, **137 (1)**:55-71.

Funes, A., De Vicente, J., Cruz-Pizarro, L. & De Vicente, I. (2014). The influence of pH on manganese removal by magnetic microparticles in solution. *Water Res*, **53**:110-122.

Haarhoff, J., Kubare, M., Mamba, B., Krause, R., Nkambule, T., Matsebula, B. & Menge, J. (2009). NOM characterization and removal at six Southern African water treatment plants. *Drink Water Eng. Sci. Discuss*, **2**:231-257.

Lobanga, K.P., Haarhoff, J. & van Staden, S.J. (2014). Treatability of South African surface waters by enhanced coagulation. *Water SA*, **40 (3)**:529-534. .

Mamba, B.B., Krause, R.W., Matsebula, B. & Haarhoff, J. (2009). Monitoring natural organic matter and disinfection by-products at different stages in two South African water treatment plants. *Water SA*, **35 (1)**:121–127.

Matilainen, A., Vepsäläinen, M. & Sillanpää, M. (2010). Natural organic matter removal by coagulation during drinking water treatment: A review. *Adv Colloid Interface Sci*, **159 (2)**:189-197.

Matilainen, A, Gjessing, E.T., Lahtinen, T., Hed, L., Bhatnagar, A. & Sillanpää, M. (2011). An overview of the methods used in the characterisation of natural organic matter (NOM) in relation to drinking water treatment. *Chemosphere*, **83 (11)**:1431-1442.

Nkambule, T.I., Krause, R.W, Mamba, B.B. & Haarhoff, J. (2009a). Removal of natural organic matter from water using ion-exchange resins and cyclodextrin polyurethanes. *Phys. Chem. Earth*, **34 (13-16)**:812-818.

Nkambule, T.I., Krause, R.W.M., Haarhoff, J. & Mamba, B.B. (2011). Treatability and characterization of Natural Organic Matter (NOM) in South African waters using newly developed methods. *Phys. Chem. Earth*, **36 (14-15)**:1159-1166.

Nkambule, T. I., Krause, R. W. M., Haarhoff, J. & Mamba, B. B. (2012a). Natural Organic Matter (NOM) in South african waters: characterization of NOM, treatability and method development for effective NOM removal from water. Ph.D thesis, University of Johannesburg.

Nkambule, T.I., Krause, R.W.M., Haarhoff, J. & Mamba, B.B. (2012b). Natural organic matter (NOM) in South African waters: NOM characterisation using combined assessment techniques. *Water SA*, **38 (5)**:697-706.

Nkambule, T.I., Krause, R.W.M., Haarhoff, J. & Mamba, B.B. (2012c). The characterisation of Natural organic matter (NOM) in South African waters. *Water Sci. Technol. Water Supply*, **12:648**-657.

Obi, C., Momba, M., Green, E., Igumbor, J., Samie, A. & Musie, E. (2009). Microbiological, physico-chemical and management parameters impinging on the

efficiency of small water treatment plants in the Limpopo and Mpumalanga Provinces of South Africa. *Water SA*, **33 (2)**, 229–238.

Ritson, J.P., Graham, N.J.D., Templeton, M.R., Clark, J.M., Gough, R. & Freeman, C. (2014). The impact of climate change on the treatability of dissolved organic matter (DOM) in upland water supplies : A UK perspective. *Sci. Total Environ*, 473-474:714-730.

Särkkä, H., Vepsäläinen, M. & Sillanpää, M. (2015). Natural organic matter (NOM) removal by electrochemical methods –A review. *J Electroanal Chem*, 1-46.

Sharp, E.L., Parsons, S.A. & Jefferson, B. (2006). Seasonal variations in natural organic matter and its impact on coagulation in water treatment. *Science of Total Environment*, **363**:183-194.

Świetlik, J. & Sikorska, E. (2006). Characterization of natural organic matter fractions by high pressure size-exclusion chromatography, specific UV absorbance and total luminescence spectroscopy. *Polish J. Environ. Stud*, **15 (1)**:145-153.

Teixeira, M.R. & Nunes, L.M. (2016). The impact of natural organic matter seasonal variations in drinking water quality. *Desalination and Water treatment*, **36 (1-3)**:344-353.

Thebe, T., Swartz, C.D., Morrison, I.R., Engelbrecht, W.J. & Loewenthal, R.E. (2000). Characterisation of Natural Organic Matter in South African coloured surface waters. *Water Institute of Southern Africa (WISA) Biennial Conference, Sun City, South Africa, 28 May -1 June 2000*, 1-11.

Uyak, V., Ozdemir, K. & Toroz, I. (2008). Seasonal variations of disinfection by-product precursors profile and their removal through surface water treatment plants*. Sci. Total Environ*, **390 (2-3)**:417-424.

Wershaw, R.L., Leenheer, J.A. & Cox, L. (2005). Characterization of dissolved and particulate natural organic matter (NOM) in Neversink Reservoir, New York Scientific Investigations Report 2005-5108. *US Geol. Surv. Sci. Investi*.

Zhang, Y., Zhao, J., Jiang, Z., Shan, D. & Lu, Y. (2014). Biosorption of Fe (II) and Mn (II) Ions from Aqueous Solution by Rice Husk Ash. *Biomed Res Int*, **2014**:1-10.

# CHAPTER 5

## SYNTHESIS, CHARACTERIZATION AND APPLICATION OF Pd SUPPORTED N DOPED $TiO_2$ (N, Pd CO-DOPED $TiO_2$) FOR THE PHOTOCATALYTIC DEGRADATION OF NATURAL ORGANIC MATTER (NOM) IN WATER.

### 5.1 INTRODUCTION

The available water treatment processes do not effectively remove all of the NOM present in water, however it only deals with the hydrophobic fraction of NOM. This is mainly due to the complexity and the size of NOM, thus in the process of removing NOM, it also reduces the efficiency of other treatment processes which in turn increases the operational costs (Urbanowska & Kabsch-Korbutowicz 2016). Owing to this, methods that will degrade NOM into smaller fractions are required and one of the currently used degradation method is ozonation. Although NOM can be effectively degraded during ozonation, the process can end up increasing the amount biodegradable NOM fractions, which promote bacterial regrowth in the treatment and distribution systems (Haarhoff *et al.*, 2009; Urbanowska & Kabsch-Korbutowicz 2016). The limitation of the ozonation process has, as a result, led to more research being geared towards the development of far more advanced and less toxic oxidation processes with higher removal capabilities.

Photocatalysis is of much interest and one of the promising photocatalyst which has gained a lot of attention due to its superior characteristics and its various applications in resolving global challenges such as water pollution is $TiO_2$ (Matilainen & Sillanpää, 2010). However, the main limitation of $TiO_2$ is its wide band gap (3.2 eV) and fast electron-hole recombination, which negatively affects its performance under visible region (Kuvarega *et al*., 2011). It is for this reason that researchers are now focusing on developing methods for addressing these shortcomings without necessarily compromising the photoactivity of $TiO_2$ (Nosaka *et al.*, 2005). In line with these research efforts, different dopants, which include metals and non-metals, have been introduced on the surface of $TiO_2$. This chapter is therefore focused on the synthesis, characterization and application of N, Pd co-doped $TiO_2$ (NPT) for the photodegradation of NOM in water. Co-doping with both

nitrogen and palladium induces synergistic effects on the photoactivity of $TiO_2$ by reducing the band gap of $TiO_2$ and electron-hole recombination thereby improving the photoactivity of the material (Sakthivel *et al.*, 2004; Yang *et al.*, 2014). Photocatalysis is based on generation of free radicals initiated by the generation of electrons and holes following photoactivation. The oxidative species such as hydroxyl radicals then degrade the targeted pollutant by oxidizing them to $CO_2$ and $H_2O$ (Nkambule *et al.*, 2012). Studies have shown that co-doped $TiO_2$ (with non-metals and metals) can effectively degrade various organics present in water (Kuvarega *et al.,* 2011; Nkambule,*et al*., 2012; Yang *et al*., 2014; Luo *et al*., 2015).

## 5.2 EXPERIMENTAL METHODOLOGY

NPT was synthesized using a modified sol-gel method, whereby ammonium hydroxide ($NH_4OH$) was used as a source of nitrogen and hydrolysis reagent while palladium diamine dichloride (Pd $(NH_3)_2$ $Cl_2$) was used as the Pd precursor as described in **Section 3.7**.

Techniques such as; FTIR, UV-Vis, Raman, XRD, TGA, SEM and EDS were employed in order to characterize the physio-chemical properties of NPT. Further details are discussed in **Section 3.9**.

## 5.3 RESULTS AND DISCUSSIONS

### 5.3.1 FTIR analysis of NPT

FTIR was used to define the available functional groups and to study the surface changes occurring on the material at various palladium concentrations (Gole *et al.*, 2004) (**Figure 5.3.1**). The broad band observed around 3295 $cm^{-1}$ for all samples corresponds to the OH groups on the surface of the particles. Moreover, at 1615 $cm^{-1}$, the OH bending peak is observed and is corresponding to adsorbed water on the surface of the material (Cheng *et al.*, 2012). The intensity of the OH peaks increased with the introduction and the increase in palladium dopant, which proves

that the number of hydroxyl and water adsorbed on the material's surface was increasing. The presence of the OH groups enhances the photoactivity of $TiO_2$ (Kuvarega *et al.*, 2011). A intense peak around 510 corresponds to Ti-O bond and was present for all samples (Yu *et al*., 2005).

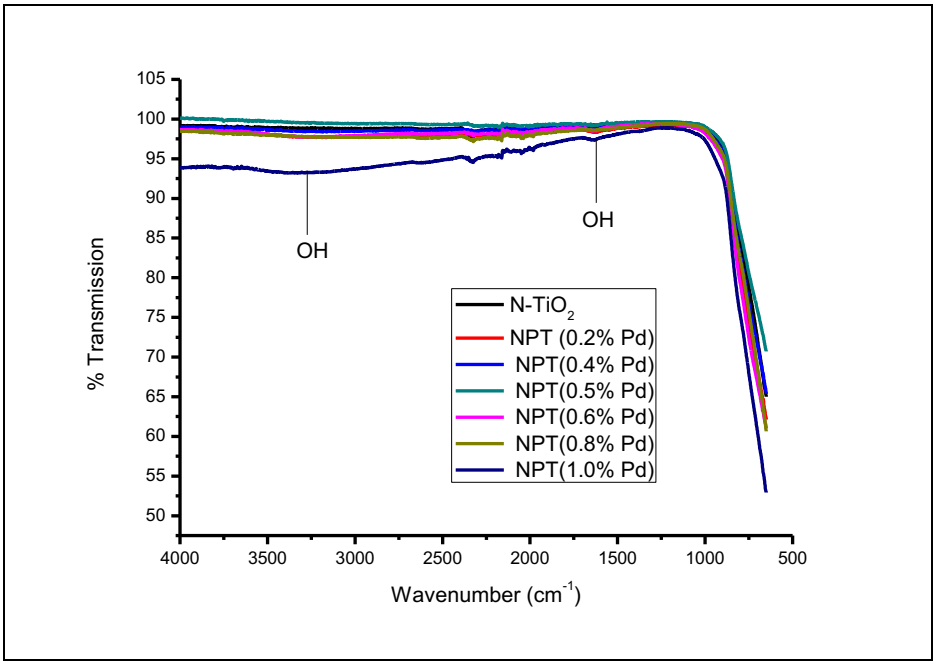


**Figure 5.3.1: FTIR spectra of NPT with various Pd concentrations.**

### 5.3.2 UV-Vis analysis of NPT

The UV-Vis absorption spectra of the photocatalysts is shown in **Figure 5.3.2 (A)**. It can be observed from the figure that the N doped titanium dioxide has a significant absorption appearing between 400-600 nm. This can be attributed to the electrons from the 2p levels of the nitrogen atom being excited to the unoccupied CB (Kuvarega *et al*., 2011). This can also be due to the formation of the intra-band levels between the CB and VB of the $TiO_2$, which then reduces the band gap thus enhancing the activity of the doped material in the visible region (Mekprasart *et al*., 2013). Most importantly, it must be noted that N-$TiO_2$ showed enhanced absorption under the visible region compared to NPT (0.2-0.6% Pd). This could be due to the fact that doping with nitrogen alone, there are more

defects on $TiO_2$ which are occupied by N atoms, however, introducing both N and Pd may results in some interaction/competition between N and Pd for the active site. Increasing the Pd concentration was found to cause a red shift in the absorption edge towards the visible region and thus showing the synergistic effect of co-doping in the reduction of the band gap of $TiO_2$ (Kuvarega *et al.*, 2011).

As shown in **Figure 5.3.2 (B)**, N-$TiO_2$ and NPT absorbs at a higher wavelength (>400 nm) compared to the commercial $TiO_2$ (Burda *et al.*, 2003). The commercial $TiO_2$ shows a single, strong absorption at about 400 nm, which is attributed to the charge transfer between the 2p orbital of oxygen in the VB and a $Ti^{4+}$ ion in the CB of titania (Gole *et al*., 2004; Sakthivel *et al*., 2004; Kuvarega *et al*., 2011). In addition, the red shift observed after doping the titania with nitrogen may be due to the replacement of oxygen with nitrogen in the $Ti^{4+}$-O centres on the surface of the material (Gole *et al*., 2004).

It is noteworthy that the increase in the amount of Pd was concordant to the increase in the absorption wavelength of the material (Kuvarega *et.al*., 2012a). This is due to the fact that Pd reduces the band gap of $TiO_2$, thus making it more active under visible region. Pd also introduces a localized energy level between the VB and CB, thus introducing the red shift in $TiO_2$ (Sakthivel *et al.*, 2004).

The diffuse reflectance spectra were constructed as the Kubelka-Munk function, F(R), versus wavelength based on the Kubelka-Munk equation: $F(R) = (1-R)^2 / R$ (R = Rsample/Rreference (**Figure 5.3.2 (C)**) (Murphy 2007). It was shown that there was a strong absorption peak that appeared below 400 nm for both the doped and pristine $TiO_2$. This strong peak is a result of the charge transfer from the VB to the CB of $TiO_2$ (Kuvarega *et al.*, 2011). The spectra of NPT shows a red shift resulting from the sp to d transition between the electrons from the band of $TiO_2$ and localized d-electrons from palladium ions (Kuvarega *et al.*, 2011).

The Kubelka-Munk data was used to construct a Tauc Plot for the semiconductor material (**Figure 5.3.2 (C)** & **(D)**). Research has shown that the type of transition mode of $TiO_2$ is not clear (Kuvarega *et al.*, 2011). Whereas, a direct allowed band gap semiconductor will show a linear Tauc plot with n = ½; for the indirect allowed

band gap, n = 2. By extrapolating the Tauc line to the x-axis, a semiconductor band gap is obtained.

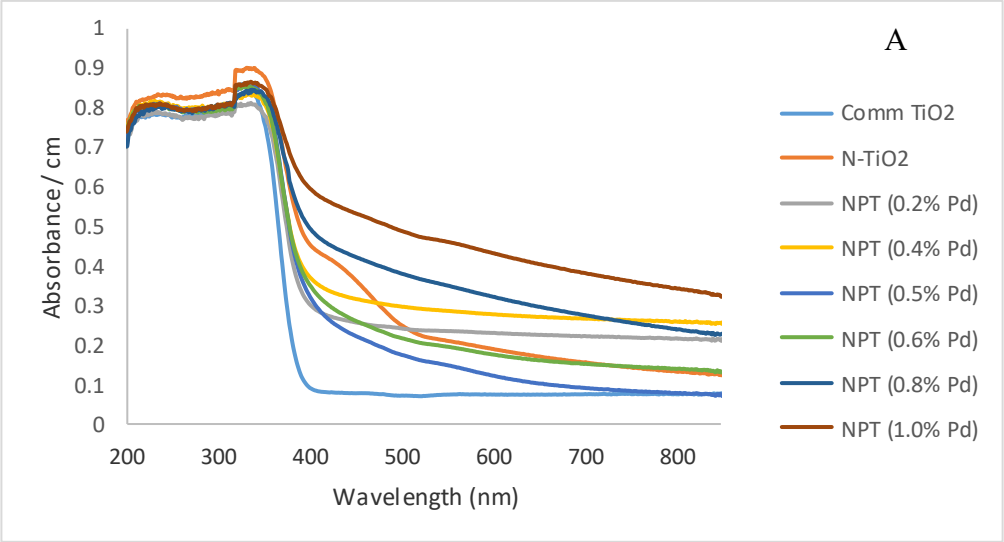


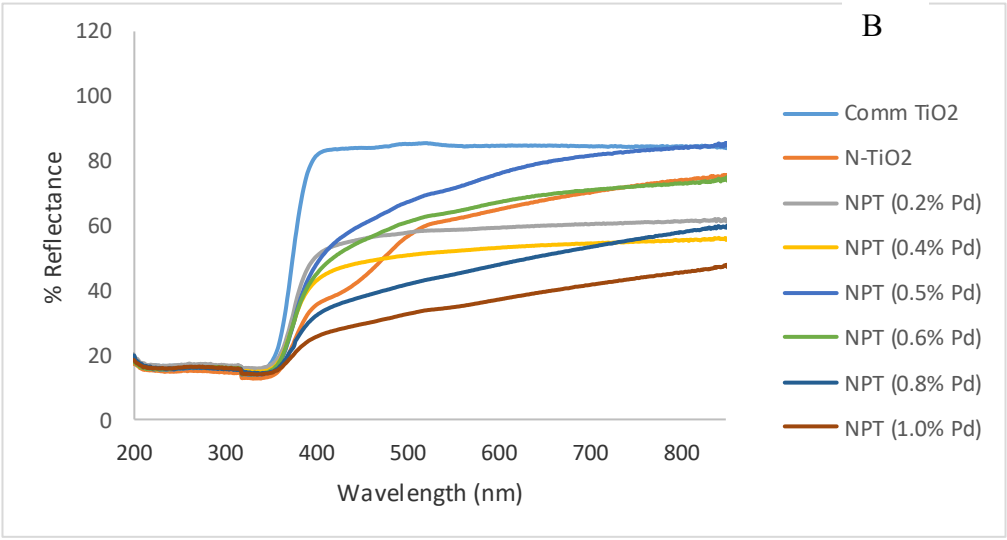

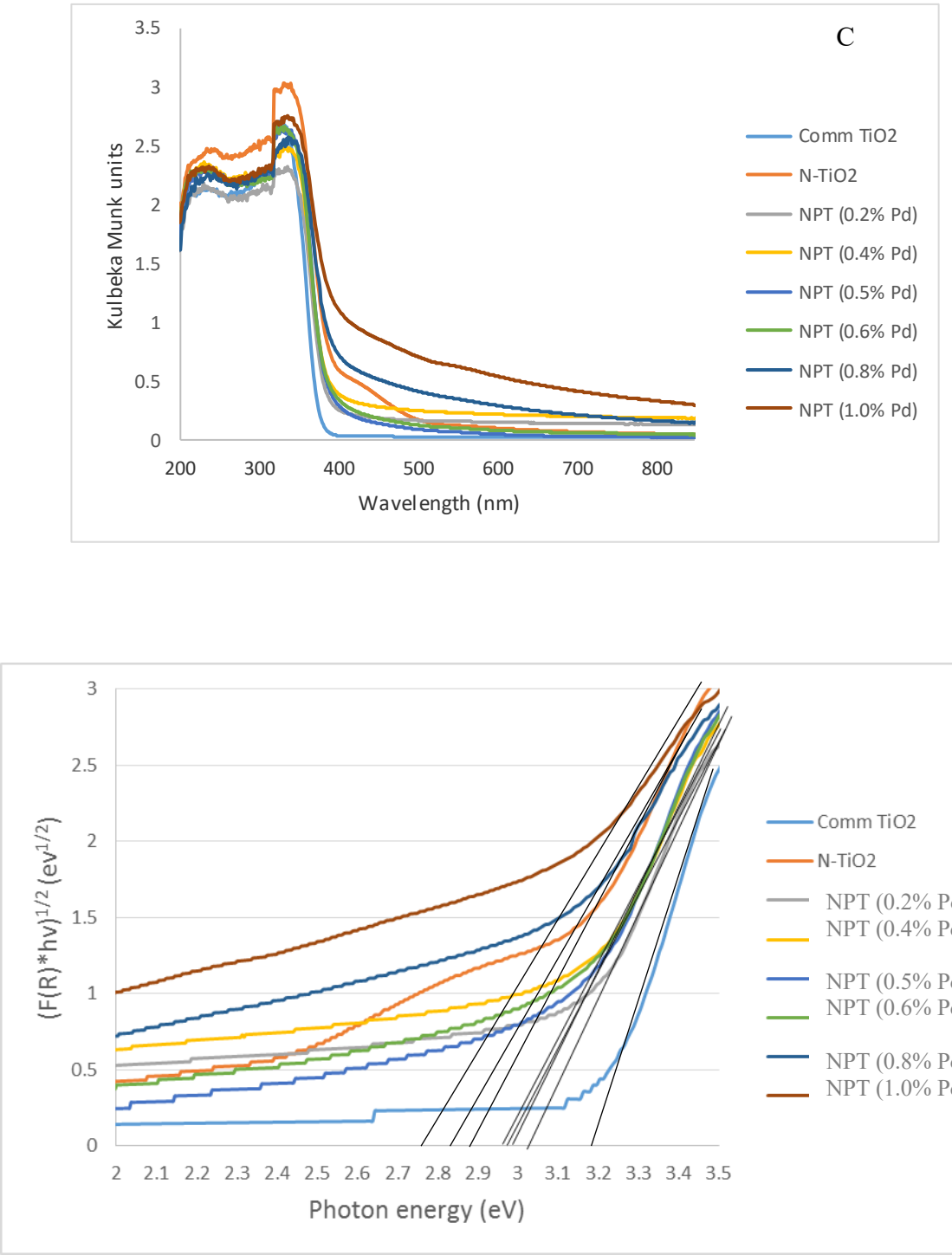


**Figure 5.3.2: UV-vis absorption (A), diffuse reflectance (B), Kubelka-Munk plots (C) and Tauc plots (D) of NPT with various Pd concentrations.**

**Table 5.1** shows the effect of Pd dopant on the band gap of the material. A decrease in the band gap is generally seen when the concentration of Pd is increased; this confirms the positive effect of co-doping the $TiO_2$ material. The higher than usual band gap that was observed for NPT (0.2% Pd) compared to the other doped materials is attributable to the fact that as Pd ions are being introduced, they tend to compete with the N ions for the active sites on the $TiO_2$. The higher band gap could also be attributed to the preferential formation of the d-d transitions over sp-d transition, which serve as evidence for the formation of the Pd-O band (Kuvarega *et al.*, 2011).

**Table 5.1: Effect of Pd Dopant level on Band Gap**

| Sample | Band gap (eV) |
|---|---|
| Commercial $TiO_2$ | 3.20 |
| N - $TiO_2$ | 2.90 |
| NPT (0.2% Pd) | 3.02 |
| NPT (0.4% Pd) | 2.97 |
| NPT (0.5% Pd) | 2.95 |
| NPT (0.6% Pd) | 2.93 |
| NPT (0.8% Pd) | 2.82 |
| NPT (1.0% Pd) | 2.75 |

### 5.3.3 Raman analysis of NPT

Raman analysis was performed with the purpose of evaluating the surface information of $TiO_2$. **Figure 5.3.3** shows six Raman active fundamental modes at 144 $cm^{-1}$ ($E_g$), 197 $cm^{-1}$ ($E_g$), 397 $cm^{-1}$ ($B_{1g}$), 518 $cm^{-1}$($A_{1g}$+$B_{1g}$) and 640 $cm^{-1}$ ($E_g$), which correspond to anatase $TiO_2$ (Cheng *et al.,* 2012). Both the $B_{1g}$ and $E_g$ peaks were due to the 001 and 110 face scatterings, respectively (Kuvarega *et al.*, 2012b). There were no peaks corresponding to PdO for all the samples because of low Pd dosages in the material. It can also be concluded that by calcinating

$TiO_2$, sharp and intense peaks were formed, which in turn proves the improvement of the degree of crystallinity of the material (Cheng *et al*., 2012).

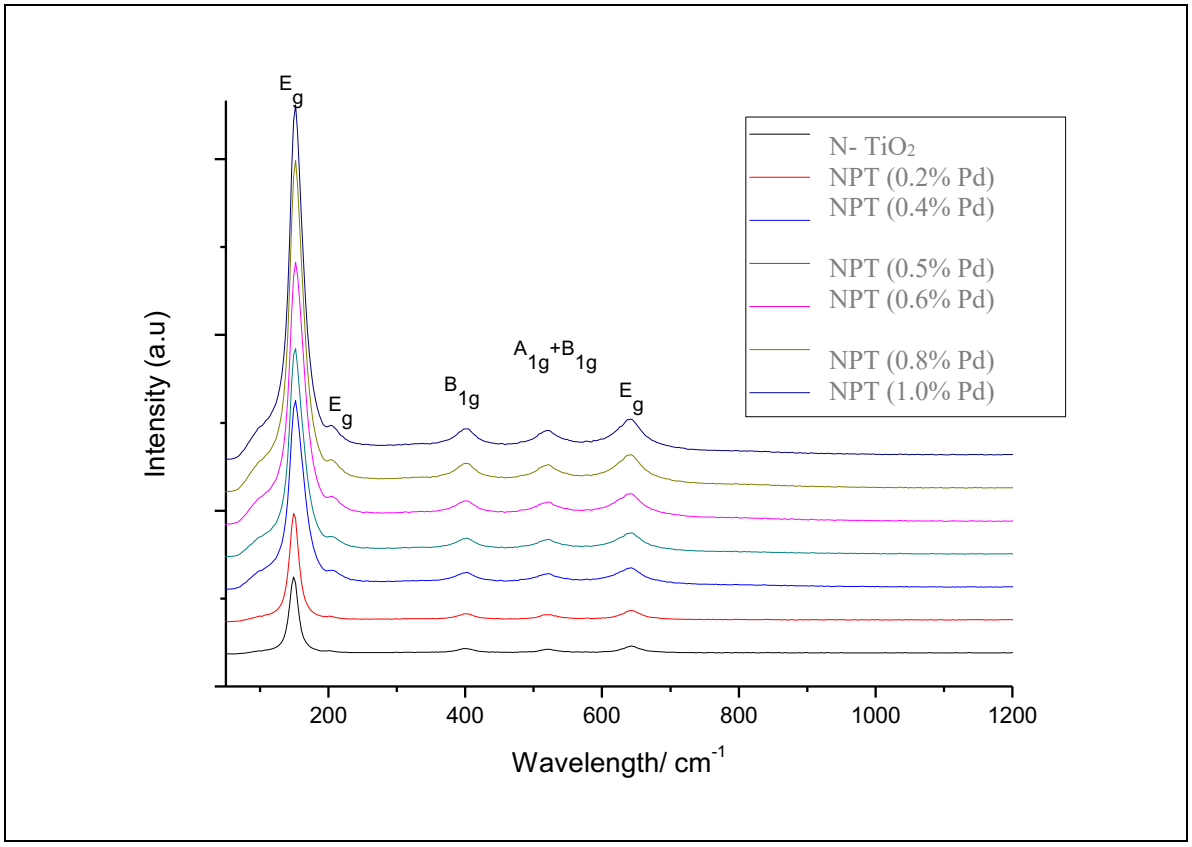


**Figure 5.3.3: Raman spectrum of NPT with various Pd concentrations.**

### 5.3.4 XRD analysis of NPT

Post synthesis treatment by calcining the material at 500 ˚C caused an increase in the material's crystallinity with anatase as the predominant phase, and this is in concordant to the Raman results depicted in **Figure 5.3.3** (Kuvarega *et al*., 2011). In principle peaks at 2 θ values of 25.3 and 27.4 corresponds to anatase and rutile phases, respectively (Cheng *et al*., 2012). Peaks appearing at 2 θ values of 25.3, 37.6, 48.2, 53.9, 54.8, 62.7, and 75.2, which correspond to the (101), (004), (200), (105), (211), (204), and (215) planes, respectively, they all confirm the presence of anatase $TiO_2$ (**Figure 5.3.4**) (Kuvarega *et al*., 2011; Najjar *et al*., 2015; Seifvand & Kowsari 2016). Due to a low dosages of palladium and nitrogen dopants, no diffraction peaks that correspond to these dopants were depicted. However, the

PdO peak was observed at a 2 θ value of about 42; the intensity of this peak was increased upon the introduction of Pd (Kuvarega *et al.*, 2011). There were no peaks corresponding to N and this indicates that the N atoms were properly distributed in or on the $TiO_2$, which caused the $TiO_2$ to maintain its anatase phase (Kuvarega *et al.*, 2011). In the N-$TiO_2$, the N atoms can easily replace the oxygen in the lattice due to similar atomic radii (Kuvarega *et al*., 2012b).

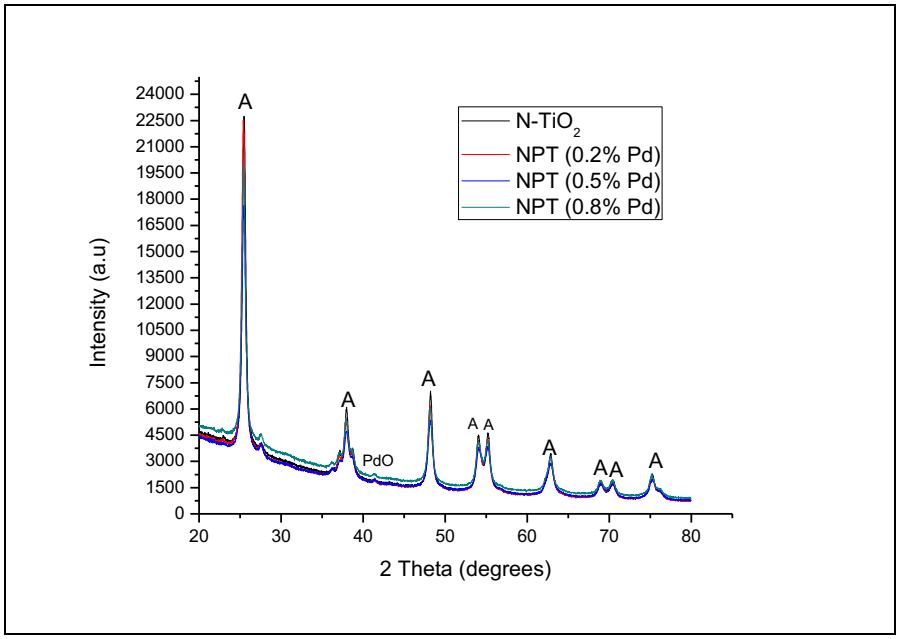


**Figure 5.3.4: XRD pattern of NPT with various Pd concentrations.**

### 5.3.5 TGA analysis of NPT

The thermograms illustrated in **Figure 5.3.5**, shows a weight loss at about 100 ˚C, which was attributed to the loss of water adsorbed onto the particle surface (Nkambule *et al.*, 2012). A mass loss from 100-900 ˚C is because of the loss of mainly carbon based materials entangled within the nanomaterials (Kuvarega *et al.*, 2011). The total weight loss of between 2.0% and 3.0% indicates that the materials are chemically stable, which means that a lot carbon based material was lost via the calcination process.

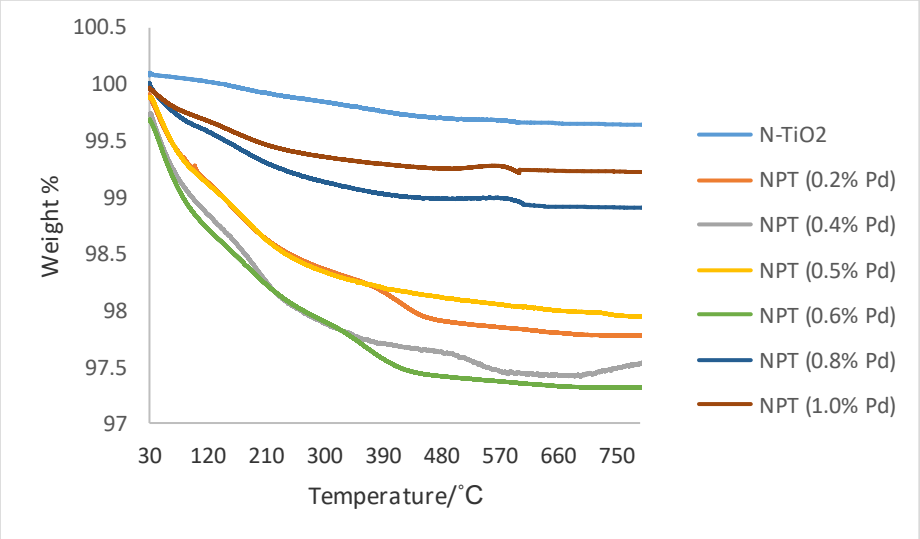


**Figure 5.3.5: TGA plot of NPT with various Pd concentrations.**

### 5.3.6 SEM analysis of NPT

**Figure 5.3.6** shows the SEM images and EDS spectrum of NPT (0.5% Pd). The SEM images confirm that the $TiO_2$ is made up of small and spherical particles (Cheng *et al.*, 2012; Najjar *et al*., 2015; Seifvand & Kowsari 2016). The particles also showed some degree of agglomeration (Kuvarega *et al*., 2011). The EDS results was used to confirm the elemental composition of the synthesized material. It was found that the oxygen and titanium were the main components, while Pd was contained in small proportions (Lee *et al*., 2015). The C peak which was observed is associated with the carbon tape upon which the sample was mounted. However, the perceived absence of obvious N peaks is due to possible overlap with some other peaks (Nkambule *et al*., 2012).

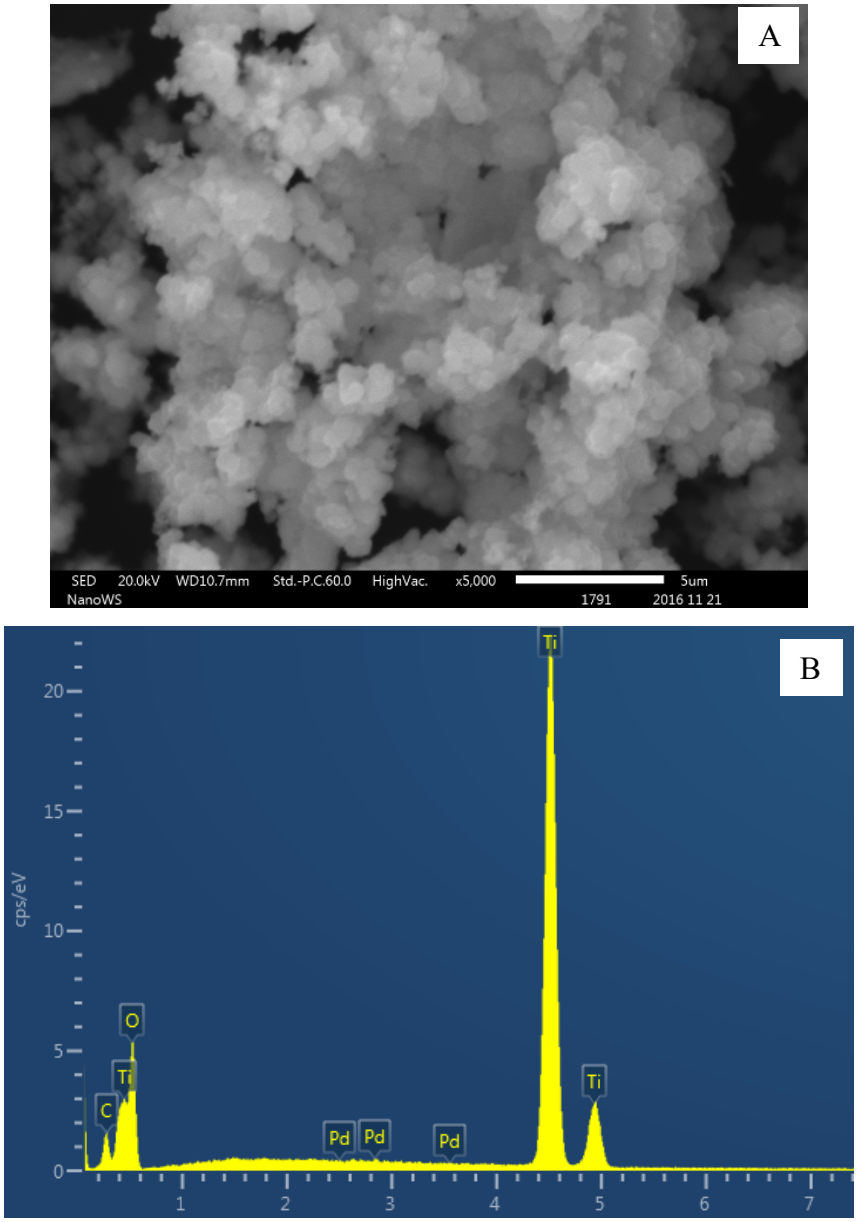


**Figure 5.3.6: SEM image (A) and EDS spectrum (B) of NPT (0.5% Pd).**

## 5.4 EVALUATION OF THE PHOTOCATALYTIC ACTIVITY OF NPT

The procedure followed to evaluate the photoactivity of NPT under solar simulation is described in **section 3.10**. The performance of the NPT was studied by evaluating the degree of NOM (from Midvaal (MV) treatment plant) degradation after 2 hours under visible light irradiation. The effect of NPT on NOM degradation was examined using a UV-Vis spectrometer.

A photocatalytic degradation of NOM using nanomaterials that were synthesized have shown the N-$TiO_2$ to have the lowest NOM reduction efficiency compared to the NPT (0.2-1.0% Pd) (**Table 5.2**). This was expected because the nitrogen in N-$TiO_2$ only reduces the band gap, whereas for the co-doped $TiO_2$ there is additional synergistic effect that improves the photoactivity of $TiO_2$ under visible light. According to literature, increasing the amount of palladium introduces a red shift in $TiO_2$, thus enhances the phototoactivity of the material under visible light (Kuvarega *et al*., 2011; Seifvand & Kowsari 2016). However, experimentally increasing the Pd amount does not always lead to high NOM degradation rates (**Table 5.2**). Similar findings have been reported in instances where different pollutants were degraded using metal and non-metal doped $TiO_2$ (Burda *et al*., 2003; Sakthivel *et al*., 2004; Kuvarega *et al.*, 2011; Kuvarega *et al*., 2012a; Lee *et al*., 2015; Li *et al*., 2016). In this study, an increase in NOM degradation (up to 58.9%) was noted when the Pd content was increased to up to 0.5%, and thereafter decreased to 42.1% for the sample with the highest amount of palladium (**Figure 5.4.1** & **Table 5.2**). The observed decrease in NOM degradation at higher Pd concentrations can be due to the agglomeration at high concentration of Pd, which reduces the surface area of $TiO_2$, which in turn reduces its photocatalytic activity (Sakthivel *et al*., 2004). In addition, at high concentrations of Pd, metals can act as recombination centres for electrons and holes by attracting holes with the purpose of recombining them with electrons (Najjar *et al.*, 2015; Lee *et al.*, 2015). The enhanced photoactivity that was observed at Pd concentration levels of 0.5% was therefore due the formation of a Schottky junction between the metal and $TiO_2$, which reduces the electron-hole recombination thus improving the photocatalytic activity of the material (Kuvarega *et al.*, 2011; Lee *et al*., 2015).

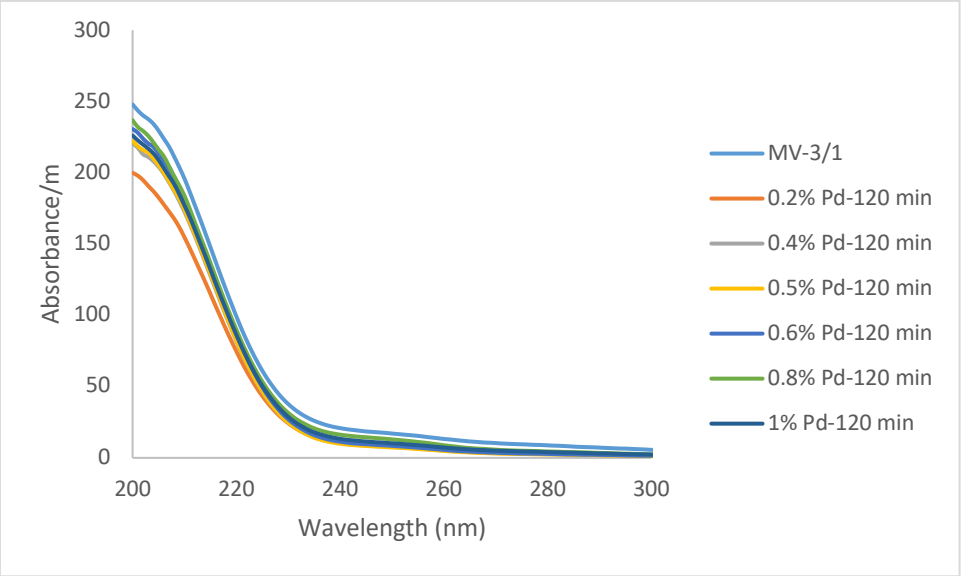


**Figure 5.4.1: UV scan of the raw water sample (round 3) obtained from Midvaal treatment plant (MV1) sample and treated with NPT, at various Pd concentrations.**

**Table 5.2: Illustrating the $UV_{254}$ reduction of MV1 (Round 3) by various % Pd of NPT**

| Sample name | $UV_{254}$ / m | % Reduction |
|---|---|---|
| MV-3 (conventional methods) | 15.76 | 60.0% |
| MV1 with N-$TiO_2$ | 11.96 | 24.1% |
| MV1 with NPT (0.2% Pd) | 7.24 | 54.1% |
| MV1 with NPT (0.4% Pd) | 6.85 | 56.5% |
| MV1 with NPT (0.5% Pd) | 6.47 | 58.9% |
| MV1 with NPT (0.6% Pd) | 7.43 | 52.9% |
| MV1 with NPT (0.8% Pd) | 11.55 | 26.7% |
| MV1 with NPT (1.0% Pd) | 9.12 | 42.1% |

A review of the literature has shown that non-metals doped $TiO_2$, metal doped $TiO_2$ and co-doped $TiO_2$ can degrade various forms of aromatic compounds under visible light illumination (Kuvarega *et al.*, 2011; Nkambule *et al.*, 2012; Lee *et al.*, 2015; Seifvand & Kowsari 2016; Li *et al*., 2016) and results emanating from this study (**Figure 5.4.2**) seem to support these findings. When compared to other light sources such as UV; visible light has been reported to have an enhanced degradation efficiency for various pollutants (Nkambule *et al*., 2012).

**Figure 5.4.2** shows the comparison of the percentage $UV_{254}$ removal **(A)** and $UV_{254}$ **(B)** for raw water samples of all the treatment plants under study (results presented are for the final rounds of sampling). $UV_{254}$ define the amount of the aromatic content of NOM present in water. The figure illustrates that raw water samples with high $UV_{254}$ also shows a high percentage reduction of the aromatic content of NOM as evidenced by the decrease in $UV_{254}$ for both the conventional treatment processes and NPT (0.5% Pd). HL, VP and P treatment plants were reported to have the highest percentage removal and the LE treatment plant having the lowest removal rate. This is mainly due to the fact that the higher the $UV_{254}$, the higher the aromatic content of NOM.

Literature has revealed that the hydrophobic fraction (which is highly aromatic in nature) can be easily and effectively removed during the coagulation process (Murray & Parsons 2004; Matilainen *et al.*, 2010; Baghoth *et al.*, 2011). Similar findings were reported by Nkambule *et.al*., (2012), whereby the hydrophobic fraction of NOM was effectively removed compared to the hydrophilic and transphilic when using the N, Pd co-doped $TiO_2$. The differences in $UV_{254}$ for raw water samples proves that the character of NOM is not uniform in various regions due to different locations, geology, topography, industrial and agricultural activities being practised in that particular location (Mamba *et al*., 2009). Most importantly, the percentage of NOM removal was also different when using conventional treatment processes at various plants; this is due to the fact that different plants use different treatment processes, chemicals and dosages. The same treatment process and dosage (NPT) was applied for various treatment plants with different compositions of NOM and it was observed that the treatability was different due to

different locations at which the raw water samples were collected from, thus variations in NOM compositions.

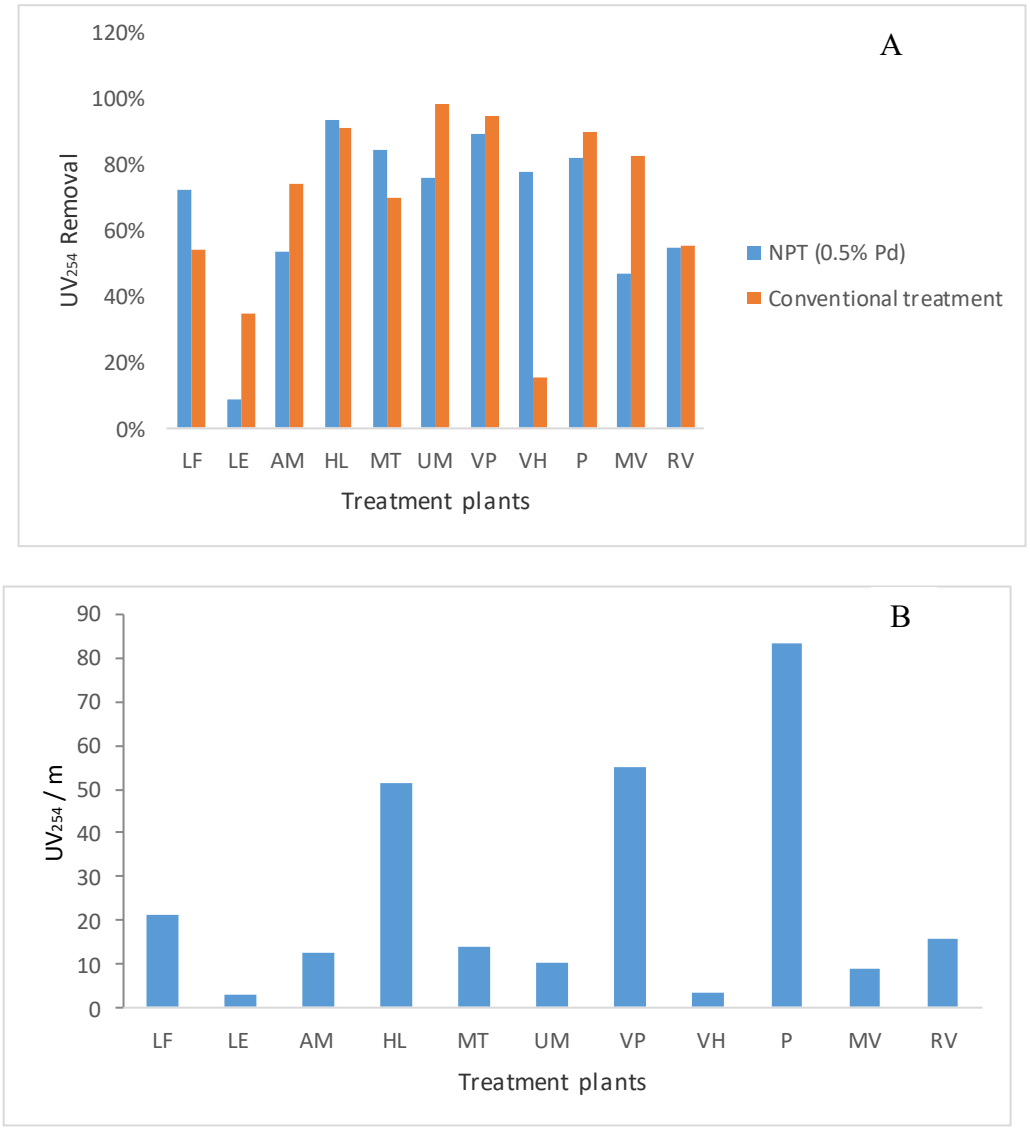


**Figure 5.4.2: A comparison of the treatability of NOM from various South African water treatment plants using NPT (0.5% Pd) and conventional treatment processes (A); and $UV_{254}$ for raw waters (final sampling round) (B).**

## 5.5 CONCLUSION

The study showed that not all the NOM is being removed by using the available conventional methods, thus there is a need for the development of new technologies that will complement the available NOM removal methods. Methods such as XRD and Raman analysis revealed that the synthesized NPT consisted of anatase $TiO_2$. FTIR proved that all the expected functional groups (OH and TiO) were present for the synthesized NPT. UV-Vis spectra showed that doping $TiO_2$ with N and Pd, was accompanied by a red shift, which was indicated by the decrease in the band gaps of NPT. An increase in the palladium concentration caused a red shift in the absorption edge towards the visible region. The material with the highest photocatalytic activity (58.8%) was NPT (0.5% Pd), when evaluated against the Midvaal (MV) raw water sample. Photodegradation of various raw water samples obtained from the various water treatment plants located in South Africa using NPT (0.5% Pd) revealed that the treatability of NOM was not uniform in various water sources. This was attributed by the fact that the character of NOM is not uniform in various places as it depends on geology, topography, industrial and agricultural activities being practised in that area. It was also evident that the raw water samples with the high content of hydrophobic fraction of NOM had a highest removal efficiency. HL, VP and P showed the highest percentage $UV_{254}$ removal and LE having the lowest.

## 5.6 REFERENCES


Baghoth, S.A. (2012). Characterizing Natural organic matter in drinking water treatment processes and trains. UNESCO-IHE institute for Water Education, MSc dissertation, The Netherlands University.

Burda, C., Lou, Y., Chen, X., Samia, A.C.S., Stout, J. & Gole, J.L. (2003). Enhanced Nitrogen Doping in $TiO_2$ Nanoparticles. *Nano Lett*, **3**:1049-1051.

Cheng, X., Yu, X., Xing, Z. & Yang, L. (2012). Synthesis and characterization of N-doped $TiO_2$ and its enhanced visible-light photocatalytic activity. *Arab J. Chem*, 1-7.

Gole, J.L., Stout, J.D., Burda, C., Lou, Y. & Chen, X. (2004). Highly efficient formation of visible light tunable $TiO_{2-x}N_x$ photocatalysts and their transformation at the nanoscale. *J. Phys. Chem. B*, **108 (4)**:1230-1240.

Haarhoff, J., Kubare, M., Mamba, B., Krause, R., Nkambule, T., Matsebula, B. & Menge, J. (2009). NOM characterization and removal at six Southern African water treatment plants. *Drink Water Eng. Sci. Discuss*, **2**:231-257.

Joshi, M., Bhattacharyya, A. & Ali, S.W. (2008). Characterization techniques for nanotechnology applications in textiles. *Indian J. Fibre Text. Res*, **33 (3)**:304-317.

Kuvarega, A.T., Krause, R.W.M. & Mamba, B.B. (2011). Nitrogen/Palladium-codoped $TiO_2$ for efficient visible light photocatalytic dye degradation. *Society*, 22110–22120.

Kuvarega, A.T., Krause R.W.M. & Mamba, B.B. (2012a). Photocatalytic performance of nitrogen-platinum group metal co-doped $TiO_2$ supported on carbon nanotubes for visible-light degradation of organic pollutants in water. PhD thesis, University of Johannesburg.

Kuvarega, A.T., Krause, R.W.M., Mamba, B.B. (2012b). Multiwalled carbon nanotubes decorated with nitrogen, palladium co-doped $TiO_2$ (MWCNT / N, Pd co-doped $TiO_2$) for visible light photocatalytic degradation of Eosin Yellow in water. *J Nanopart Res*, **14:776.**

Kuvarega, A.T. & Mamba, B.B. (2016). $TiO_2$ -based Photocatalysis: Toward Visible Light-Responsive Photocatalysts Through Doping and Fabrication of Carbon-based Nanocomposites. *Critical Reviews in Solid State and Materials Sciences*, 1–52.

Lee, J., Youn, J., Kim, Y. & Oh, H. (2015). Effect of Palladium Nanoparticles on Photocatalytic Characteristics of N doped Titania Catalyst. *J. Mater. Sci Technol*, **31 (6)**:664-669.

Li, C., Zong, L., Li, Q., Zhang, J., Yang, J. & Jin, Z. (2016). Photocatalytic oxidation of propylene on Pd-loaded Anatase $TiO_2$ nanotubes under visible light irradiation. *Nanoscale Res. Lett*, **11**:271.

Mamba, B.B., Krause, R.W., Matsebula, B. & Haarhoff, J. (2009). Monitoring natural organic matter and disinfection by-products at different stages in two South African water treatment plants. *Water SA*, **35 (1)**:121–127.

Matilainen, A., Vepsäläinen, M. & Sillanpää, M. (2010). Natural organic matter removal by coagulation during drinking water treatment: A review. *Adv Colloid Interface Sci*, **159 (2)**:189-197.

Mekprasart, W., Khumtong, T., Rattanarak, J., Techitdheera, W. & Pecharapa, W. (2013). Effect of nitrogen doping on optical and photocatalytic properties of $TiO_2$ thin film prepared by spin coating process. *Energy Procedia*, **34**:746-750.

Murphy, A.B. (2007). Band-gap determination from diffuse reflectance measurements of semiconductor films, and application to photoelectrochemical water-splitting. *Sol. Energy Mater. Sol. Cells*, **91 (14)**:1326-1337.

Murray, C.A. & Parsons, S.A. (2004). Removal of NOM from drinking water: Fenton's and photo-Fenton's processes. *Chemosphere*, **54**:1017-1023.

Najjar, R., Shokri, M. & Farsadi, S. (2015). Preparation of Pd-doped nano-$TiO_2$ in microemulsion and their application in photodegradation of C.I. Acid Yellow 23. *Desalin. Water Treat*, **54 (9)**:2581-2591.

Nkambule, T. I., Kuvarega, A. T., Krause, R. W. M., Haarhoff, J. & Mamba, B. B. (2012). Synthesis and characterisation of Pd-modified N-doped $TiO_2$ for photocatalytic degradation of natural organic matter (NOM) fractions. *Environ. Sci. Pollut. Res*, **19**, 4120–4132.

Nosaka, Y., Matsushita, M., Nishino, J. & Nosaka, A.Y. (2005). Nitrogen-doped titanium dioxide photocatalysts for visible response prepared by using organic compounds. *Sci. Technol. Adv. Mater*, **6 (2)**:143-148.

Sakthivel, S., Shankar, M.V., Palanichamy, M., Arabindoo, B., Bahnemann, D.W. & Murugesan, V. (2004). Enhancement of photocatalytic activity by metal deposition: Characterisation and photonic efficiency of Pt, Au and Pd deposited on $TiO_2$ catalyst. *Water Res*, **38 (13)**:3001-3008.

Seifvand, N. & Kowsari, E. (2016). Synthesis of Mesoporous Pd-doped $TiO_2$ templated by a magnetic recyclable ionic liquid for efficient photocatalytic air treatment. *Ind. Eng. Chem. Res*, **55 (40)**:10533-10543.

Urbanowska, A. & Kabsch-Korbutowicz, M. (2016). Characteristics of Natural Organic Matter removed from water along with its treatment. *Envi Prot Engin*, **42 (2)**:183-195.

Uyak, V., Ozdemir, K. & Toroz, I. (2008). Seasonal variations of disinfection by-product precursors profile and their removal through surface water treatment plants. *Sci. Total Environ*, **390 (2-3)**:417-424.

Yang, G., Jiang, Z., Yang, G. & Yan, Z. (2010). Preparation of highly visible-light active N-doped $TiO_2$ photocatalyst. *J. Mater. Chem*, **20 (25)**: 5301.

Yang, Z., Lan-lan, Q., Peng-wei, T. & You-xian, Z. (2014). Review of N and Metal co-doped $TiO_2$ for water purification under visible light irradiation. *Int. Conf. Environ. Chem. Biol*, **78 (7)**:139-142.

Yu, Y., Yu, J.C., Chan, C.Y, Che, Y.K., Zhao, J.C., D, L., Ge, W.K. & Wong, P.K. (2005). Enhancement of adsorption and photocatalytic activity of $TiO_2$ by using carbon nanotubes for the treatment of azo dye. *Appl. Catal. B Environ*, **61 (1-2):**1-11.

# CHAPTER 6
# SYNTHESIS, CHARACTERIZATION AND APPLICATION OF MULTIWALLED CARBON NANOTUBES DECORATED WITH NITROGEN, PALLADIUM CO-DOPED $TiO_2$ (MWCNTs/N, Pd CO-DOPED $TiO_2$) FOR THE PHOTOCATALYTIC DEGRADATION OF NATURAL ORGANIC MATTER (NOM) IN WATER.

## 6.1 INTRODUCTION

Carbon nanotubes (CNTs) have been used in the enhancement of the photoactivity of $TiO_2$ (Yu *et al.*, 2011; Di Paola *et al.*, 2012; Kuvarega *et al.*, 2012b). Due to their nanoporous character and high mechanical and chemical stabilities, CNTs are excellent supports, especially for semiconductors that have some photocatalytic activity. Decorating $TiO_2$ with CNTs has gained a lot of attention from researchers due to enhanced properties of the resulting nanocomposites that make them suitable to deal with a number of global problems including water purification (Kuvarega *et al.*, 2012b). Even though $TiO_2$ is an n-type semiconductor; the availability of CNTs in the material allows the photogenerated electrons to freely move towards the CNTs surface, which may have a lower Fermi level, thus increasing the lifetime of the holes in the VB of $TiO_2$ (decreasing electron-hole recombination) (An *et al.*, 2007; Kuvarega *et.al.*, 2012a). This in turn increases the photocatalytic activity of the $TiO_2$ (Kuvarega *et al.*, 2012a). However, not much work has been carried out on MWCNTs decorated with metals/non-metals for water purification purposes. To the best of our knowledge, no work has been undertaken on the use of MWCNTs/N, Pd co-doped $TiO_2$ for the photodegradation of NOM in water. Based on the work reported by Kuvarega *et.al.*, (2012b), whereby the MWCNT/N, Pd co-doped $TiO_2$ was used for the photodegradation of Eosin yellow in water, it is envisaged that MWCNTs/N, Pd co-doped $TiO_2$ nanocomposite will show a synergistic effect on the photoactivity of $TiO_2$ under visible light. Consequently, this chapter will deal with the

characterization of the synthesized MWCNTs/N, Pd co-doped $TiO_2$ nanocomposites and their efficiency towards NOM photodegradation in water.

## 6.2 EXPERIMENTAL METHODOLOGY

MWCNTs/N, Pd co-doped $TiO_2$ (1.0% Pd) (also reffered as CT) was synthesized using a modified sol-gel method, whereby $NH_4OH$ was used as a source of nitrogen and hydrolysis reagent while Pd $(NH_3)_2$ $Cl_2$ was used as Pd precursor as described in **Section 3.8**.

FTIR, UV-Vis, Raman, XRD, TGA and SEM were employed in order to characterize the physio-chemical properties of CT. Further details are provided in **Section 3.9**.

## 6.3 RESULTS AND DISCUSSION

### 6.3.1 FTIR analysis of CT nanocomposites

FTIR was used to confirm the availability of specific functional groups in the nanocomposites and also to study the variations on $TiO_2$ surface at different MWCNTs concentrations (Gole *et al.*, 2004) (**Figure 6.3.1**). The broad band appearing at around 3295 $cm^{-1}$ in the spectra of all the samples corresponds to the OH groups located on the surface of the material (Kuvarega *et al*., 2012a). At 1615 $cm^{-1}$ the OH bending peak was observed and this is ascribed to the adsorbed water on the surface of the material (Wang *et al*., 2009; Cheng *et al*., 2012). The intensity of the OH peaks was found to be increasing with the increase in the amount of the MWCNTs. This proves that the number of hydroxyl groups and the amount of water adsorbed on the surface of the $TiO_2$ was increasing thus enhancing the photoactivity of $TiO_2$ (Kuvarega *et al.*, 2011). This occurs when the water and the hydroxyl groups get scavenged by the holes in the VB (which are formed during the activation of $TiO_2$) to form OH radicals which then attacks and degrades NOM (present on the particle's surface) into smaller molecules. Most importantly, the CT (1.0% MWCNTs) was found to have the highest intensity of OH peaks and was therefore expected to have the highest photodegradation

efficiency. On the other hand, the OH peaks of the CT (5.0% MWCNTs) were less intense even though this material had the highest MWCNTs loading. This may be due to agglomeration at high CNT levels which reduces the surface area of $TiO_2$ as well as the number of OH groups and $H_2O$ molecules adsorbed on the surface of the material. This in turn reduces the number of $OH^{\bullet}$ produced to degrade NOM in water. An intense peak that appeared at around 510 $cm^{-1}$ and was present in the spectra of all the samples corresponds to the Ti-O bond (Yu *et al.*, 2005). There were no peaks corresponding to CNTs because of low loadings of the MWCNTs in the nanocomposites and possibly the $TiO_2$ bands have shielded most of the CNT peaks (Kuvarega *et al.*, 2012a).

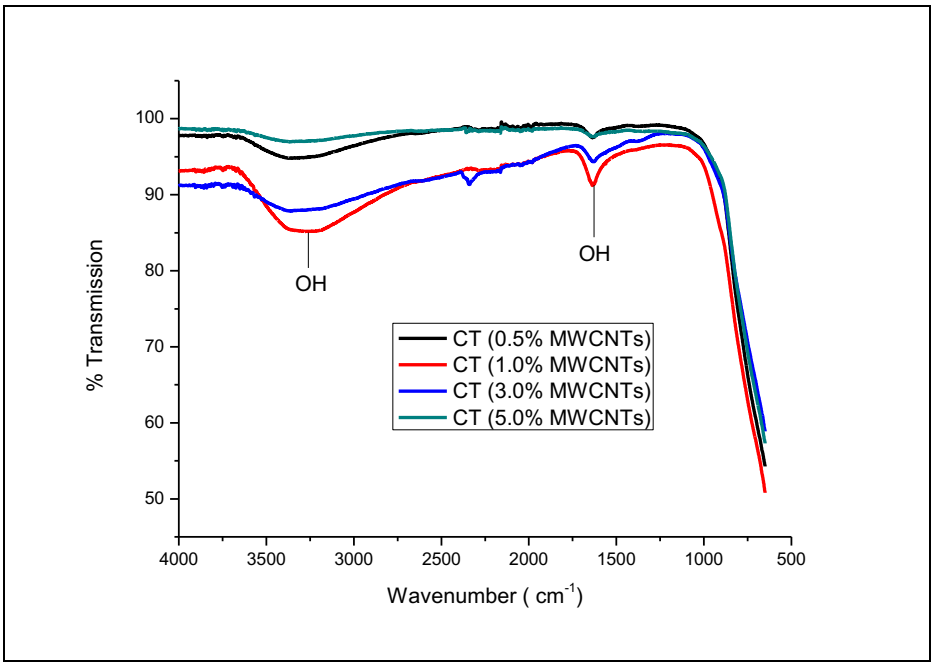


**Figure 6.3.1: FTIR spectra of CT with various MWCNTs ratios.**

### 6.3.2 UV-Vis analysis of CT nanocomposites

**Figure 6.3.2 (A)** shows the UV-Vis absorbance spectra of the various nanocomposites. As expected, the spectrum of the pristine $TiO_2$ showed an intense absorption peak at about 400 nm, which is attributed to the charge transfer between the oxide and central titanium ion (Kuvarega *et al*., 2011). An intense peak that appears at around 375 nm and is present in the spectra of all the samples; correspond to the anatase $TiO_2$ (Kuvarega *et al*., 2012b). An increase in the concentration of the MWCNTs caused the red shift in the absorption edge of the nanocomposites which is observed by a shift towards the longer wavelength in the absorption spectra (Wang *et al.*, 2005). The MWCNTs are responsible for causing an increase in the electric charge of the oxide ion occurring on the surface of the material; an increased electric charge reduces the electron-hole recombination, and by extension, enhances the photoactivity of $TiO_2$ (Wang *et al*., 2009).

The diffuse reflectance spectra shown in **Figure 6.3.2 (B)** were plotted as the Kubelka-Munk function [F(R)] versus wavelength using the Kubelka-Munk equation: $F(R) = (1-R)^2 / R$ (R = Rsample/Rreference (Murphy 2007). The Kubelka-Munk function was used to construct a Tauc Plot (**Figure 6.3.2 (C)** & **D**) for the semiconductor material. The Tauc line was extrapolated to the x-axis to obtain the band gaps of the materials (Nkambule *et al*., 2012).

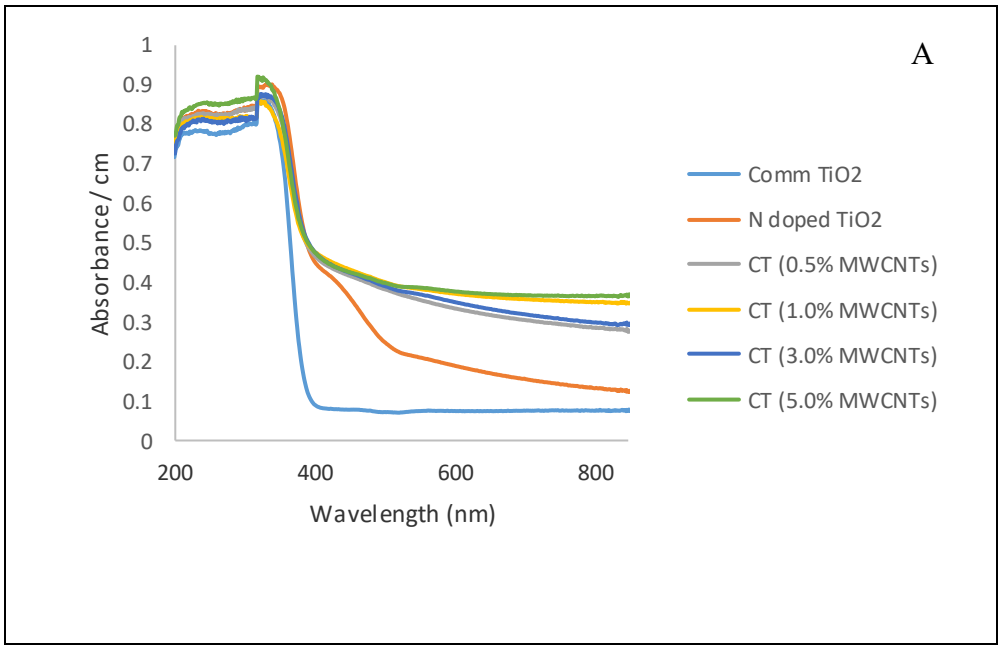
A
Absorbance/cm
1
0.9
0.8
0.7
0.6
0.5
0.4
0.3
0.2
0.1
0
200
400
600
800
Wavelength (nm)
Comm TiO2
N doped TiO2
CT (0.5% MWCNTs)
CT (1.0% MWCNTs)
CT (3.0% MWCNTs)
CT (5.0% MWCNTs)

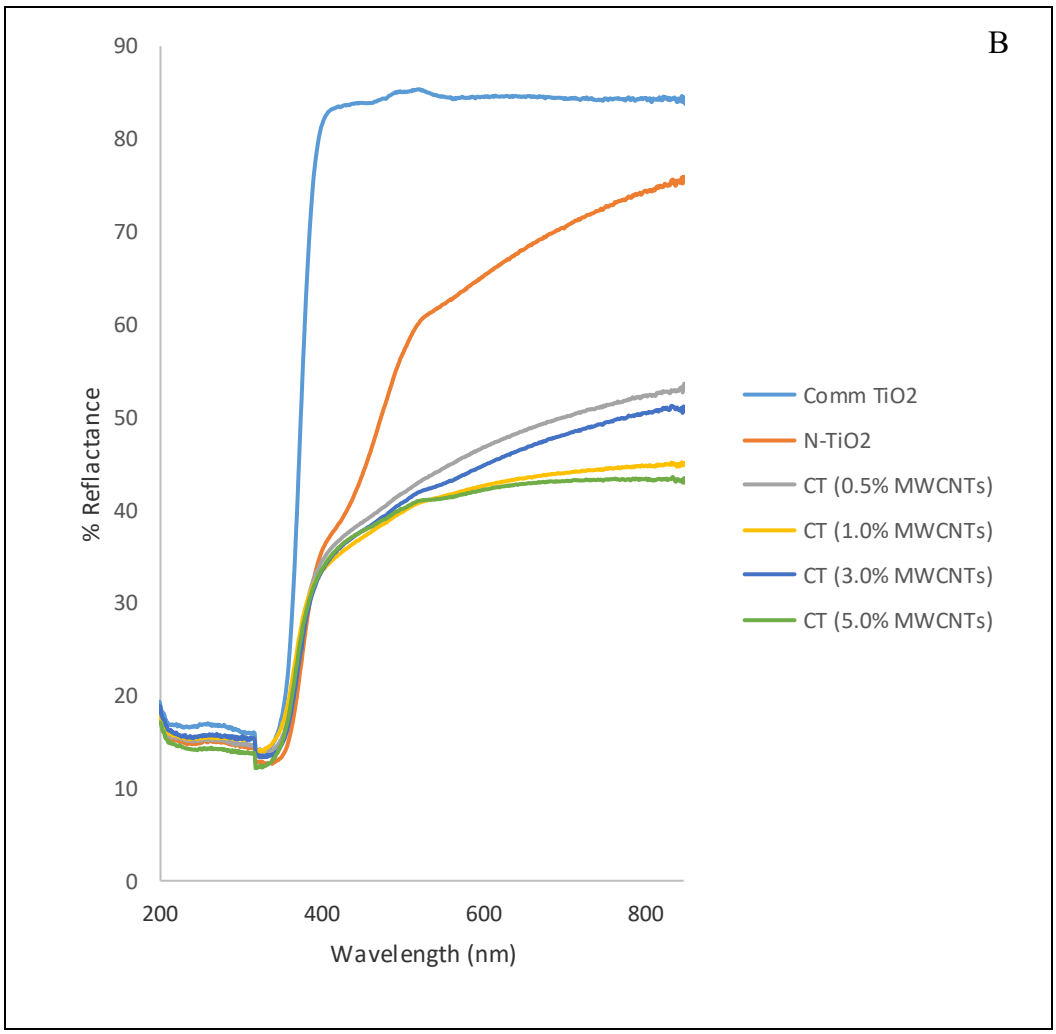
B
% Reflactance
90
80
70
60
50
40
30
20
10
0
200
400
600
800
Wavelength (nm)
Comm TiO2
N-TiO2
CT (0.5% MWCNTs)
CT (1.0% MWCNTs)
CT (3.0% MWCNTs)
CT (5.0% MWCNTs)

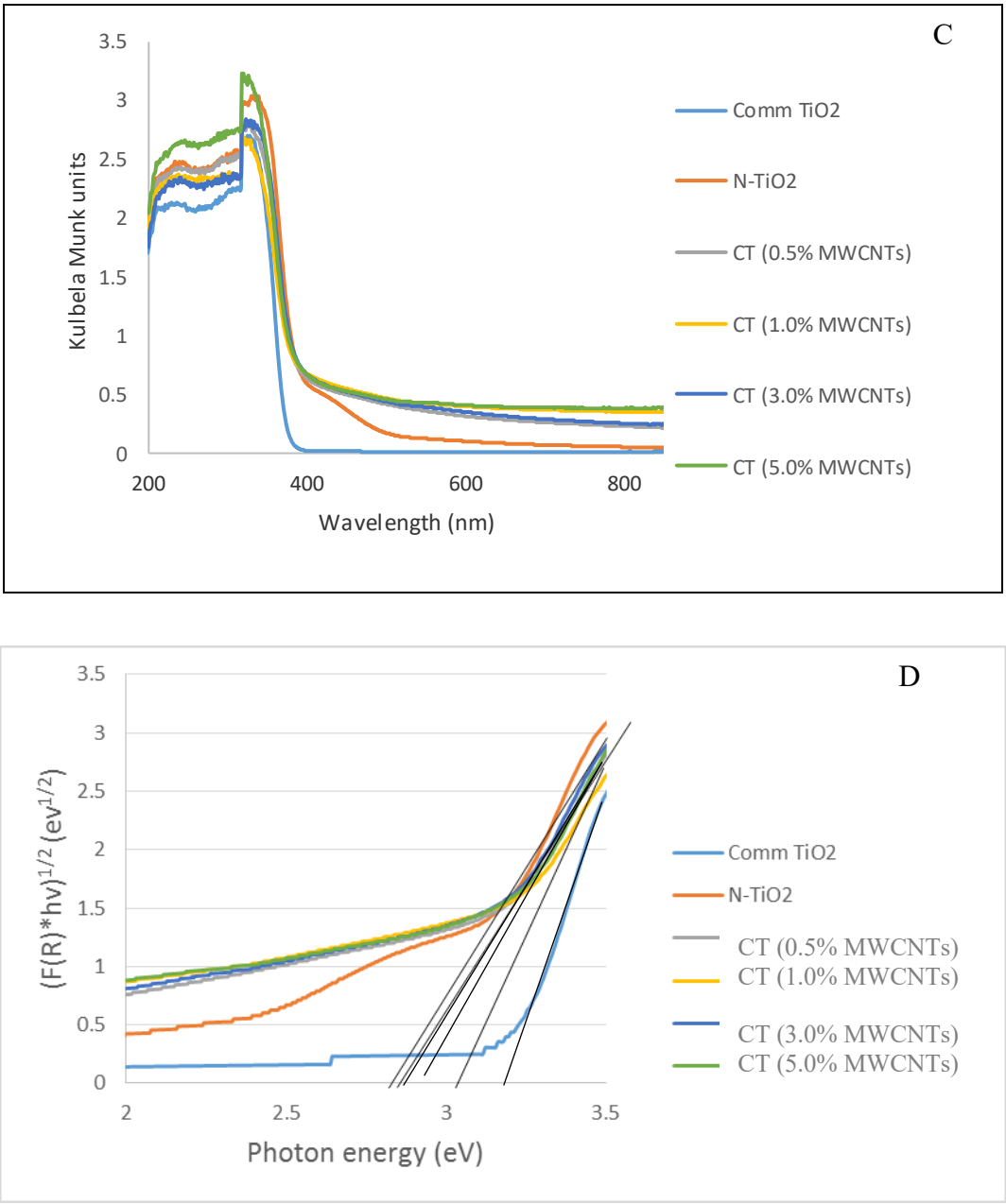


**Figure 6.3.2: UV-vis absorption (A), diffuse reflectance (B), Kubelka-Munk plots (C) and Tauc plots (D) of CT with various MWCNT concentrations.**

**Table 6.1** shows the band gaps of the synthesized materials. Upon the introduction of the MWCNTs (0.5–1.0 %), an initial decrease in the band gap was observed; the smallest band gap was observed for the nanocomposite consisting of 3.0% MWCNTs. More importantly, all the band gaps for the doped materials were lower than that of the pristine $TiO_2$, thus confirming the positive effect of co-

doping and the positive interaction between the doped materials and MWCNTs, which could improve the photoactivity of the nanocomposite under visible light illumination (Wang *et al.,* 2009; Kuvarega *et al*., 2012b).

**Table 6.1: Effect of MWCNTs on band gap in CT nanocomposites**

| Sample | Indirect band gap (eV) |
|---|---|
| Commercial $TiO_2$ | 3.20 |
| N – $TiO_2$ | 3.05 |
| CT (0.5% MWCNTs) | 2.90 |
| CT (1.0% MWCNTs) | 2.93 |
| CT (3.0% MWCNTs) | 2.80 |
| CT (5.0% MWCNTs) | 2.83 |

### 6.3.3 Raman analysis of CT nanocomposites

The Raman spectra of the CT (**Figure 6.3.3**) confirmed the presence of $TiO_2$ and CNTs in the synthesized nanocomposite. The six Raman peaks appearing at 144 $cm^{-1}$ ($E_g$), 197 $cm^{-1}$ ($E_g$), 397 $cm^{-1}$ ($B_{1g}$), 518 $cm^{-1}$ ($A_{1g}$ + $B_{1g}$) and 640 $cm^{-1}$ ($E_g$) correspond to anatase $TiO_2$ (Kuvarega *et al.*, 2012b). The peak that appears at around 1353 $cm^{-1}$ and 1585 $cm^{-1}$ corresponds to the D and G bands of the CNTs, respectively (Yu *et al.*, 2011; Yadav *et al.*, 2011; Kuvarega *et al.*, 2012a). The D band represents the defect sites in the hexagonal framework of the MWCNTs due to the disordered $sp^3$-hybridised carbon. Whereas, the G band is for the ordered $sp^2$-hybridisation (Kuvarega *et al*., 2012a). This accounts for covalent functionalization of NPT on MWCNTs (Yadav *et al*., 2011).

**Figure 6.3.3** also shows that the peak intensity of D and G bands increases with the increase in MWCNTs loadings in the nanocomposites, with a 5.0% MWCNTs loadings having the highest intensity. This could be explained based on the fact that at low MWCNTs loadings, the CNTs were well covered by the NPT. Whereas,

with high MWCNTs concentrations, the CNTs were poorly covered by the NPT due to issues of aggregation and poor dispersion during synthesis as confirmed by the SEM images (Kuvarega *et al.*, 2012a).

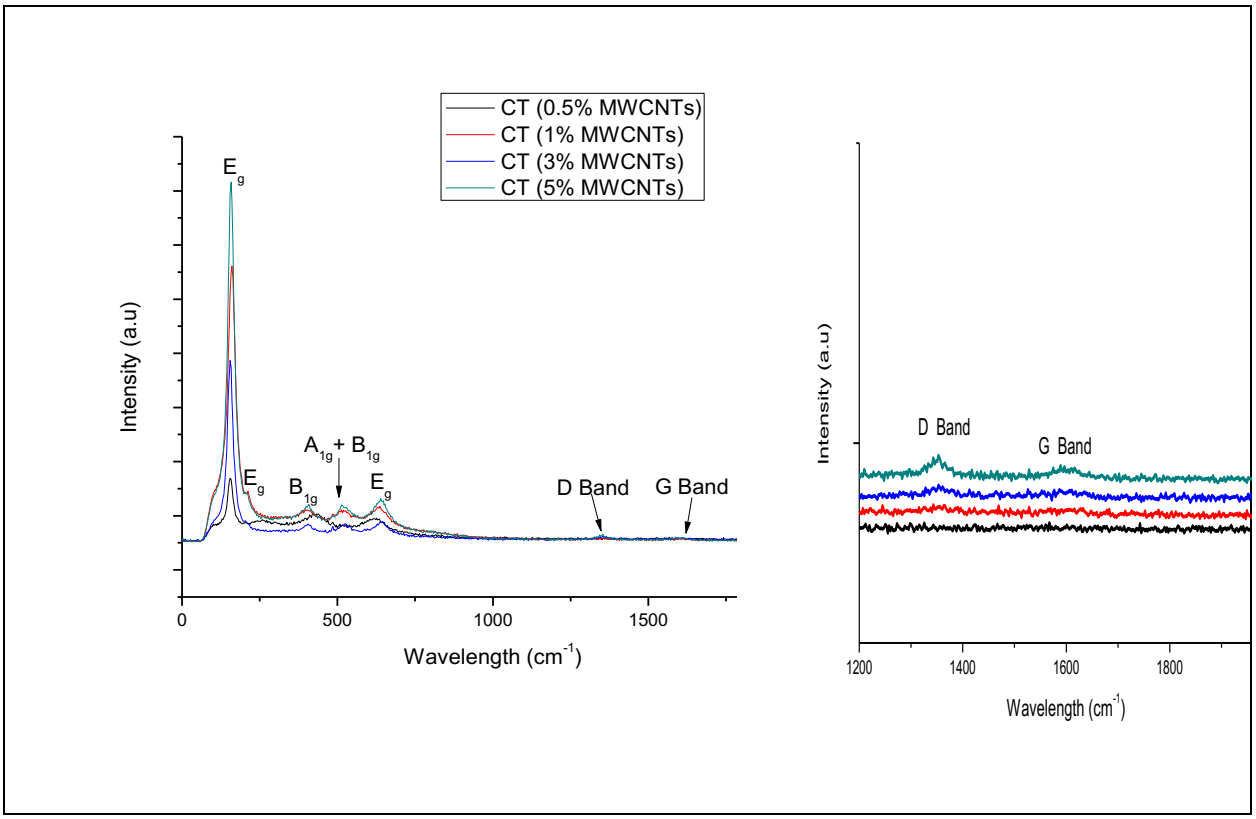


**Figure 6.3.3: Raman spectrum of CT nanocomposites.**

### 6.3.4 TGA analysis of CT nanocomposites

TGA analysis (**Figure 6.3.4 (A)** & (**B)**) was for studying the thermal stability of the synthesized nanocomposite and to estimate the amount of MWCNTs present in the nanocomposite (Kuvarega *et al.*, 2011). **Figure 6.3.4 (A)** shows that the MWCNTs decomposes at around 450 ˚C. A mass loss occurring at 30-100 ˚C was noted and this was found to be due to the loss of water adsorbed onto the surface of the material (**Figure 6.3.4 (B)**) (Wang *et al.*, 2009). The mass loss around 250 ˚C could be related to the loss of C and N-related compounds from the precursors. Another mass loss which was recorded at about 450 ˚C was attributed to the decomposition of MWCNTs. Mass losses occurring at temperatures above 450 ˚C which account for approximately 0.2, 0.25, 0.50 and 0.95% of the total masses of

the nanocomposites for the 0.5, 1.0, 3.0 and 5.0% CT nanocomposites, respectively, were observed. This means that the CT ratios used during the preparation of the nanocomposites are concordant to the TGA results of the nanocomposites. It is suspected that the observed negligible mass losses of MWCNTs occurred during the synthesis of the nanocomposites (Kuvarega *et al.*, 2012b). **Figure 6.3.4** also shows that the decomposition temperature's for the MWCNTs in the pristine CNTs and nanocomposites are different. The CNTs in nanocomposites are decomposing at the higher temperature compared to pure MWCNTs. In addition, at lower CNT dosages, where there is good coverage of CNTs by NPT, the decomposition temperature is much higher compared to nanocomposites with higher CNT loadings (poor coverage of CNTs by NPT). The observed difference could be due to the presence of NPT coated on MWCNTs which may limit the transfer of heat to the CNTs thus delaying the CNTs oxidation (Kuvarega *et al*., 2012a).

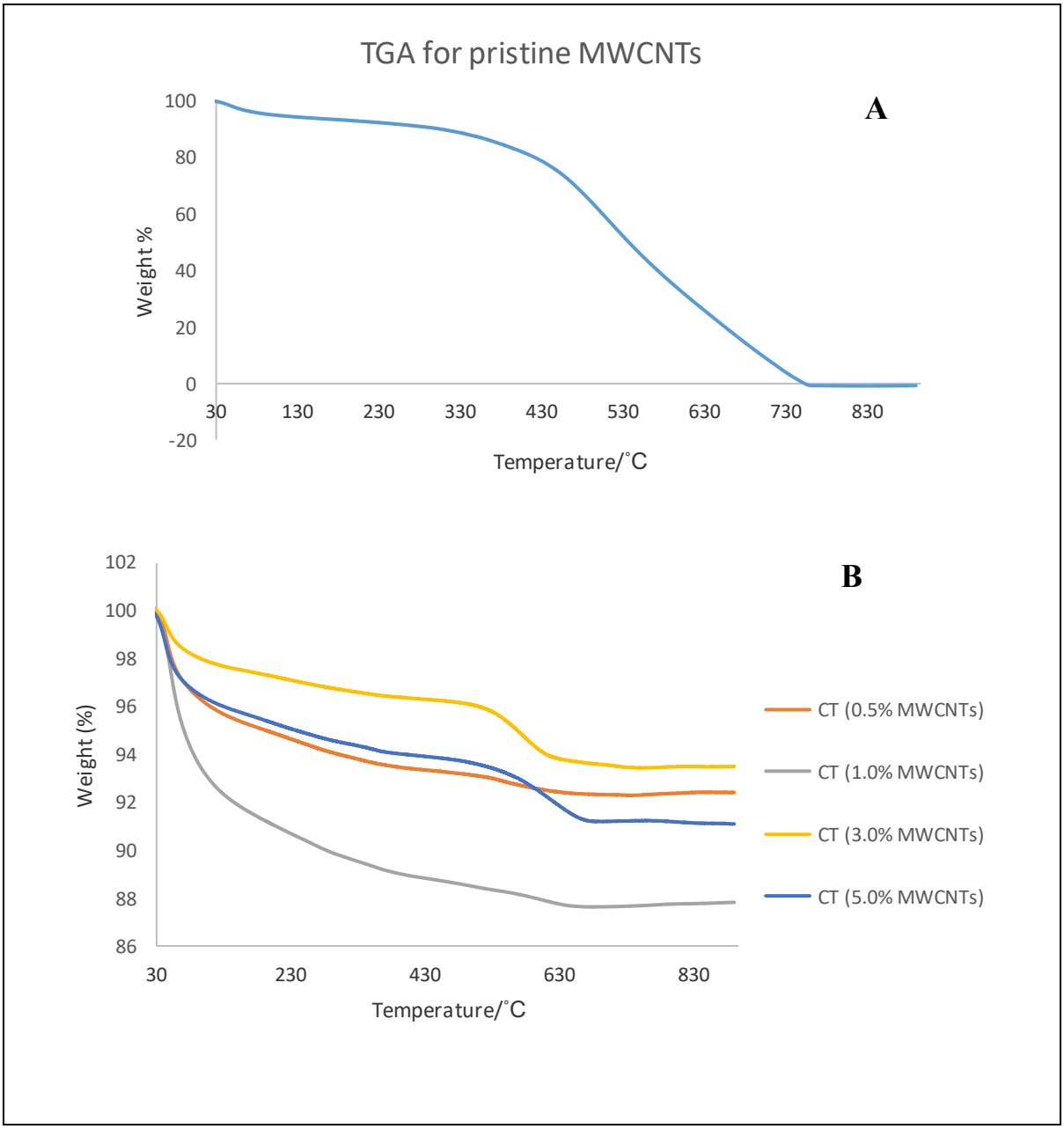


**Figure 6.3.4: TGA plot of pristine MWCNTs (A) and CT nanocomposites (B).**

### 6.3.5 SEM and EDS analysis of CT

**Figure 6.3.5.1** shows the SEM images of the synthesized CT (1.0% Pd). The SEM images of the pristine MWCNTs shows that the CNTs are highly aggregated (**Figure 6.3.5.1(A)**). **Figure 6.3.5.1 (B)** shows that the $TiO_2$ has nano-sized and nearly spherical shaped particles. The particles also show some degree of

aggregation. Moreover, **Figure 6.3.5.1 (C)** and **(D)** shows that the MWCNTs are covered with NPT (Kuvarega *et al.*, 2012b). CT (5.0% MWCNTs) show some CNTs structures protruding from the $TiO_2$ aggregates (marked with a circle). This proves poor coverage of CNTs by NPT at higher CNT loadings due to issues of poor dispersion of MWCNTs in 2-propanol thus leading to higher degree of aggregation (Kuvarega *et al.*, 2012b).

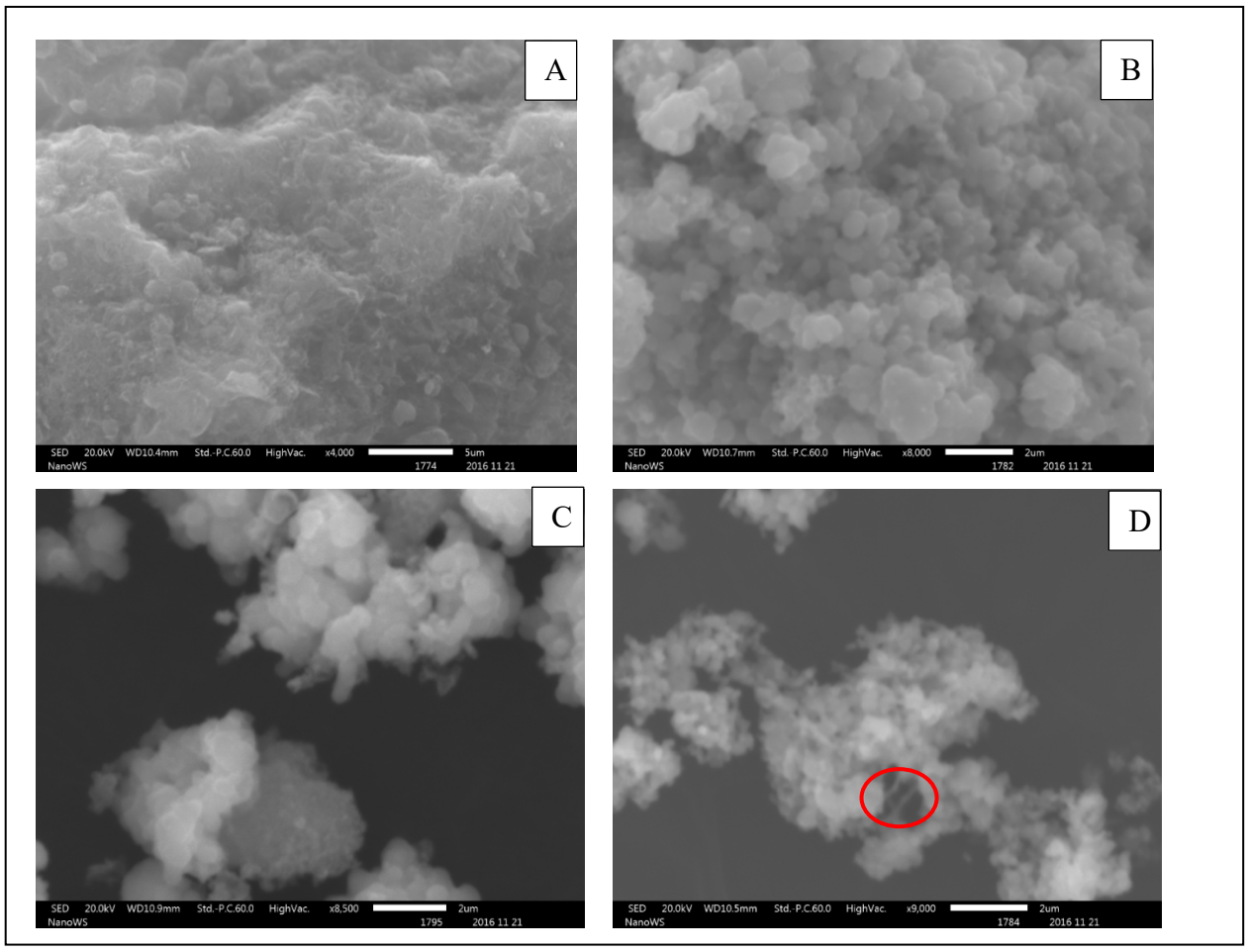


**Figure 6.3.5.1: SEM images of (A) Pristine MWCNTs, (B) CT (0.5% MWCNTs); (C) CT (1.0% MWCNTs); and (D) CT (5.0% MWCNTs).**

**Figure 6.3.5.2** illustrates the EDS spectrum of CT (1.0% MWCNTs), which confirms the elemental composition of the synthesized material. The spectrum confirms the presence of Ti, Pd, O,C and Cl; with Ti and O as the main components (Wang *et al.*, 2005; Yadav *et al.*, 2011). Cl most probably emanates

from the palladium diammine dichloride, which was used as a palladium source; it is suspected that the C is from both from the carbon tape that was used to mount the sample and/or the MWCNTs (Kuvarega *et al.*, 2012a).

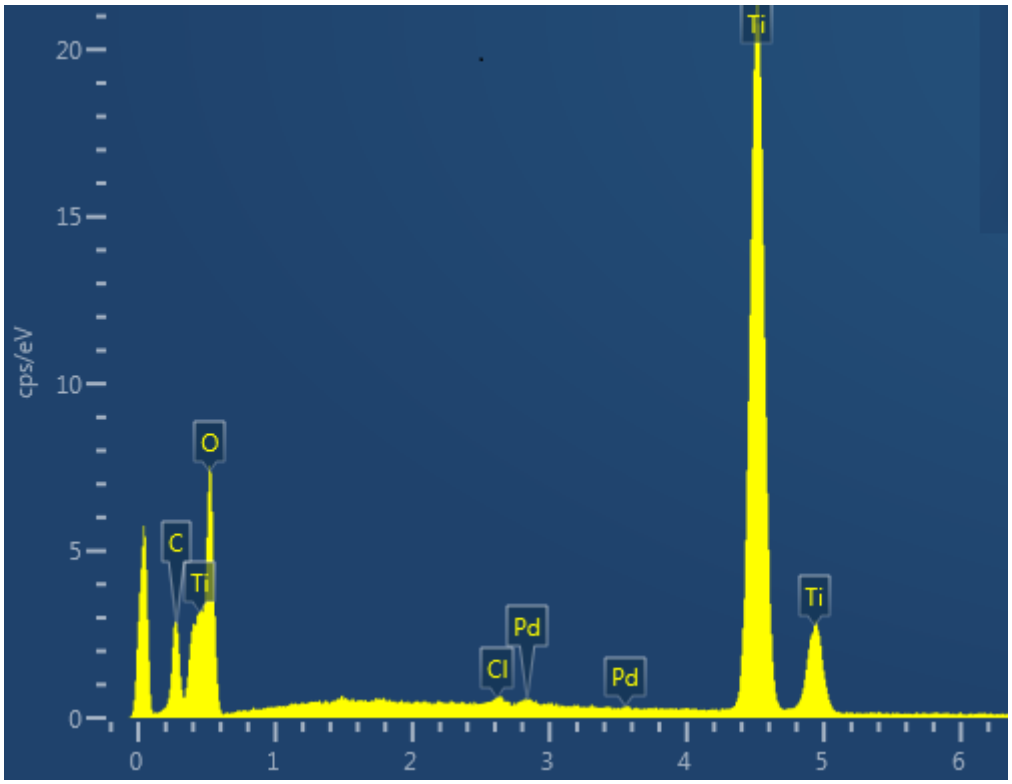


**Figure 6.3.5.2: EDS spectrum of CT (1.0% MWCNTs).**

## 6.4 PHOTOCATALYTIC DEGRADATION OF NOM USING MWCNTs/N, Pd CO-DOPED $TiO_2$

The procedure followed to evaluate the photoactivity of CT is described in **Section 3.10**. The performance of CT was studied by evaluating the degree of NOM (from Plettenberg Bay (P)) degradation under visible light irradiation after 2 hours (**Figure 6.4.1**). The effect of the catalyst (CT) on NOM was monitored using a UV-Vis spectrometer.

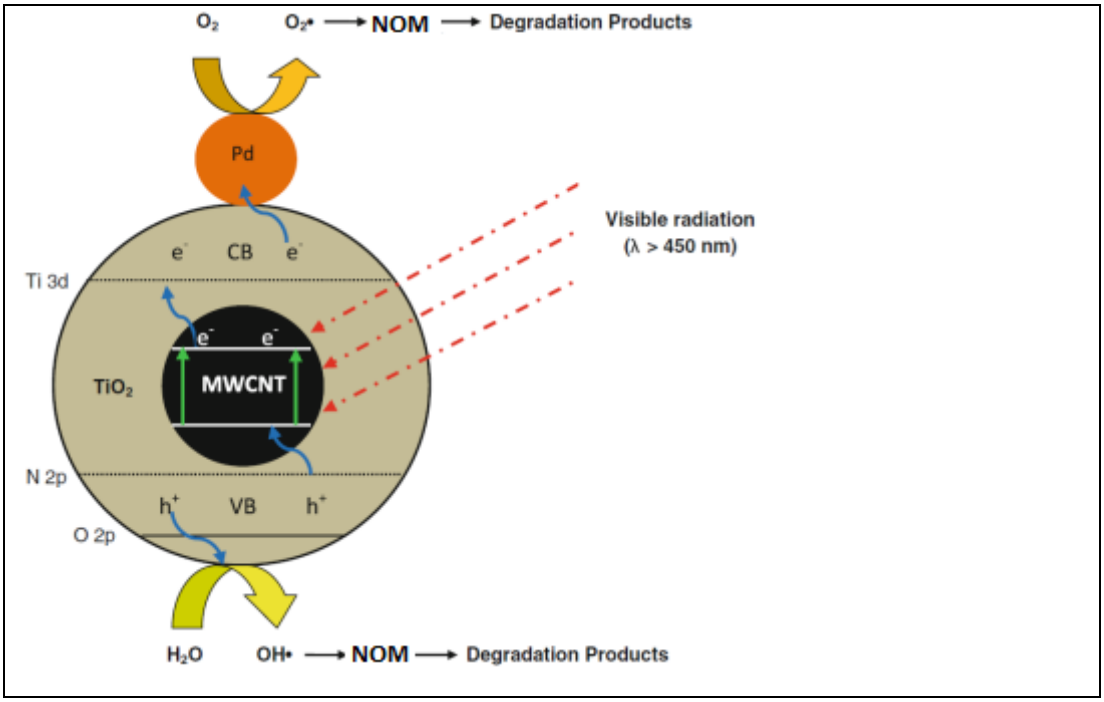


**Figure 6.4.1: Proposed scheme for the photocatalytic mechanism of NOM degradation by MWCNTs decorated with NPT** (Kuvarega *et al*., 2012a).

**Figure 6.4.2** shows the UV scan for the P raw water that was treated with CT, at various MWCNTs concentrations. The results show that raw water samples had the highest UV absorbance compared to the treated samples due to the suspended particles present in raw water which are known to absorb some UV light. Various concentrations of MWCNTs were loaded onto the prepared nanocomposites and the highest photodegradation rate for NOM under visible light was noted for CT (1.0% MWCNTs). This observation is concordant with the UV results presented in **Figure 6.3.2**. This could be due to the fact that at higher CNT loadings there is agglomeration which could end up reducing the surface area of the nanocomposites thus resulting in less NOM being adsorbed and degraded on the material's surface. However 5.0% MWCNT loadings is showing higher degradation efficiency compared to 3.0% MWCNTs and this could mean that the CT (5.0% MWCNTs) has a higher surface area available compared to 3.0% MWCNTs thus more NOM will be adsorbed onto its surface and more NOM is then degraded. The lifetime of OH radicals is very short, so if more is adsorbed on the

surface that will mean more NOM will have enough time to interact with the radicals.

**Figure 6.4.3** on the other hand shows a decrease in the aromatic content of NOM as evident by the $UV_{254}$ reduction of the P-1 (Round 2) water samples when various CT nanomposites were used. The results demonstrate that the nanocomposites had a high $UV_{254}$ (aromatic content of NOM) removal efficiency compared to NPT (1.0% Pd); with CT (1.0% MWCNTs) having the highest photodegradation efficiency compared to the other nanocomposites. Likewise, **Figure 6.4.4** shows the percentage DOC (amount of NOM present in water after it has been filtered through a 0.45 µm filter) removal for the nanocomposites at various MWCNTs loadings. These results show that CT (1.0% MWCNTs) has the highest percentage of DOC removal, with CT (3.0% MWCNTs) having the lowest. These results are concordant with the results presented in **Figure 6.4.3**, which shows the percentage $UV_{254}$ removal for the nanocomposites, with CT (1.0% MWCNTs) having the highest removal. The 0.5% and 5.0% MWCNTs loaded nanocomposites were shown to have similar DOC percentage removals. This contrast with results obtained for the aromatic content ($UV_{254}$) percentage removal (**Figure 6.4.3**), where the aromatic content ($UV_{254}$) percentage removal for 5.0% MWCNTs was higher than that of 0.5% MWCNTs. The MWCNTs are well decorated with N, Pd co-doped $TiO_2$ which enhances the surface area of the material and thus proves the occurrence of the synergistic effect of MWCNTs on NPT (Kuvarega *et al.,* 2012a).

CNTs are excellent acceptors of photogenerated electrons and have a lower Fermi level compared to $TiO_2$, which allow for free movement of electrons between the bands; it is because of these properties, that MWCNTs have a great potential of reducing electron-hole recombination (An *et al.*, 2007; Kuvarega *et al.*, 2012b). CNTs are also good adsorbents, and for this reason CNT-derived nanocomposites increase the adsorption of the targeted pollutant onto the surface of the nanocomposite (Gao *et al.*, 2009; Wang *et al.*, 2009; Kuvarega *et al.*, 2012b). Owing to the colour of CNTs and the fact that they can act as a photosensitizer, the nanocomposites absorb more light under the visible region (Gao *et al*., 2009; Wang *et al*., 2009). Moreover, the presence of N (which reduces the band gap of

$TiO_2$) and Pd (which reduces the electron-hole recombination) in the nanocomposite introduces a synergistic effect on the nanocomposite, which then results in the improved photoactivity of the material (Kuvarega *et al*., 2012b).

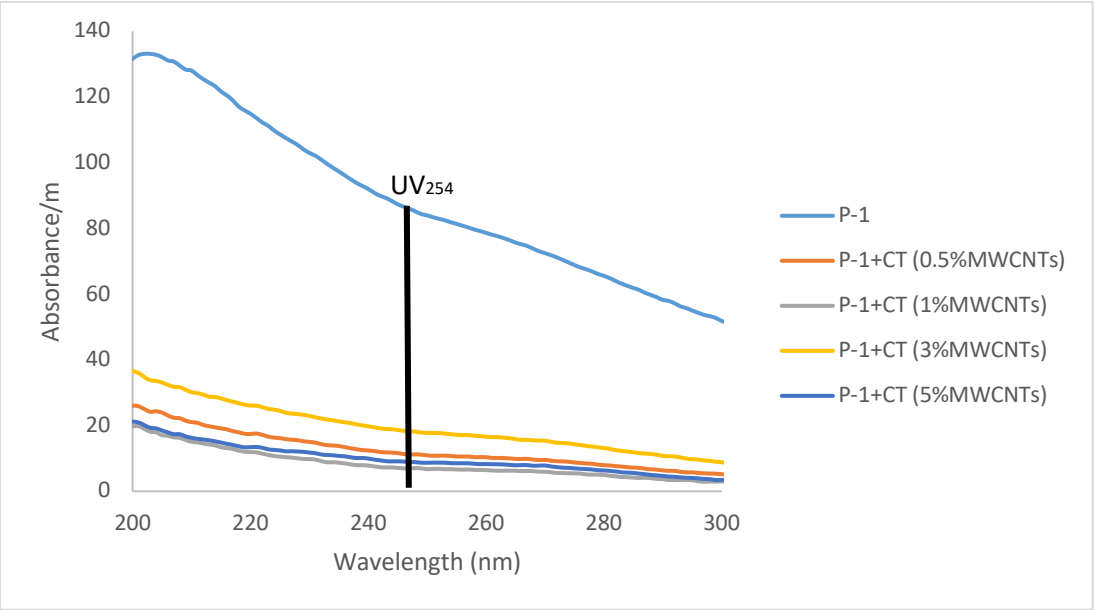


**Figure 6.4.2: UV scan of Plettenberg Bay raw water (P) sample (Round 2) with CT, at various MWCNTs concentrations after 2 hours.**

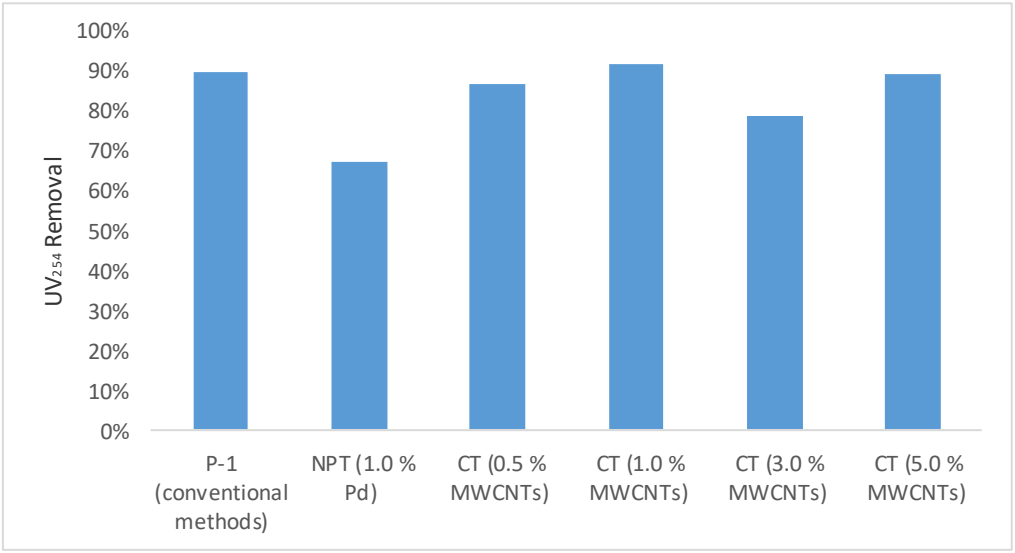


**Figure 6.4.3: Percentage $UV_{254}$ removal of the Plettenberg Bay raw water (P) sample (Round 2) using CT, at various MWCNTs concentrations after 2 hours.**

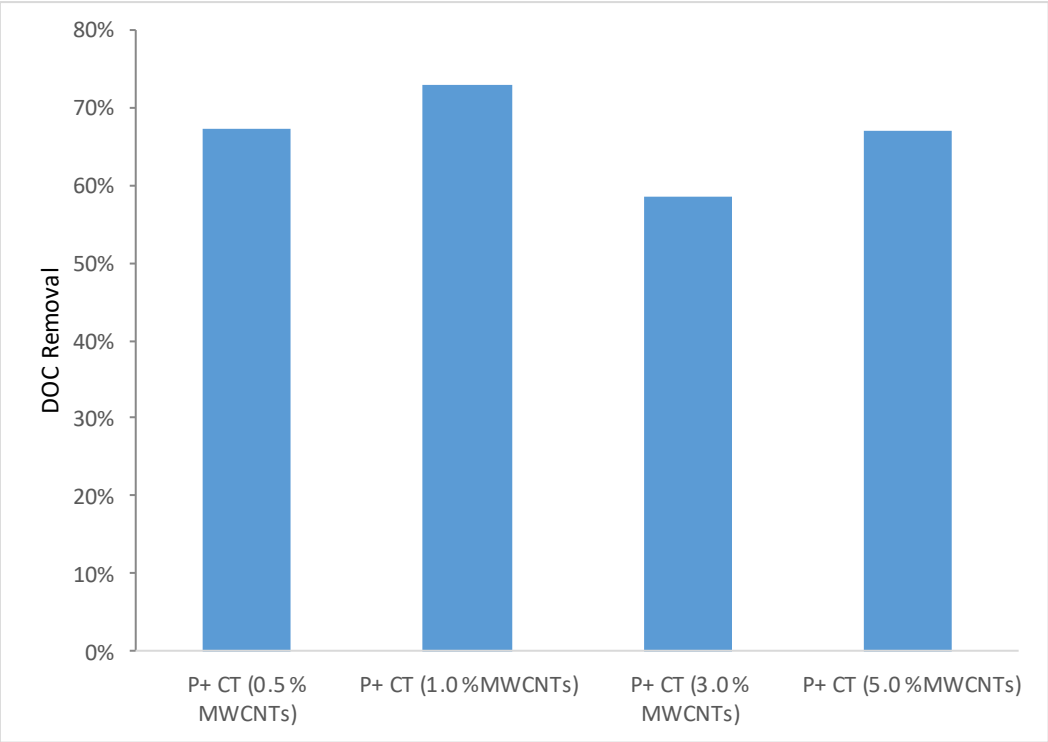


**Figure 6.4.4: Percentage DOC removal of Plettenberg Bay raw water (P) sample (Round 2) using CT, at various MWCNTs concentrations after 2 hours.**

## 6.5 CONCLUSION

In this chapter MWCNTs loaded (0.5-5.0% MWCNTs) on CT nanocomposites that were synthesized *via* a modified sol-gel method were effectively characterized and tested for their photodegradation efficiency towards NOM containing sample obtained from the Plettenberg Bay water treatment plant. This plant was chosen because of its high NOM content, specifically the hydrophobic fraction which has previously been shown to be effectively removed using treatment processes such as coagulation. In Chapter 5, the NPT nanomaterial was shown to be a promising nanomaterial for the photodegradation of NOM in water.

MWCNTs, have been reported as excellent adsorbants and photosensitizers that have a low Fermi level, which contributes towards the reduction of electron-hole recombination. Therefore, loading of the nanocomposites with MWCNTs was expected to improve the photoactivity of the resulting the nanocomposite in the visible region. To this end, CT nanocomposites showed the increased levels of photodegradation when compared with NPT nanomaterials; with a percentage loading of 1.0% MWCNTs having the highest photoactivity compared to other nanocomposites. The enhanced photodegradation is attributable to the large surface area of the material, which allows a huge amounts of NOM to be adsorbed onto the surface of the material (Lu & Su 2007). Adsorption of high amounts of the pollutant on the surface of the $TiO_2$ permits the photogenerated radicals to have enough time to interact with NOM (Kuvarega *et al.*, 2012a). All the above mentioned observations prove the existence of the synergistic effect of decorating the MWCNTs with NPT on the photoactivity of $TiO_2$ for water decontamination.

## 6.6 REFERENCES


An, G., Ma, W., Sun, Z., Liu, Z., Han, B., Miao, S., Miao, Z. & Ding, K. (2007) Preparation of titania/carbon nanotube composites using supercritical ethanol and their photocatalytic activity for phenol degradation under visible light irradiation. *Carbon N Y*, **45 (9)**:1795-1801.

Casbeer, E., Sharma, V.K. & Li, X.Z. (2012). Synthesis and photocatalytic activity of ferrites under visible light: A review. *Sep Purif. Technol*, **87**:1-14.

Chatterjee, D. & Dasgupta, S. (2005). Visible light induced photocatalytic degradation of organic pollutants. *J. Photochem. Photobiol*, **6 (2-3)**:186-205.

Cheng, X., Yu, X., Xing, Z. & Yang, L. (2012). Synthesis and characterization of N-doped $TiO_2$ and its enhanced visible-light photocatalytic activity. *Arab. J. Chem*, 1-5.

Di Paola, A., García-López, E., Marcì, G. & Palmisano, L. (2012). A survey of photocatalytic materials for environmental remediation. *J. Hazard. Mater*, 211-212:3-29.

Gao, B., Chen, G.Z. & Li Puma, G. (2009). Carbon nanotubes/titanium dioxide ($CNTs/TiO_2$) nanocomposites prepared by conventional and novel surfactant wrapping sol-gel methods exhibiting enhanced photocatalytic activity. *Appl. Catal. B Environ*, **89 (3-4)**, 503–509.

Gole, J.L., Stout, J.D., Burda, C., Lou, Y. & Chen, X. (2004). Highly Efficient Formation of Visible Light Tunable $TiO_{2-x}N_x$ Photocatalysts and Their Transformation at the Nanoscale. *J. Phys. Chem. B*, **108 (4)**:1230-1240.

Khairy, M. & Zakaria, W. (2014). Effect of metal-doping of $TiO_2$ nanoparticles on their photocatalytic activities toward removal of organic dyes. *Egypt J Pet*, **23 (4)**:419-426.

Kuvarega, A.T., Krause, R.W.M. & Mamba, B.B. (2011). Nitrogen / Palladium-codoped $TiO_2$ for efficient visible light photocatalytic dye degradation. *Society*, 22110–22120.

Kuvarega, A.T., Krause R.W.M. & Mamba, B.B. (2012a). Photocatalytic performance of nitrogen-platinum group metal co-doped $TiO_2$ supported on carbon nanotubes for visible-light degradation of organic pollutants in water. PhD thesis, University of Johannesburg.

Kuvarega, A.T., Krause, R.W.M. & Mamba, B.B. (2012b). Multiwalled carbon nanotubes decorated with nitrogen, palladium co-doped $TiO_2$ (MWCNT/N, Pd co-doped $TiO_2$) for visible light photocatalytic degradation of Eosin Yellow in water. *J Nanopart Res*, **14:776.**

Kuvarega, A.T. & Mamba, B.B. (2016). $TiO_2$ -based Photocatalysis: Toward Visible Light-Responsive Photocatalysts Through Doping and Fabrication of Carbon-based Nanocomposites. *Critical Reviews in Solid State and Materials Sciences*, 1–52.

Lu, C. & Su, F. (2007). Adsorption of natural organic matter by carbon nanotubes. *Sep. Purif. Technol*, **58 (1)**:113-121.

Luo, X. Chen, C., Yang, J., Wang, J., Yan, Q, Shi, H. & Wang, C. (2015). Characterization of La/Fe/$TiO_2$ and Its Photocatalytic Performance in Ammonia Nitrogen Wastewater. *Int. J. Environ. Res. Public health*, **12 (11)**:14626–39.

Mahlambi, M.M., Mishra, A.K., Mishra, S.B., Krause, R.W.M., Mamba, B.B. & Raichur, A.M. (2015). $TiO_2$ Nanocatalysts Supported on a Hybrid Carbon-Covered Alumina Support : Comparison between Visible Light and UV Light Degradation of Rhodamine B. *Journal of Nanotech*, 2015:1-8.

Murphy, A.B. (2007). Band-gap determination from diffuse reflectance measurements of semiconductor films, and application to photoelectrochemical water-splitting. *Sol. Energy Mater. Sol. Cells*, **91 (14)**:1326-1337.

Najjar, R., Shokri, M. & Farsadi, S. (2015). Preparation of Pd-doped nano-$TiO_2$ in microemulsion and their application in photodegradation of C.I. Acid Yellow 23. *Desalin. Water Treat*, **54 (9)**:2581-2591.

Nkambule, T. I., Kuvarega, A. T., Krause, R. W. M., Haarhoff, J., & Mamba, B. B. (2012). Synthesis and characterisation of Pd-modified N-doped $TiO_2$ for photocatalytic degradation of natural organic matter (NOM) fractions. *Environ Sci Pollut Res*, **19**, 4120–4132.

Wang, H., Wang, H.L. & Jiang, W.F. (2009). Solar photocatalytic degradation of 2, 6-dinitro-*p*-cresol (DNPC) using multi-walled carbon nanotubes (MWCNTs)-$TiO_2$ composite photocatalysts. *Chemosphere*, **75 (8)**:1105-1111.

Wang, W., Serp, P., Kalck, P. & Faria, J.L. (2005). Visible light photodegradation of phenol on MWNT-$TiO_2$ composite catalysts prepared by a modified sol-gel method. *J. Mol. Catal. A Chem*, **235 (1-2)**:194-199.

Yadav, S.K., Madeshwaran, S.R. & Cho, J.W. (2011). Synthesis of a hybrid assembly composed of titanium dioxide nanoparticles and thin multi-walled carbon nanotubes using “click chemistry.” *J. Colloid. Interface Sci*, **358 (2)**:471-476.

Yang, Z., Lan-lan, Q., Peng-wei, T. & You-xian, Z. (2014). Review of N and Metal co-Doped $TiO_2$ for Water Purification under Visible Light Irradiation. *Int. Conf. Environ. Chem. Biol*, **78 (7)**:139-142.

Yu, J., Ma, T. & Liu, S. (2011). Enhanced photocatalytic activity of mesoporous $TiO_2$ aggregates by embedding carbon nanotubes as electron-transfer channel. *Phys. Chem. Chem. Phys*, **13 (8)**:3491-3501.

Yu, Y., Yu, J.C., Chan, C.Y., Che, Y.K., Zhao, J.C., D, L., Ge, W.K. & Wong, P.K. (2005). Enhancement of adsorption and photocatalytic activity of $TiO_2$ by using

carbon nanotubes for the treatment of azo dye. *Appl. Catal. B Environ*, **61 (1-2):**1-11.

# CHAPTER 7
# CONCLUSION AND RECOMMENDATIONS

Owing to the fact that the character of NOM is not uniform in different locations due to geology, climate changes and human activities practised in the various regions and that NOM in the same location may differ seasonally due to issues of rainfall events, drought or floods and snowmelts runoff; the first objective of this study was to characterize NOM occurring in selected South African water sources. This was accomplished by collecting samples from seven various South African drinking water treatment plants via extensive sampling to account for different water types present in South Africa. The sampling was done during the period of September 2015 to September 2016 to account for seasonal variations. Samples were collected after each treatment stage for each treatment plant to study the treatability of NOM by various treatment processes. The obtained samples were characterized using conventional methods such as DOC, $UV_{254}$ and SUVA and advanced methods such as FEEM in order to understand the character of NOM occurring various geographic locations in South Africa. Lastly, owing to the size and complexity of NOM, which limits its removal efficiency from water by the available water treatment technologies, thus the second and the third objectives were to synthesize and characterize NPT and CT and to evaluate their photodegradation efficiency of NOM into smaller molecules prior to its removal. The overall findings obtained in this study were as follows:

- The character of NOM was not uniform in various South African raw water sources for various treatment plants under study and based on this, the treatability of NOM was not uniform. The treatability of NOM throughout the treatment train was also different with coagulation being more effective in removing NOM than other treatment steps.

- Conventional characterization methods showed that the raw water for VP had high SUVA values thus high content of high molecular weight and hydrophobic fraction of NOM compared to other raw water sources. However, the use of traditional NOM characterization methods such as DOC, $UV_{254}$, SUVA turbidity, conductivity and pH did not give enough information about the composition of NOM in water; SUVA and DOC/UV only serve as qualitative and quantitative tools, respectively. In order to get more information about the composition of NOM, advanced characterization method such as FEEM was used. The FEEM results showed that NOM samples with high humic substances (e.g. in HL, P and VP treatment plants) were effectively treated as they showed high $UV_{254}$ (aromatic character of NOM) removal percentages. FEEM also provided information regarding the treatability of NOM throughout the water treatment train, with the P samples after the coagulation process showing little traces of humic and fluvic components compared to its raw water samples. This proves that coagulation removes mostly the hydrophobic fractions of NOM. The treated water after filtration process showed very little or no traces of humic fractions and this proved the effectiveness of the filters used at P treatment plant in removing NOM.
- The synthesized NPT showed a red band shift in the absorption edge towards the visible region, which was indicated by the reduction of the band gaps of NPT with an increase in palladium concentrations. The NPT (0.5% Pd) showed the highest photocatalytic activity (58.8%) towards the aromatic character of NOM ($UV_{254}$), when evaluated against the Midvaal (MV) raw water sample under visible light irradiation. This proved the synergistic effect of co-doping with N and Pd which resulted in the reduction of band gap and possible reduced electron-hole recombination of the $TiO_2$. Various raw water samples obtained from the various water treatment plants located in South Africa revealed that the treatability of NOM using NPT was not uniform.
- Decorating MWCNTs with NPT resulted in further photocatalytic enhancement for NOM containing samples obtained from the P water treatment plant. MWCNTs are excellent adsorbents and photosensitizers

that have a low Fermi level, which contributes towards the reduction of electron-hole recombination. Therefore, loading of the MWCNTs of up to 1.0% increased the photocatalytic activity of the nanocomposite for up to 91.2% $UV_{254}$ reduction, compared to 68.2% achieved with NPT (1.0% Pd). The enhanced photoactivity of the $TiO_2$ was due to the synergistic effect of NPT with MWCNTs. CNTs are good adsorbents thus increases the adsorption of NOM on the surface of the $TiO_2$ thereby allowing enough time for the photogenerated radicals to interact with NOM.

All of the objectives brought forth in this study have been achieved and the study has raised the following questions/insights which need to be investigated further:

- There is a need to find more information regarding NOM treatability. It is well-known that coagulation removes most of the hydrophobic fraction. A similar conclusion need to be reached with regards to other treatment processes such as activated carbon filtration, disinfection etc.
- There is a need to establish a clear relationship between NOM fractions and different climatic seasons, so that the correct NOM removal methods can be implemented during the respective season in order to enhance the effective removal of NOM in water. For example, which fraction is more dominant in which season?
- The treatability of various fractions of NOM using CT needs to be determined in order to evaluate the efficiency of CT on different NOM fractions. The formed by product (if there are any) needs to be tested for their toxicity towards animals and their negative impact on the environment.

## APPENDIX A: CHARACTERIZATION OF NOM

**Table 1: Parameters used to study the character of NOM for the Magalies water (Round 1)**

| Sample Codes | pH | Conductivity (mS/cm) | Turbidity (NTU) | DOC (mg/l) |
|---|---|---|---|---|
| MP1-1 | 8.11±0.37 | 982±1.54 | 30.8±005 | 7.44 ± 0.28 |
| MP1-2 | 7.25±0.44 | 1040±2.02 | 5.42±0.02 | 5.19 ± 0.03 |
| MP1-3 | 7.18±0.21 | 1020±1.55 | 2.94±0.12 | 5.25 ± 0.07 |
| MP1-4 | 7.11±0.18 | 1043±0.15 | 0.36±0.03 | 4.25 ± 0.01 |
| MP1-5 | 7.05±055 | 1049±0.21 | 0.26±0.12 | 4.59 ± 0.11 |
| MP2-1B | 7.95±0.16 | 990±0.48 | 39.2±0.00 | 6.59 ± 0.12 |
| MP2-2 | 7.77±0.42 | 977±0.00 | 0.82±0.22 | 4.85 ± 0.07 |
| MP2-3 | 7.97±004 | 998±0.00 | 0.67±0.11 | 4.82 ± 0.06 |
| MP2-4 | 7.86±0.26 | 996±0.10 | 0.44±0.00 | 4.56 ± 0.09 |
| MP2-5 | 7.63±0.00 | 1005±0.01 | 0.42±0.014 | 4.52 ± 0.07 |
| MP3-2 | 7.72±0.08 | 655±0.08 | 4.25±0.21 | 5.24 ± 0.06 |
| MP3-3 | 7.76±0.01 | 1003±0.00 | 0.097±1.00 | 4.83 ± 0.02 |
| MP3-5 | 7.63±0.01 | 1009±0.15 | 0.57±0.58 | 4.77 ± 0.07 |

**Table 2: Parameters used to study the character of NOM for the Magalies water (Round 2)**

| Sample Codes | pH | Conductivity (mS/cm) | Turbidity (NTU) | DOC (mg/l) |
|---|---|---|---|---|
| MP1-1 | 8.37±0.78 | 528.0±2.35 | 24.50±1.55 | 4.96 ± 0.08 |
| MP1-2 | 7.63±0.62 | 577.0±1.82 | 8.11±1.08 | 3.83 ± 0.07 |
| MP1-3 | 7.63±0.60 | 507.5±1.42 | 0.02±0.06 | 3.55 ± 0.26 |
| MP1-4 | 7.69±0.04 | 562.2±0.64 | 0.00±0.00 | 2.93 ± 0.20 |
| MP1-5 | 7.32±0.09 | 567.4±0.03 | 0.00±0.00 | 3.08 ± 0.13 |
| MP2/-1B | 7.88±0.23 | 549.5±0.01 | 41.2±0.15 | 5.22 ± 0.17 |

| | | | | |
|---|---|---|---|---|
| MP2-2 | 8.04±0.21 | 531.3±0.02 | 0.00±0.00 | 3.99 ± 0.01 |
| MP2-3 | 8.05±0.71 | 533.3±0.55 | 0.00±0.00 | 4.16 ± 0.01 |
| MP2-5 | 7.54±0.23 | 541.4±2.28 | 0.00±0.00 | 3.47 ± 0.10 |
| MP3-1 | 8.27±0.01 | 530.7±1.77 | 54.2±0.37 | 5.36 ± 0.11 |
| MP3-2 | 7.98±0.01 | 538.2±0.22 | 6.35±0.44 | 4.26 ± 0.10 |
| MP3-3 | 7.90±0.55 | 541.5±0.25 | 0.00±0.00 | 4.05 ± 0.13 |
| MP3-5 | 7.67±0.13 | 545.3±0.11 | 0.00±0.00 | 3.81 ± 0.22 |

**Table 3: Parameters used to study the character of NOM for the Magalies water (Round 3)**

| Sample Codes | pH | Conductivity (mS/cm) | Turbidity (NTU) | DOC (mg/l) |
|---|---|---|---|---|
| MP1-1 | 7.63±0.26 | 559.7±12.01 | 1.49±0.05 | 5.94 ± 0.08 |
| MP1-2 | 7.62±0.81 | 570.5±2.45 | 2.03±0.01 | 5.28 ± 0.02 |
| MP1-3 | 7.79±0.81 | 568.2±1.50 | 0.03±0.01 | 4.58 ± 0.08 |
| MP1-4 | 7.84±2.12 | 579.1±3.52 | 0.00±0.00 | 4.35 ± 0.07 |
| MP1-5 | 7.60±0.05 | 589.3±2.09 | 0.00±0.00 | 4.48 ± 0.03 |
| MP2-1B | 7.93±0.01 | 579.2±4.1 | 0.00±0.00 | 3.96 ± 0.11 |
| MP2-2 | 8.59±0.01 | 568.2±9.21 | 0.35±0.03 | 4.44 ± 0.12 |
| MP2-3 | 8.60±0.65 | 574.5±2.27 | 0.02±0.01 | 4.63 ± 0.08 |
| MP2-5 | 7.90±0.00 | 573.1±3.05 | 0.00±0.00 | 4.35 ± 0.01 |
| MP3-1 | 8.23±0.27 | 588.2±0.12 | 1.26±0.05 | 6.06 ± 0.23 |
| MP3-2 | 8.29±0.89 | 558.9±0.01 | 2.46±0.12 | 4.44 ± 0.02 |
| MP3-3 | 8.20±0.005 | 557.6±0.02 | 0.00±0.00 | 4.26 ± 0.19 |
| MP3-5 | 7.81±0.55 | 574.3±0.00 | 0.00±0.00 | 4.06 ± 0.02 |

**Table 4: Parameters used to study the character of NOM for the Rietvlei plant**

| Sample code | pH | Conductivity (mS/cm) | Turbidity (NTU) | DOC (mg/l) |
|---|---|---|---|---|
| RV-1/1 | 8.58 ±0.03 | 665.3 ±0.01 | 13.19 ±0.00 | 8.25 ± 0.08 |
| RV-1/2 | 8.33 ±0.01 | 681.0 ±0.707 | 10.06 ±0.01 | 6.22 ± 0.13 |
| RV-1/3 | 7.94 ±0.00 | 707.8 ±0.707 | 0.01 ±0.55 | 4.83 ± 0.05 |
| RV-1/4 | 7.96 ±0.028 | 441.8 ±1.05 | 0.07 ±0.00 | 5.59 ± 0.09 |
| RV-1/5 | 7.84 ±0.084 | 558.6 ±2.83 | 0.45 ±0.01 | 3.67 ± 0.14 |
| RV-2/1 | 9.04 ±0.07 | 450.3 ±0.12 | 5.82 ±0.13 | 10.12 ± 0.16 |
| RV-2/4 | 9.30 ±0.02 | 451.0 ±0.09 | 0.22 ±0.27 | 6.62 ± 0.06 |
| RV-2/5 | 8.99 ±0.03 | 392.3 ±0.15 | 0.28 ±0.05 | 5.16 ± 0.17 |
| RV-3/1 | 8.13 ±0.035 | 402.0 ±0.03 | 2.61 ±0.84 | 7.42 ± 0.00 |
| RV-3/3 | 8.06 ±0.005 | 421.5 ±0.00 | 0.07 ±0.26 | 4.32 ± 0.15 |
| RV-3/4 | 8.11 ±0.015 | 416.7 ±0.75 | 0.00 ±0.09 | 4.73 ± 0.04 |
| RV-3/5 | 8.05 ±0.005 | 373.3 ±0.06 | 0.00 ±0.00 | 2.87 ± 0.12 |
| RV-4/1 | 8.08 ±0.00 | 407.8 ±0.71 | 3.32 ±0.01 | 7.53 ± 0.12 |
| RV-4/3 | 7.62 ±0.0275 | 425.6 ±0.015 | 0.00 ±0.01 | 4.20 ± 0.13 |
| RV-4/4 | 7.72 ±0.061 | 425.6 ±0.20 | 0.00 ±0.27 | 4.62 ± 0.14 |
| RV-4/5 | 7.44 ±0.50 | 385.0 ±0.59 | 0.00 ±0.06 | 2.97 ± 0.11 |
| RV-5/1 | 7.98 ±0.01 | 427.0 ±0.71 | 1.07 ±0.11 | 1.58 ± 0.06 |
| RV-5/3 | 7.60 ±0.01 | 430.0 ±0.35 | 0.87 ±0.09 | 1.43 ± 0.02 |
| RV-5/4 | 7.63 ±0.04 | 436.0 ±0.00 | 0.27 ±0.00 | 1.37 ± 0.03 |
| RV-5/5 | 7.67 ±0.11 | 384.5 ±2.47 | 0.46 ±0.01 | 1.54 ± 0.04 |

**Table 5: Parameters used to study the character of NOM for the Ebenezer plant**

| Sample code | pH | Conductivity (mS/cm) | Turbidity (NTU) | DOC (mg/l) |
|---|---|---|---|---|
| LE-1/1 | 7.21±0.005 | 96.1±0.98 | 1.87±0.05 | 2.50 ± 0.05 |
| LE-1/2 | 9.33±0 | 77.4±0.25 | 2.22±0.88 | 1.62 ± 0.10 |
| LE-1/3 | 7.95±0.005 | 72.3±0.09 | 2.10±0.16 | 1.52 ± 0.07 |
| LE-1/4 | 7.20±0.01 | 86.9±0.05 | 1.35±0.00 | 1.23 ± 0.09 |
| LE-1/5 | 7.19±0.007 | 209.7±0.12 | 1.71±0.01 | 1.23 ± 0.10 |
| LE-2/1 | 7.25±0.04 | 39.6±0.10 | 2.46±0.03 | 0.21 ± 0.04 |
| LE-2/2 | 7.22±0.07 | 48.2±0.00 | 1.09±0.12 | 0.26 ± 0.11 |
| LE-2/3 | 7.52±0.12 | 44.3±0.23 | 1.37±0.01 | 0.38 ± 0.10 |
| LE-2/4 | 7.33±0.52 | 45.0±0.10 | 0.07±0.00 | 0.06 ± 0.07 |
| LE-2/5 | 7.55±0.05 | 47.9±0.10 | 0.00±0.00 | 0.00 ± 0.00 |
| LE-3/1 | 6.94±0.07 | 40.7±0.21 | 3.2±0.35 | 0.13 ± 0.06 |
| LE-3/2 | 6.90±0.42 | 48.4±0.42 | 2.6±0.01 | 0.00 ± 0.00 |
| LE-3/3 | 7.07±0.00 | 44.4±0.35 | 9.7±0.74 | 0.00 ± 0.00 |
| LE-3/4 | 7.08±0.15 | 43.5±0.21 | 0±0.00 | 0.00 ± 0.00 |
| LE-3/5 | 7.06±0.36 | 44.3±0.14 | 1.3±0.38 | 0.00 ± 0.00 |
| LE-4/1 | 7.37±0.19 | 37.8±0.28 | 0.81±0.05 | 0.79 ± 0.05 |
| LE-4/2 | 7.49±0.22 | 45.85±0.35 | 0.73±0.04 | 0.92 ± 0.03 |
| LE-4/3 | 7.71±0.23 | 41.3±0.57 | 0.82±0.21 | 1.92 ± 0.01 |
| LE-4/4 | 7.57±0.24 | 40.9±0.00 | 0.54±0.10 | 0.18 ± 0.02 |
| LE-4/5 | 7.39±0.37 | 45.4±2.83 | 0.66±0.08 | 1.73 ± 1.01 |

**Table 6: Parameters used to study the character of NOM for the Olifantspoort plant**

| Sample code | pH | Conductivity | Turbidity | DOC |
|---|---|---|---|---|

| | | (mS/cm) | (NTU) | (mg/l) |
|---|---|---|---|---|
| LO-1/1 | 7.75±0.01 | 600.1±1.00 | 38.30±0.66 | 6.69 ± 0.05 |
| LO-1/2 | 8.27±0.01 | 601.0±1.00 | 3.69±0.43 | 6.39 ± 0.17 |
| LO-1/3 | 8.15±0.00 | 606.7±2.08 | 0.22±0.05 | 6.03 ± 0.12 |
| LO-1/4 | 7.62±0.01 | 616.3±0.58 | 0.26±0.00 | 5.67 ± 0.12 |
| LO-2/1 | 7.88±0.15 | 588.2±0.15 | 13.8±0.37 | 4.49 ± 0.19 |
| LO-2/2 | 7.91±0.01 | 625.9±2.45 | 7.55±1.16 | 4.03 ± 0.05 |
| LO-2/3 | 7.83±0.04 | 645.4±0.05 | 0.00±0.00 | 3.81 ± 0.12 |
| LO-2/4 | 7.41±0.00 | 638.6±0.19 | 0.00±0.00 | 3.46 ± 0.09 |
| LO-3/1 | 8.24±0.03 | 1124.5±0.00 | 15.05±1.11 | 3.04 ± 0.09 |
| LO-3/2 | 8.20±0.00 | 1097.5±0.70 | 4.42±0.32 | 2.57 ± 0.05 |
| LO-3/3 | 8.13±0.00 | 1077.5±3.52 | 0.62±0.27 | 2.43 ± 0.04 |
| LO-3/4 | 7.84±0.00 | 1089.0±8.48 | 0.74±0.10 | 2.26 ± 0.10 |

**Table 7: Parameters used to study the character of NOM for the Flag Boshielo plant**

| Sample code | pH | Conductivity (mS/cm) | Turbidity (NTU) | DOC (mg/l) |
|---|---|---|---|---|
| LF-1/1 | 7.61±0.01 | 512±1.00 | 10.79±0.29 | 7.20 ± 0.21 |
| LF-1/2 | 7.63±0.03 | 521±1.00 | 2.91±0.10 | 6.06 ± 0.05 |
| LF-1/3 | 7.61±0.01 | 533±0.58 | 1.85±0.11 | 5.83 ± 0.23 |
| LF-1/4 | 7.43±0.01 | 537±1.53 | 0.61±0.05 | 6.30 ± 0.17 |
| LF-2/1 | 8.42±0.02 | 528.0±4.24 | 6.50±1.00 | 8.27± 0.45 |
| LF-2/2 | 8.23±0.55 | 552.2±2.12 | 2.4±0.31 | 6.52 ± 0.12 |
| LF-2/3 | 7.93±0.13 | 545.5±3.53 | 2.4±1.01 | 6.69 ± 0.16 |
| LF-2/4 | 7.49±0.00 | 546.2±0.70 | 2.4±1.13 | 7.09 ± 0.13 |
| LF-3/1 | 7.72±0.05 | 531.5±2.12 | 14.37±1.77 | 11.30 ± 0.22 |
| LF-3/2 | 8.75±0.11 | 549.5±3.54 | 4.40±0.55 | 8.53 ± 0.22 |
| LF-3/3 | 8.51±0.08 | 543.0±4.95 | 3.66±0.25 | 8.40 ± 0.31 |
| LF-3/4 | 7.79±0.41 | 559.0±5.66 | 6.06±0.11 | 8.71 ± 0.01 |

**Table 8: Parameters used to study the character of NOM for the Plettenburg plant**

| Sample code | pH | Conductivity (mS/cm) | Turbidity (NTU) | DOC (mg/l) |
|---|---|---|---|---|
| P-1/1 | 6.28±0.16 | 96.6±5.21 | 0.01±0.02 | 4.91± 0.12 |
| P-1/2 | 5.61±0.07 | 114.4±0.32 | 3.45±0.71 | 0.45 ± 0.07 |
| P-1/3 | 6.60±0.23 | 127.7±2.65 | 0.14±0.09 | 0.21 ± 0.02 |
| P-1/4 | 6.54±0.32 | 130.1±3.78 | 0.00±0.00 | 0.10 ± 0.09 |
| P-1/5 | 6.65±0.16 | 135.6±9.8 | 0.05±0.08 | 0.84 ± 0.05 |
| P-2/1 | 5.17±0.00 | 67.55±3.18 | 2.68±0.30 | 21.11 ± 0.04 |
| P-2/2 | 4.78±0.01 | 118.35±1.63 | 19.02±0.64 | 1.16 ± 0.05 |
| P-2/3 | 4.89±0.01 | 103.50±0.99 | 1.54±0.14 | 1.27 ± 0.03 |
| P-2/4 | 5.09±0.06 | 101.85±1.63 | 0.58±0.13 | 1.31 ± 0.02 |
| P-2/5 | 9.65±0.13 | 135.00±0.85 | 0.49±0.08 | 1.69 ± 0.04 |

**Table 9: Parameters used to study the character of NOM for the Preekstoel (VP) and Hermanus (VH) plants**

| Sample code | pH | Conductivity (mS/cm) | Turbidity (NTU) | DOC (mg/l) |
|---|---|---|---|---|
| VP-1/1 | 2.50±0.02 | 1732.7±4.20 | 4.44±4.04 | 8.50 ± 0.26 |
| VP-1/2 | 5.32±0.01 | 295.0±2.15 | 13.06±0.56 | 4.97 ± 0.05 |
| VP-1/3 | 2.76±0.01 | 964.7±0.15 | 0.00±0.00 | 3.09 ± 0.13 |
| VP-1/4 | 3.55±0.01 | 403.7±2.18 | 0.00±0.00 | 2.45 ± 0.15 |
| VP-1/5 | 8.30±0.01 | 310.7±2.07 | 0.39±1.52 | 3.00 ± 0.05 |
| VP-2/1 | 6.75±0.21 | 235.7±4.72 | 8.15±0.47 | 6.19 ± 0.17 |
| VP-2/2 | 4.71±0.02 | 251.7±1.5 | 20.8±1.91 | 5.90 ± 0.15 |
| VP-2/3 | 4.99±0.01 | 250.3±0.6 | 2.71±0.12 | 5.57 ± 0.09 |
| VP-2/4 | 5.51±0.06 | 250.3±0.6 | 0.24±0.01 | 4.60 ± 0.23 |
| VP-2/5 | 7.15±0.15 | 549.0±4.6 | 0.16±0.04 | 0.44 ± 0.05 |
| VH-1/1 | 6.24±0.02 | 709.0±0.05 | 8.02±1.00 | 0.00 ±0.00 |
| VH-1/4 (Mn) | 6.91±0.01 | 667.5±0.01 | 0.12±2.65 | 0.00 ±0.00 |

| | | | | |
|---|---|---|---|---|
| VH-1/4 (Fe) | 5.62±0.01 | 715.7±0.01 | 1.14±1.53 | 0.00 ±0.00 |
| VH-2/1 | 5.46±0.02 | 483.3±2.89 | 12.93±1.55 | 0.07 ± 0.01 |
| VH-2/4 (Mn) | 5.27±0.07 | 474.7±2.31 | 10.23±3.22 | 0.11 ± 0.02 |
| VH-2/4 (Fe) | 7.86±0.28 | 540.7±1.00 | 0.28±0.10 | 0.24 ± 0.10 |

**Table 10: Parameters used to study the character of NOM for the AM, HL, UM & MT plants**

| Sample code | pH | Conductivity (mS/cm) | Turbidity (NTU) | DOC (mg/l) |
|---|---|---|---|---|
| AM-1/1 | 7.18±0.02 | 138.4±0.63 | 6.32±0.15 | 14.8 ± 0.09 |
| AM-1/2 | 9.03±0.00 | 166.3±0.35 | 9.15±0.18 | 14.78 ± 0.10 |
| AM-1/3 | 8.93±0.01 | 167.7±0.21 | 0.22±0.07 | 14.75 ± 0.11 |
| AM-1/4 | 8.82±0.22 | 168.5±0.71 | 0.00±0.00 | 14.73 ± 0.03 |
| AM-1/5 | 7.68±0.00 | 236.0±0.00 | 0.00±0.00 | 23.8 ± 0.13 |
| AM-2/1 | 6.745±0.01 | 130.65±7.14 | 9.33±0.00 | 4.26 ± 0.10 |
| AM-2/2 | 8.425±0.02 | 150.1±0.71 | 6.23±0.57 | 3.66 ± 0.07 |
| AM-2/3 | 8.08±0.04 | 148.65±0.21 | 1.115±0.01 | 3.53 ± 0.06 |
| AM-2/4 | 7.79±0.13 | 146.9±0.57 | 0.30±0.13 | 3.51 ± 0.06 |
| AM-2/5 | 7.65±0.01 | 210.5±4.95 | 0.415±0.21 | 3.328 ± 0.07 |
| HL-1/1 | 8.81±0.03 | 172.3±3.82 | 8.81±0.03 | 16.59 ± 0.07 |
| HL-1/2 | 8.27±0.01 | 186.4±1.70 | 8.22±0.02 | 18.76 ± 0.09 |
| HL-1/3 | 8.47±0.01 | 189.7±2.83 | 0.07±0.04 | 18.46 ± 0.07 |
| HL-1/4 | 7.81±0.06 | 187.4±1.06 | 0.00±0.00 | 17.06 ± 0.04 |
| HL-1/5 | 7.28±0.18 | 187.5±0.64 | 0.00±0.00 | 17.13 ± 0.12 |
| HL-2/1 | 6.85±0.11 | 163.8±0.99 | 57.95±0.07 | 4.82 ± 0.17 |
| HL-2/2 | 8.505±0.05 | 185.9±0.99 | 11.27±5.56 | 3.47 ± 0.09 |
| HL-2/3 | 8.75±0.01 | 186.65±1.91 | 1.37±0.48 | 3.40 ± 0.08 |
| HL-2/4 | 8.705±0.02 | 188.9±0.00 | 0.33±0.18 | 3.37 ± 0.02 |
| HL-2/5 | 8.69±0.01 | 193.45±1.48 | 0.63±0.05 | 3.25 ± 0.0745 |
| UM-1/1 EJ | 7.37±0.02 | 353.5±0.00 | 3.95±0.20 | 36.9± 0.14 |

| | | | | |
|---|---|---|---|---|
| UM-1/1 U | 7.53±0.05 | 386.0±0.00 | 0.02±0.01 | 24.69± 0.09 |
| UM-1/2 | 8.37±0.03 | 371.5±7.78 | 4.02±0.24 | 29.74± 0.38 |
| UM-1/3 | 8.35±0.06 | 374.5±1.42 | 0.63±0.08 | 22.49± 0.31 |
| UM-1/4 | 7.61±0.00 | 360.5±0.71 | 0.00±0.00 | 4.46 ± 0.19 |
| UM-1/5 | 7.57±005 | 373.7±4.21 | 0.00±0.00 | 3.74 ± 0.05 |
| UM-2/1 EJ | 7.63±0.01 | 314.5±0.71 | 2.32±0.23 | 4.46 ± 0.19 |
| UM-2/1 U | 6.95±0.00 | 282.5±0.71 | 10.325±0.19 | 6.01 ± 0.25 |
| UM-2/2 | 7.94±0.02 | 311±1.41 | 6.19±0.65 | 4.56 ± 0.16 |
| UM-2/3 | 9.04±0.01 | 271±19.80 | 3.695±0.59 | 4.57 ± 0.16 |
| UM-2/4 | 8.43±0.01 | 309.5±4.95 | 0.595±0.35 | 4.46 ± 0.09 |
| UM-2/5 | 7.56±0.01 | 315.5±0.72 | 0.545±0.28 | 4.37 ± 0.22 |
| MT-1/1 | 7.75±0.02 | 305.5±1.41 | 26.1±0.11 | 30.05 ± 0.25 |
| MT-1/2 | 7.74±0.09 | 310.0±4.24 | 22.4±2.24 | 29.02 ± 0.15 |
| MT-1/3 | 7.69±0.06 | 309.5±1.41 | 3.54±1.66 | 28.74 ± 0.11 |
| MT-1/4 | 7.74±0.05 | 310.5±2.12 | 0.00±0.00 | 28.69 ± 0.07 |
| MT-1/5 | 7.55±0.00 | 305.2±1.41 | 1.87±1.56 | 26.52 ± 0.13 |
| MT-2/1 | 7.79±0.05 | 267.0±4.24 | 13.55±0.45 | 3.75 ± 0.13 |
| MT-2/2 | 8.93±0.03 | 285.0±4.24 | 4.62±0.04 | 1.88 ± 0.22 |
| MT-2/3 | 7.86±0.02 | 269.5±7.78 | 1.29±0.56 | 2.91 ± 0.13 |
| MT-2/4 | 7.72±0.01 | 274.0±1.4 | 0.58±0.04 | 2.80 ± 0.11 |
| MT-2/5 | 7.36±0.04 | 269.5±4.9 | 0.82±0.04 | 2.46 ± 0.09 |

**Table 11: Parameters used to study the character of NOM for the Midvaal**

| Sample code | pH | Conductivity (mS/cm) | Turbidity (NTU) | DOC (mg/l) |
|---|---|---|---|---|
| MV-1/1 | 9.15±0.83 | 606.3±2.50 | 19.01±1.35 | 5.53 ± 0.05 |
| MV-1/2 | 9.06±0.02 | 610.3±1.52 | 17.79±0.01 | 6.45 ± 0.12 |
| MV-1/3 | 8.98±0.01 | 665.0±0.15 | 12.92±0.01 | 5.48 ± 0.12 |
| MV-1/4 | 8.76±0.05 | 619.0±0.27 | 5.33±0.01 | 5.14 ± 0.07 |
| MV-1/5 | 8.74±0.00 | 621.7±1.57 | 4.78±0.00 | 5.14 ± 0.09 |
| MV-1/6 | 9.09±0.30 | 621.3±2.77 | 5.59±0.04 | 5.10 ± 0.08 |
| MV-1/7 | 8.99±0.07 | 617.3±0.48 | 2.82±0.07 | 5.02 ± 0.08 |
| MV-1/8 | 8.01±0.14 | 614.0±0.04 | 0.41±0.12 | 4.44 ± 0.06 |
| MV-1/9 | 7.96±0.00 | 620.7±0.09 | 0.44±0.00 | 4.28 ± 0.04 |
| MV-2/1 | 9.07±0.01 | 480±1.53 | 10.27±0.73 | 5.31 ± 0.09 |
| MV-2/2 | 9.05±0.01 | 491±0.58 | 5.84±0.78 | 5.49 ± 0.24 |
| MV-2/3 | 8.94±0.01 | 495±1.00 | 6.65±0.77 | 5.25 ± 0.02 |
| MV-2/4 | 8.17±0.01 | 516±1.53 | 3.64±0.61 | 5.13 ± 0.11 |
| MV-2/5 | 8.57±0.17 | 494±1.53 | 10.68±0.28 | 4.87 ± 0.04 |
| MV-2/6 | 8.34±0.01 | 510±1.00 | 6.20±0.28 | 4.48 ± 0.14 |
| MV-2/7 | 8.22±0.02 | 523±1.53 | 2.07±0.47 | 4.56 ± 0.01 |
| MV-2/8 | 7.39±0.01 | 523±3.05 | 0.00±0.00 | 3.87 ± 0.06 |
| MV-2/9 | 7.32±0.01 | 531±1.00 | 0.00±0.00 | 3.50 ± 0.80 |
| MV-3/1 | 8.82±0.02 | 644.0±7.07 | 11.35±1.35 | 5.45 ± 0.12 |
| MV-3/2 | 8.84±0.01 | 640.0±4.24 | 13.38±5.26 | 5.37 ± 0.06 |
| MV-3/3 | 8.80±0.08 | 637.5±2.12 | 9.53±7.74 | 4.81 ± 0.16 |

| | | | | |
|---|---|---|---|---|
| MV-3/4 | 8.58±0.01 | 643.3±2.83 | 15.05±1.31 | 4.68 ± 0.02 |
| MV-3/5 | 8.30±0.26 | 647.2±0.71 | 9.22±0.93 | 4.76 ± 0.02 |
| MV-3/6 | 7.95±0.05 | 643.3±2.82 | 10.68±1.02 | 4.53 ± 0.17 |
| MV-3/7 | 7.91±0.11 | 661.5±2.82 | 2.38±2.21 | 4.61 ± 0.08 |
| MV-3/8 | 7.56±0.10 | 660.0±7.07 | 0.01±0.00 | 3.72 ± 0.05 |
| MV-3/9 | 7.66±0.19 | 731.5±5.67 | 0.00±0.00 | 3.62 ± 0.03 |
| MV-4/1 | 8.85±0.71 | 675.5±7.48 | 11.50±1.55 | 8.13 ± 0.28 |
| MV-4/2 | 8.65±0.78 | 679±5.36 | 2.03±1.42 | 8.16 ± 0.25 |
| MV-4/3 | 8.65±0.23 | 643±1.72 | 3.12±0.64 | 7.82 ± 0.22 |
| MV-4/4 | 8.17±0.21 | 682±5.15 | 2.09±0.15 | 7.67 ± 0.26 |
| MV-4/5 | 8.54±0.62 | 690.5±8.49 | 3.12±0.33 | 7.26 ± 0.12 |
| MV-4/6 | 8.28±0.23 | 682.5±27.58 | 1.47±1.08 | 6.92 ± 0.03 |
| MV-4/7 | 8.35±0.04 | 662±28.28 | 1.27±0.06 | 6.65 ± 0.20 |
| MV-4/8 | 7.48±0.60 | 686±32.53 | 0.39±1.82 | 5.64 ± 0.19 |
| MV-4/9 | 7.54±0.09 | 687±8.28 | 0.30±0.03 | 5.83 ± 0.22 |

## APPENDIX B: UV VALUES AT DIFFERENT WAVELENGTHS

**Table 12: UV values at different wavelengths for Magalies plant (in $m^{-1}$) (Round 1)**

| Sample Codes | UV Absorbance | | | |
|---|---|---|---|---|
| | 214 | 254 | 272 | 300 |
| MP1-1 | 23.87 | 11.26 | 10.31 | 11.44 |
| MP1-2 | 15.75 | 3.14 | 2.19 | 2.08 |
| MP1-3 | 17.63 | 5.02 | 4.07 | 3.99 |
| MP1-4 | 18.82 | 6.21 | 5.26 | 5.75 |
| MP1-5 | 14.69 | 2.08 | 1.13 | 1.33 |
| MP2-1B | 26.79 | 14.18 | 13.23 | 15.09 |
| MP2-2 | 18.41 | 5.71 | 4.84 | 3.27 |
| MP2-3 | 17.79 | 5.18 | 4.23 | 3.67 |
| MP2-4 | 16.32 | 3.70 | 2.76 | 2.81 |
| MP2-5 | 16.94 | 4.33 | 5.51 | 2.60 |
| MP3-2 | 19.16 | 6.55 | 2.42 | 4.91 |
| MP3-3 | 16.61 | 3.91 | 3.05 | 2.22 |
| MP3-5 | 15.98 | 3.37 | 3.38 | 2.46 |

**Table 13: UV values at different wavelengths for Magalies plant (in $m^{-1}$) (Round 2)**

| Sample Codes | UV Absorbance | | | |
|---|---|---|---|---|
| | 214 | 254 | 272 | 300 |
| MP1-1 | 25.08 | 10.04 | 7.43 | 4.55 |
| MP1-2 | 22.14 | 8.27 | 5.82 | 3.27 |
| MP1-3 | 29.00 | 9.67 | 6.99 | 4.31 |

| | | | | |
|---|---|---|---|---|
| MP1-4 | 29.97 | 5.57 | 3.9 | 1.92 |
| MP1-5 | 31.29 | 8.00 | 5.47 | 3.34 |
| MP2-1B | 26.39 | 11.38 | 8.64 | 5.83 |
| MP2-2 | 28.66 | 12.09 | 9.21 | 6.26 |
| MP2-3 | 23.44 | 9.70 | 7.53 | 5.07 |
| MP2-5 | 30.61 | 10.67 | 8.13 | 5.82 |
| MP3-1 | 26.24 | 11.44 | 8.78 | 5.44 |
| MP3-2 | 27.72 | 11.62 | 8.75 | 5.64 |
| MP3-3 | 21.87 | 8.74 | 6.51 | 4.09 |
| MP3-5 | 27.43 | 11.17 | 8.42 | 5.83 |

**Table 14: UV values at different wavelengths for Magalies plant (in $m^{-1}$) (Round 3)**

| Sample Codes | UV Absorbance | | | |
|---|---|---|---|---|
| | **214** | **254** | **272** | **300** |
| MP1-1 | 57.98 | 10.4 | 8.37 | 4.55 |
| MP1-2 | 85.15 | 8.46 | 6.55 | 3.44 |
| MP1-3 | 30.18 | 7.01 | 5.41 | 2.70 |
| MP1-4 | 51.93 | 6.68 | 5.07 | 2.42 |
| MP1-5 | 31.82 | 5.4 | 3.7 | 1.83 |
| MP2-1B | 30.85 | 5.53 | 3.8 | 1.84 |
| MP2-2 | 26.24 | 7.2 | 5.62 | 2.78 |
| MP2-3 | 26.3 | 7.01 | 5.35 | 2.59 |
| MP2-5 | 27.58 | 5.43 | 3.64 | 1.73 |
| MP3-1 | 178.26 | 12.09 | 9.8 | 5.77 |
| MP3-2 | 26.32 | 8.5 | 6.44 | 3.52 |
| MP3-3 | 25.83 | 7.98 | 6.03 | 3.28 |
| MP3-5 | 22.77 | 5.32 | 3.53 | 1.57 |

**Table 15: UV values at different wavelengths for Rietvlei water treatment plant (Round 1-5) (in $m^{-1}$)**

| Sample Codes | UV Absorbance | | | |
|---|---|---|---|---|
| | 214 | 254 | 272 | 300 |
| RV-1/1 | 24.21 | 11.69 | 10.74 | 9.24 |
| RV-1/2 | 32.27 | 19.66 | 18.71 | 21.17 |
| RV-1/3 | 17.51 | 4.89 | 3.95 | 4.87 |
| RV-1/4 | 20.26 | 7.65 | 6.61 | 5.34 |
| RV-1/5 | 18.05 | 5.44 | 4.48 | 3.06 |
| RV-2/1 | 45.97 | 23.30 | 19.57 | 13.10 |
| RV-2/4 | 46.59 | 16.51 | 13.88 | 9.42 |
| RV-2/5 | 42.11 | 12.09 | 9.70 | 6.93 |
| RV-3/1 | 67.67 | 23.32 | 19.40 | 13.14 |
| RV-3/3 | 68.32 | 14.04 | 11.59 | 8.10 |
| RV-3/4 | 68.66 | 15.72 | 12.92 | 8.83 |
| RV-3/5 | 61.26 | 10.21 | 7.96 | 5.99 |
| RV-4/1 | 103.1 | 18.39 | 15.04 | 9.38 |
| RV-4/3 | 94.13 | 8.12 | 6.34 | 3.70 |
| RV-4/4 | 94.58 | 9.52 | 7.5 | 4.34 |
| RV-4/5 | 83.45 | 5.54 | 3.81 | 2.20 |
| RV-5/1 | 103.64 | 15.89 | 13.08 | 7.49 |
| RV-5/3 | 93.31 | 10.9 | 8.93 | 5.29 |
| RV-5/4 | 110.69 | 9.59 | 7.75 | 4.39 |

| | | | | |
|---|---|---|---|---|
| RV-4/5 | 98.04 | 7.07 | 5.15 | 3.19 |

**Table 16: UV values at different wavelengths for Ebenezer water treatment plant (in $m^{-1}$)**

| Sample Codes | UV Absorbance | | | |
|---|---|---|---|---|
| | **214** | **254** | **272** | **300** |
| LE-1/1 | 11.28 | 6.49 | 5.42 | 4.21 |
| LE-1/2 | 12.00 | 6.79 | 5.99 | 4.72 |
| LE-1/3 | 9.58 | 5.58 | 4.91 | 3.91 |
| LE-1/4 | 10.34 | 5.44 | 4.83 | 3.90 |
| LE-1/5 | 12.38 | 6.38 | 5.58 | 4.74 |
| LE-2/1 | 19.57 | 9.19 | 7.87 | 6.17 |
| LE-2/2 | 16.49 | 8.11 | 7.14 | 5.76 |
| LE-2/3 | 20.77 | 9.83 | 8.47 | 6.58 |
| LE-2/4 | 13.60 | 5.82 | 5.13 | 4.18 |
| LE-2/5 | 18.43 | 7.50 | 6.18 | 5.08 |
| LE-3/1 | 10.86 | 5.6 | 4.88 | 3.76 |
| LE-3/2 | 14.81 | 5.23 | 4.53 | 3.52 |
| LE-3/3 | 5.85 | 1.76 | 1.4 | 0.83 |
| LE-3/4 | 6.15 | 1.33 | 0.97 | 0.51 |
| LE-3/5 | 6.89 | 1.89 | 1.55 | 1.39 |
| LE-4/1 | 7.46 | 3.07 | 2.56 | 1.66 |
| LE-4/2 | 7.84 | 3.17 | 2.65 | 1.65 |
| LE-4/3 | 26.27 | 10.64 | 8.36 | 4.84 |
| LE-4/4 | 8.79 | 2.97 | 2.42 | 1.54 |

| | | | | |
|---|---|---|---|---|
| LE-4/5 | 7.84 | 2.01 | 1.57 | 1.03 |

**Table 17: UV values at different wavelengths for Olifanspoort plant (in $m^{-1}$)**

| Sample Codes | UV Absorbance | | | |
|---|---|---|---|---|
| | **214** | **254** | **272** | **300** |
| LO -1/1 | 55.36 | 14.03 | 11.70 | 8.08 |
| LO -1/2 | 54.35 | 13.37 | 11.14 | 7.70 |
| LO -1/3 | 54.45 | 12.58 | 10.51 | 7.25 |
| LO -1/5 | 53.12 | 10.36 | 8.06 | 6.06 |
| LO -2/1 | 47.36 | 9.77 | 7.5 | 4.24 |
| LO -2/2 | 49.23 | 9.06 | 6.64 | 3.38 |
| LO -2/3 | 43.14 | 5.67 | 3.79 | 1.19 |
| LO -2/4 | 51.18 | 13.58 | 11.01 | 8.84 |
| LO -3/1 | 59.39 | 8.67 | 7.03 | 4.59 |
| LO -3/2 | 54.64 | 5.31 | 4.07 | 2.30 |
| LO -3/3 | 55.48 | 5.26 | 4.06 | 2.28 |
| LO -3/4 | 54.93 | 3.69 | 2.2 | 1.20 |

**Table 18: UV values at different wavelengths for Flag Boshielo plant (in $m^{-1}$)**

| Sample Codes | UV Absorbance | | | |
|---|---|---|---|---|
| | **214** | **254** | **272** | **300** |
| LF 1-1 | 26.66 | 12.51 | 9.7 | 5.44 |
| LF 1-2 | 28.26 | 11.11 | 8.41 | 4.81 |
| LF 1-3 | 28.93 | 9.19 | 7.01 | 3.68 |
| LF 1-4 | 32.64 | 10.82 | 7.73 | 4.98 |
| LF 2-1 | 36.52 | 18.11 | 14.7 | 9.44 |

| | | | | |
|---|---|---|---|---|
| LF 2-2 | 25.41 | 12.56 | 9.93 | 6.99 |
| LF 2-3 | 24.4 | 10.14 | 7.74 | 4.94 |
| LF 2-4 | 25.78 | 10.68 | 8.01 | 5.36 |
| LF 3-1 | 39.23 | 21.1 | 17.75 | 12.9 |
| LF 3-2 | 22.12 | 7.94 | 6.01 | 3.48 |
| LF 3-3 | 21.71 | 7.17 | 5.48 | 3.08 |
| LF 3-4 | 27.52 | 9.64 | 6.81 | 4.25 |

**Table 19: UV values at different wavelengths for Midvaal plant (Round 1 and 2) (in $m^{-1}$)**

| Sample Codes | UV Absorbance | | | |
|---|---|---|---|---|
| | **214** | **254** | **272** | **300** |
| MV-1/1 | 38.32 | 15.74 | 13.17 | 8.50 |
| MV-1/2 | 41.53 | 17.82 | 15.04 | 10.46 |
| MV-1/3 | 39.28 | 16.70 | 14.26 | 9.87 |
| MV-1/4 | 39.36 | 16.90 | 14.26 | 9.98 |
| MV-1/5 | 38.16 | 15.65 | 13.22 | 9.32 |
| MV-1/6 | 37.74 | 14.33 | 11.85 | 8.58 |
| MV-1/7 | 34.27 | 12.35 | 10.24 | 7.18 |
| MV-1/8 | 39.69 | 10.84 | 8.43 | 6.15 |
| MV-1/9 | 37.03 | 9.36 | 7.28 | 5.19 |
| MV-2/1 | 55.18 | 19.2 | 16.35 | 11.23 |
| MV-2/2 | 56.54 | 20.01 | 16.77 | 11.52 |
| MV-2/3 | 55.58 | 19.23 | 16.23 | 11.22 |
| MV-2/4 | 51.94 | 17.71 | 15.01 | 10.37 |
| MV-2/5 | 51.68 | 16.36 | 13.64 | 9.48 |

| | | | | |
|---|---|---|---|---|
| MV-2/6 | 46.38 | 11.65 | 9.65 | 6.91 |
| MV-2/7 | 47.62 | 12.64 | 10.50 | 7.46 |
| MV-2/8 | 52.13 | 10.73 | 8.50 | 6.34 |
| MV-2/9 | 51.62 | 10.48 | 8.37 | 6.31 |

**Table 20: UV values at different wavelengths for Midvaal plant (Round 3 and 4) (in $m^{-1}$)**

| Sample Codes | UV Absorbance | | | |
|---|---|---|---|---|
| | **214** | **254** | **272** | **300** |
| MV-3/1 | 144.99 | 12.48 | 10.44 | 6.75 |
| MV-3/2 | 144.08 | 11.86 | 9.89 | 6.34 |
| MV-3/3 | 144.78 | 12.09 | 10.14 | 6.46 |
| MV-3/4 | 142.87 | 11.13 | 9.35 | 5.76 |
| MV-3/5 | 145.59 | 11.85 | 9.9 | 6.42 |
| MV-3/6 | 140.68 | 8.61 | 7.02 | 4.59 |
| MV-3/7 | 143.31 | 8.39 | 6.82 | 4.46 |
| MV-3/8 | 142.49 | 5.19 | 3.6 | 2.02 |
| MV-3/9 | 142.27 | 4.99 | 3.43 | 1.88 |
| MV-4/1 | 90.61 | 8.68 | 7.15 | 4.38 |
| MV-4/2 | 90.31 | 8.25 | 6.81 | 4.01 |
| MV-4/3 | 91.95 | 10.48 | 8.48 | 5.6 |
| MV-4/4 | 90.92 | 11.15 | 9.56 | 6.64 |
| MV-4/5 | 90.34 | 9.24 | 7.58 | 4.85 |
| MV-4/6 | 89.44 | 8.53 | 6.83 | 4.48 |
| MV-4/7 | 83.89 | 6.07 | 4.64 | 2.86 |
| MV-4/8 | 81.21 | 2.03 | 3.17 | 3.13 |
| MV-4/9 | 80.11 | 1.52 | 2.66 | 2.77 |

**Table 21: UV values at different wavelengths for AM, HL, UM & MT plants (Round 1) (in $m^{-1}$)**

| Sample Codes | UV Absorbance | | | |
|---|---|---|---|---|
| | **214** | **254** | **272** | **300** |
| AM-1/1 | 72.87 | 23.65 | 20.34 | 15.00 |
| AM-1/2 | 50.67 | 7.72 | 6.24 | 4.00 |
| AM-1/3 | 50.98 | 7.83 | 6.42 | 3.98 |
| AM-1/4 | 51.38 | 7.7 | 6.22 | 3.92 |
| AM-1/5 | 43.46 | 4.3 | 2.96 | 1.66 |
| AM-2/1 | 45.49 | 12.44 | 10.52 | 7.77 |
| AM-2/2 | 28.64 | 0.27 | 0.36 | 0.72 |
| AM-2/3 | 28.49 | 0.04 | 0.51 | 0.88 |
| AM-2/4 | 27.95 | 0.46 | 0.95 | 1.28 |
| AM-2/5 | 31.86 | 3.15 | 3.67 | 3.26 |
| HL-1/1 | 45.22 | 19.55 | 17.06 | 12.96 |
| HL-1/2 | 27.45 | 5.77 | 4.24 | 2.63 |
| HL-1/3 | 27.09 | 5.3 | 3.88 | 2.29 |
| HL-1/4 | 24.84 | 3.41 | 2.25 | 1.11 |
| HL-1/5 | 25.4 | 3.92 | 2.77 | 1.70 |
| HL-2/1 | 96.14 | 51.35 | 45.45 | 36.23 |
| HL-2/2 | 38.53 | 6.04 | 4.79 | 3.21 |
| HL-2/3 | 38.95 | 6.38 | 5.04 | 3.1 |
| HL-2/4 | 38.93 | 6.39 | 4.92 | 3.17 |
| HL-2/5 | 36.71 | 4.54 | 3.27 | 1.9 |
| UM-1/1 U | 19.95 | 10.42 | 8.53 | 5.43 |
| UM-1/1 EJ | 50.6 | 15.25 | 12.4 | 7.60 |
| UM-1/2 | 29.92 | 10.13 | 8.14 | 4.98 |
| UM-1/3 | 30.79 | 10.26 | 8.23 | 5.11 |

| | | | | |
|---|---|---|---|---|
| UM-1/4 | 25.84 | 6.4 | 4.27 | 2.34 |
| UM-1/5 | 25.41 | 6.41 | 4.25 | 2.28 |
| UM-2/1 U | 14.72 | 15.57 | 12.85 | 8.73 |
| UM-2/1 EJ | 38.75 | 5.09 | 3.88 | 2.32 |
| UM-2/2 | 16.45 | 2.96 | 1.84 | 0.48 |
| UM-2/3 | 17.61 | 3.56 | 2.36 | 0.98 |
| UM-2/4 | 17.54 | 2.92 | 1.81 | 0.57 |
| UM-2/5 | 14.51 | 0.14 | 1.16 | 1.74 |
| MT-1/1 | 16.11 | 8.99 | 7.8 | 5.68 |
| MT-1/2 | 27.49 | 21.21 | 20.21 | 18.96 |
| MT-1/3 | 8.79 | 3.38 | 2.69 | 1.62 |
| MT-1/4 | 9 | 3.23 | 2.57 | 1.55 |
| MT-1/5 | 7.81 | 2.41 | 1.67 | 1.08 |
| MT-2/1 | 32.94 | 14.07 | 12.02 | 8.70 |
| MT-2/2 | 25.29 | 8.20 | 6.82 | 4.62 |
| MT-2/3 | 21.21 | 5.92 | 4.84 | 3.13 |
| MT-2/4 | 21.28 | 5.8 | 4.44 | 2.93 |
| MT-2/5 | 19.23 | 4.19 | 3.05 | 1.94 |

**Table 22: UV values at different wavelengths for Veolia plant (Round 1) (in $m^{-1}$)**

| Sample Codes | UV Absorbance | | | |
|---|---|---|---|---|
| | **214** | **254** | **272** | **300** |
| VP-1/1 | 102.39 | 55.96 | 46.88 | 32.65 |
| VP-1/2 | 80.44 | 46.34 | 41.4 | 31.92 |
| VP-1/3 | 39.68 | 12.91 | 10.09 | 6.20 |
| VP-1/4 | 34.19 | 9.07 | 7.16 | 4.11 |

| | | | | |
|---|---|---|---|---|
| VP-1/5 | 39.85 | 11.49 | 8.75 | 5.81 |
| VP-2/1 | 102 | 55.14 | 46.85 | 33.44 |
| VP-2/2 | 53.9 | 27.21 | 24.19 | 18.86 |
| VP-2/3 | 34.48 | 10.3 | 8.51 | 5.52 |
| VP-2/4 | 9.84 | 7.23 | 6.17 | 4.23 |
| VP-2/5 | 25.61 | 2.96 | 2.11 | 0.35 |
| VH-1/1 | 3.16 | 1.92 | 1.46 | 1.39 |
| VH-1/4 (Mn) | 1.52 | 0.52 | 0.4 | 0.17 |
| VH-1/4 (Fe) | 2.8 | 1.05 | 0.59 | 0.35 |
| VH-2/1 | 9.79 | 3.49 | 3.59 | 4.02 |
| VH-2/4 (Mn) | 5.19 | 0.31 | 0.29 | 0.35 |
| VH-2/4 (Fe) | 5.35 | 0.77 | 0.66 | 0.56 |

**Table 23: UV values at different wavelengths for Plattensburg plant (Round 3) (in $m^{-1}$)**

| Sample Codes | UV Absorbance | | | |
|---|---|---|---|---|
| | **214** | **254** | **272** | **300** |
| P-1/1 | 37.19 | 23.86 | 20.37 | 14.47 |
| P-1/2 | 9.76 | 6.34 | 5.5 | 4.06 |
| P-1/3 | 8.81 | 5.77 | 4.91 | 3.55 |
| P-1/4 | 4.14 | 2.19 | 1.66 | 1.02 |
| P-1/5 | 10.91 | 6.19 | 5.1 | 3.44 |
| P-2/1 | 125.33 | 83.37 | 72.61 | 53.09 |
| P-2/2 | 25.59 | 19.46 | 17.41 | 13.71 |

| | | | | |
|---|---|---|---|---|
| P-2/3 | 16.56 | 11.28 | 9.37 | 6.63 |
| P-2/4 | 13.52 | 8.43 | 6.89 | 4.58 |
| P-2/5 | 14.69 | 8.55 | 7.17 | 4.66 |

## APPENDIX C: SUVA VALUES FOR VARIOUS TREATMENT PLANTS

**Table 24: SUVA values Magalies water and as for Magalies water plant 1, 2 & 3 (Round 1)**

| Sample Codes | SUVA (ℓ/mg·m) |
|---|---|
| MP1-1 | 1.51 |
| MP1-2 | 0.60 |
| MP1-3 | 0.96 |
| MP1-4 | 1.46 |
| MP1-5 | 0.45 |
| MP2-1B | 2.15 |
| MP2-2 | 1.20 |
| MP2-3 | 1.06 |
| MP2-4 | 0.81 |
| MP2-5 | 0.96 |
| MP3-2 | 1.25 |
| MP3-3 | 0.83 |
| MP3-5 | 0.71 |

**Table 25: SUVA values Magalies water and as for Magalies water plant 1, 2 & 3 (Round 2)**

| Sample Codes | SUVA (ℓ/mg·m) |
|---|---|
| MP1-1 | 2.02 |
| MP1-2 | 2.16 |
| MP1-3 | 2.72 |
| MP1-4 | 1.90 |
| MP1-5 | 2.60 |
| MP2-1B | 2.18 |
| MP2-2 | 3.03 |
| MP2-3 | 2.33 |
| MP2-5 | 3.07 |
| MP3-1 | 2.13 |
| MP3-2 | 2.73 |
| MP3-3 | 2.09 |
| MP3-5 | 2.93 |

**Table 26: SUVA values Magalies water and as for Magalies water plant 1, 2 & 3 (Round 3)**

| Sample Codes | SUVA (ℓ/mg·m) |
|---|---|
| MP1-1 | 1.75 |
| MP1-2 | 1.60 |

| | |
|---|---|
| MP1-3 | 1.53 |
| MP1-4 | 1.54 |
| MP1-5 | 1.20 |
| MP2-1B | 1.40 |
| MP2-2 | 1.62 |
| MP2-3 | 1.51 |
| MP2-5 | 1.25 |
| MP3-1 | 1.99 |
| MP3-2 | 1.91 |
| MP3-3 | 1.87 |
| MP3-5 | 1.31 |

**Table 27: SUVA values for samples from Rietvlei water treatment plant**

| Sample Codes | SUVA (ℓ/mg·m) |
|---|---|
| RV-1/1 | 1.42 |
| RV-1/2 | 3.16 |
| RV-1/3 | 1.01 |
| RV-1/4 | 1.37 |
| RV-1/5 | 1.48 |
| RV-2/1 | 2.30 |
| RV-2/4 | 2.49 |
| RV-2/5 | 2.34 |
| RV-3/1 | 3.14 |
| RV-3/3 | 3.25 |

| | |
|---|---|
| RV-3/4 | 3.32 |
| RV-3/5 | 3.56 |
| RV-4/1 | 2.44 |
| RV-4/3 | 1.93 |
| RV-4/4 | 2.06 |
| RV-4/5 | 1.86 |
| RV-5/1 | 10.06 |
| RV-5/3 | 7.62 |
| RV-5/4 | 7.00 |
| RV-5/5 | 4.59 |

**Table 28: SUVA values for samples from Ebenezer treatment plant**

| Sample Codes | SUVA (ℓ/mg·m) |
|---|---|
| LE-1/1 | 2.51 |
| LE-1/2 | 4.19 |
| LE-1/3 | 3.67 |
| LE-1/4 | 4.42 |
| LE-1/5 | 5.19 |
| LE-2/1 | 0.21 |
| LE-2/2 | 0.20 |
| LE-2/3 | 0.20 |
| LE-2/4 | 0.24 |
| LE-2/5 | 1.28 |
| LE-3/1 | 5.6 |
| LE-3/2 | 5.23 |
| LE-3/3 | 1.76 |
| LE-3/4 | 1.33 |

| | |
|---|---|
| LE-3/5 | 1.89 |
| LE-4/1 | 3.89 |
| LE-4/2 | 3.45 |
| LE-4/3 | 5.54 |
| LE-4/4 | 16.50 |
| LE-4/5 | 116 |

**Table 29: SUVA values for samples from Olifartespoort treatment plant**

| Sample Codes | SUVA (ℓ/mg·m) |
|---|---|
| LO-1/1 | 2.10 |
| LO-1/2 | 2.09 |
| LO-1/3 | 2.09 |
| LO-1/4 | 1.83 |
| LO-2/1 | 2.18 |
| LO-2/2 | 2.25 |
| LO-2/3 | 1.49 |
| LO-2/4 | 3.92 |
| LO-3/1 | 2.85 |
| LO-3/2 | 2.07 |
| LO-3/3 | 2.16 |
| LO-3/4 | 1.63 |

**Table 30: SUVA values for samples from Flag Boshielo treatment plant**

| Sample code | **SUVA (ℓ/mg·m)** |
|---|---|
| LF-1/1 | 1.74 |
| LF-1/2 | 1.83 |
| LF-1/3 | 1.58 |
| LF-1/4 | 1.72 |
| LF-2/1 | 2.19 |
| LF-2/2 | 1.93 |
| LF-2/3 | 1.51 |
| LF-2/4 | 1.51 |
| LF-3/1 | 1.87 |
| LF-3/2 | 0.93 |
| LF-3/3 | 0.85 |
| LF-/4 | 1.11 |

**Table 31: SUVA values for samples from Midvaal treatment plant (Round 1)**

| Sample Codes | SUVA (ℓ/mg·m) |
|---|---|
| MV-1/1 | 2.85 |
| MV-1/2 | 1.62 |
| MV-1/3 | 1.80 |
| MV-1/4 | 1.94 |
| MV-1/5 | 1.81 |
| MV-1/6 | 1.68 |
| MV-1/7 | 1.43 |
| MV-1/8 | 1.38 |
| MV-1/9 | 1.21 |

**Table 32: SUVA values for samples from Midvaal treatment plant (Round 2)**

| Sample Codes | SUVA (ℓ/mg·m) |
|---|---|
| MV-2/1 | 3.61 |
| MV-2/2 | 3.64 |
| MV-2/3 | 3.66 |
| MV-2/4 | 3.45 |
| MV-2/5 | 3.36 |
| MV-2/6 | 2.60 |
| MV-2/7 | 2.77 |

| | |
|---|---|
| MV-2/8 | 2.77 |
| MV-2/9 | 2.99 |

**Table 33: SUVA values for samples from Midvaal treatment plant (Round 3)**

| Sample Codes | SUVA (ℓ/mg·m) |
|---|---|
| MV-3/1 | 2.29 |
| MV-3/2 | 2.21 |
| MV-3/3 | 2.51 |
| MV-3/4 | 2.38 |
| MV-3/5 | 2.49 |
| MV-3/6 | 1.90 |
| MV-3/7 | 1.82 |
| MV-3/8 | 1.40 |
| MV-3/9 | 1.38 |

**Table 34: SUVA values for samples from Midvaal treatment plant (Round 4)**

| Sample Codes | SUVA (ℓ/mg·m) |
|---|---|
| MV-4/1 | 1.07 |
| MV-4/2 | 1.01 |
| MV-4/3 | 1.34 |
| MV-4/4 | 1.45 |
| MV-4/5 | 1.27 |

| | |
|---|---|
| MV-4/6 | 1.23 |
| MV-4/7 | 0.91 |
| MV-4/8 | 0.004 |
| MV-4/9 | 0.002 |

**Table 35: SUVA values for samples from Plattenberg Bay treatment plant (Round 1&2)**

| Sample Codes | SUVA (ℓ/mg·m) |
|---|---|
| P-1/1 | 4.56 |
| P-1/2 | 1.4 |
| P-1/3 | 2.70 |
| P-1/4 | 2.93 |
| P-1/5 | 0.72 |
| P-2/1 | 4.05 |
| P-2/2 | 16.77 |
| P-2/3 | 8.88 |
| P-2/4 | 6.43 |
| P-2/5 | 5.06 |

**Table 36: SUVA values for samples from Preekstoel treatment plant (Round 1&2)**

| Sample Codes | SUVA (ℓ/mg·m) |
|---|---|
| VP-1/1 | 6.58 |
| VP-1/2 | 9.32 |
| VP-1/3 | 4.18 |
| VP-1/4 | 3.70 |
| VP-1/5 | 3.82 |
| VP-2/1 | 8.91 |
| VP-2/2 | 461 |
| VP-2/3 | 1.85 |
| VP-2/4 | 1.57 |
| VP-2/5 | 6.73 |

**Table 37: SUVA values for samples from Amanzimtoti treatment plant (Round 1&2)**

| Sample Codes | SUVA (ℓ/mg·m) |
|---|---|
| AM-1/1 | 1.60 |
| AM-1/2 | 0.52 |
| AM-1/3 | 0.53 |

| | |
|---|---|
| AM-1/4 | 0.52 |
| AM-1/5 | 0.18 |
| AM-2/1 | 2.92 |
| AM-2/2 | 0.07 |
| AM-2/3 | 0.01 |
| AM-2/4 | 0.13 |
| AM-2/5 | 0.96 |

**Table 38: SUVA values for samples from Hazelmere (HL) treatment plant (Round 1&2)**

| Sample Codes | SUVA (ℓ/mg·m) |
|---|---|
| HL-1/1 | 1.18 |
| HL-1/2 | 0.31 |
| HL-1/3 | 0.29 |
| HL-1/4 | 0.20 |
| HL-1/5 | 0.23 |
| HL-2/1 | 10.65 |
| HL-2/2 | 1.74 |
| HL-2/3 | 1.88 |
| HL-2/4 | 1.90 |
| HL-2/5 | 1.40 |

**Table 39: SUVA values for samples from Umzinto treatment plant (Round 1&2)**

| Sample Codes | SUVA (ℓ/mg·m) |
|---|---|
| UM-1/1 EJ | 0.28 |
| UM-1/1 U | 0.62 |
| UM-1/2 | 0.34 |
| UM-1/3 | 0.46 |
| UM-1/4 | 1.43 |
| UM-1/5 | 1.71 |
| UM-1/1 EJ | 1.14 |
| UM-1/1 U | 2.59 |
| UM-1/2 | 0.65 |
| UM-1/3 | 0.78 |
| UM-1/4 | 0.65 |
| UM-1/5 | 0.03 |

**Table 40: SUVA values for samples from Mtwalume treatment plant (Round 1&2)**

| Sample Codes | SUVA (ℓ/mg·m) |
|---|---|
| MT-1/1 | 0.30 |
| MT-1/2 | 0.73 |
| MT-1/3 | 0.12 |
| MT-1/4 | 0.11 |
| MT-1/5 | 0.09 |
| MT-2/1 | 3.75 |
| MT-2/2 | 4.36 |
| MT-2/3 | 2.03 |
| MT-2/4 | 2.07 |
| MT-2/5 | 1.70 |

**Table 41: SUVA values for samples from Veolia (Borehole) treatment plant (Round 1&2)**

| Sample Codes | SUVA (ℓ/mg·m) |
|---|---|
| VB-1 | 49.86 |
| VB-4 Mn | 2.82 |
| VB-4 Fe | 3.21 |

## APPENDIX D: UV SCANS FOR VARIOUS TREATMENT PLANTS

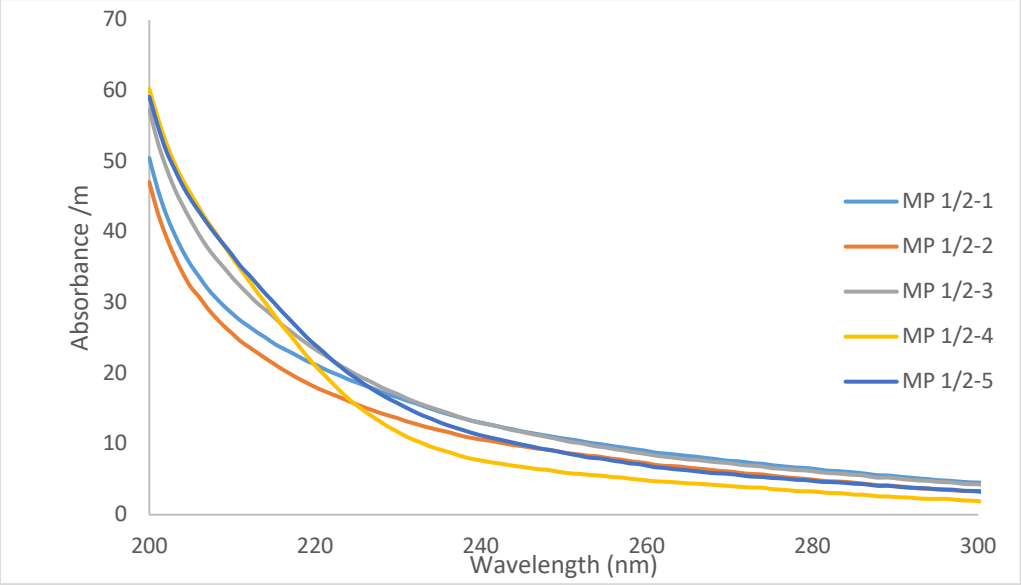


**Figure 1: UV scan for the Magalies plant 1 water (Round 2)**

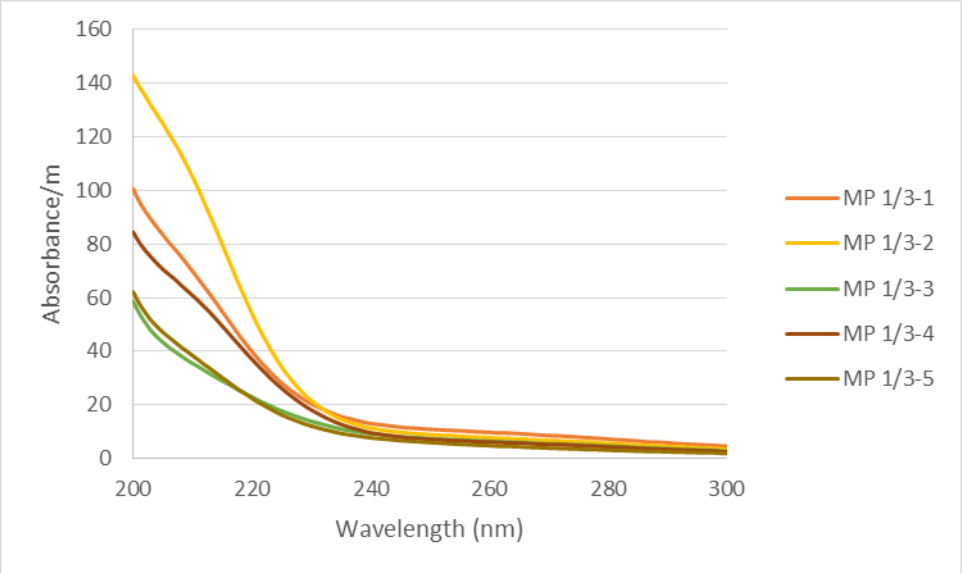


**Figure 2: UV scan for the Magalies plant 1 water (Round 3)**

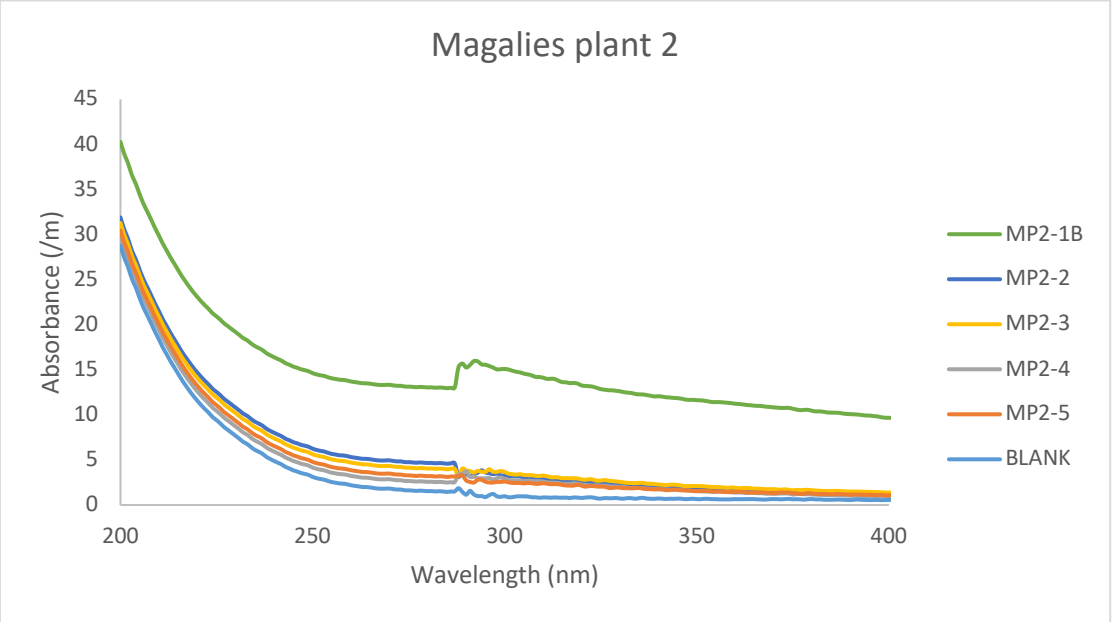


**Figure 3: UV scan for the Magalies plant 2 water (Round 1)**

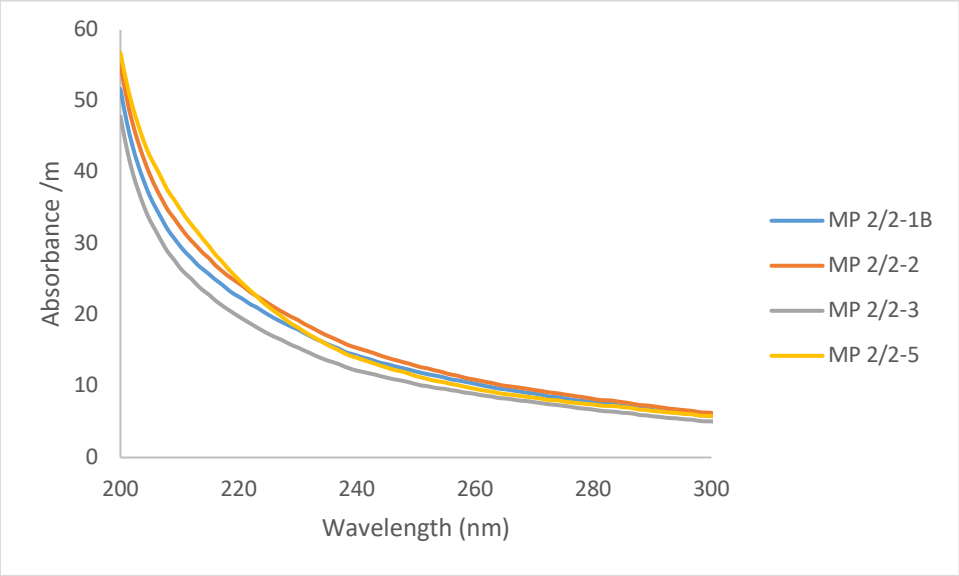


**Figure 4: UV scan for the Magalies plant 2 water (Round 2)**

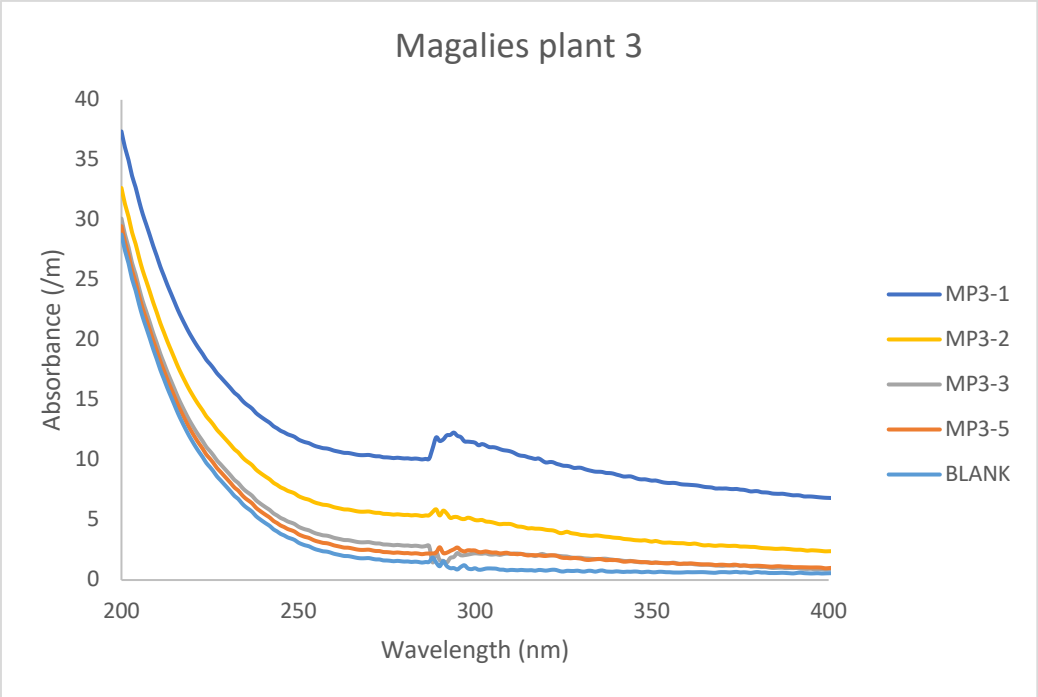


**Figure 5: UV scan for the Magalies plant 3 water (Round 1)**

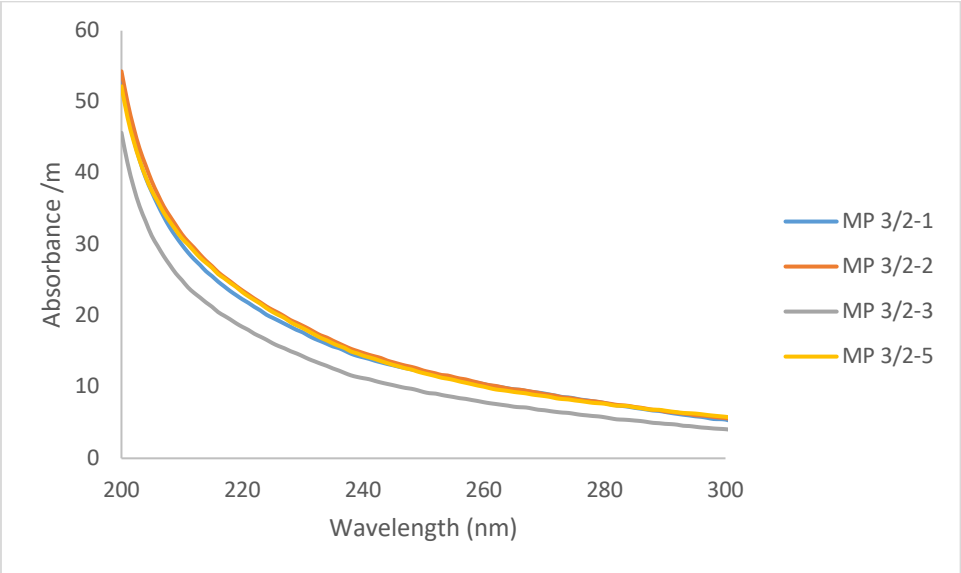


**Figure 6: UV scan for the Magalies plant 3 water (Round 2)**

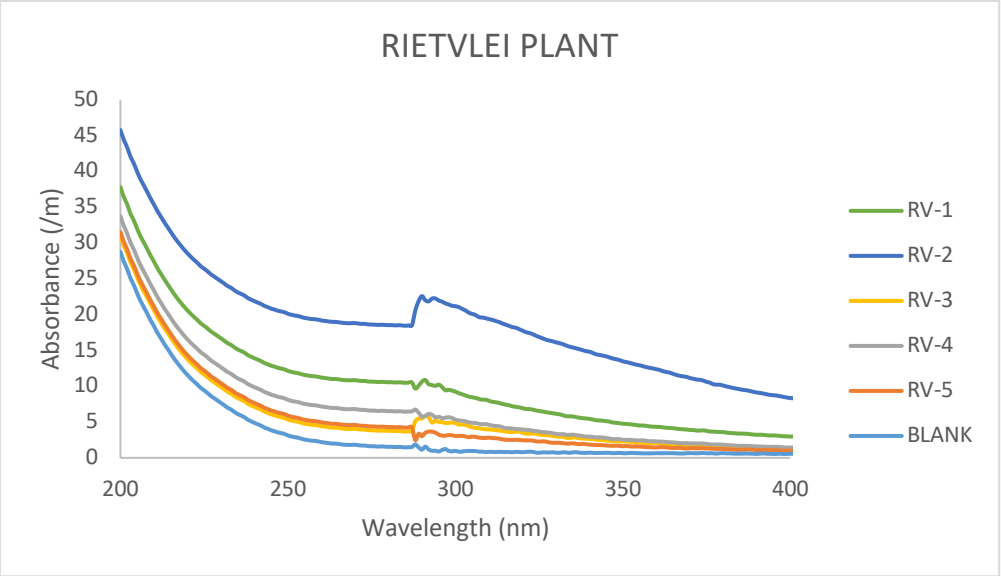


**Figure 7: UV scan for the Reitvlei plant (Round 1)**

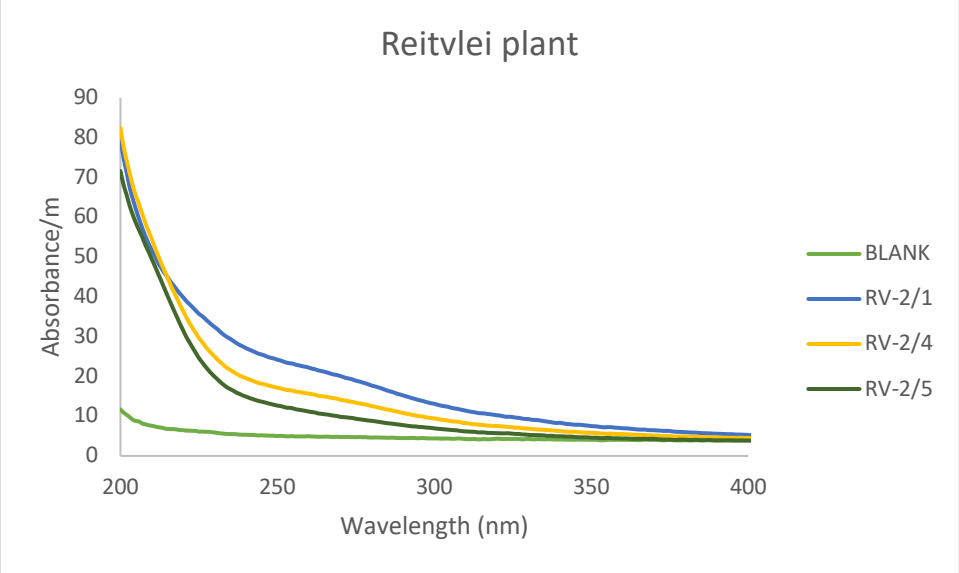


**Figure 8: UV scan for the Reitvlei plant (Round 2)**

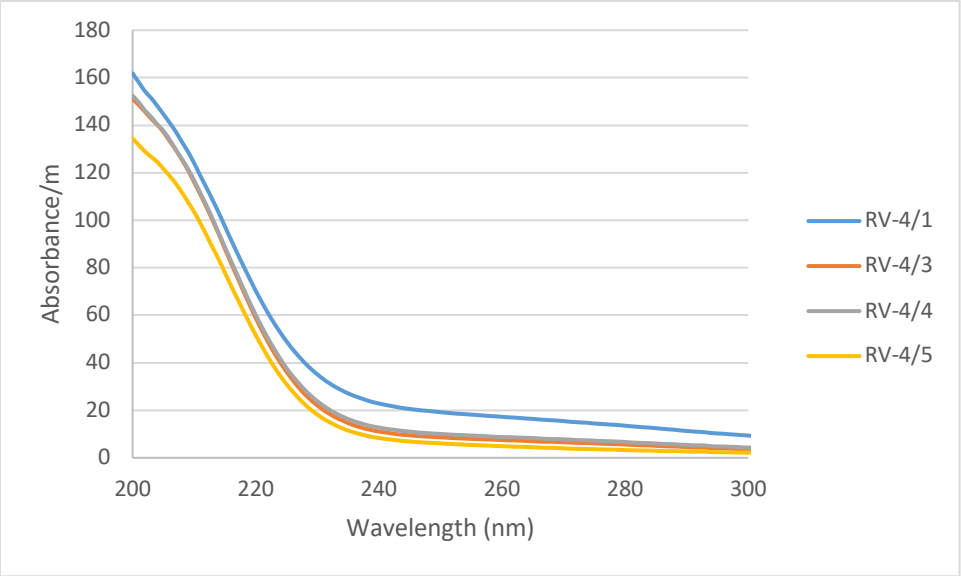


**Figure 9: UV scan for the Reitvlei plant (Round 4)**

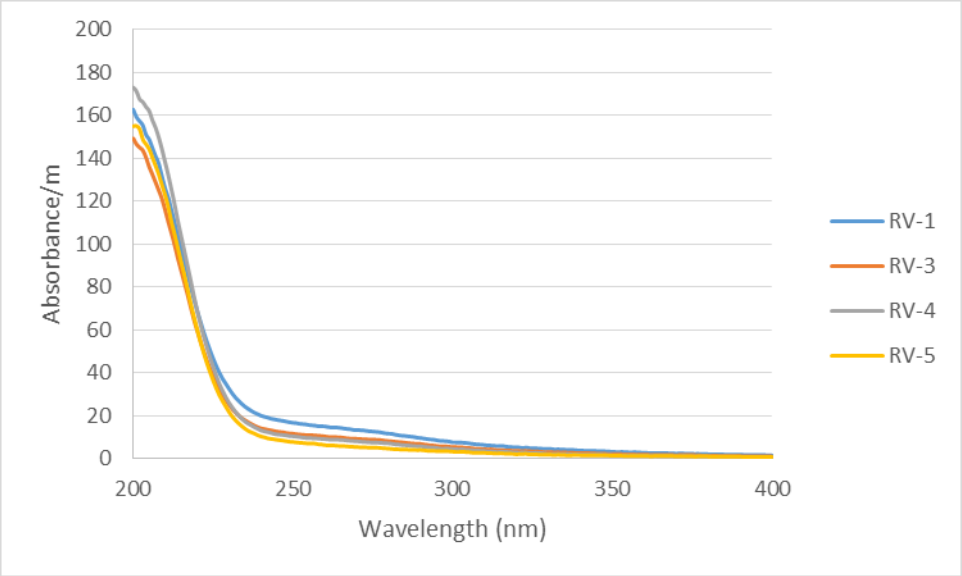


**Figure 9: UV scan for the Reitvlei plant (Round 5)**

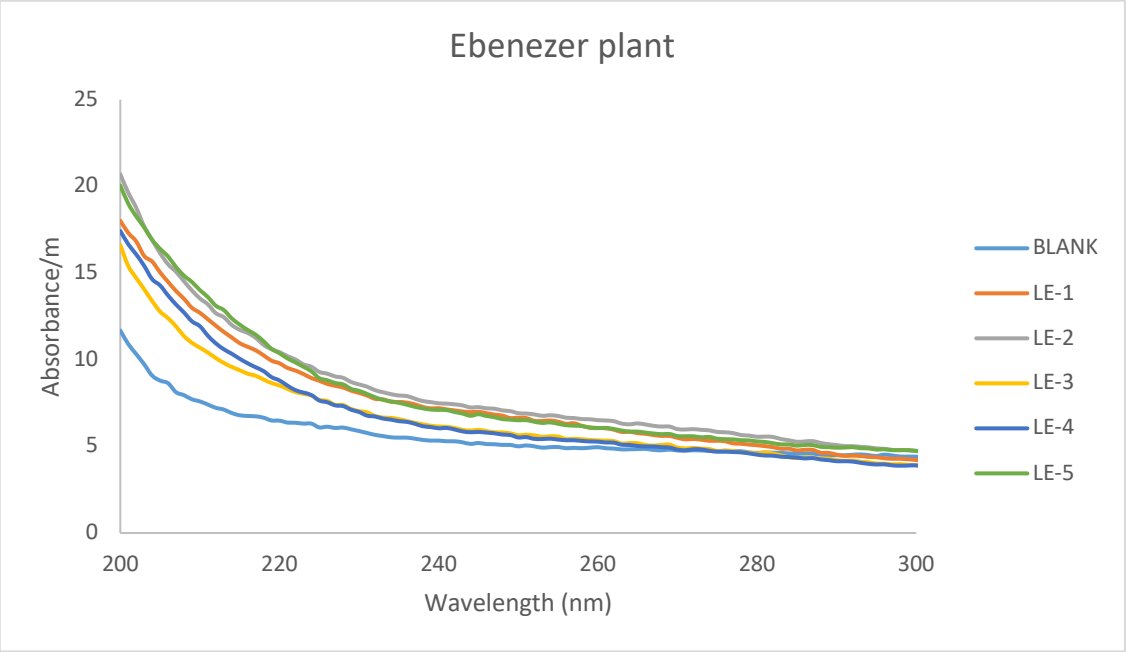


**Figure 10: UV scan for the Ebenezer plant (Round 1)**

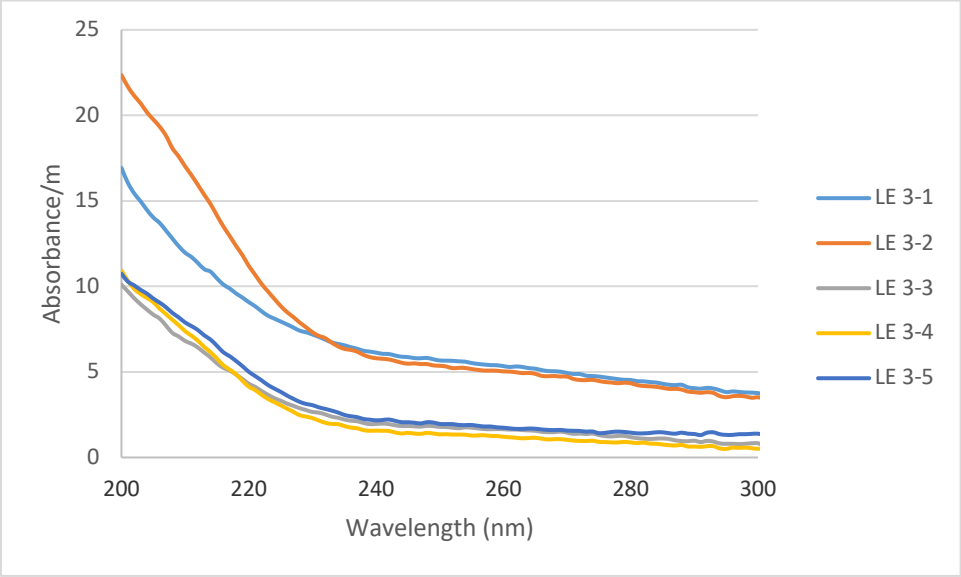


**Figure 11: UV scan for the Ebenezer plant (Round 3)**

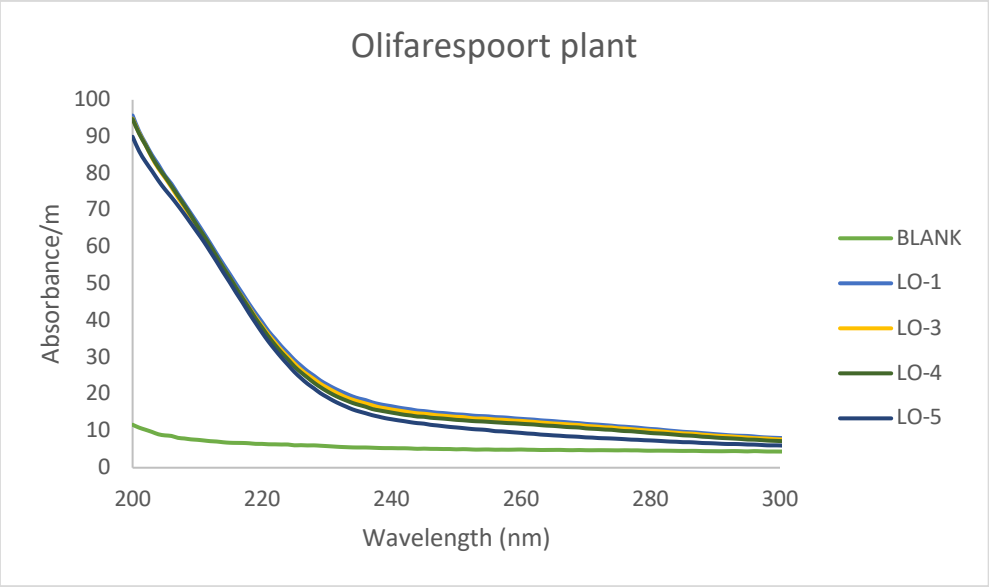


**Figure 12: UV scan for the Olifarnspoort plant (Round 1)**

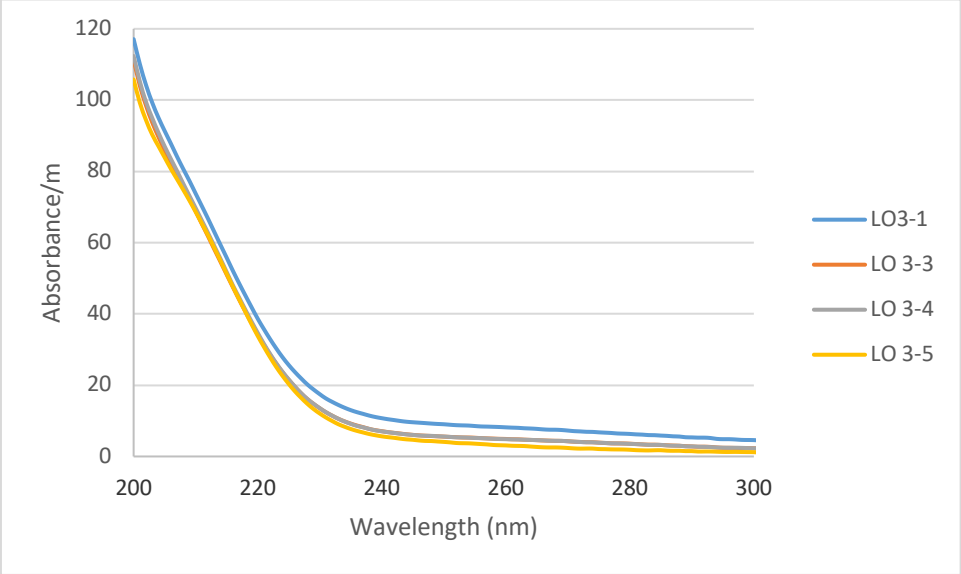


**Figure 13: UV scan for the Olifarnspoort plant (Round 3)**

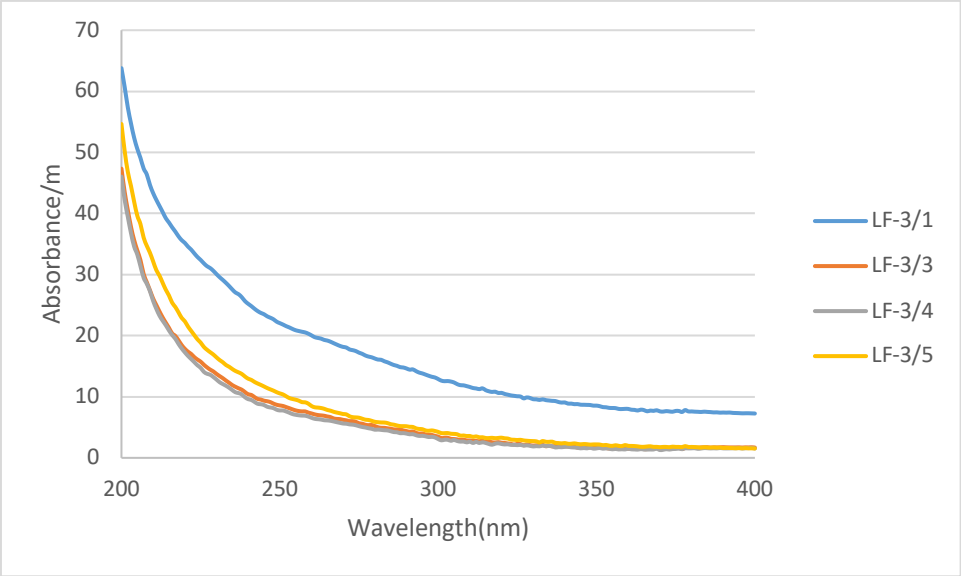


**Figure 14: UV scan for the Olifarnespoort plant (Round 4)**

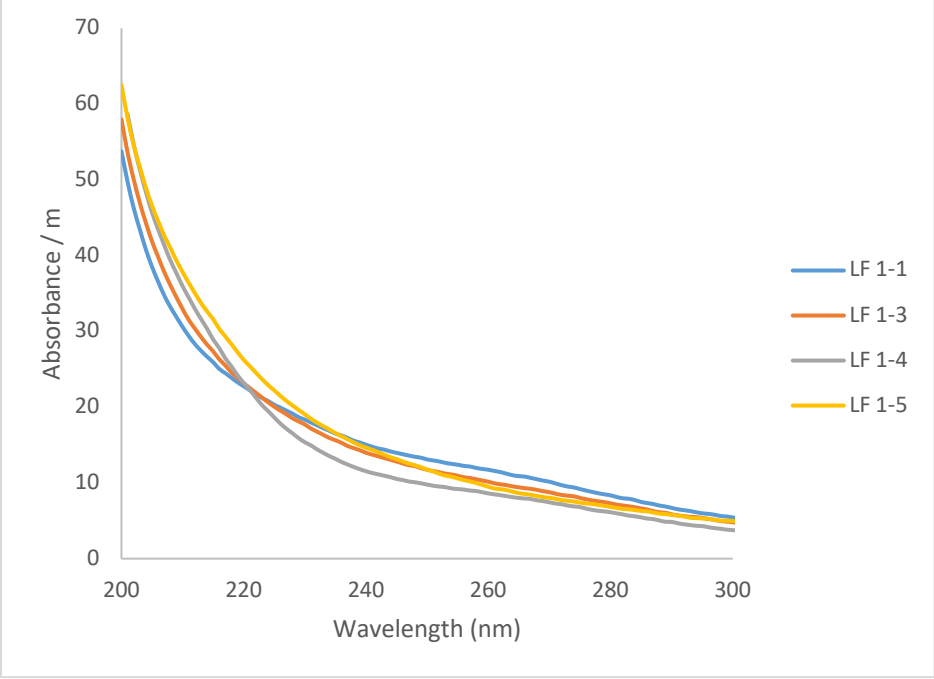


**Figure 14: UV scan for the Flag Boshielo plant (Round 1)**

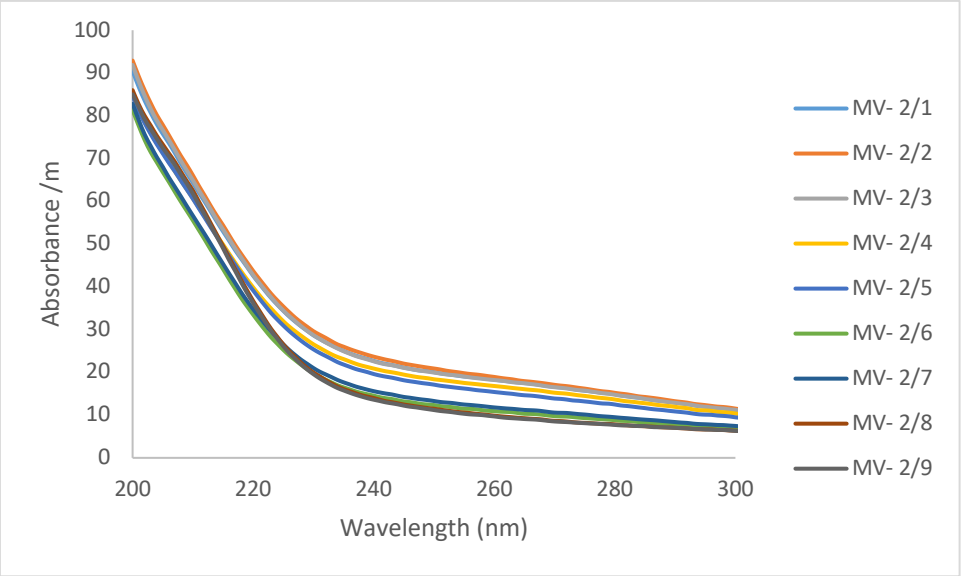


**Figure 15: UV scan for the Midvaal plant (Round 2)**

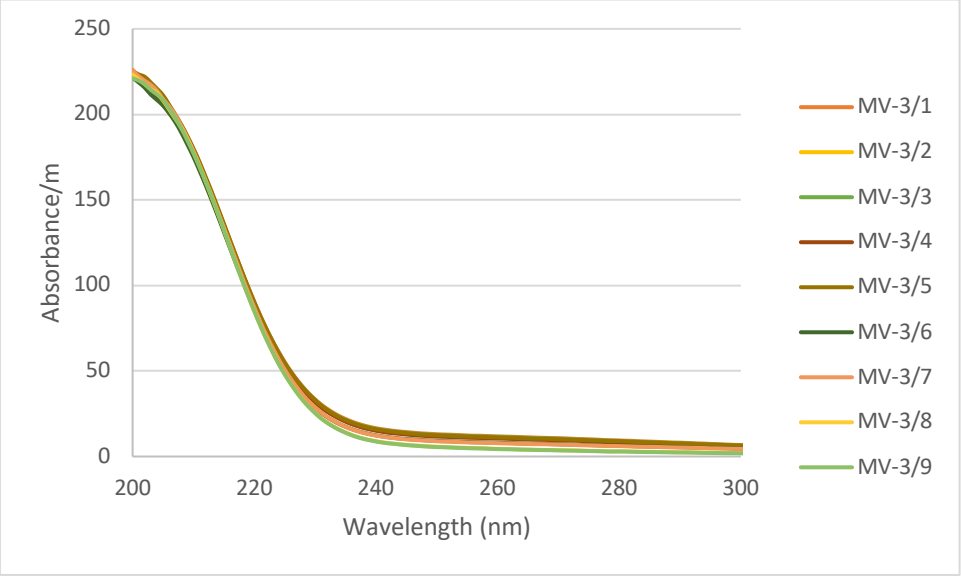


**Figure 16: UV scan for the Midvaal plant (Round 3)**

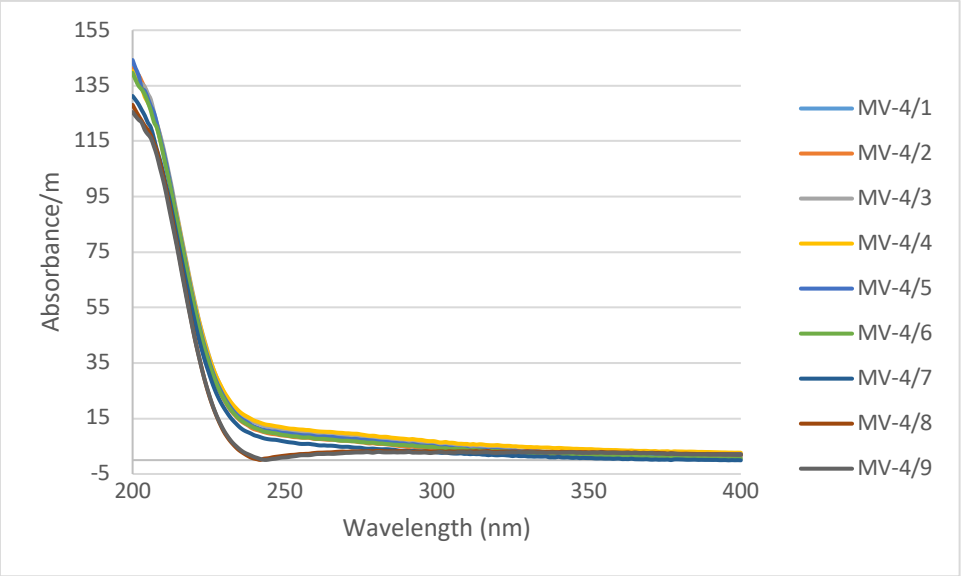


**Figure 17: UV scan for the Midvaal plant (Round 4)**

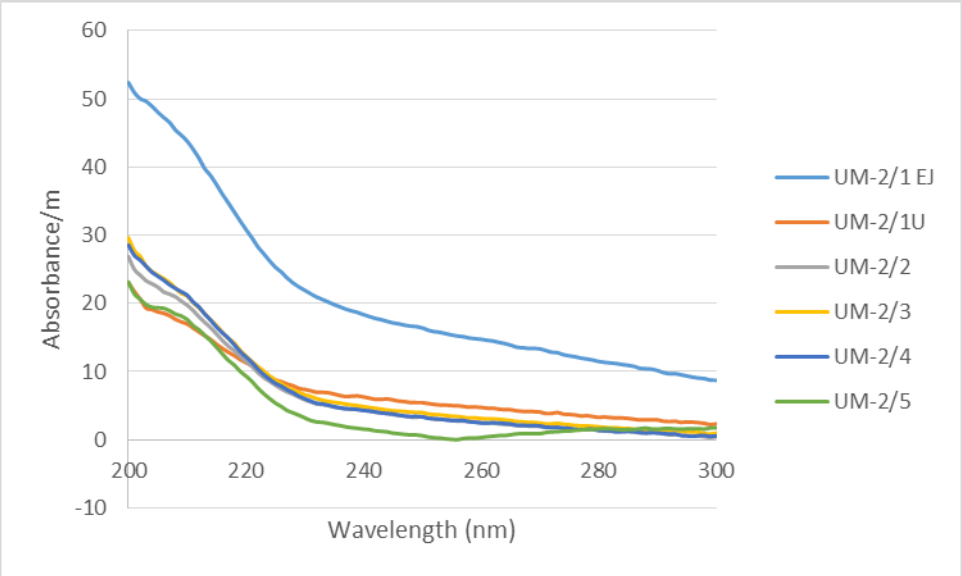


**Figure 18: UV scan for the Umzinto plant (Round 2)**

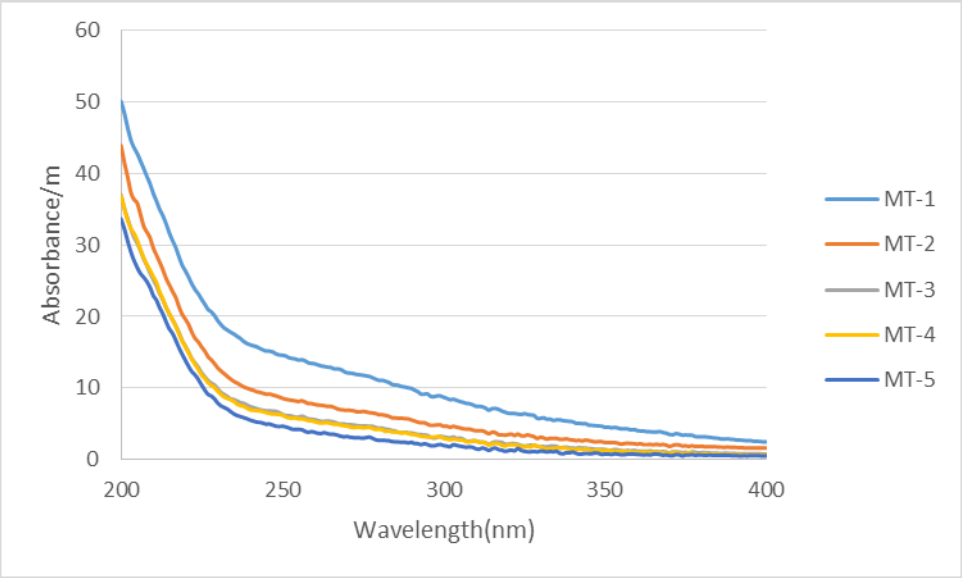


**Figure 19: UV scan for Mtwalume (MT) plant (Round 2)**

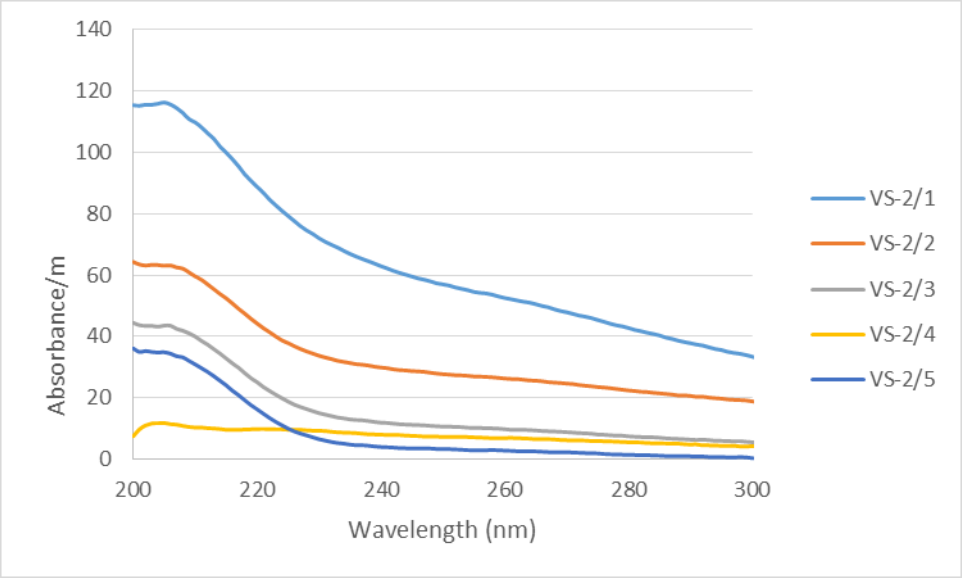


**Figure 20: UV scan for the Preekstoel plant (Round 2)**

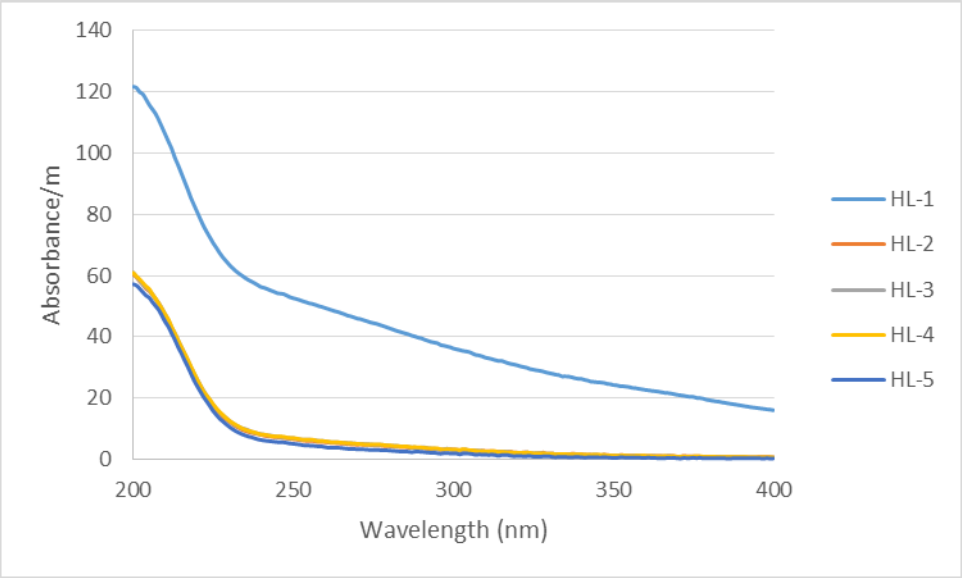


**Figure 21: UV scan for the Hazelmere (HL) plant (Round 2)**

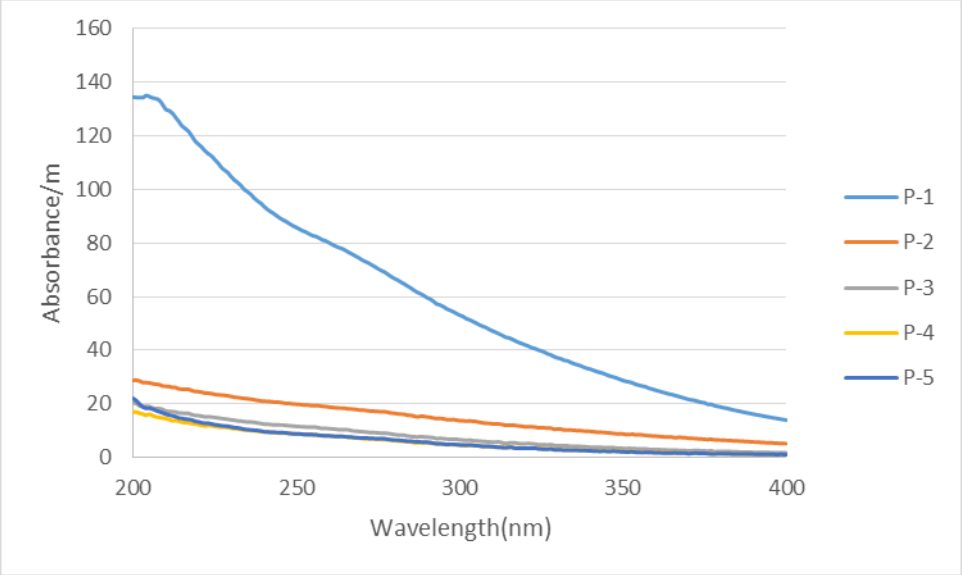


**Figure 22: UV scan for the Preekstoel (VP) plant (Round 2)**

## Appendix E: FEEM SPECTRA OF VARIOUS TREATMENT PLANTS

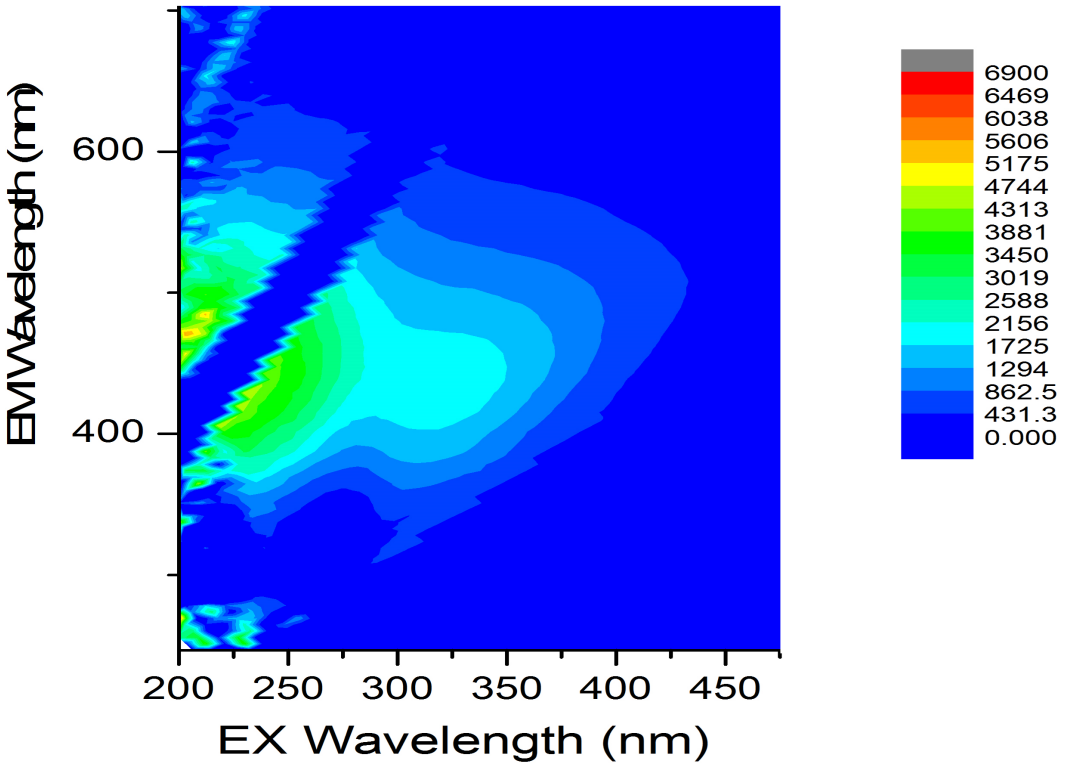


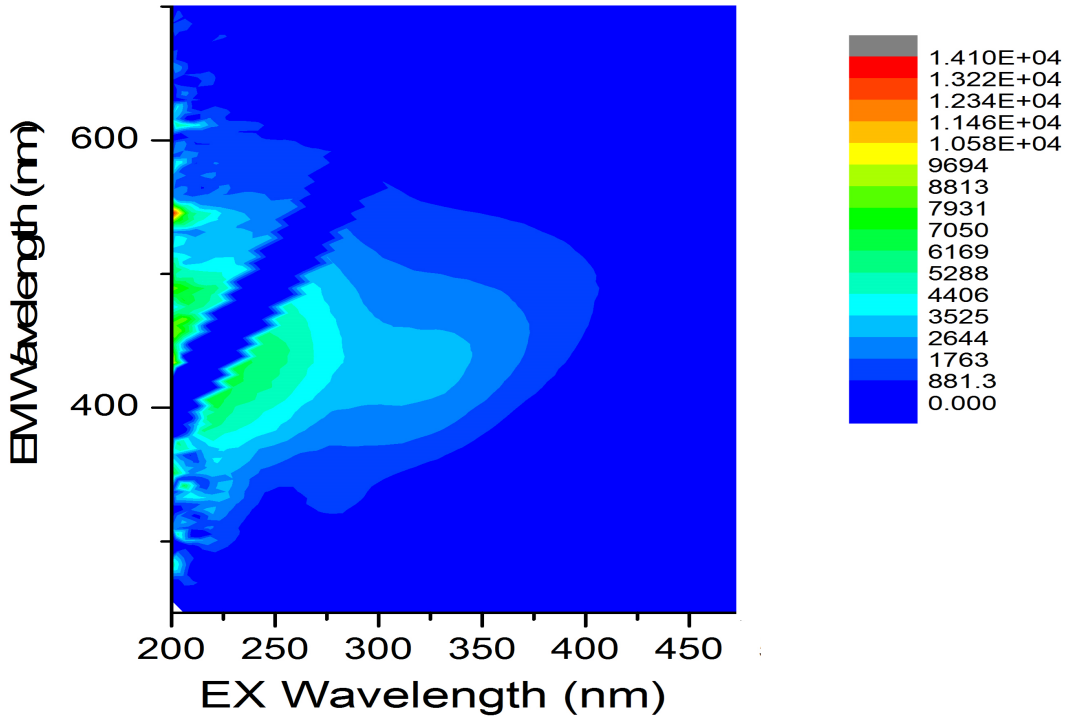

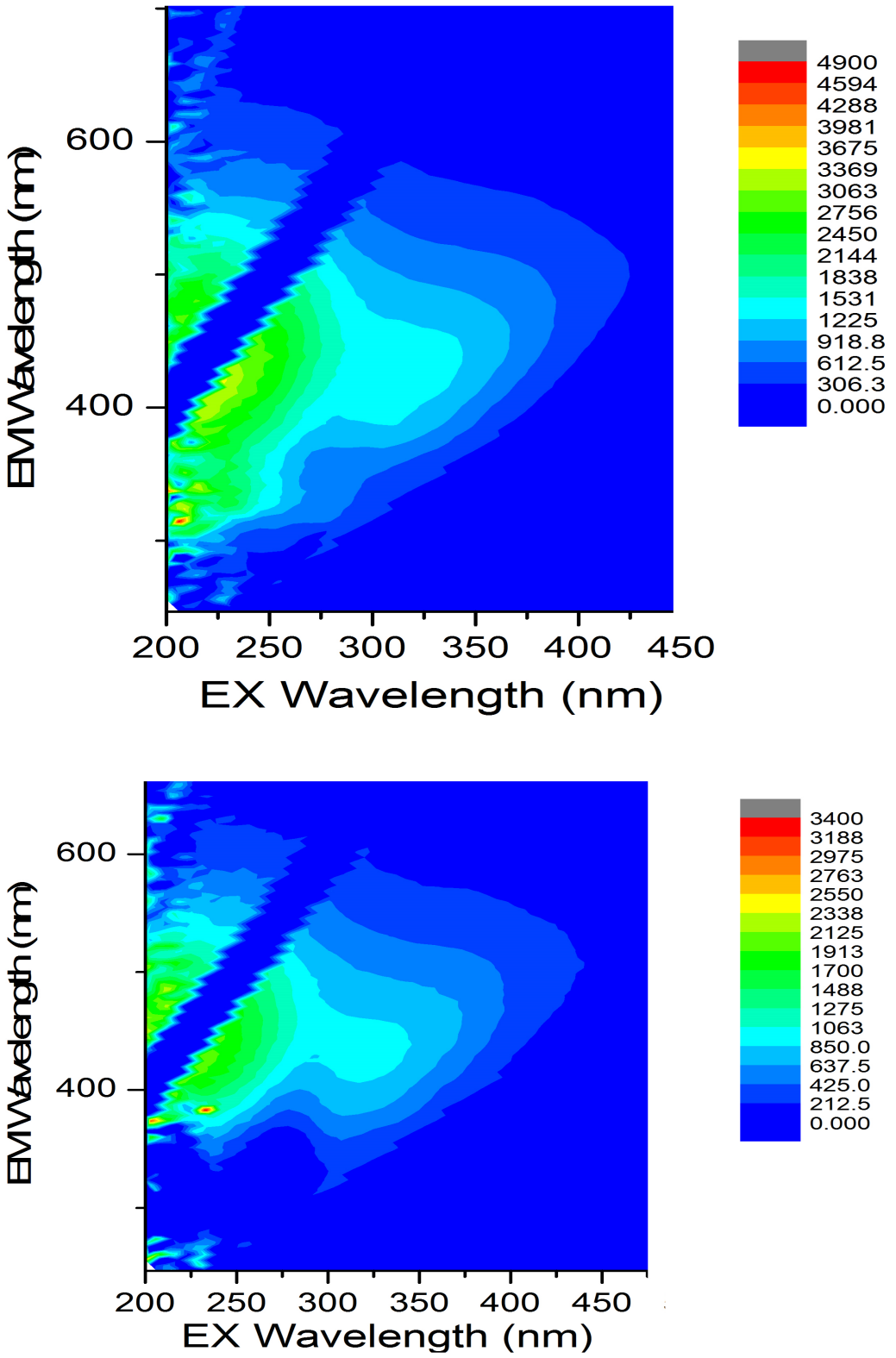


**Figure 23: FEEM spectra of the AM (a), UM (b), HL (c), MT (d) raw water.**

## Appendix F: TREATABILITY OF NOM WITH NANOMATERIALS AND NANOCOMPOSITES

**Table 42: Treatability of NOM from various South African water treatment plants using NPT (0.5 % Pd)**

| Treatment plants | $UV_{254}$ (Raw water samples) / m | $UV_{254}$ (Raw water + NPT (0.5 % Pd)) | % $UV_{254}$ reduction |
|---|---|---|---|
| LF | 21.10 | 5.90 | 72.1 % |
| RV | 15.89 | 7.22 | 54.6 % |
| VS | 55.14 | 5.80 | 89.5 % |
| AM | 19.46 | 9.00 | 53.7 % |
| HL | 53.43 | 3.46 | 93.5 % |
| LE | 3.01 | 2.75 | 8.6 % |
| MT | 14.82 | 2.32 | 84.3 % |
| UM | 12.56 | 2.99 | 76.2 % |
| VB | 1.92 | 0.42 | 78.1 % |
| P | 83.74 | 14.64 | 82.3 % |
| MV | 8.68 | 4.63 | 46.7 % |

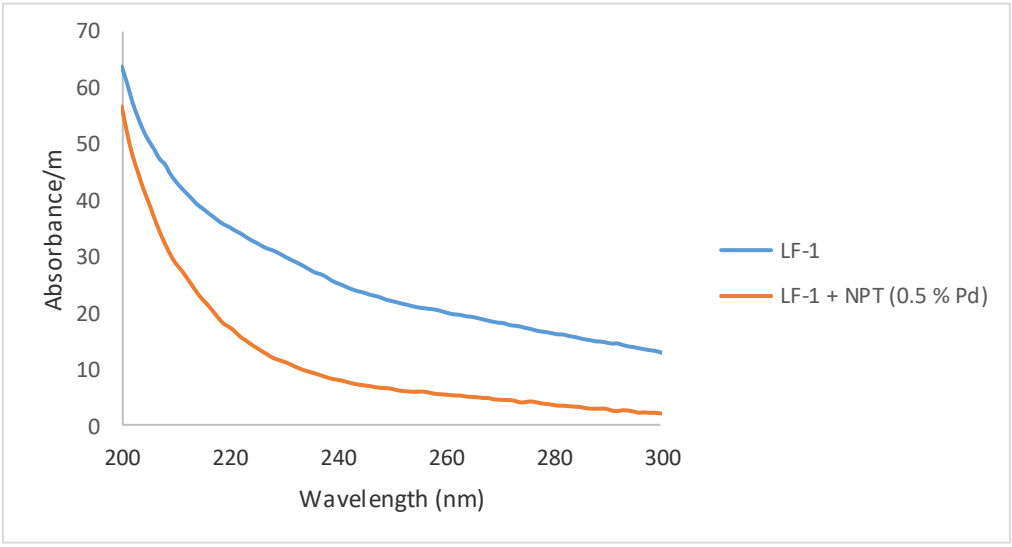


**Figure 24: Treatability of NOM from LF treatment plant**

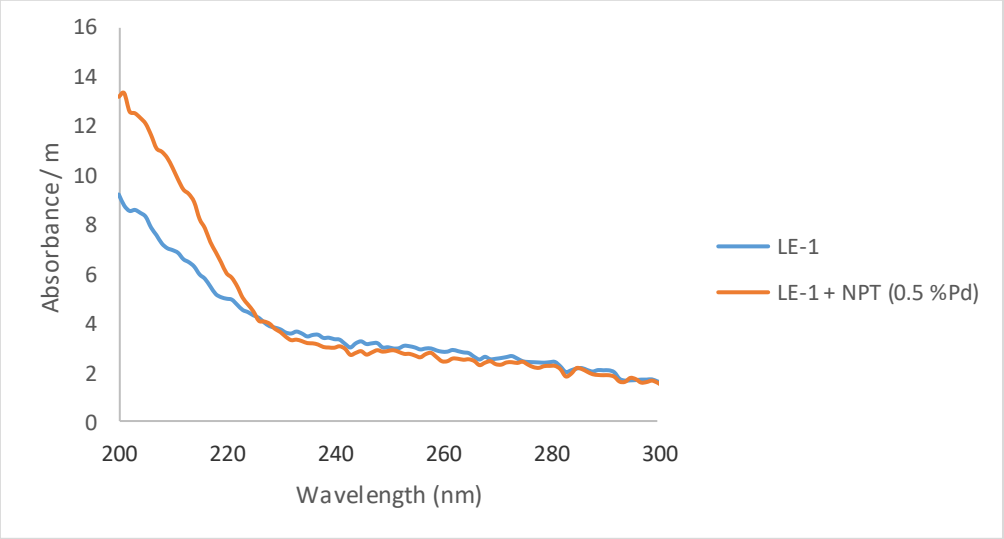


**Figure 25: Treatability of NOM from LE treatment plant**

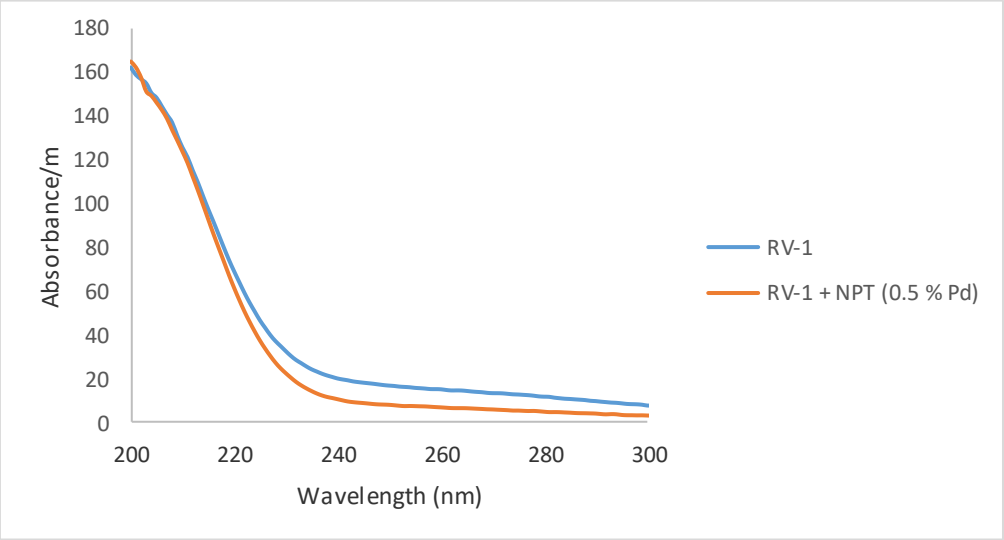


**Figure 26: Treatability of NOM from RV treatment plant**

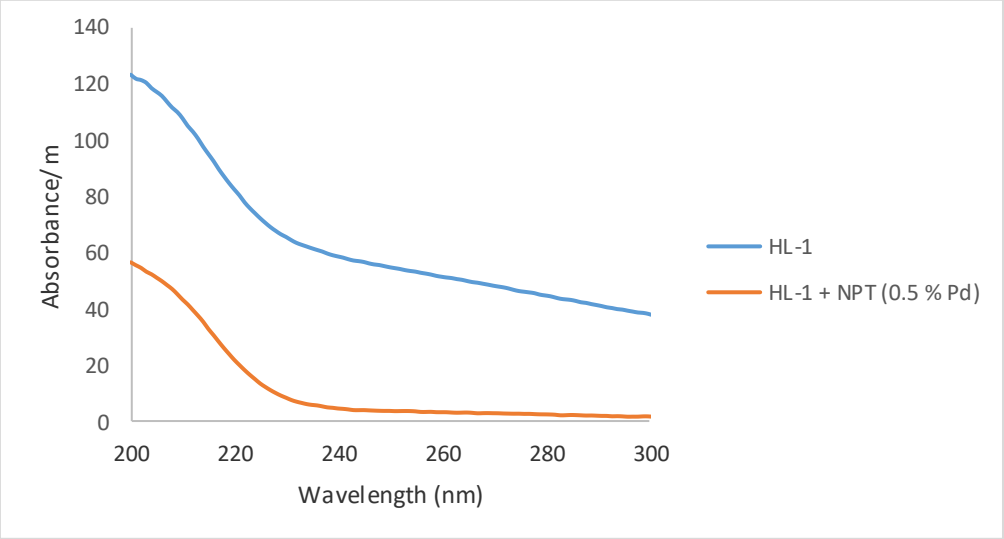


**Figure 27: Treatability of NOM from HL treatment plant**

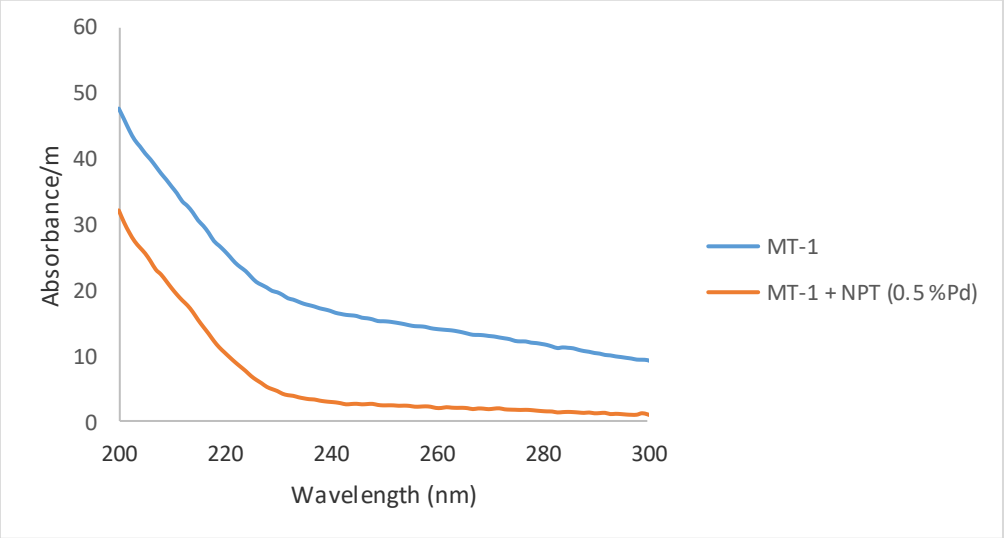


**Figure 28: Treatability of NOM from MT treatment plant**

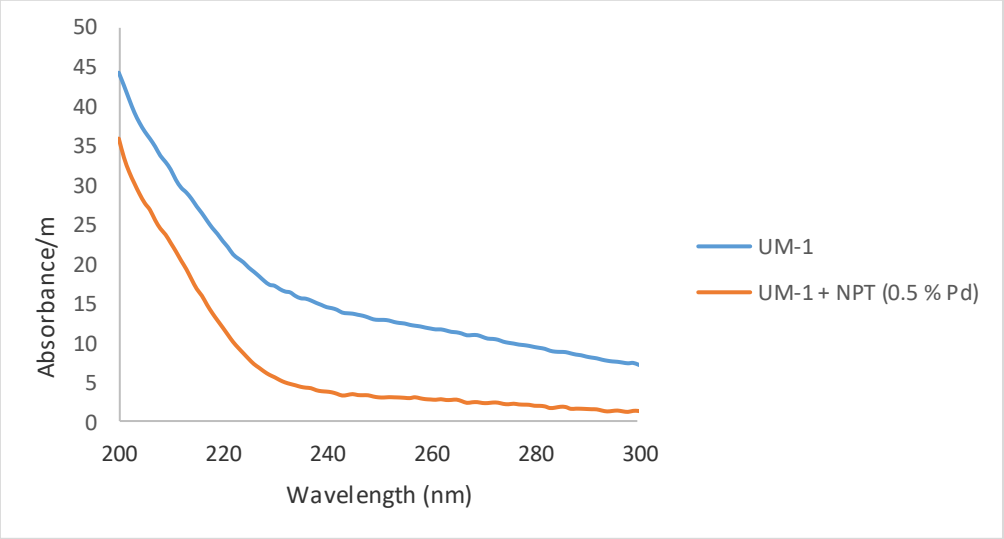


**Figure 29: Treatability of NOM from UM treatment plant**

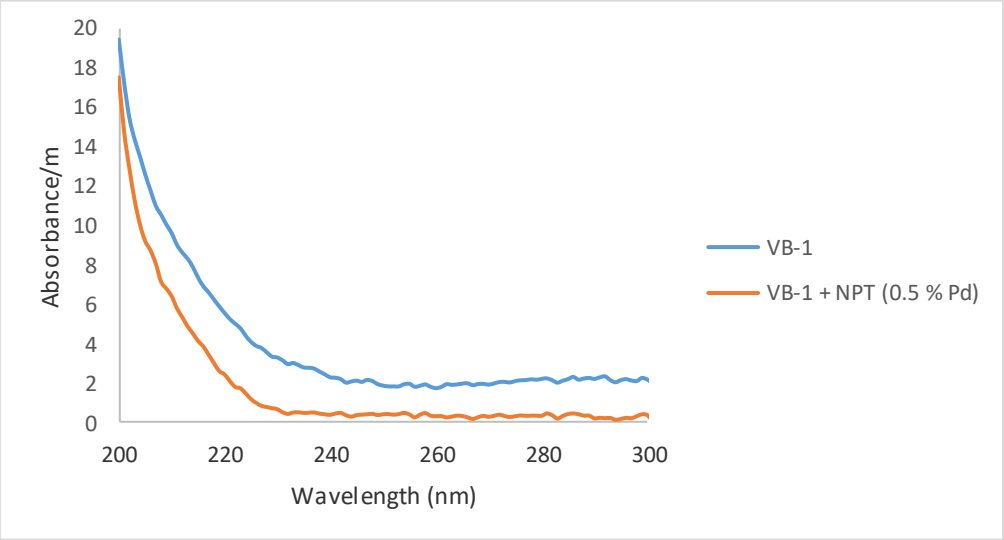


**Figure 30: Treatability of NOM from VB treatment plant**

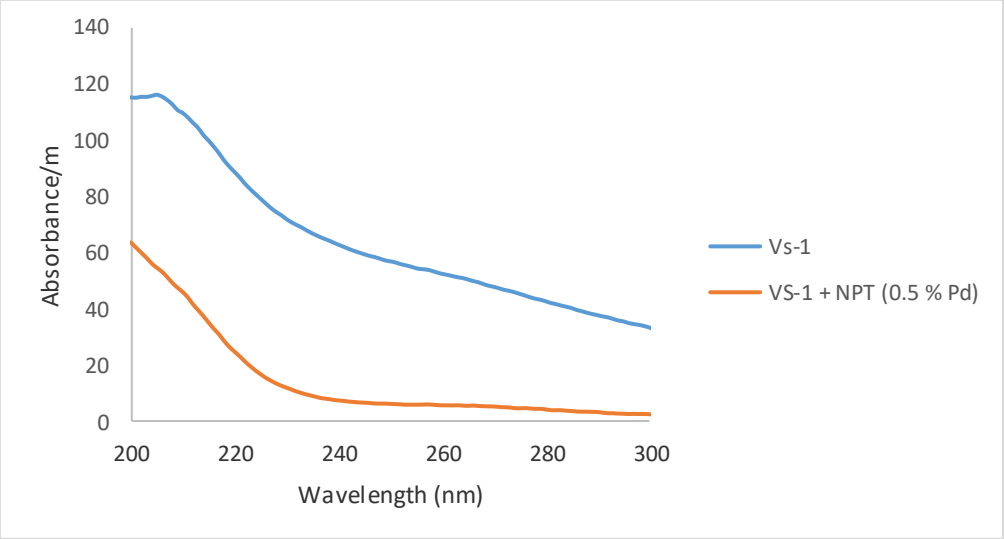


**Figure 31: Treatability of NOM from VS treatment plant**

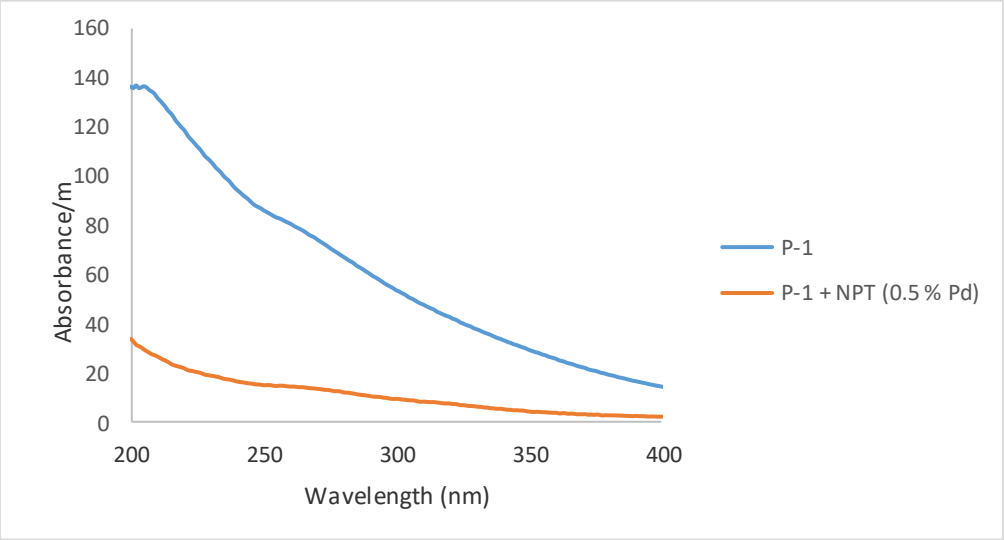


**Figure 32: Treatability of NOM from P treatment plant**

**Table 43: Illustrating the $UV_{254}$ reduction of P-1 (Round 2) by various %MWCNTs of CT nanocomposites**

| Sample name | $UV_{254}$ / m | % Reduction |
|---|---|---|
| P-1 ( conventional methods) | 81.86 | 89.7 % |
| P-1 with NPT (1.0 % Pd) | 26.67 | 67.4 % |
| P-1 with CT (0.5 % MWCNTs) | 10.74 | 86.9 % |
| P-1 with CT (1.0 % MWCNTs) | 6.71 | 91.8 % |
| P-1 with CT (3.0 % MWCNTs) | 17.37 | 78.8 % |
| P-1 with CT (5.0 % MWCNTs) | 8.55 | 89.5 % |